



Carnegie Mellon University
 PITTSBURGH, PENNSYLVANIA 15213

**DEPARTMENT OF
 MECHANICAL ENGINEERING**

Final Report NASA Grant NAG 3-166

March 15, 1981 to November 18, 1988

**"DYNAMICS OF FACE AND ANNULAR SEALS
 WITH TWO-PHASE FLOW"**

*LEWIS
 8-11-88
 175001
 p-270*

**William F. Hughes, Principal Investigator
 Prithwish Basu
 Paul A. Beatty
 Richard M. Beeler
 Stephen Lau**

**Mechanical Engineering Department
 Carnegie Mellon University
 Pittsburgh, Pennsylvania 15213**

November 1988

(NASA-CR-183352) DYNAMICS OF FACE AND
 ANNULAR SEALS WITH TWO-PHASE FLOW Final
 Report, 15 Mar. 1981 - 18 Nov. 1988
 (Carnegie-Mellon Univ.) 270 p

N89-12870

CSCL 11A

G3/37

Unclas
 C175001

Final Report NASA Grant NAG 3-166
March 15, 1981 to November 18, 1988
"DYNAMICS OF FACE AND ANNULAR SEALS
WITH TWO-PHASE FLOW"

William F. Hughes, Principal Investigator
Prithwish Basu
Paul A. Beatty
Richard M. Beeler
Stephen Lau

Mechanical Engineering Department
Carnegie Mellon University
Pittsburgh, Pennsylvania 15213

November 1988

Contents

Summary	3
Nomenclature	5
1. Introduction to the General Theory of Face Seals	7
2. The Theory and Equations of Two-Phase Laminar Face Seals	49
3. A Simplified Model for Laminar Two-Phase Face Seal Design	67
4. The Theory and Equations of Turbulent Two-Phase Face Seals and Annular Seals	79
5. A Methodology for Turbulent Face Seal Design	96
6. A Methodology for Turbulent Annular Seal Design	130
7. A Combined Laminar and Turbulent Computer Code for Face Seal Performance Predictions and Design	144
8. A Summary of Detailed Work and Key to Publications	187
9. References	190
10. Appendices	199
A. Derivation of the Energy Equation	200
B. The Steady State Influence Coefficient Matrix	202
C. Derivation of the Time-Dependent Influence Coefficient Matrix	204
D. Documentation of the Computer Code (Chapter 7)	209
11. Floppy Disk (inside back cover)	

Summary

A detailed study has been made of face and annular seals under conditions where boiling, i.e., phase change of the leaking fluid, occurs within the seal. Many seals operate in this mode because of flashing due to pressure drop and/or heat input from frictional heating. We mention high pressure, water pumps, industrial chemical pumps, and cryogenic pumps as a few of many applications. The initial motivation for this work was the LOX-GOX seals for the space shuttle main engine, but the study has been expanded to include any face or annular seal where boiling occurs.

We have discussed some of the distinctive behavior characteristics of two-phase seals, particularly their axial stability. While two-phase seals probably exhibit instability to disturbances of other degrees of freedom such as wobble, etc., under certain conditions, such analyses are too complex to be treated at present. Since an all liquid seal (with parallel faces) has a neutral axial stiffness curve, and is stabilized axially by convergent coning, other degrees of freedom stability analyses are necessary. However, the axial stability behavior of the two-phase seal is always a consideration no matter how well the seal is aligned and regardless of the speed. Hence, we might think of the axial stability as the primary design consideration for two-phase seals and indeed the stability behavior under sub-cooling variations probably overshadows other concerns. The main thrust of this work has been the dynamic analysis of axial motion of two-phase face seals, principally the determination of axial stiffness, and the steady behavior of two-phase annular seals.

The main conclusions are that seals with two-phase flow may be unstable if improperly balanced. Detailed theoretical analyses of low (laminar) and high (turbulent) leakage seals are presented along with computer codes, parametric studies, and in particular a simplified PC based code that allows for rapid performance prediction: calculations of

stiffness coefficients, temperature and pressure distributions, and leakage rates for parallel and coned face seals.

A simplified combined computer code for the performance prediction over the laminar and turbulent ranges of a two-phase seal is described and documented.

This report summarizes the analyses, results, and computer codes, but for more details the reader is referred to the more complete detailed studies presented in the various papers and reports listed in Chapter 8.

NOMENCLATURE

F_o	opening force [N]
F_o^*	nondimensional opening force
F_c	closing force [N]
G	mass velocity, ρu , [kg/m ² s]
h	film thickness (seal clearance) [m]
h^*	nondimensional film thickness
H	film coefficient for heat transfer [J/(s.m ² K)]
i	specific enthalpy [J/kg]
k	thermal conductivity [W/(m.K)], inlet loss coefficient
m	mass leakage rate [kg/s];
M	nondimensional mass leakage rate
M	Mach Number
p	pressure [Pa]
p^*	nondimensional pressure
Q	torque [Nm]
q	rate of heat conduction per unit area into the seal plates from the fluid [J/(s.m ²)]
r	radial location [m]
R	shaft radius
R	ideal gas constant [J/(kg.K)]
T	temperature [K]
u	velocity in r , velocity in axial -direction [m/s]
U	average velocity in r - direction [m/s]
v	specific volume [m ³ /kg]
V	relative axial velocity of the seal rings [m/s]
w	velocity in θ - direction [m/s]
W_s	control volume shaft work
x	nondimensional radial distance
z	axial coordinate [m]

α	thermal diffusivity [m ² /s]
β	coning angle
θ	circumferential location [rad]
λ	molecular mean free path [m], quality or mass fraction of vapor in two-phase mixture
μ	viscosity [Pa.s]
ν	kinematic viscosity [m ² /s]
ρ	density [kg/m ³]
$\tau_{z r}$	wall shear stress in radial direction [N/m ²]
$\tau_{z \theta}$	wall shear stress in circumferential direction [N/m ²]
Φ	viscous dissipation function [J/s.m ³]
ω	angular velocity [rad/s]
Ω	nondimensional angular velocity
$()_b$	value at the discrete boiling interface
$()_{bal}$	value at the balance radius
$()_f$	saturated liquid value
$()_{fg}$	properties [$()_g - ()_f$]
$()_g$	gas property, saturated vapor property
$()_i$	value at the inner radius (low-pressure side)
$()_l$	liquid property
$()_o$	value at the outer radius (high-pressure side)
$()_w$	value at the wall
$()_\infty$	sealed fluid property away from the seal; exhaust back pressure

CHAPTER 1

INTRODUCTION

Seals are mechanical devices used to restrict leakage of fluids, for example, when a rotating shaft penetrates a stationary housing which encloses the pressurized fluid. The tolerable leakage rate depends on the nature of the sealed fluid; leakage of expensive, toxic, corrosive, explosive or flammable fluids must be reduced to a minimum. The life and reliability of seals are also of major concerns amount the users to reduce equipment and process downtime. Sometimes when system redundancy is kept at a bare minimum, for example in airborne and space vehicles, a seal failure could cause serious system malfunctioning.

In January 1986, the whole world suddenly became aware of the crucial importance of fluid sealing technology when the US shuttle "Challenger" tragically exploded shortly after leaving the launch pad. A joint sealed by rubber O-rings had failed. This episode had the characteristics of many a sealing problem. The component involved was of relatively low-value in its own merit, but the consequential cost of failure was totally disproportionate. The failed O-ring was a static seal and much less complicated in operation than the dynamic seals discussed here.

The Figure 1-1 [1] gives an overview of different types of industrial sealing devices available. Among the different kinds of seals, 'Mechanical End Face Seals' (also simply called Face Seal) are the dominating category of major industrial seals and have been given special and extensive considerations. Fluids that need to be sealed range from water, petroleum products, oil, natural gas, air and toxic chemicals to cryogenic fluids like liquid oxygen and hydrogen (Space Shuttle Turbo Pumps). These seals may handle pressure up

to 5000 psi (~350 atm.), temperatures up to 1000°C and a rotational speed of up to 60,000 RPM.

A good treatise on mechanical face seal designs, basic configurations, operation and lubrication mechanisms has been given by Ludwig & Griener [2, 3]. Figure 1-2 shows the schematic diagram of a face seal. The primary sealing is accomplished by a nonrotating ring (called primary seal ring or stator) that bears against the face of a rotating ring (called seal seat or rotor) mounted on the shaft. Occasionally co-rotating and counter-rotating seals (advanced aircraft engines) are encountered where both the rings are rotating. Between the stator and the housing, there are multiple springs which give it the flexibility in the axial and two angular modes about orthogonal diametrical directions. Secondary seals are provided between the stator ring and the housing. Typically these seals are elastomeric O-rings. They self-energize under pressure and tend to fill in the asperities and voids on the surfaces in contact and hence minimize leakage through secondary sealing surfaces. Successful operation of seals requires satisfaction of seemingly competing demands. In order to reduce wear and maintain integrity of the sealing surfaces, it is desirable, if not essential, to achieve and maintain separation of faces by a lubricating film. At the same time face separation must be kept extremely small (~ 2-3 μ m) in order to minimize leakage. These requirements must be dynamically met in changing operating conditions and in the presence of machinery vibrations.

Figure 1-3 shows the typical forces a stator experiences. This is an 'outside-pressurized' arrangement with the high pressure fluid at the Seal OD. This configuration offers a few advantages as the centrifugal forces tend to retard leakages and centrifuge solid particles away from the sealing surfaces giving a self-cleaning feature. The sealed fluid leaks through the gap between the seal rings and pressure drops due to friction and inertia. A typical pressure profile, $P(r)$, for an axisymmetric gap is shown in the figure. If the

gap is nonaxisymmetric, hydrodynamic pressure will build up inside the seal due to relative tangential motion of the seal faces and the pressure profile becomes also a function of the circumferential location, i.e. $P(r, \theta)$. For an axisymmetric gap, there is no hydrodynamic pressure generation and the pressure distribution inside the seal is same as if both the seal faces are stationary (if centrifugal inertia effects are neglected). The pressure distribution, so obtained, often referred to as hydrostatic component. This fluid pressure P , tends to open the seal gap. On the other hand, the axial loading from the sealed fluid pressure and the spring force, F_s , acts behind the stator and tends to close the seal. The expressions for the opening and closing forces are given below.

$$F_o = \int_0^{2\pi} \int_{r_i}^r P(r, \theta) r dr d\theta$$

$$F_c = \pi(r_o^2 - r_{bal}^2) P_o + F_s + \pi(r_{bal}^2 - r_i^2) P_i$$

' r_{bal} ' is called the 'balance radius' by which the closing force, F_c , can be controlled. If the closing force, F_c , is equal to the opening force, F_o , at the operating point, then a lubricating fluid film is maintained at the seal interface. Under this situation, the seal operates in a 'non-contacting mode' and is called a 'balanced seal.' The corresponding clearance is called the 'operating clearance or film thickness.' On the other hand, if the closing force is greater than the available opening force, the asperity contact takes place at the seal interface and the force balance is achieved with the help of the mechanical contact pressure. In this case, the seal operates in a 'contacting mode' and is called an 'unbalanced seal.' The contacting seals are supposed to operate with a minimal contact pressure; otherwise, heavy wear at the surfaces would cause premature seal failure. These seals are generally used for low to moderate pressure services and noncontacting seals for high pressure applications. In chemical and petrochemical industries, the contacting mode is primarily chosen for almost all sealing applications to reduce leakage of hazardous fluid as

much as possible even at the expense of seal life. The third situation arises when the opening force exceeds the applied closing force. In that case, the seal pops open causing high leakage and seal failure is said to have taken place. For a given design with a certain balance radius, r_{bal} , the closing force is constant for a given operating pressure, whereas the opening force is dependent on the gap geometry and speed. The information most useful to the seal designers is the 'Opening Force vs. Nominal Clearance' curves, typically known as 'F-h' curves, for different speeds and system pressures. One necessary requirement for a stable and successful seal operation is to have a negatively sloped 'F-h' curve around the operating point (which means positive film stiffness); otherwise, seal faces will collapse and give unacceptable contact load and rapid wear. Examples of typical 'F-h' curves are shown in Figures 1-9 and 1-10 and they are explained later.

The seal lubricating film is usually very thin (in the range of few microns) and, therefore, very small irregularities, thermal and pressure distortions, and face runout motions can have a dramatic effect on seal performance. Thus, the primary seal cannot, in general, be visualized as two perfectly flat and parallel surfaces. Some possible geometries are illustrated in Figure 1-4[2]. The waviness (geometry a) and angular misalignment (geometry b) are most likely sources of hydrodynamic pressure build-up. Coning (geometry c) affects the hydrostatic pressure distribution and film stiffness. Externally imposed axial vibration (geometry d) can produce squeeze film damping. Parallel misalignment (also called radial eccentricity) and shaft whirl (geometry e & f) impart a radial velocity component to the fluid particles which can affect the leakage. Some of these seal geometries, particularly the angular misalignment (geometry b) introduces dynamic forcing function with frequency same as the shaft rotation rate on the flexible ring which would consequently exhibit oscillations in axial and angular modes. One particular interest to the seal designers is to whether the flexible ring would be able to dynamically track the rotor without metal to metal contact, for a given amount of rotor misalignment (commonly

called 'runout'). In the 'dynamic tracking' analysis, the fluid film is modeled as nonlinear springs and dampers. The damping comes from the 'squeeze film' effects. The elastomeric O-ring also provides considerable amount of stiffness and damping both of which are frequency dependent. If O-ring starts slipping, Coulomb damping also comes into play. It has been found that higher the film stiffness is, the better the dynamic tracking ability of the seal ring becomes.

The engineering of seals involves fluid mechanics, heat transfer, elasticity, thermodynamics - equilibrium and nonequilibrium, statistical mechanics, dynamics, chemistry and metallurgy, to name a few of the most frequent areas of concern. Usually each effect can be analyzed by itself, but then the integrated effects must be evaluated for a complete analysis of a sealing system. As indicated previously, seals are characterized by surfaces in relative motion separated by a very narrow gap. In order to ensure proper operation, very small differences in the dimensions of the seal part must be maintained while in operation. Deformations in geometry due to imposed thermal gradients, frictional heating, pressure and mechanical contact forces must be held to a minimum. In any case, net deformation must be no more than microvalues. Depending on the imposed conditions, seals operate basically in three different lubrication flow regimes shown in Figure 1-5[2]. The 'non-contacting' seals usually operate with 'full film lubrication' whereas the 'contacting' seals can operate either in the 'boundary (also called 'mixed friction') lubrication' or 'dry sliding lubrication' regime depending on the excess magnitude of the closing force over the available opening force.

If the sealed fluid is a gas (usually operating in a noncontacting mode), sometimes the 'mean free path' of the molecules may be of the same order or more than the nominal operating seal clearance (Knudsen No. > 1) in which case continuum fluid mechanics with

no-slip boundary conditions is no longer valid and 'slip flow theory' and 'statistical mechanics' are needed to describe the fluid flow.

The selection of materials for seal rings is also a very important aspect of seal design. It requires extensive tribological testing to come up with a suitable material combinations for a certain specific application. In general, the seal ring materials should have good mechanical and thermal shock resistance, wear characteristics, corrosion resistance, self lubrication property, high modulus of elasticity, to name just the important ones. Carbon-graphite usually meets most of the requirements. It is quite frequently chosen in combination with some other compatible hard material like tungsten or silicon carbide. There are other combinations of seal materials used also, e.g., carbon-graphite vs. stainless steel, tungsten carbide vs. tungsten carbide, etc., depending on the operating conditions.

With all the complexities and highly coupled effects that govern a seal behavior, it is not a secret that reliable and accurate design analysis for face seals does not exist. Any new seal design must be tested in the laboratory because a prediction of eventual performance is not possible on purely theoretical basis. Again there is a wide variation in performance of seals of "identical design;" a particular seal may fail after a few hours whereas another seal belonging to the same class can last for several years or so. It is because of this reason that seals are often termed the 'most unpredictable machine element' used in industry. However good a design and analysis tool is quite useful in evaluating one design against others. This procedure eliminates the need for building expensive prototypes and running time intensive laboratory tests for those designs which seem not so viable at the analysis phase [4]. Also modeling and analysis give more insight into the complex mechanism of seal behavior. Hence there has been quite a bit of analytical and experimental work done in the face seal area over the last 25 years and efforts are constantly being made by the engineers and scientists to come up with better theoretical models for seal operation. Since

it is extremely difficult to perform a comprehensive seal analysis including all different coupled effects, most analytical work has been focused on one or two aspects. As of yet some of the individual effects (e.g., two phase flow modeling, high Knudsen number flow, mixed friction regime, wear model, nonequilibrium effects, to name a few) are not fully understood.

1.1 Liquid Seals

A number of investigators have analyzed face seals operating with incompressible liquid for different flow geometries. Etsion has extensively studied the angular misalignment effects on seal performance and stability. A misaligned face seal is shown schematically in Figure 1-6 [11]. He obtained a complete system of forces and moments acting on the flexible ring for different values of angular misalignment. These can then be used in a seal dynamic tracking analysis. Etsion [5] observed that any angular misalignment produces a radial force on the flexible ring which in turn causes a radial eccentricity. When this eccentricity is large enough, the pumping of fluid may take place which will affect the leakage. The seal coning, however, tends to reduce the magnitude of the radial force [6]. When the pumping takes place in a direction opposite to the hydrostatic pressure drop, it is known as 'inward pumping.' This phenomenon was studied both analytically and experimentally by Findlay [7, 8]. Analysis also showed that a flat outside pressurized seal with angular misalignment has negative axial and angular stiffness [9]. Also the hydrodynamic forces creates a transverse moment which leads the tilting moment by 90 degrees [10] that can cause seal wobble. However, with coning the stiffnesses might change sign depending on the relation between the angle of tilt and angle of coning [11, 12]. For noncavitating flow, the effect of coning reduces the hydrodynamic transverse moment which would improve seal stability. The 'narrow seal approximation' is usually made in seal analysis for simplification. With this approximation, the

circumferential pressure gradient and seal curvature can be neglected. Etsion [13] compared the accurate results from numerical solutions with the approximate results and found that over a radius ratio, r_i/r_o , greater than 0.8, an accuracy to within 1% can be obtained and hence in most cases this approximation is justified.

For low pressure and/or high speed seals, lubricant cavitation is possible due to hydrodynamic effects. This has been experimentally observed. An interesting work on this subject has been published by Findlay [14]. The lubricant cavitation helps generating extra opening force because it prevents the generation of hydrodynamic pressure below the local vapor pressure of the liquid while not restricting the upper bound of the pressure. If cavitation did not occur, the components of hydrodynamic force would usually balance out and no net increase over the hydrostatic force would exist, which is not the case for low pressure seals.

Sneck was one of the early investigators who made a very important contribution in the face seal analysis under incompressible flow. He published a series of papers [15] through [20] in '68 - '69 in which he addressed different aspects affecting seal performances, e.g., angular misalignment, radial eccentricity, tangential waviness, flow turbulence, centrifugal inertia and thermal effects. The centrifugal inertia term is included in the misalignment analysis in [15]. The centrifugal effects are shown to play a significant role in seal performance at higher speeds. For an outside pressurized seal, the regions of flow field may exist with a radially inward flow along the stationary surface and outward along the rotating one and under certain circumstances, there can be net zero leakage. The existence of such a region is a direct consequence of centrifugal inertial effects. This reverse flow phenomenon has been studied in detail in another paper [16]. The combined effects of misalignment and radial eccentricity is presented in [19]. The resulting leakage component can be outward (opposite to the direction of hydrostatic pressure drop) or

inward (in the same direction as the hydrostatic pressure drop) depending on the phase angle between the misalignment and radial eccentricity. Sneek also studied eccentricity combined with surface waviness [20]. Again the direction of leakage component is shown to be dependent on the phase angle. The once per revolution waviness is found to be the main contributor in the pumping effect. Turbulent flow is analyzed in [17]. The turbulent nature of the flow is described by an isotropic apparent viscosity model and a power law velocity profile. The misalignment and surface waviness are found to be somewhat less influential with turbulent flow than with laminar flow.

The analysis of face seals is often based on the isothermal flow assumption within the seal clearance. The validity of this assumption is usually argued on the basis that seal faces are often good thermal conductors and hence will not permit large radial temperature variations. But even when the seal operates approximately isothermally, the temperature within the seal clearance need not necessarily be same as the cavity fluid temperature. An accurate prediction of seal performance requires an accurate evaluation of the fluid viscosity within the clearance space. A general thermal analysis procedure is presented in [18] to estimate the fluid operating temperature level inside the seal. No attempt has been made here to model the heat conduction through the seal rings. The upper and lower bound on the operating temperature are obtained by assuming adiabatic wall condition and zero thermal convection by the fluid, respectively. In a recent review paper by Khonsari [21], an extensive survey of literatures pertaining to thermal effects in slider and thrust bearings is presented with summary of important contributors of leading researchers and designers. Since thrust bearings and seals have some similarity, this paper is referred here. One very common assumption made by the seal analysts is to neglect the fluid temperature variations across the film. But viscosity variation across the lubricant film has been sometimes found to be responsible for generation of an appreciable load. In [21] many papers are cited which indicate the importance of transverse viscosity variation. King and Lauer [22]

presented an experimental method by infrared spectroscopy to verify the existence of the temperature gradients through the film.

Pinkus and Lund [23] also considered the effects of centrifugal forces in high speed seals. They mentioned that at the upper limits of laminar conditions, centrifugal forces reduce the load capacity considerably and alter the pattern of the lubricant flow. Koga & Fujita [24] included both the radial and centrifugal inertia terms in their analysis of high pressure water pump seals. They obtained better correlation of the analytical predictions and experimental results when inertia effects are considered than their previous analysis neglecting these effects.

As mentioned before, the total closing force is supported by hydrostatic and hydrodynamic fluid pressures and often by partial contact of seal faces (in contacting mode of operation only). For moderate to high pressure applications, the hydrostatic force component is predominant over the hydrodynamic component [25]. Since the film thickness is usually very small (of the order of a few microns), any local surface deformations due to the interfacial pressure and the angular twist of the seal rings under pressure strongly influence the hydrostatic load support and hence the seal performance [26]. For carbon rings with a relatively low modulus of elasticity, the distortions can easily be of the same order of magnitude as the nominal clearance of the seal. Thermal distortions can also occur due to both axial and radial temperature gradients in the seal rings caused by the frictional heat generated at the interface. Any radial taper in the direction of the flow changes the hydrostatic pressure distribution and the film stiffness. A diverging seals (in the leakage direction) exhibits a negative axial stiffness which may lead to seal collapse and high wear.

With the availability of digital computers and necessary softwares, the finite element (FE) analysis is commonly used for accurate predictions of pressure deformation and thermal distortion. A very important series of papers [27, 28, 29, to mention a few of them] have been published over the years by Metcalfe and his research staff at the Atomic Energy of Canada Ltd. (AECL) describing these analytical techniques. Analysis of seal-ring deflections due to applied pressure loadings, to thermal effects and to Coulomb friction between components is described in [28]. The deflection sensitivity of seal components is expressed as 'influence coefficients,' evaluated with finite element analysis. He noted that Coulomb friction gives rise to undesirable performance hysteresis when operating conditions are changed. The correlation of experimental results and theoretical predictions is presented in [29]. Salant [30] presented an analytical model of a generalized mechanical seal incorporating the fluid dynamics of the film and the mechanical and thermal distortions of various seal components. He utilized the concept of 'influence coefficients' used in [28]. He found that the hydrodynamic forces due to waviness, roughness, misalignment and eccentricity produce insignificant opening force effects in comparison with the available closing force for high pressure seals. The hydrostatic pressure is responsible in carrying most of the applied load. Hence the face deformation, particularly 'coning' is the most likely controlling mechanism for load support for these kinds of seals. Based on this idea, Salant presented a novel design of an electronically controlled seal in [31]. A microcomputer based real time control system and electro-mechanical actuator dynamically adjust the seal coning and hence the film thickness, based on information received from the stator which monitors conditions of the film. This arrangement can greatly reduce face contact while limiting leakage by continuously optimizing film thickness. This would lead to a reduction in seal damage and wear and increase in seal life.

Li [32] presented a finite difference heat conduction model for calculating the temperature distribution in the seal rings and resulting deformations. He considered one

dimensional toroidal deformation model in which the seal rings will preserve the geometry of the radial cross section after deformations. Doust and Parmar [33, 34] numerically analyzed axisymmetric distortions due to the pressure and thermal effects using 'boundary integral element' (BIE) method and correlated the results with the experimental measurements. They remarked that the BIE method is substantially more economical in terms of both computing time and storage than FE for the same level of accuracy. The main object of their test was to measure the fluid film geometry using capacitance type proximity probe, as a function of pressure. The sealant pressure and thermal effects essentially caused toroidal rotation of the faces for those seals used by them. Their rotation rate was found to be fairly insensitive to the interface pressure profile. They also observed hysteresis effect due to secondary seal friction. In a recent paper [35] by them, the effects of thermoelastic transients have been presented. The transient thermal distortion can be an order of magnitude greater than that at steady state. Transient response is worse for a shorter section than a longer one, although the time to reach steady state can be more than an hour for a long seal component. This is an interesting work since field surveys do suggest that transient operations can be more detrimental to the seal life than steady state running.

Not as much work has been done in the 'mixed-friction lubrication' area for the contacting seals as in the 'full-film lubrication' regime for the noncontacting mode of operation. The obstacle to further advancement in contacting seal technology is that relationship between controllable design parameters and performance parameters are not well understood. Lebeck has published a number of papers [36, 37, 38, 91] on 'mixed-friction' flow modeling and contacting seal analysis. He developed a model [36] which takes into account load sharing between mechanical and fluid hydrostatic pressure. The effect of wear is also modeled in order to predict how the radial profile alters and influences the hydrostatic pressure distribution with time. The experimental evaluation of the model is

reported in [37]. In a contacting seal operation, an unstable phenomenon is observed by a number of researchers, including Kennedy and Grim [39], in which case a very slight amount of initial waviness on seal faces grows during seal operation. When this unstable condition, called 'thermoelastic instability' occurs in an operating face seal, the consequences - nonuniform wear, accentuated waviness, and high localized stresses and temperatures - can be very detrimental to seal performances. Kiryu et al. [40, 41] reported the generation of a "ringing" sound in a contacting water pump seal. They attributed this phenomenon to self-excited vibration due to 'stick-slip' action, caused by transferring from fluid lubrication to dry sliding condition. Vibration mode in ringing sound generation is found to be mainly caused by the torsional and axial vibrations of the rotating shaft system.

The previous investigations, mentioned so far, are mainly based on steady state analyses. However, the angular misalignment is inevitably present on the rotating ring which introduces a dynamic forcing function on the flexibly mounted stator. Hence the ability of the stator ring to track the rotor in a controlled manner is of great importance for safe seal operation and as the demand for higher operating speeds in rotating machinery increases, the importance of seal dynamics becomes more and more evident. Several researchers, namely Etsion, Green, Metcalfe and others, have addressed this issue analytically and experimentally in [42] through [55]. A review of face seal dynamics covering the literature until 1981 is presented in [50].

The flexibly mounted stator has basically three major degrees of freedom - axial and angular about any two orthogonal diameters. The twisting motion about axial direction is prevented by antirotation locks. If the radial stiffness of the O-ring secondary seal is low, which is usually not the case, then the stator can also move in the two perpendicular radial directions. The rotor transmits its angular motion to the stator via the thin fluid film

separating the two seal rings. For a given forcing function, the response of the stator depends on its own inertia, the stiffness and damping of the fluid film and the elastomeric O-ring. The fluid film damping comes from the squeeze effects. In some cases the squeeze effects are an order of magnitude higher than the combined hydrodynamic and hydrostatic effects and hence play an important role in dynamic behavior of face seals. The stiffness and damping coefficients of the fluid film, both direct and cross-coupled, in the three major d.o.f. are calculated in [44, 51] based on small perturbation theory. It has been found that the narrower the seal, the less is the damping coefficients and at very small tilt, translation and rotational direct damping coefficients are an order of magnitude higher than the cross-coupled ones. The damping and stiffness characteristics of elastomeric O-ring are dependent on the amplitude and frequency of excitation and amount of squeeze. The experimental determination of the O-ring dynamic properties are presented in [54, 56, 57]. With a large rotor misalignment, the stator response is usually large and sometimes sliding and takes place at the O-ring interfaces and then the Coulomb friction becomes important.

Dynamic analysis [45, 46, 48, 52] based on linearized small perturbation theory revealed three modes of operation: a stable mode in which a misaligned rotor is synchronously tracked by the flexibly mounted stator; a transition mode in which half-frequency wobble of the stator is superimposed on the previous synchronous tracking mode; and an unstable mode characterized by uncontrolled vibration of the stator, eventually causing failure. In the unstable mode, a seal will fail even with zero rotor runout. For low and moderate speeds, the stable mode seems to predominate. The stator tilt, however, differs from that of the rotor both in magnitude and direction. The difference and phase shift between two tilts result in relative angular misalignment between the rotor and stator. If this relative misalignment becomes too large, seal failure due to excessive leakage or even rubbing contact can occur even though the seal is dynamically stable. In [55], the complete nonlinear equations of motion of the stator are solved numerically. The

assembly tolerances in the form of initial stator misalignment and the dynamic properties of the elastomeric O-ring are accounted for in the analysis. Both stability threshold and steady-state response of the stator are investigated. In general, it was found that the critical shaft speed corresponding to stability threshold is quite high. Hence, the dynamic stability should not be a problem in the majority of noncontacting seals. A more practical problem is the steady-state dynamic response of the stator resulting from rotor runout and assembly tolerances. The results of the numerical analysis were compared with those of the previous small perturbation analysis that provides much simpler closed form analytical solution. Very good correlation was found between the two analyses for most cases of practical applications.

Etsion and Burton [43] observed self-excited oscillations of seal ring in the form of precession and nutation. The wobble frequency was measured to be about 43% of the rotational frequency. Metcalfe [49] analyzed and tested a well-aligned face seal. He found that if the balance ratio is below a certain critical value the seal becomes hydrostatically unstable. If the elastomer stiffness in the tilting mode is insufficient to overcome this hydrostatic instability, the stator will exhibit wobble motion. The precession rate is theoretically found to be half the shaft speed if elastomer damping is insignificant (pure "whirl") and progressively slower as damping increases. Etsion presented an experimental observation of the dynamic behavior of face seals in [53]. The forced response of the stator due to the rotor runout was monitored by means of three proximity probes. It was found that both the stator tilt and its phase shift with respect to rotor tilt are time dependent and vary synchronously with the rotor rotation. The time variation is attributed to the presence of two components of stator tilt. One component is fixed in magnitude but tracks the rotor tilt. The other component is fixed both in magnitude and direction and is due to nonaxisymmetric effects in the flexible support of the stator. As a result, the relative misalignment between the stator and rotor was found to be time dependent. The

dynamically unstable seal behavior was also observed. At low supply pressure which means low film stiffness, result showed a sinusoidal perturbation at double the shaft frequency superimposed on the initial wobble due to angular misalignment. In the previous experiments, perturbation was always observed at half rather than double the shaft rotation rate. As the supply pressure was increased, this double frequency stable to unstable transition became a half-frequency transition instead. This higher frequency instability was not fully understood.

1.2 Gas Seals

The efforts on gas seal development started a little later than the liquid seals, and the work in this area are not so voluminous. In earlier times, the machinery, having gases as working fluids, like gas compressors, used, and some of them still use, liquid seals with an oil-buffered arrangement. The reason for this is that proper technology was not available to insure a non-contacting mode of operation, which is absolutely essential for gas seals because of the poor lubrication properties and high speed of operation. The oil is kept at a pressure a little higher than the sealed gas to ensure that only oil leakage could take place into the gas and seal would never run dry. In addition oil also leaks to atmosphere through another seal. Apart from the cost factor (about two orders of magnitude higher than the corresponding single phase seals), this design has some major disadvantages in terms of auxiliary equipment and space requirements. Also, since product contamination with just a small amount of buffer fluid may create enough problems, contacting liquid seals are typically used, which have inherently low and unpredictable life. Hence the need for a noncontacting seal development did arise for sealing gaseous fluids.

Although the basic concepts are the same, the main difference between the liquid and gas seal analyses is that the governing equations describing the gas flow are nonlinear

because of compressibility effects and inclusion of flow inertia, which are sometimes too important to ignore. The flow is often turbulent and choking may occur at the outlet. Also under conditions of high velocity, the entrance loss effects cannot be neglected. The gas seals should also operate with a high film stiffness in order to have good dynamic tracking ability to prevent contact. As mentioned before, the pressure within the fluid film is generated hydrodynamically by the relative motion between uneven sealing surfaces and hydrostatically by frictional pressure drop through the seal. The hydrodynamic action ceases when the motion stops. There is no hydrodynamic pressure generation with parallel faces. To a limited extent all seals possess some hydrodynamic characteristics as a consequence of geometric imperfections and unplanned unevenness such as inherent or pressure induced circumferential waviness or micro-irregularities. These effects are usually quite small. The hydrostatic effects alone impart zero stiffness to a seal unless there is a radial coning in the flow direction. Because of these facts, some conscious efforts have been made to enhance the hydrodynamic action rather than rely on chance variation, by having planned uneven hydrodynamic patterns on the seal surfaces. Some of the commonly used patterns are spiral groove, Rayleigh-step pads, radial grooves, as shown in Figure 1-7 [58]. These are called 'hybrid' seals.

The hydrodynamic pattern is followed by a seal dam which offers restrictions to the fluid flow and most of the pressure drop takes place there. Because of hydrodynamic action, there are some areas of higher pressure and other areas with lower pressure. Figure 1-8 [58] shows the elevated pressure areas on the two seals. Figure 1-9 shows the components of 'F-h' curves for the hydrodynamic and the hydrostatic sections of a 'hybrid' seal with Rayleigh-step pads, analytically obtained by Shapiro [59]. The two curves must be combined to get the net film characteristics for the seal under consideration. No angular misalignment effect is considered in this analysis. It is evident from this figure that the hydrodynamic action indeed imparts a very high film stiffness, particularly at small

clearances and prevents the seal faces from touching each other. The closing force is usually chosen so that the seal operates near the high stiffness region. Also it is seen that hydrostatic stiffness is almost zero and hence it does not contribute to the seal stability, although it may carry a major part of the closing force. Experiments performed by Ludwig [60] showed that seals with hydrodynamic pads outperformed the conventional seals used in small gas turbines.

Some of the important research work on gas seals is documented in [59] through [72]. Cheng [61] analyzed a few different designs and found that the spiral groove design gives higher stiffness than Rayleigh-step pad one. This same conclusion was also drawn by Sedy [58]. He also brought out an interesting point. As mentioned before, most of the gas expansion takes place over the dam. The cooling effect associated with the expansion is sometimes several times more than the heating effect due to viscous dissipation. The net effect is the cooling of the gas near the dam and consequently a considerable amount of heat conduction takes place from the seal rings to the gas in the vicinity of the dam. The temperature gradient, thus set up in seal rings, tends to distort the seal face in a way to produce a divergent flow passage which has an unstable effect and sometimes causes seal contact at the outer diameter. Sedy suggested a wider dam design to overcome this problem because a wider dam would cause a higher heat generation which in effect tends to neutralize the cooling effect due to gas expansion. Zuk [64] presented a quasi one-dimensional analysis for the flow of gas through seals. This model includes fluid inertia and entrance losses, in addition to viscous friction which is accounted for by a friction factor. Subsonic and choked flow conditions have been predicted and analyzed. This model is valid for both laminar and turbulent flows. Hsing and Carraro [74] used an efficient algorithm based on fourth order Runge-Kutta with adaptive step size to solve the same governing differential equation. Shapiro [59] performed both steady state and dynamic analyses of a gas seal for jet engines. The seal dynamic response was found as a

function of rotor misalignment and secondary seal friction. He theoretically obtained superharmonic response, about four times the shaft RPM, which has been confirmed experimentally. This phenomenon has been attributed to nonlinear characteristics of the O-ring. The flexible ring is found to lose its tracking ability if the rotor runout or the friction force is too large.

If the gas inside a seal is at sufficiently low pressure, the molecular mean free path can become comparable to the film thickness. The fluid subjected to this condition does not behave entirely as a continuum fluid but rather exhibits some characteristics of molecular chaos. One may also expect to encounter these effects in regions having very sharp gradients of fluid properties such that these properties change appreciably in the space of a few mean free paths, regardless of whether or not the absolute density of the gas flow is especially low. The dimensionless ratio, λ/h (Knudsen number), is a measure of the degree of rarefaction. When this ratio is large, the flow phenomena are mostly dictated by the molecular-surface interaction. This class of fluid flow is defined as "free-molecular flow." For flows in which the value of Knudsen number is small, typically $0.01 \leq \lambda/h \sim 0.1$, but not negligible as those in continuum mechanics, some departures from the usual continuum flow phenomena may be expected to occur. The layer of gas immediately adjacent to the solid surface no longer assumes the same kinematic condition as the solid boundaries but has a finite relative "slip velocity" and hence produces an apparent diminution in fluid viscosity. This is called the "slip-flow regime."

The few research works covering these non-continuum effects in lubrication are documented in [73] through [78]. Hsing and Malanoski [74] found that if the lubricant is one of the gases having a large molecular mean free path, such as Helium, Neon or Hydrogen, the slip-flow phenomena could contribute substantial reduction in the performance of a thrust bearings, which is quite similar to face seals. Gans [75] derived a

slip flow lubrication equation for an arbitrary Knudsen number from kinetic theory. Fukui and Kaneko [76] developed a more accurate generalized lubrication equation based on linearized Boltzmann's equation. The experimental results obtained by them [77] agreed well with their numerical results. Kubo et al. presented a finite element solution of the Boltzmann's equation in [78].

1.3 Two-phase Seals

When liquid is sealed at temperature higher than its saturation temperature at the outlet pressure, it flashes inside the seal due to the pressure drop and/or the viscous heat dissipation. Typical examples of applications where such two-phase flow may be encountered are light hydrocarbons in petroleum refineries, hot water in boiler feed pumps and reactor coolant pumps, and cryogenic fluids like liquid oxygen and hydrogen (LOX/LH₂) in rocket turbopumps. The two-phase seals generally exhibit more erratic behavior than their single phase counterparts. The seals also have more stringent requirements in their performances because of severity in applications. As, for example, light hydrocarbons are potentially flammable and explosive and hence certainly dangerous if allowed to leak. Since these hydrocarbons in gaseous phase are heavier than air, they usually form a thick dense cloud on the ground around the source. It constitutes a severe hazard [79]. In LOX/LH₂ turbopumps, any seal failure due to excessive leakage can be, needless to say, extremely dangerous. Actually the face seals in the space shuttle turbopumps failed repeatedly on the test pads until they had been replaced with annular seals. Although annular seals are safer in operation, they allow very high leakage. At a later date, the face seals have been adopted successfully in the LOX/LH₂ turbopumps for the Japanese H-1 rocket [80]. Two-phase seal operation is also encountered in boiler feed pumps. It has been estimated that the boiler feed pump outages alone cost power companies several hundred million dollars each year in lost power revenues. It is believed

that a high percentage of these problems is related to seal failures [97]. The reactor coolant pump (RCP) seals can also experience change of phase of the sealed fluid during station blackout conditions and exhibit excessive leakage. Failure of these precision components may result in a small loss of coolant accident (LOCA) in nuclear reactors [82].

Because of the severity of application, the two-phase operation mechanisms must be better understood in order to come up with a suitable design. The research works done in this area are reported in [79] through [102]. An interesting earlier paper on this subject was published by Orcutt [83]. He used a quartz runner to permit visual observation of the seal interface during operation. The experimental observations indicated the existence of a multiple phase film, characterized by two large scale regions. The first region adjacent to the seal cavity was occupied almost entirely by water. The second annular region extends from the atmospheric edge of the interface to a semi-stable boundary with the liquid-filled region. This region was occupied by a mixture of liquid and vapor. The boundary moved towards the edge adjacent to the seal cavity with the rise in liquid and seal surface temperatures. Unstable operation was encountered with visible leakage as the cavity fluid temperature was increased. More than a decade later, Harrison and Watkins [84] and Wallace [79] reported a similar unstable two-phase operation with light petroleum products at elevated temperature. Under the unstable operation, the fluid film periodically broke down and reformed with violent fluctuations in torque. Seals showed both audible (while in operation) and visible (when taken apart) signs of distress. Seal operation was, however, stable at lower temperature. Barnard and Weir [85] reported seals operating successfully with no visible leakage because of vaporization. The seal faces, they examined, all exhibited three concentric bands across their surfaces. Will [86] also observed the similar three banded appearance on successfully operating two-phase seals. No convincing causes are known.

In theoretical modeling of two-phase flow through seals, most of the work so far has been done by Hughes and his coworkers and are reported in [87] through [93]. Basically two different models have been presented in [87, 88, 89] for low and high leakage flows, respectively. The low leakage flow model is based on laminar flow and it considers heat conduction into the seal rings but neglects heat convection by the fluid and heat of vaporization. Boiling is assumed to be taking place at a discrete interface. The high leakage flow model is based on turbulent flow. This model disregards heat conduction through seal rings but takes into account convection, heat of vaporization, radial and centrifugal inertias. This model could predict continuous boiling over a finite region and also choking at the outlet under certain conditions. Beatty and Hughes [90] refined the turbulent flow model with better treatment of inlet losses. They obtained an anomalous 'all-liquid choking' situation in which the flow is choked but remains liquid all the way up to the seal exit. Beyond the exit, the liquid flashes immediately into vapor.

Lebeck presented a mixed-friction model with phase change in [91]. He modified the flow equation for roughness effects and considered the load support due to asperity contacts. Hughes and his coworkers assumed an idealized semi-infinite heat conduction model, whereas Lebeck used a more realistic seal geometry and boundary conditions and implemented a finite difference scheme to solve for seal ring face temperature distributions. Lebeck's model is valid for low leakage rates only.

Beeler and Hughes [98] performed a dynamic analysis in the axial mode. They used the quasistatic 'F-h' curve obtained by using the adiabatic model to represent the fluid film. Squeeze film effects were ignored. With this limited dynamic model, they predicted self-sustained oscillations under certain conditions whereas failure due to metal-to-metal contact under other situations. Zuber and Dougherty [94] modeled the process of condensation and evaporation and derived a generalized lubrication equation. The two-phase region is

treated as a dispersed homogeneous flow with thermodynamic nonequilibrium between the vapor and the liquid. Although research efforts in this aspect are somewhat limited because of the difficulty involved, experiments showed that the effects of condensation and evaporation can become of primary importance in determining static and dynamic characteristics of saturated vapor bearings and seals.

The 'F-h' curves for two-phase seal operation obtained by different investigators has a peculiar feature and is shown schematically in Figure 1-10. The positively sloped side of this curve implies a negative film stiffness whereas the negatively sloped side means positive film stiffness. For a given closing force, there can be two operating clearances with the smaller one giving rise to unstable operation and the larger one stable. Vaporization also seems to inhibit leakage.

The two models for two-phase seal operation, developed by Beeler and Beatty [104,112], work reasonably well at the two extremes - very low leakage rates with convection neglected and very high leakage rates with conduction neglected. Both models break down as soon as the effect neglected in the respective model begins to become important. In actuality, most two-phase seal operations take place in the intermediate leakage range when both conduction and convection are important. A preliminary model is developed here to bridge the gap between the two previous models. This model, known as the 'Film Coefficient Model,' is valid over the entire laminar flow regime unlike the earlier model developed by Beeler which only worked at the very low leakage rate end. The new model considers both conduction and convection and allows continuous boiling over an extended region whereas the earlier model which neglects convection always forces a discrete boiling interface and exhibits numerical instability as soon as leakage rate starts becoming a little higher. With the inclusion of turbulence and radial inertia effects, the applicability of the 'Film Coefficient model' can be extended to high leakage rate end with

the ability to predict choking. Hence this model has the potential for describing the seal behavior over the entire range of possible leakage rates - low to high.

Another simplified and semi-analytical model, known as 'Isothermal Model," has also been developed for low leakage rates. This is based on the model developed by Beeler. The assumptions of isothermal condition along the seal interface and ideal gas behavior of the vapor permit closed form solutions which may be used for preliminary design and analysis. However, to obtain more accurate and realistic description, the 'Film Coefficient Model' may be used.

Under certain two-phase operation, seals seem to exhibit self-sustained oscillations even when all the applied conditions remain quite steady. These have been observed as axisymmetric fluctuations in the film thickness accompanied with periodic interface temperature variations.

1.4 Two-Phase Seals - How They Work

We continue the general background on two-phase seals, laminar (low leakage) and turbulent (high leakage). Details of the equations and computational techniques will be presented in Chapter 2 and in more detail in the appendices, except for the simplified model which is discussed in detail in Chapter 3.

Again, many phenomena associated with all liquid on all gas seals have been discussed in considerable detail and do provide insight into their behavior. However, many effects, such as popping, chattering, and some failure modes are associated with two-phase effects in that the behavior changes in response to temperature, subcooling of the sealed liquid and generally whether boiling occurs.

Liquid and gas face seals have, generally, neutral axial stiffness but can be unstable to wobble. In general, coning (convergence in the flow direction) tends to give positive axial stiffness to liquid seals and many are designed this way.

However, two-phase seals can have a negative axial stiffness and be inherently unstable to axial disturbances over certain ranges of parameters. Coning may serve to mitigate the negative stiffness, but not always. In fact, a stably operating seal may become unstable by changing the operating conditions, particularly by increasing the temperature of the sealed liquid (i.e., decreasing the subcooling and approaching saturation conditions). These observations apply both to laminar and turbulent seals.

In order to understand the characteristics of a two-phase face seal let us consider the flow through the seal. Figure 1-11 shows the trajectory in a T-s plane for flow through a seal. The actual distance from f to g on the seal face can vary from a negligible distance to the entire seal face. For most low leakage seals the points will be close together and boiling takes place almost at a discrete radius. For high leakage turbulent seals the boiling may occur over the entire seal face. Further, the closer to isothermal operation, the shorter the region over which boiling occurs. Clearly if there is no temperature change then the boiling must occur at a discrete interface in order to satisfy both momentum and the Clapeyron relation.

Now consider the pressure drop through the seal, Figure 1-12. If the seal is all liquid, the pressure is nearly linear, and if all gas the pressure is nearly quadratic. However, if boiling occurs, then for a given film thickness (seal face separation), the leakage rate is reduced and the pressure is higher than for an all liquid or all gas seal. A plot of the total opening force produced by this pressure vs. the seal face separation then

produces the axial stiffness curve Figure 1-10, which is shown again in Figure 1-13 with the liquid and gas asymptotes. A positive slope here represents a negative axial stiffness (i.e., instability), and a negative slope represents a positive axial stiffness (stability). Figure 1.14 shows a set of actual curves generated from the simplified theory which will be discussed in Section 3.

These axial stiffness curves are the key to the distinctive two-phase operation. Operation on right hand side of the curve in Figure 1-14 is stable to an axial disturbance but the left side is unstable. Now, the seal may be balanced for any level by changing the balance ratio. An arbitrary line is shown in Figure 1-14 as the balance point. At each speed there are two equilibrium points. The one with the larger film thickness is stable, the one with the smaller film thickness unstable. Depending on the location of the balance line the seal may be unstable for an all liquid seal, all gas, or both. For instance, if the balance were established at 1000 N, the seal would open if it were all gas and collapse if all liquid. At the balance shown, about 1250 N, the seal would collapse if the seal were either all gas or all liquid and relies on two-phase operation for stability.

However, the situation is more complex. The behavior depends critically on the subcooling of the sealed liquid. As the sealed fluid nears saturation conditions the stiffness curve tends to become entirely positive in slope and the seal is totally unstable. Hence, a seal balanced properly at one level of operation may become unstable if the temperature is changed sufficiently. These considerations are critical in such situations as nuclear power plant "black-outs." Consider Figure 1-15. The saturation temperature is 453 K. At about 440 K the curve shows a monotonic positive slope (unstable) and the seal would tend to pop open. Interestingly, if the seal temperature were very close to saturation the opening load tends to correspond to all gas and the seal would collapse. During a transient, opening would occur first with possible catastrophic consequences.

As opening continues, what happens as the leakage flow increases and become turbulent? We can answer that with the turbulent flow model which is discussed in detail in Chapters 4 and 5. Figures 1-16 and 11-7 show turbulent curves. Generally, the turbulent curves show the same trend and we conclude that an instability is exasperated as the seal continues to open or collapse.

To summarize our findings,

1. Codes developed for steady operation description, stiffness calculations, and stability analysis for annular and face seals - laminar or turbulent.
2. Axial disturbances may create instabilities and possible self-sustained oscillations.
3. All behavior critically dependent on heat transfer effects and viscous dissipation.

Before we review the general equations we use in the various models, a word about some of the necessary considerations is in order. We must consider the equations of momentum and energy, the thermodynamic equation of state, the Clapeyron equation, viscous dissipation in the fluid, centrifugal inertia in the fluid, and the heat transfer into the seal faces. The consideration of heat transfer is crucial to the behavior of the seal. In Figure 1-18 we show a schematic drawing of how the heat can flow into or out of the fluid through the seal faces.

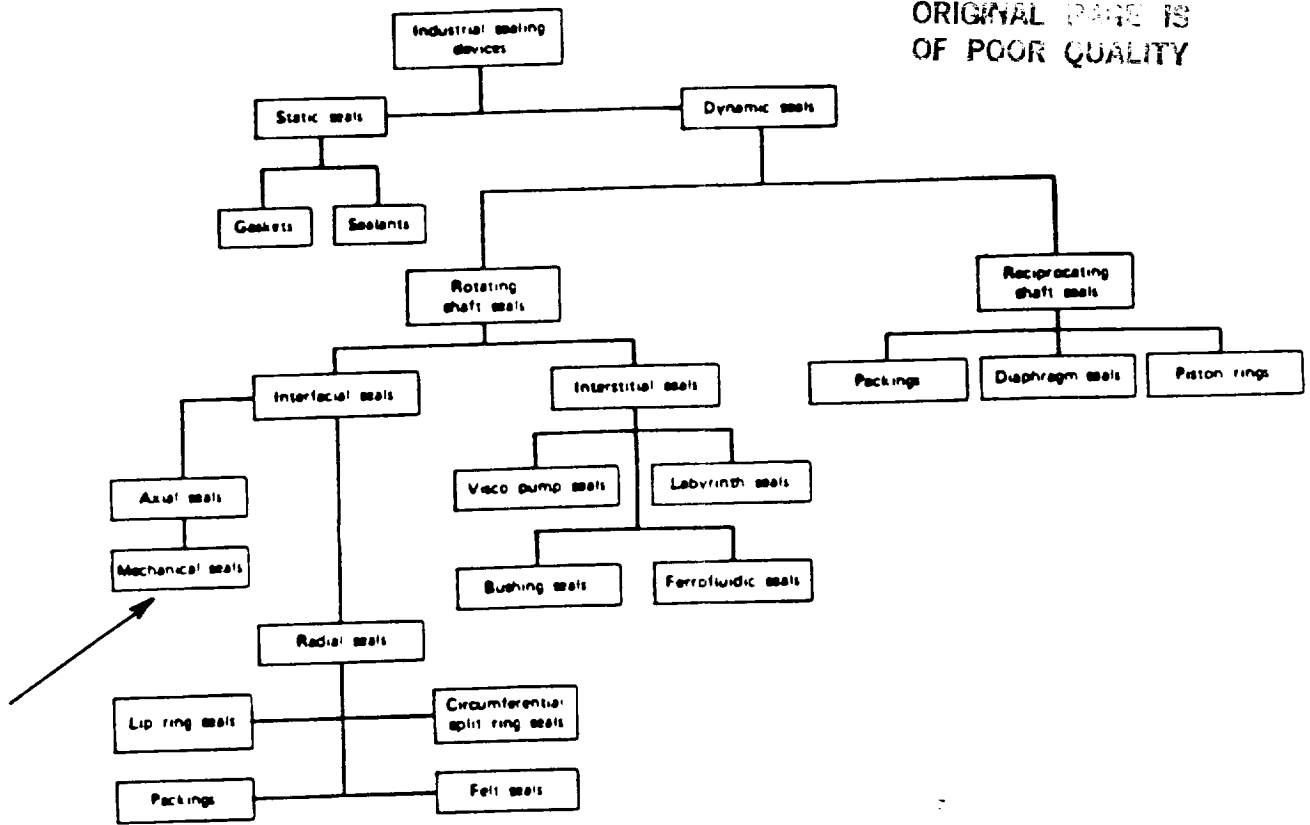


Figure 1-1: Classification Diagram - Industrial Sealing Devices

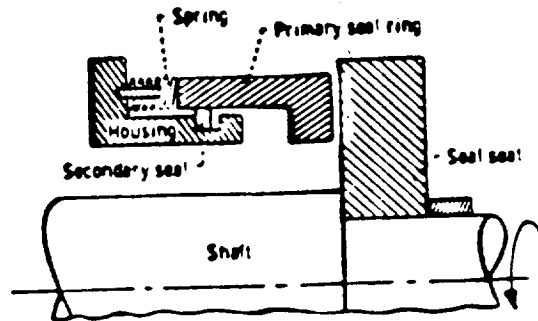


Figure 1-2: Schematic Diagram of a Face Seal

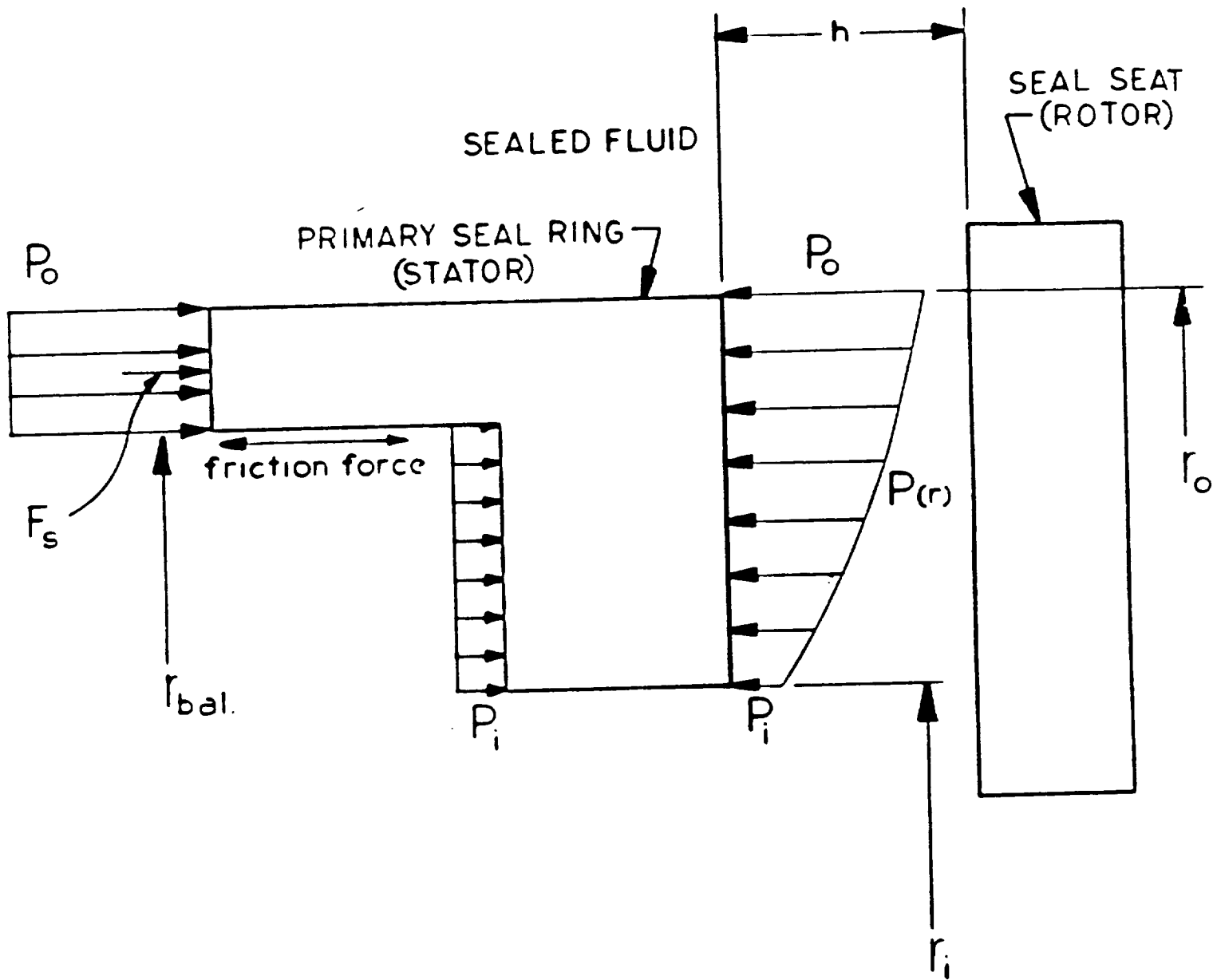


Figure 1-3: Force Diagram on a Stator

ORIGINAL PAGE IS
OF POOR QUALITY

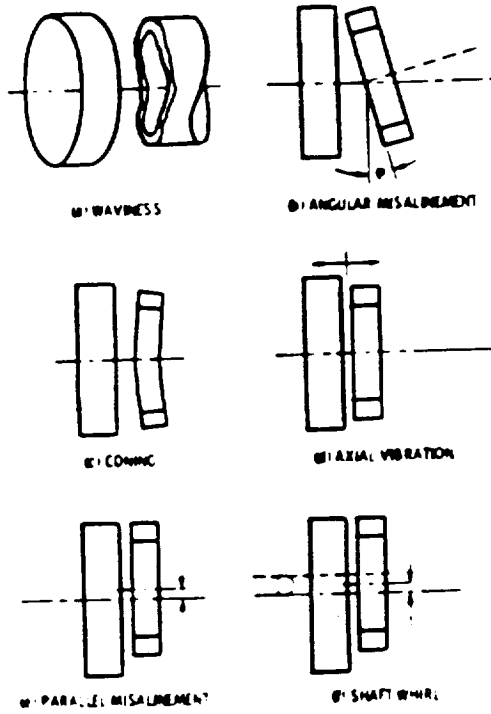


Figure 1-4: Possible Primary-Seal Geometries

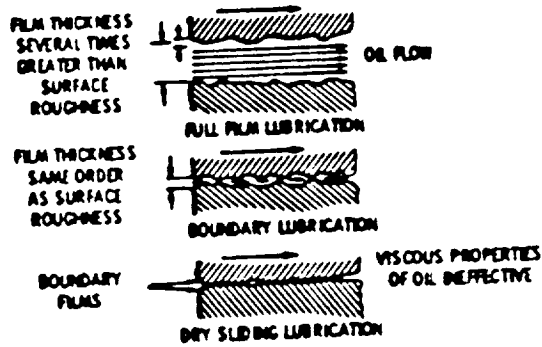


Figure 1-5: Seal Lubrication Models

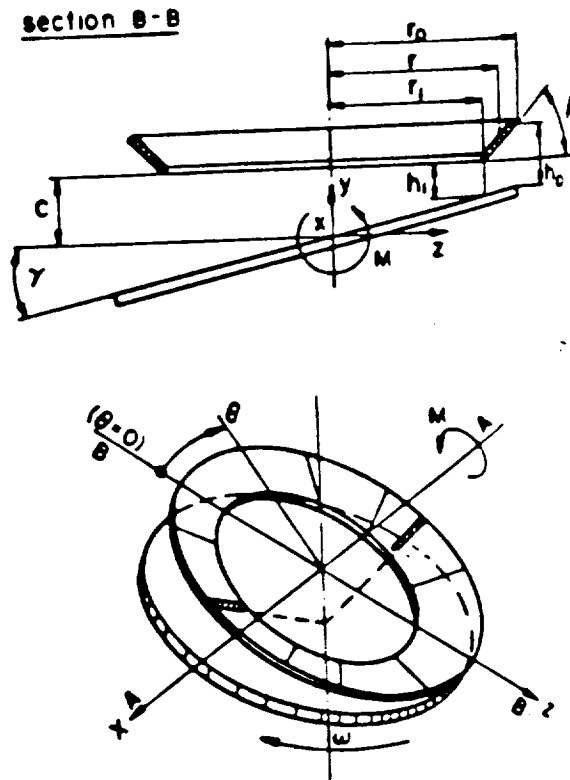
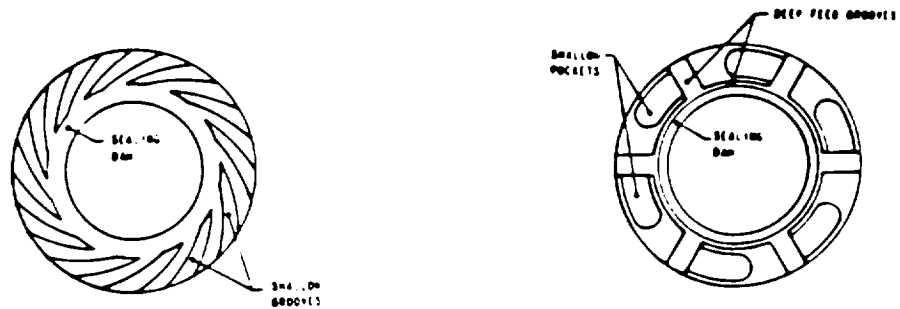


Figure 1-6: Face Seal with Angular Misalignment and Coning



SPIRAL GROOVE

**RAYLEIGH
STEP PAD**

Figure 1-7: Hydrodynamic Patterns on Face Seals



Figure 1-8: Hydrodynamic Pressure Generation

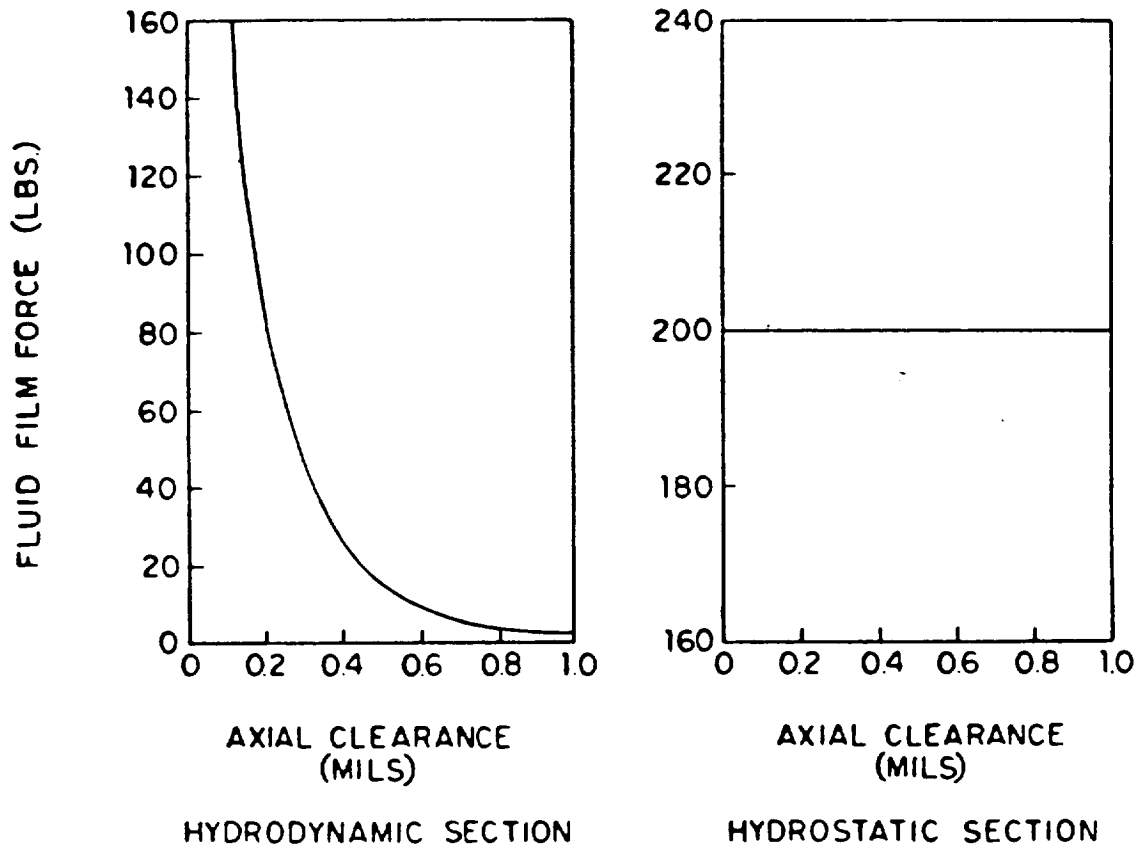


Figure 1-9: Hybrid Gas Seal F-h Curves - Hydrodynamic and Hydrostatic Components

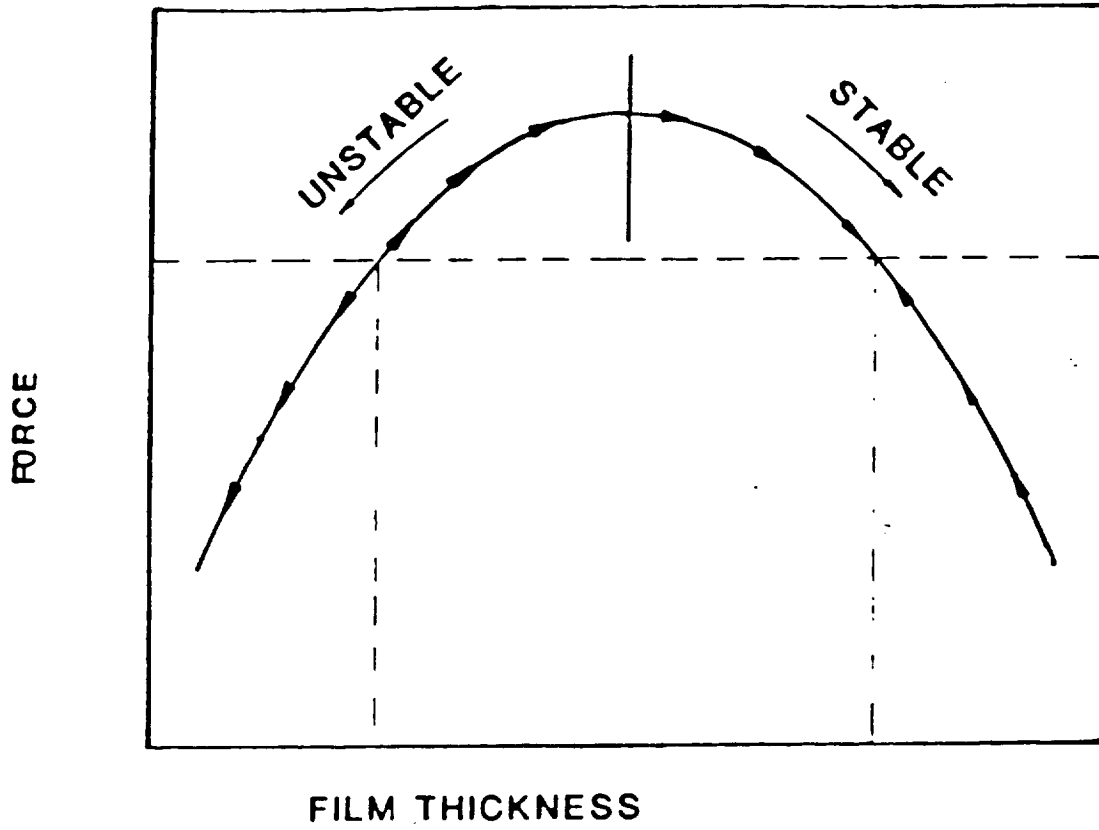


Figure 1-10: Seal F-h Curves for Two-phase Operation

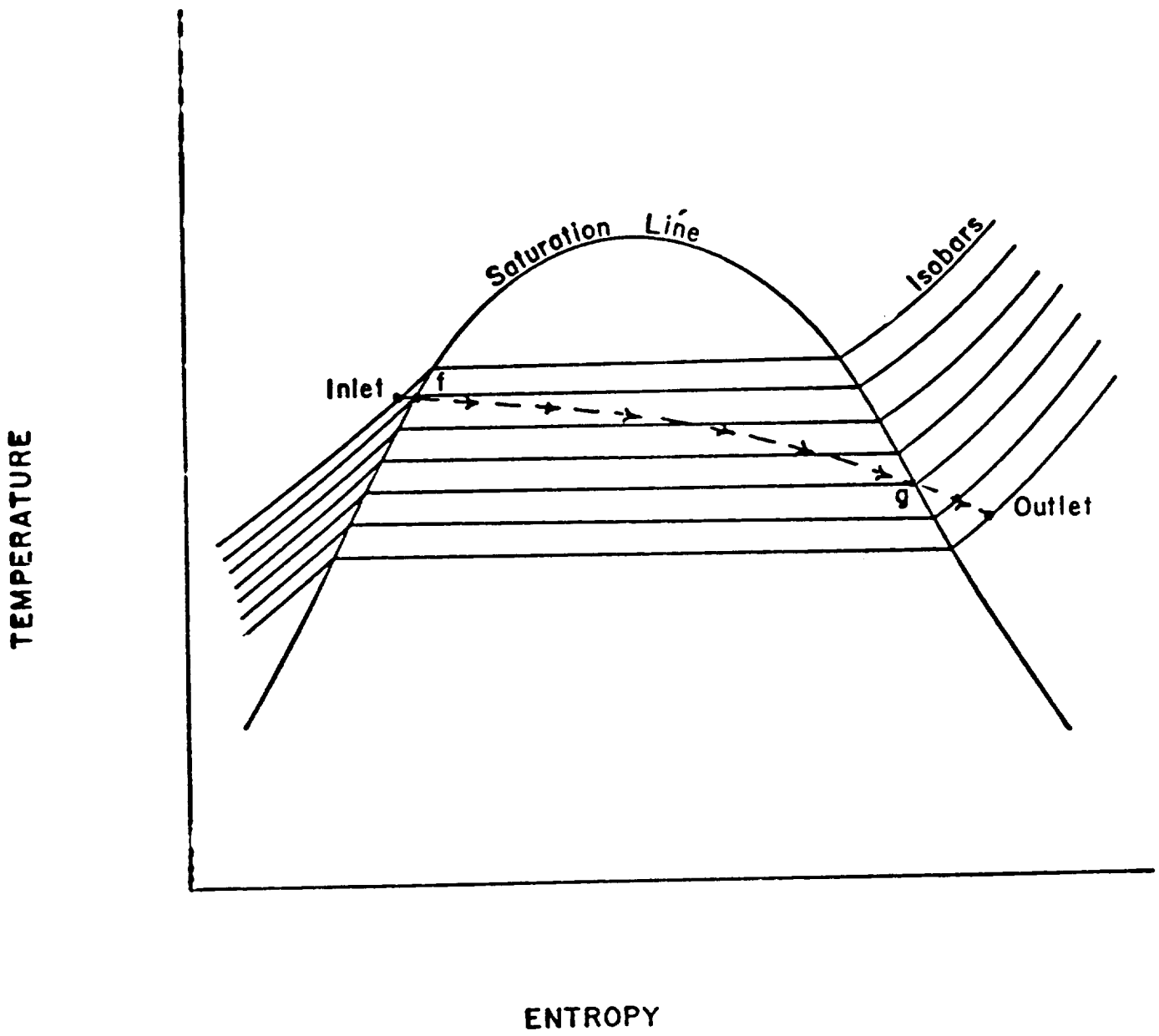


Figure 1-11: Trajectory of properties through a two-phase seal.

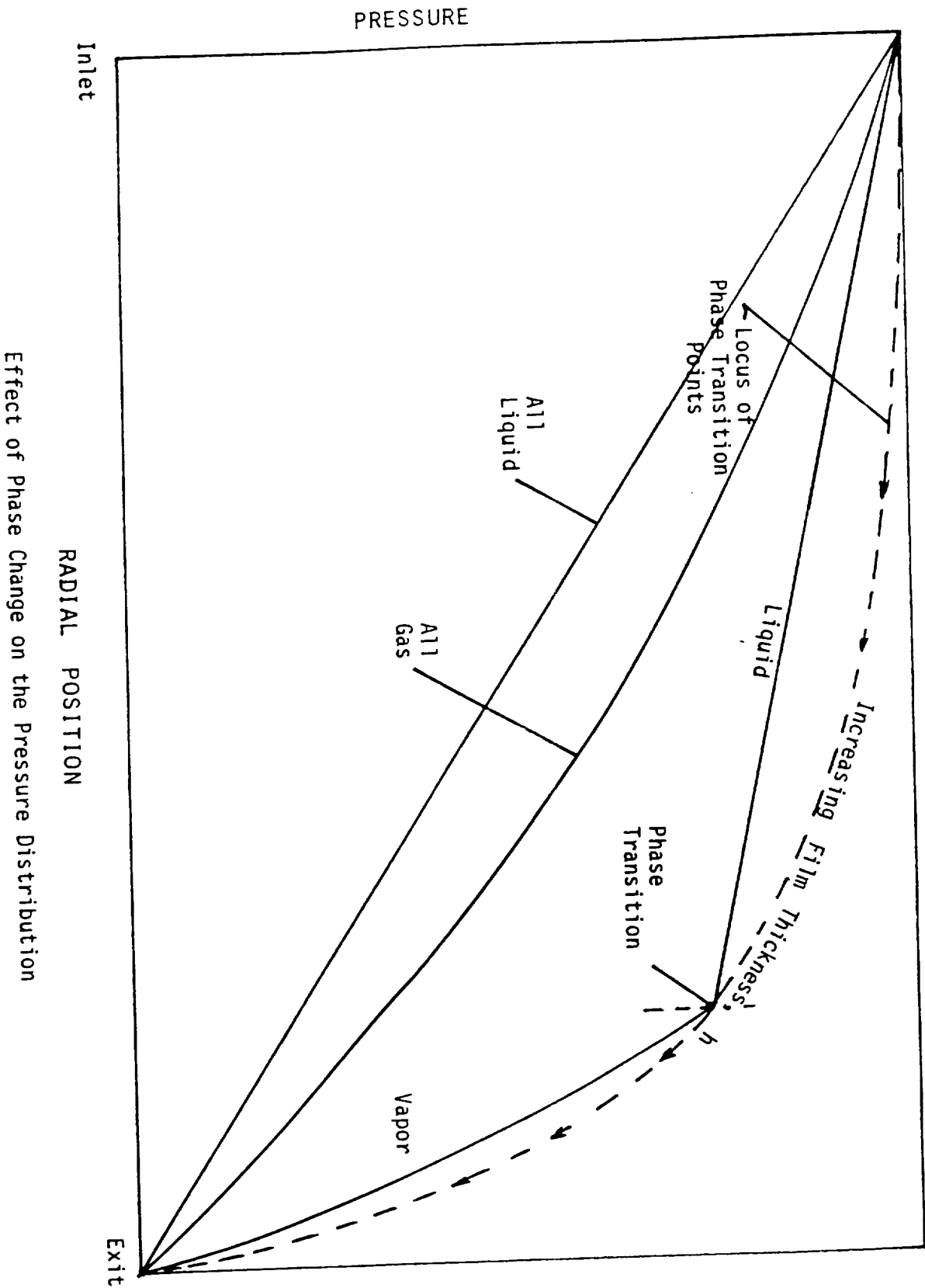


Figure 1-12: Effect of Phase Change on the Pressure Distribution

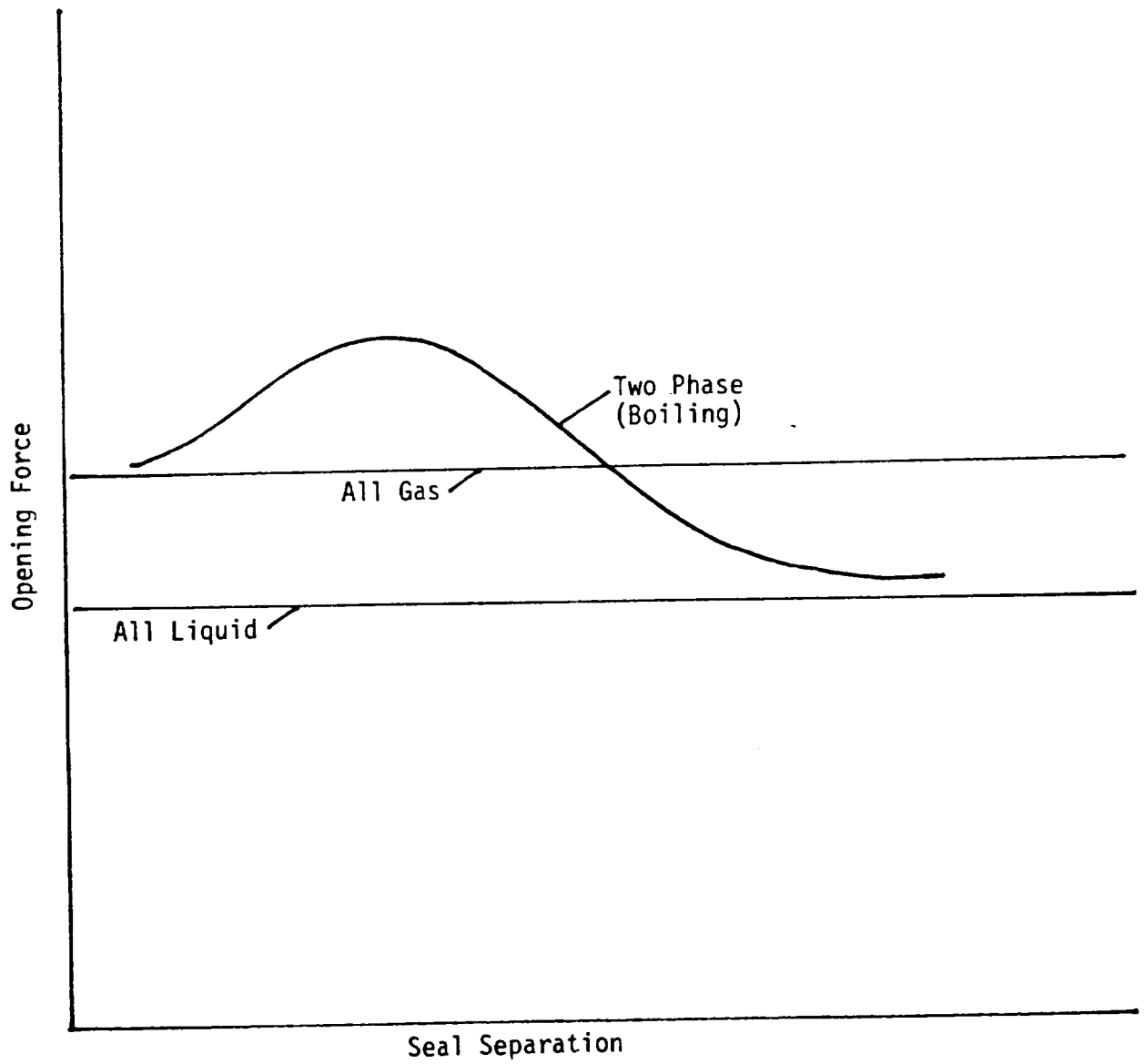
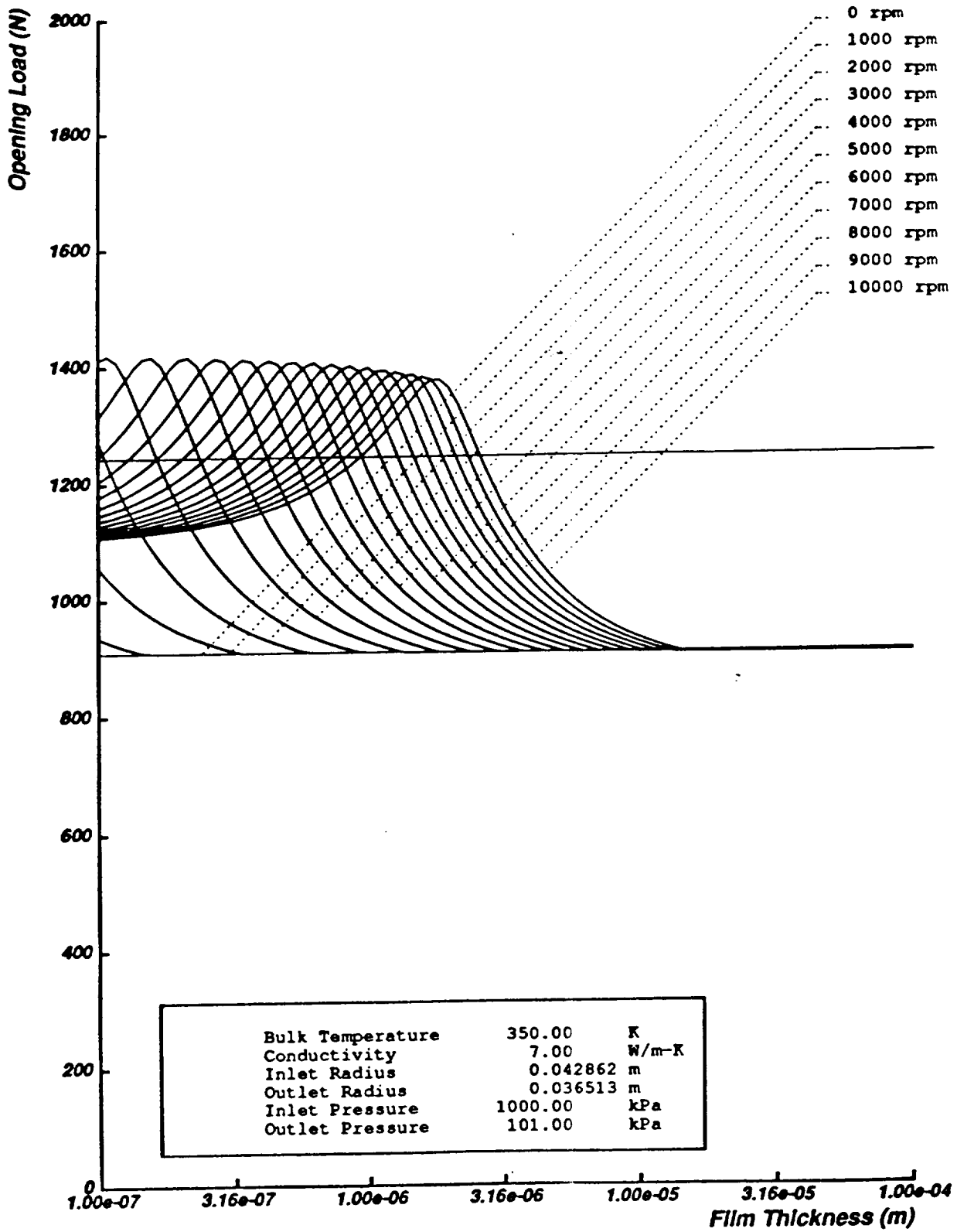
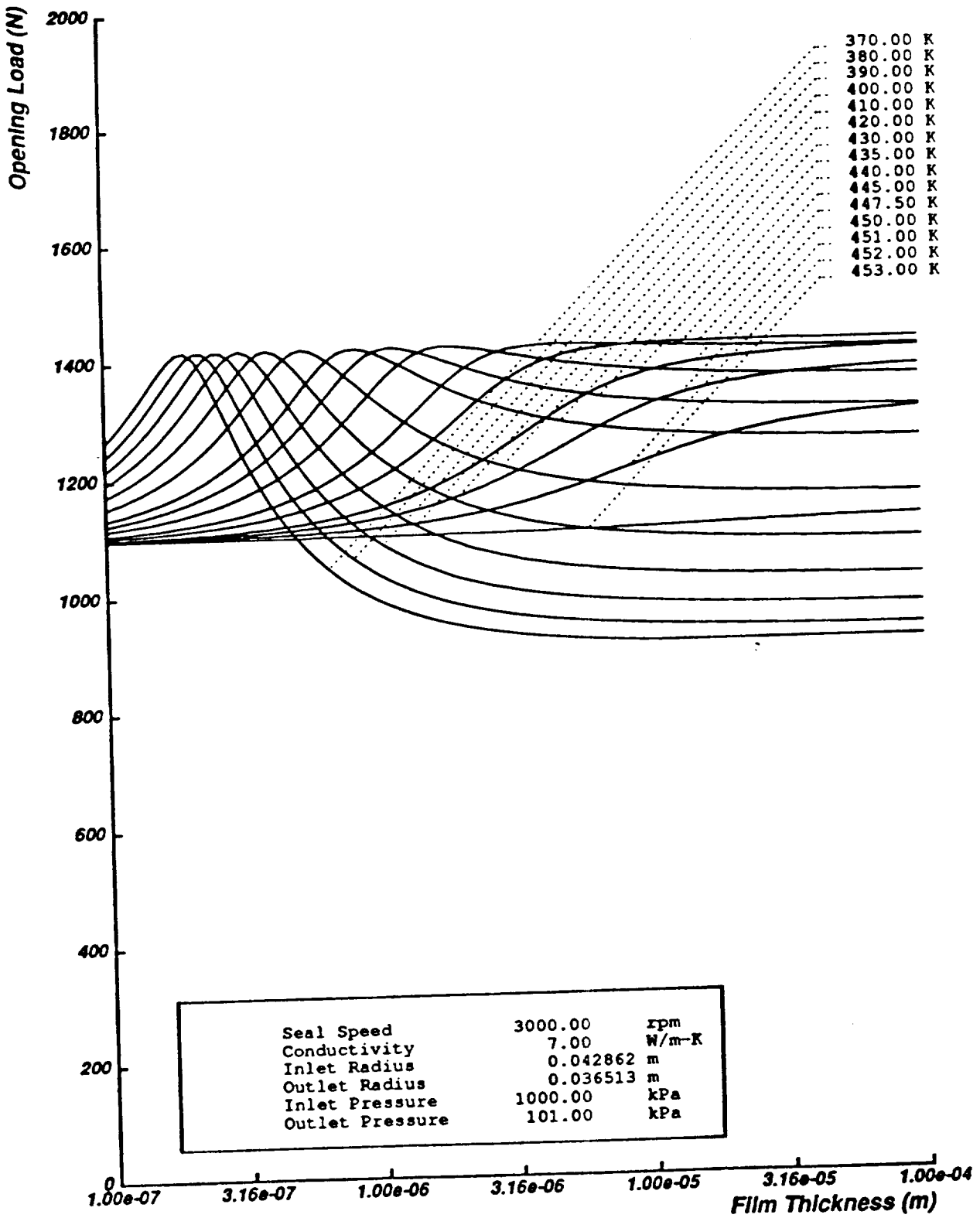


Figure 1-13: STIFFNESS CURVES



Plot of Opening Load Versus Film Thickness for Different Seal Speeds

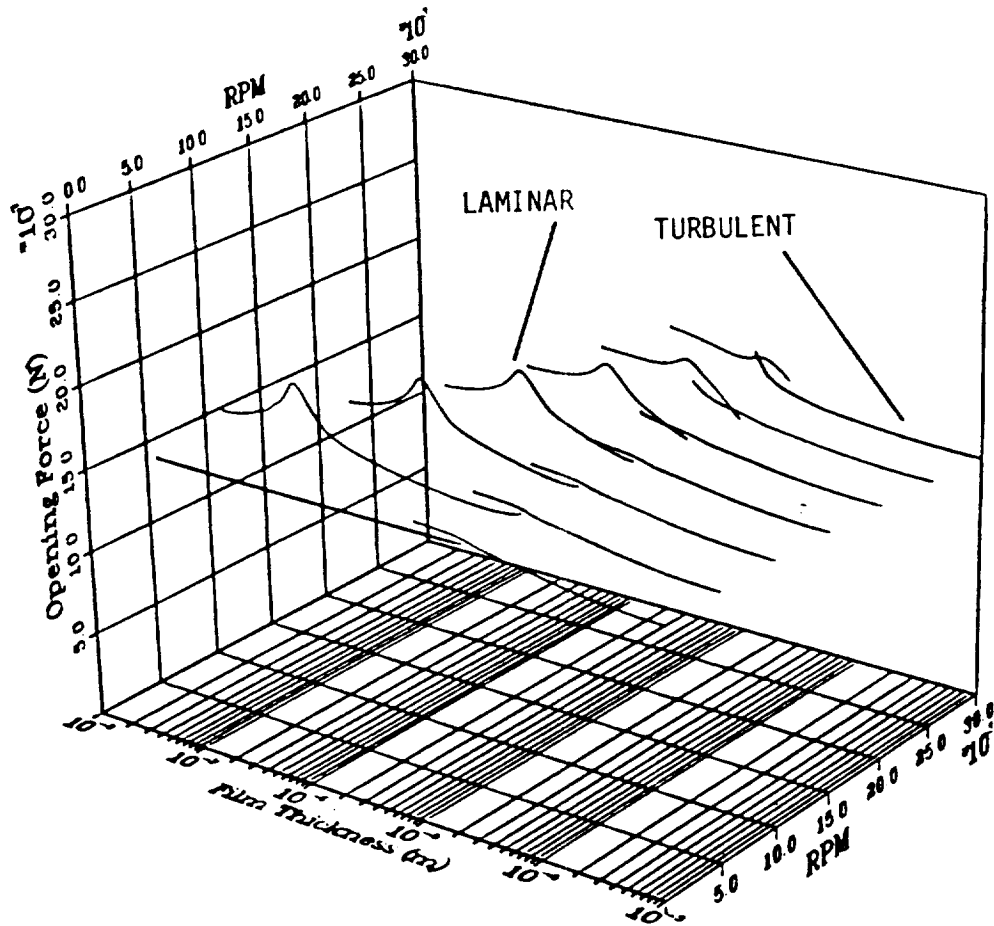
Figure 1-14



Plot of Opening Load Versus Film Thickness
for Different Bulk Fluid Temperatures

Figure 1-15

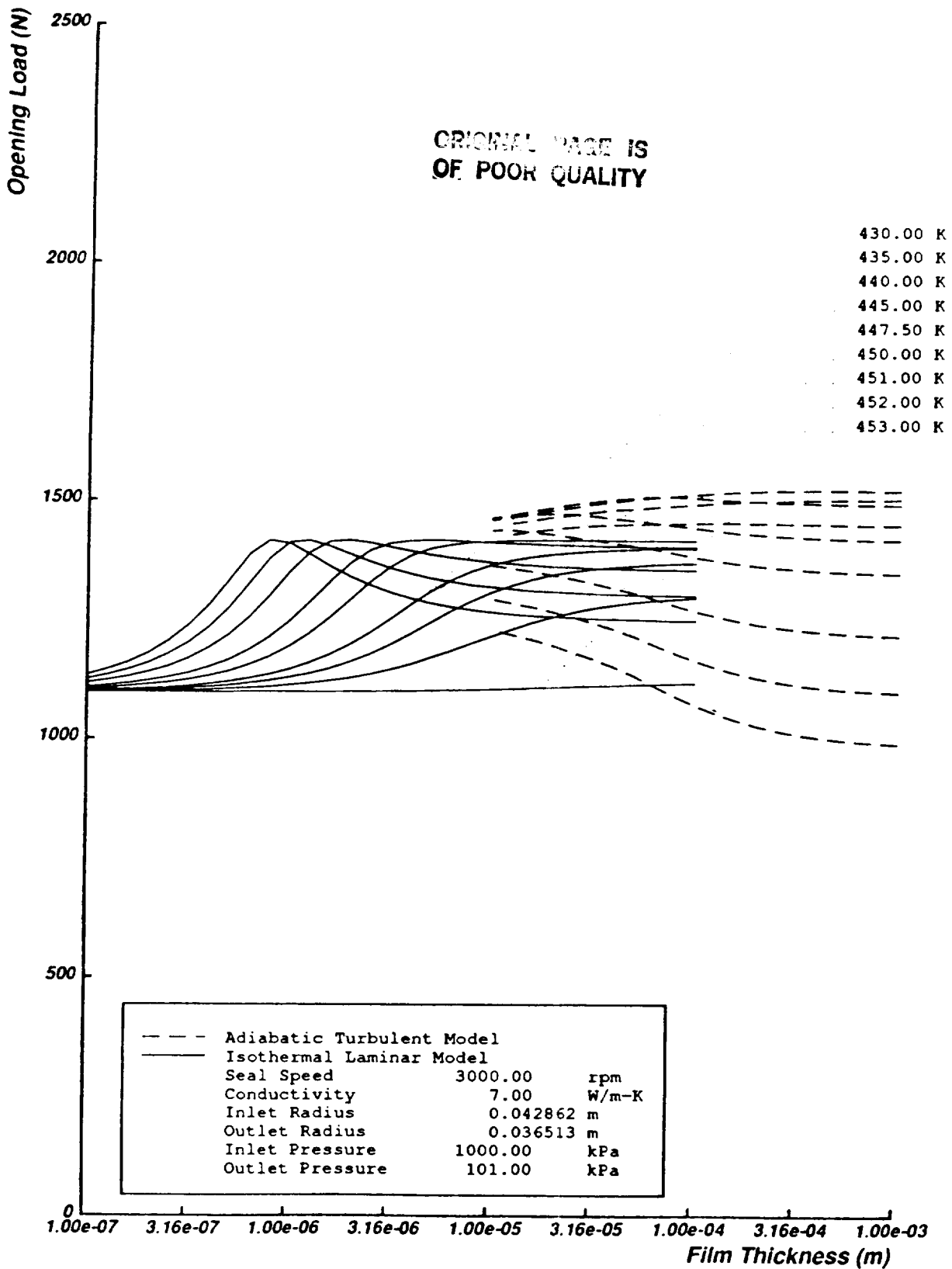
Plot of Seal Opening Force



Reservoir Temperature : 440.0 °K
Inlet Pressure : 5000.0 kPa
Back Pressure : 101.0 kPa

Figure 1-16: Stiffness Curves Showing Effect of Speed and Turbulence.

ORIGINAL PAGE IS
OF POOR QUALITY

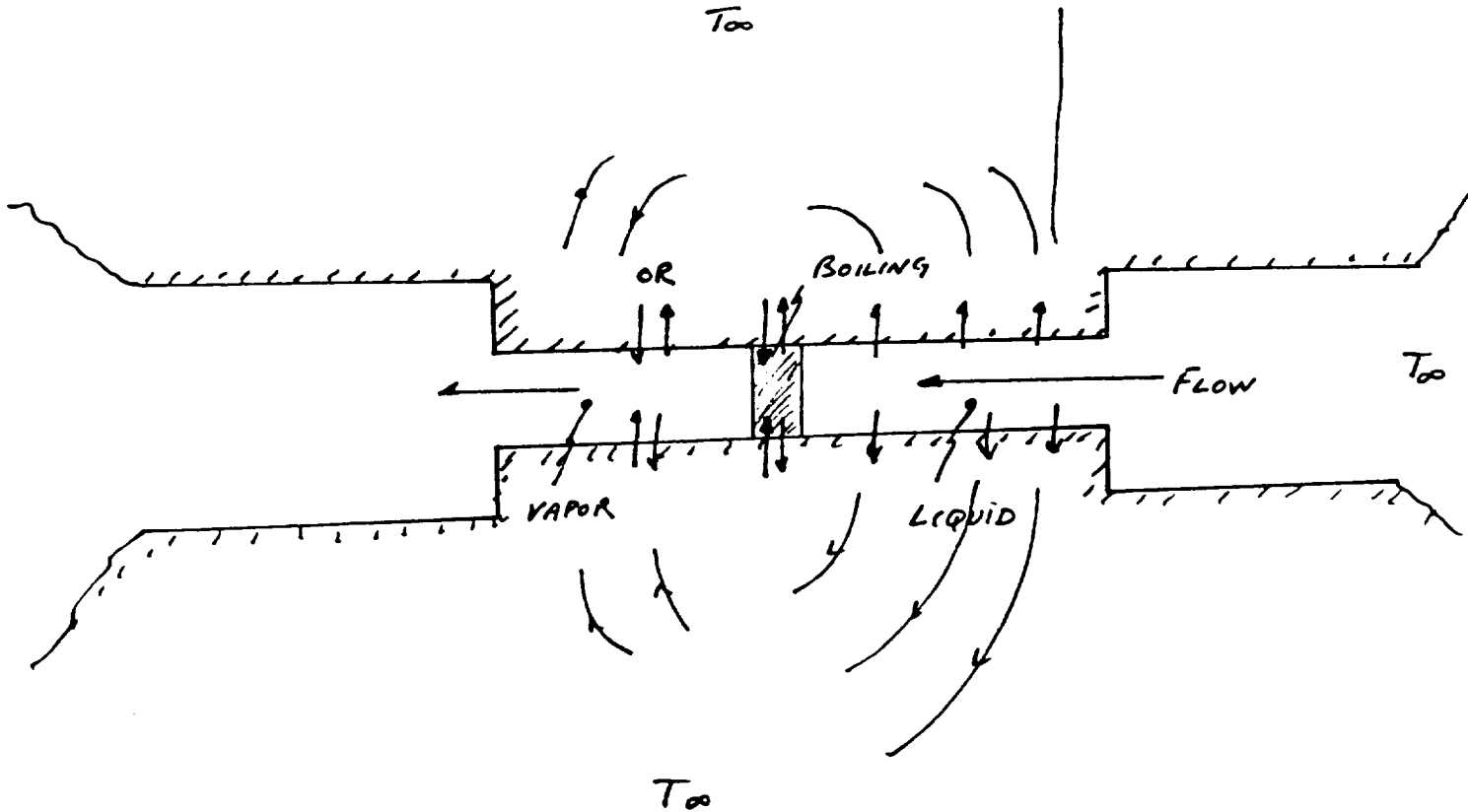


Plot of Opening Load Versus Film Thickness

for Different Bulk Fluid Temperatures

Figure 1-17

Figure 1-18: Heat Transfer to the Seal Faces.



- HEAT GENERATED IN LIQUID REGION FLOWS INTO SEALS.
- IN BOILING REGION HEAT WILL FLOW INTO FLUID TO BOIL LIQUID IF LEAKAGE RATE IS HIGH ENOUGH. HEAT WILL FLOW OUT IF LEAKAGE RATE IS LOW AND SPEED (DISSIPATION) HIGH.
- HEAT MAY FLOW IN EITHER DIRECTION IN VAPOR REGION.
- TEMPERATURE ACROSS FLUID OF FRACTIONAL DEGREE ORDER EXCEPT IN BOILING REGION WHERE THE TEMPERATURE MAY BE OF ORDER OF A FEW DEGREES IF LEAKAGE RATE IS HIGH.

CHAPTER 2

GOVERNING EQUATIONS FOR LAMINAR SEALS

2.1 Introduction

The governing equations of fluid motion and heat transfer through the seal rings are developed here. Figure 2-1 shows the radial flow passage inside a seal under two-phase operation. Although this figure indicates a parallel face, the formulations are done with a more general coned face seal with film thickness, h , varying along the radial direction, r . The moving and the fixed plates represent the rotor and the stator, respectively. For this particular case, the heat generation is high enough and the flow is low enough to cause complete boiling inside the seal. There may be situations in which the sealed liquid does not boil completely and leaves the seal as a two-phase mixture.

Heat is generated in the lubricating film due to viscous dissipation. A part of this heat is conducted into the seal rings and the rest convected downstream by the fluid. The proportion of each mode of heat removal at any radius depends mainly on the leakage rate, the material conductivities and whether or not phase change takes place. Usually under two-phase operation, conduction and convection both play important roles depending on the region under consideration - liquid, two-phase, or gas.

The following assumptions are made in this analysis:

1. For the heat conduction calculation, the seal geometry is to be modeled with the appropriate thermal boundary conditions. As the radial width of the interface is very small and backup materials on either side of the interface are large in volume, the seal rings are assumed to be semi-infinite solids of homogeneous

composition with conductivity same as the average value of the two materials. The idealized seal model is shown in Figure 2-2. The temperature very far from the interface, T_{∞} , corresponds to the bulk temperature of the liquid being sealed. These assumptions make the model independent of the actual geometrical details, and simplifies the numerical calculations. It is expected some general conclusions may be drawn about seal behavior using this model. For actual design purposes, however, the seal geometry and all the imposed thermal boundary conditions should be given proper consideration, and the methodology developed here can still be useful.

2. The film geometry is assumed to be axisymmetric, with no tilting or angular misalignment.
3. Only quasistatic, laminar flow is considered in the analysis. However, the governing equations for squeeze film effects, developed by Beeler [104] and turbulent, inertia dominated flow, developed by Beatty [90] are briefly discussed here for the sake of completeness.
4. The thermodynamic and transport properties are uniform across the film.
5. Density of liquid is constant throughout. This may be suitable for water but not for many hydrocarbons.
6. Radial inertia is neglected in laminar flow on the ground of low leakage rates. Although this is very small for low leakage seals, the speed of sound in a two-phase mixture, however, can be far less than that in either pure liquid or gaseous phase under the same conditions [105]. This usually happens around 50% quality range. Hence 'choking' may occur even at apparently low leakage rates, radial inertia and inlet losses included in the development of the turbulent equations.
7. Radial conduction of heat in the fluid film is neglected because of low conductivity of the fluid.
8. Centrifugal inertia effects are included.

2.2 Governing Equations of Fluid Motion

2.2.1 Steady Laminar flow

Momentum and Continuity

Referring to Figure 2-1, the θ momentum equations for the fluid are as follows,

$$-\frac{dp}{dr} + m \frac{\partial^2 u}{\partial z^2} = -\frac{\rho \omega^2}{r} \quad (2-1)$$

$$\frac{\partial^2 w}{\partial z^2} = 0 \quad (2-2)$$

The term on the right-hand side of the Equation (2-1) represents the centrifugal inertia effect.

Integrating (2-2) across the film twice, subject to the boundary conditions the $w = 0$ at $z = 0$ and $w = \omega r$ at $z = h$,

$$w = \frac{\omega r z}{h} \quad (2-3)$$

The Equation (2-3) is an example of the classical velocity driven Couette flow between two parallel plates.

Substituting (2-3) into (2-1) and integrating with the boundary conditions $u = 0$ at $z = 0$ and h ,

$$u = \frac{1}{m} \frac{dp}{dr} \frac{z(z-h)}{2} - \frac{\rho r \omega^2}{mh^2} \frac{z(z^3-h^3)}{12} \quad (2-4)$$

As seen in Equation (2-4), the radial velocity has two parts. The first term on the right hand side is the typical parabolic profile of Poiseuille flow. This is driven by the pressure gradient. The second term comes from the contribution of the centrifugal inertia. It has a stronger effect near the rotating face and distorts the Poiseuille profile which would otherwise be symmetric about the center of the film.

The continuity equation in integrated form is

$$m = \rho \int_0^h 2\pi r u dz \quad (2-5)$$

where m is constant along the radius for steady-state seal operation. Substituting (2-4) in (2-5), there results,

$$\frac{dp}{dr} = -\frac{6m\mu}{\pi\rho r h^3} + \frac{3\rho r \omega^2}{10} \quad (2-6)$$

The second term on the right-hand side of Equation (2-6) is due to the centrifugal inertia effects. The Equation (2-6) is valid for liquid, two-phase, or gas.

Energy Equation

The derivation of the integrated energy equation is shown in Appendix A. This equation can be written as follows:

$$\frac{m}{2\pi} \frac{di}{dr} = \mu \frac{r^2 \omega^2}{h} + \frac{3\omega^2 m}{20\pi} + \frac{\rho^2 r^2 h^3 \omega^4}{700\mu} - q \quad (2-7)$$

The left hand side term represents the convection. The first term on the right hand side is the heat generation due to viscous dissipation. The second and third terms are the correction terms due to the retention of the centrifugal inertia in the equation of motion, and q is the heat conduction flux into the seal plates from the fluid film.

Two-phase Region Model

The two-phase fluid is assumed to be a homogeneous mixture of saturated liquid and saturated vapor. The specific volume, enthalpy and thermal conductivity are obtained by linearly weighting the corresponding saturated liquid and saturated vapor properties as follows:

$$v = v_f + \lambda v_{fg} \quad (2-8)$$

$$i = i_f + \lambda i_{fg} \quad (2-9)$$

$$k = k_f + \lambda k_{fg} \quad (2-10)$$

The weighting parameter, λ , is the quality or the local mass fraction of vapor.

Often the details of the two-phase flow pattern are not known and an idealized theological model cannot be defined. Faced with the necessity of choosing some expression for viscosity, many workers have chosen averages which fit the limiting cases in which only either phase is present [105]. Two of such models are presented below:

Model 1: Weighted according to the mass fraction,

$$\mu = \mu_f + \lambda \mu_{fg} \quad (2-11)$$

Model 2: Weighted according to the volume fraction,

$$\mu = (1 - \lambda) \frac{v_f}{v} \mu_f + \lambda \frac{v_g}{v} \mu_g \quad (2-12)$$

which leads to the following expression for kinematic viscosity:

$$\nu = \nu_f + \lambda \nu_{fg}$$

With the Model 1, a two-phase region with very low quality will behave like a liquid region so far as the heat generation is concerned but the pressure drop will be rapid similar to a gas region, whereas with the Model 2, the heat generation will be sharply reduced over the same region but the pressure drop will be low as in liquid region.

Specification of Fluid Properties

Thermodynamic data and fluid transport property data is required to solve specific problems. To this end, saturation thermodynamic data tables were drawn from Reynolds' book [25] and fit to fourth-order splines. Accurate interpolation between table entries could then be done. First derivatives of the saturation thermodynamic properties with respect to pressure are also required in some analyses and can be estimated with good accuracy from the spline curve equations. Saturated liquid and vapor viscosities for a number of substances of interest were found in a variety of sources [26, 19, 29]. Viscosities of superheated vapors were given in tabular form by the same sources and bilinear interpolation between those entries was done as necessary.

Because the state of subcooled liquids and superheated vapors depends on a combination of temperature and pressure, calculation of fluid properties in those thermodynamic states can be unwieldy. However, these calculations can be simplified by some reasonably accurate approximations which are worthy of discussion:

- The viscosity of a subcooled liquid was taken to be the viscosity of saturated liquid at the same temperature. In all cases under study, the given pressure levels

were only moderately above the saturation pressures. Since the dependence of viscosity on pressure is rather weak in all the substances considered, this approximation is judged to be adequate.

- The specific volume for a subcooled liquid was likewise taken to have the value of saturated liquid at the same temperature. Liquids are, in general, highly incompressible so that this approximation is adequate as well.
- The specific internal energy of a subcooled liquid differs little from the internal energy of a saturated liquid at the same temperature. As discussed in the previous item, the specific volume also changes little between these states, allowing the specific enthalpy of a subcooled liquid to be estimated with good accuracy. The subcooled liquid enthalpy is approximately equal to the saturated liquid enthalpy taken at the subcooled temperature plus the saturated liquid specific volume multiplied by the difference of the pressures of the subcooled and saturated states.
- The need to calculate properties of superheated vapors is very seldom encountered in typical turbulent seal analysis. The means to make such calculations are included solely for completeness. Superheated vapor was considered to be an ideal gas with constant specific heats, but variations in gas viscosity with temperature and pressure were taken into account. For thermodynamic states near the saturation dome, this approximation is judged to be rather crude.

2.2.2 Transient Laminar flow & Squeeze-Film Effects

Squeeze-film effects refer to changes in the fluid properties due to relative axial motion of the seal rings. As one ring approaches the other, the lubricating film is squeezed. Usually the pressure inside the seal is higher than the steady state solution with the same film thickness. The mass flow rate will in general vary along the radius. If the film thickness decreases quickly enough the pressure in part of the fluid film may rise above the sealed fluid pressure. If this happens, fluid will be forced out of the seal at the inlet as well as the exit [104]. On the other hand, when the seal rings move apart and the film thickness increases, the pressure in the fluid film will fall below that predicted by the steady state solution. Squeeze-film effects will always produce damping because the change in opening

load resulting from an axial velocity of the primary ring always acts in the direction opposite to that velocity.

The fluid governing equations for single-phase flow, developed by Beeler [104], are given below.

Momentum and Continuity - Single Phase

Since radial and circumferential inertias are neglected, the r and z momentum equations will be the same as in the steady-state case. However, the pressure and the mass flow rate both vary along the radial direction as well as in time. Rewriting the Equations (2-3) and (2-4) for the circumferential and radial velocities,

$$w = \frac{\omega r z}{h} \quad (2-13)$$

$$u = \frac{1}{\mu} \frac{\partial p}{\partial r} \frac{z(z-h)}{2} - \frac{\rho r \omega^2}{\mu h} \frac{z(z^3 - h^3)}{12} \quad (2-14)$$

Following the derivation of the steady state flow, the Equation (2-14) is multiplied with the circumference and the density, and then integrated across the fluid film to get an expression for local leakage rate, m .

$$m = \frac{\pi r h^3 \rho}{6\mu} \left[\frac{3\rho \omega^2 r}{10} - \frac{\partial p}{\partial r} \right] \quad (2-15)$$

Note that m may now vary with radial position. Considering the annular control volume in Figure 2-3, as the film thickness changes with time, the rate at which the mass within the

control volume changes must be equal to the difference between the leakage rates on each side of the control volume. This may be written mathematically as follows:

$$m_r - m_{r+\delta r} = \frac{\partial}{\partial t} (2\pi r \rho h \delta r) \quad (2-16)$$

Now dividing through by the circumference and the width of the control volume, δr , and then letting δr approach zero, there obtains,

$$\begin{aligned} \frac{\partial(\rho h)}{\partial t} &= -\frac{1}{2\pi r} \lim_{\delta r \rightarrow 0} \frac{m_{r+\delta r} - m_r}{\delta r} \\ &= -\frac{1}{2\pi r} \frac{\partial m}{\partial r} \end{aligned} \quad (2-17)$$

Finally, using the Equation (2-15), the following form of the squeeze-film equation of motion for single phase is obtained,

$$\rho V + h \frac{\partial \rho}{\partial t} = \frac{1}{12r} \frac{\partial}{\partial r} \left[\frac{\rho r h^3}{\mu} \left\{ \frac{\partial p}{\partial r} - \frac{3\rho \omega^2 r}{10} \right\} \right] \quad (2-18)$$

where V is the relative axial velocity of the two rings.

Energy - Single Phase

The energy equation is given below, with the terms neglected consistent with the earlier assumptions,

$$\rho \left[\frac{\partial i}{\partial t} + u \frac{\partial i}{\partial r} \right] = \frac{\partial p}{\partial t} + u \frac{\partial p}{\partial r} + \mu \left[\left(\frac{\partial v}{\partial z} \right)^2 + \left(\frac{\partial u}{\partial z} \right)^2 \right] + k \frac{\partial^2 T}{\partial z^2} \quad (2-19)$$

Equation (2-19) is integrated across the film and it can be written as follows:

$$\rho \frac{\partial \dot{x}}{\partial t} - \frac{\partial p}{\partial x} = \frac{\mu \omega^2 r^2}{h^2} + \frac{\rho h^2}{\mu} \left[\frac{\rho r^2 \omega^4}{112} - \frac{r \omega^2}{40} \left(\rho \frac{\partial \dot{x}}{\partial r} + \frac{\partial p}{\partial r} \right) + \frac{1}{12} \frac{\partial \dot{x}}{\partial r} \frac{\partial p}{\partial r} \right] - q \quad (2-20)$$

Two-Phase Region

Under dynamic situations, the two-phase region model is more complex than that under steady conditions. The appropriate field equations are developed by Zuber and Dougherty [94]. The two phases may not be in thermal equilibrium and also the process of condensation and evaporation are to be modeled. Formation of condensate acts as a vapor sink, whereas the evaporation acts as a vapor source at a point. The effects of the vapor sink and/or the source term can be of primary importance in determining dynamic characteristics of two-phase seals [94]. Apart from the continuity equation for the mixture, which is same as the Equation (2-17) for the single phase, the continuity equation for the liquid is to be considered also, which is given below,

$$\frac{\partial (1 - \lambda) \rho}{\partial t} + \vec{\nabla} \cdot ((1 - \lambda) \rho \vec{v}) = \Gamma_f \quad (2-21)$$

where the source term Γ_f is the mass rate of liquid formation per unit volume.

The following constitutive equation of condensation or of evaporation is also required,

$$\Gamma_f = \Gamma_f(\rho) \quad (2-22)$$

For condensing flow, the liquid source depends on the rates of droplet nucleation and vapor condensation on these droplets. For evaporating flows, Γ_f depends on the droplet

number density, size distribution and the rate of evaporation. In either case, the constitutive equation of condensation and/or evaporation is a strong function of vapor saturation pressure. At present, the constitutive equation is not known for some flow regimes and only in a rudimentary manner for others.

The amount of complexity involved in the study of two-phase seal transients has been presented here briefly. No attempt has been made to derive the full set of governing equations for these cases.

2.3 Heat Conduction Through Seal Rings

2.3.1 Steady-State Heat Conduction Model

The heat transfer into the seal rings must be considered in order to determine the seal face (also referred to as 'wall') temperature distribution. In Figure 2-4, the face of one seal ring (both assumed to be a semi-infinite solid of thermal conductivity k) is shown. The temperature at position r may be expressed as

$$T(r) = \int_a \frac{q(r')dA}{4\pi k |\vec{r} - \vec{r}'|} \quad (2-23)$$

where k is the average conductivity of the two seal ring materials and a is the annular seal interface over which heat is generated.

Since the fluid film thickness is very small compared to the other relevant dimensions in the problem, it may be considered to be a thin heat "source" which releases or absorbs heat at a given rate, q , per unit area. The fluid film is modeled as an annular disk of infinitesimal thickness laying in a plane and divided into n coplanar annular elements of

equal width. This disk is imbedded in an infinite solid of thermal conductivity k which represents the seal ring and seal. Each element corresponds to one radial finite difference point which lies halfway between the element's inner and outer radii. With these assumptions, Equation (2-23) can be written in matrix form as follows:

$$\{T\} = [C]\{q\} + \{T_\infty\} \quad (2-24)$$

$\{T\}$ and $\{q\}$ are the temperature and heat generation vectors, respectively. $\{T_\infty\}$ is a column vector of constant elements. In this derivation, the heat dissipation q_i is assumed to be constant over the element i . $[C]$ is called the 'steady-state influence coefficient matrix.' The detail derivation of $[C]$ is done by Beeler [104] and the final expressions of its elements are shown in Appendix B. However, the elements of $[C]$ can be obtained for finite seal geometries with proper boundary conditions by using either finite difference or finite element methods.

2.3.2 Transient Heat Conduction Model

Under certain circumstances, when the fluid film is not stable and exhibits variation in thickness over time, the seal interface temperature also becomes time-dependent to determine which the following semi-infinite transient heat conduction model is developed.

The governing differential equation for transient heat conduction in three dimension is

$$\alpha \nabla^2 T = \frac{\partial T}{\partial t} - \frac{h(\vec{r}, t)}{\rho C} \quad (2-25)$$

where h is the heat generation rate per unit volume.

The initial and infinity conditions are $T(\vec{r}, 0) = f(\vec{r})$ and, as $|\vec{r}| \rightarrow \infty, T \rightarrow 0$.

The Green's function for the Equation (2.25) is given by,

$$G(\vec{r}, t; \vec{\xi}, \tau) = \frac{1}{\rho C} \frac{e^{-\left[\frac{|\vec{r}-\vec{\xi}|^2}{4\alpha(t-\tau)}\right]}}{\left[4\pi\alpha(t-\tau)\right]^{3/2}}; t > \tau$$

$$= 0; t < \tau$$
(2-26)

The Equation (2-26) gives the influence coefficient at a radius \vec{r} at time t due to a unit source at $\vec{\xi}$ at time τ .

The temperature at \vec{r} at time t is given by,

$$T(\vec{r}, t) = \int_{-\infty}^{\infty} G(\vec{r}, t; \vec{\xi}, 0) \rho C f(\vec{\xi}) d\vec{\xi} +$$
(2-27)

$$\int_0^t \int_{-\infty}^{\infty} G(\vec{r}, t; \vec{\xi}, \tau) h(\vec{\xi}, \tau) d\vec{\xi} d\tau + T_{\infty}$$

The first term in the right hand side of the Equation (2-27) represents the contribution from the initial conditions, the second term from the heat generation and the third term comes from the steady background temperature. For a seal, the heat generation is taking place over the annular interface only. Hence while the spatial integration is to be done over the entire three-dimensional region in the first term, the same integration is only necessary over the finite interface region in the second term. One way of avoiding having to calculate the initial condition integral is to perform the time integration over the entire time interval (0, t) to find the temperature at the end of each discrete time step t_n because at time $t = 0$, the initial temperature distribution $f(\vec{\xi})$ is zero everywhere.

The fluid film is again modeled as an annular disk of infinitesimal thickness lying in a plane and divided into n coplanar annular elements of equal width, as is done in the steady

state case. At any time t , the entire time interval $(0, t)$ is discretized into N intervals of varying size. The disadvantage with this semi-infinite model, as mentioned above, is finding temperature distribution at t_n , cannot be conveniently posed as an initial-value problem over the n th time interval with the known temperature distributions at the end of the previous interval t_{n-1} as the prescribed initial condition. Instead the first term in Equation (2-27) is set to zero and time integration in the second term is performed over the entire time interval $(0, t_n)$ which has been discretized into n sub-intervals. It is assumed that the heat generation vector $\{q\}$ and temperature vector $\{T\}$ are constant over each of these sub-intervals. With the chosen spatial and temporal discretization, the Equation (2-27) gives the following matrix equation with summation over all the time sub-intervals,

$$\{T(t_n)\} = \sum_{k=1}^n [C_k]\{q_k\} + \{T_\infty\} \quad (2-28)$$

where $\{T(t_n)\}$ is the temperature distribution vector at time t_n and $[C_k]$ is the 'time-dependent influence coefficient matrix,' the detail derivation of which is given in Appendix C.

2.4 Boundary Conditions

The seal inlet and outlet pressure p_o and p_i , and the bulk fluid temperature T_∞ are the given boundary conditions. The inlet pressure, p_o , is the same as the sealed fluid pressure for low leakage rates. However, the inlet losses are to be accounted for high leakage rates. The pressure p_i is same as the back pressure at the seal outlet (p_∞) except where choking occurs. The material temperature further away from the seal interface, T_∞ , is assumed to be the same as the bulk sealed fluid temperature. Although a part of the heat generated at the seal interface is conducted into the seal rings and the surrounding materials, the bulk fluid temperature will not change much because the heat will be ultimately carried out of the machinery with the fluid flow.

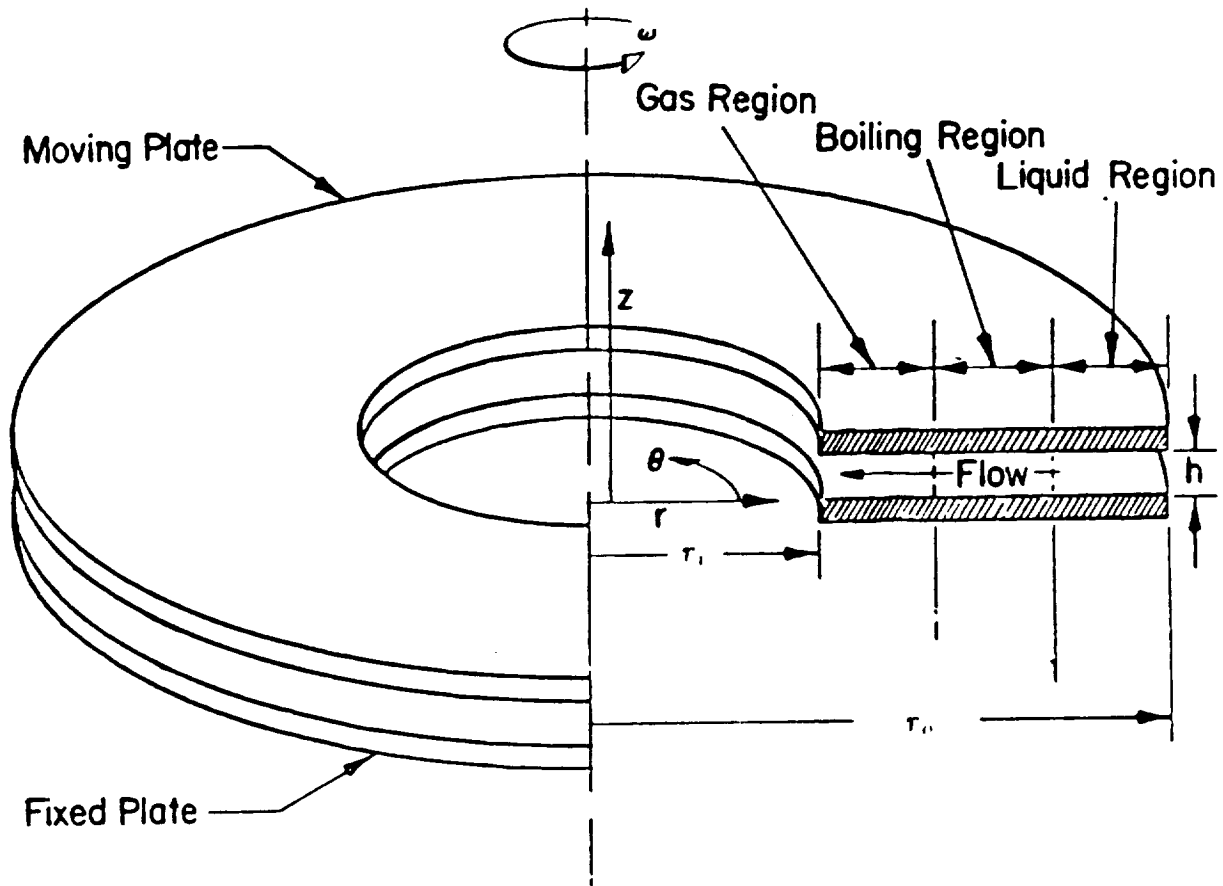


Figure 2-1: Two-phase Flow Through Face Seal

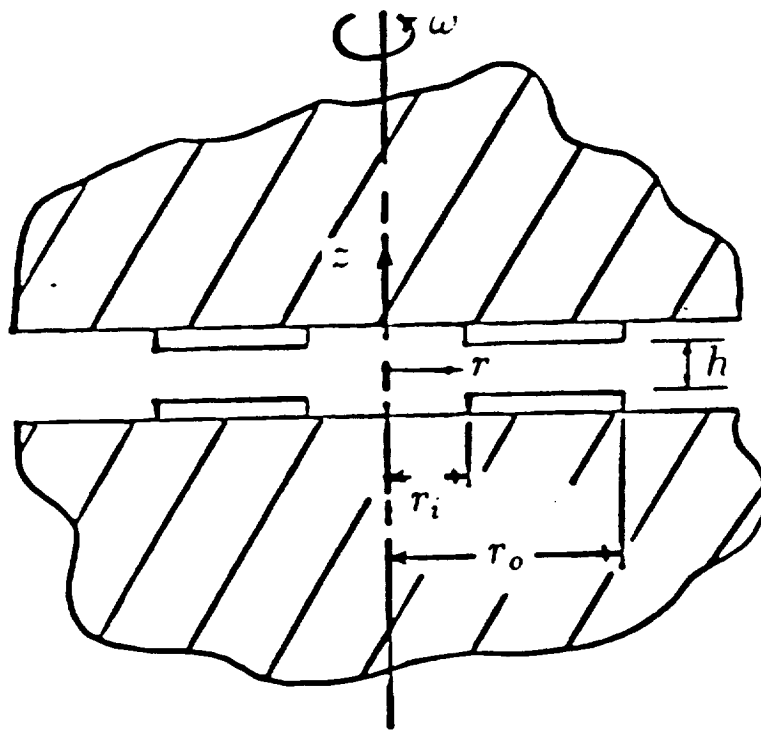


Figure 2-2: Idealized Seal Model

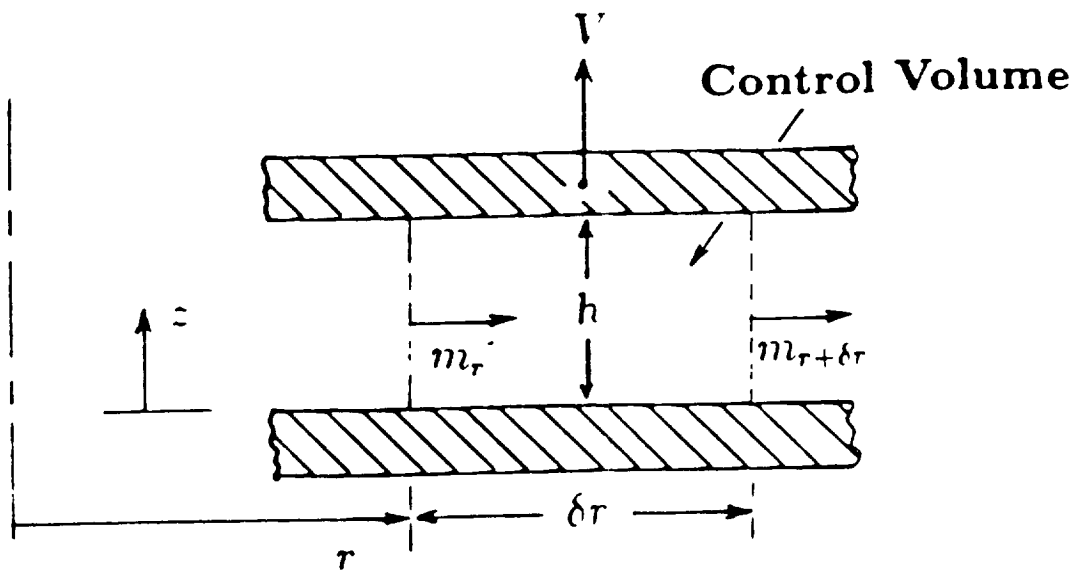


Figure 2-3: Annular Control Volume for Squeeze-film Model

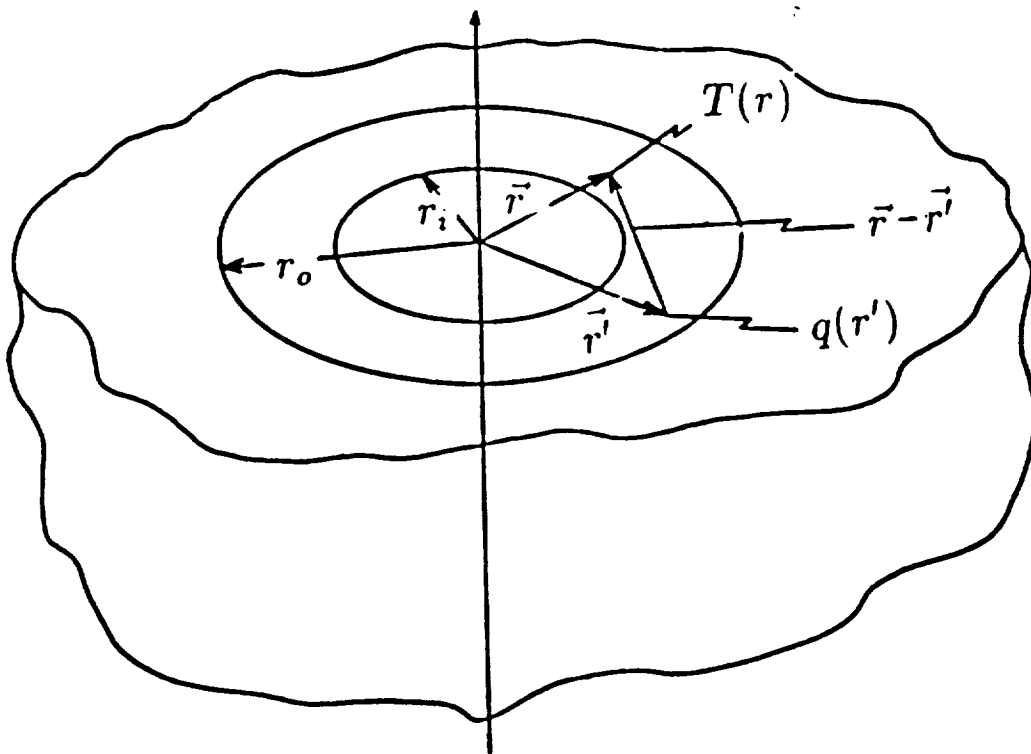


Figure 2-4: Annular Seal Flow Region on a Semi-Infinite Solid - Steady State Temperature Calculation

CHAPTER 3

A SIMPLIFIED MODEL FOR LAMINAR TWO-PHASE FACE SEAL DESIGN

3.1 Introduction

In this chapter we present a simplified model suitable for designing either parallel and coned face seals. During the early stages of designing a seal, it is usually necessary to perform extensive parametric studies before viable designs can be identified. To a seal designer, a computationally efficient model for quick and simple analyses is a very valuable tool. Fortunately, most face seals are designed to operate at very small film thicknesses and have very low leakage rates, additional simplifications to our basic laminar seal model presented in Chapter 2 can be made to greatly simplify the analysis.

When the seal film thickness is very small, the fluid mass flow (leakage) rate is low enough that the heat carried away in the fluid (convection) is very small compared to the heat generated due to viscous dissipation. Also, because of the high heat generation rate, phase change of the fluid from liquid to vapor occurs over a very short distance. It is therefore reasonable to assume that, in a low leakage seal analysis, the errors introduced by neglecting the effects of convection and continuous boiling will not be unacceptable. In our simplified model for low leakage seals, the most important simplifications made are neglecting convection and assuming discrete boiling. A computer code suitable for PC operation based on this model has been prepared and is documented in Appendix D.

3.2 Physical Model

We will be concerned primarily with outside pressurized seals although the analysis is equally valid for inside seals. Figure 3.1 shows the geometry of a face seal. For an outside face seal, the leakage path is radially inwards. High pressure fluid enters the seal from the outer radius and leaves at the inner radius. This configuration offers the

advantage of a lower leakage rate with the help of the centrifugal effect. For an all liquid outside seal, net leakage can be reduced to zero if the seal is operating above a certain critical speed. However, in most operations, this critical speed is much higher than the operating speed and the inertial effects are of minor importance.

In this simplified model, a number of physical assumptions in addition to those in Chapter 2 were made and a discussion of them is given below.

1. The seal is axisymmetric and the seal surfaces are perfectly smooth. There is no surface contact between the seal plates. For face seals operating at extremely small film thicknesses, hydrodynamic effects caused by surface roughness and surface contacts can contribute significantly to the net opening force. Since our model does not take these effects into account, the opening force estimate will err to the low side when such effects are indeed significant. However, coning is included in the model and wear at the outer radius may be approximated by an equivalent coning.
2. The density and viscosity of liquid are assumed to be the same as saturated liquid at the same temperature and is independent of pressure. Viscosity of vapor is also assumed to be equal to that of saturated vapor at the same temperature. This assumption is good for water but is not very suitable for many hydrocarbons, where densities and viscosities are sensitive to pressure variation. Since no provision is made to handle fractional boiling, the equations developed are not applicable to multi-component fluids.
3. Centrifugal inertia effects in the vapor region are small compared with those of the liquid region and are neglected.
4. The temperature of the fluid is assumed to be uniform across the film and is the same as the temperature of the surfaces of the seal plates. In reality, a temperature gradient must exist in the fluid film for heat transfer to take place between the fluid and the seal plates. However, the film thickness is so small that a very small temperature variation is sufficient to produce the required gradient.
5. The fluid flow is assumed to be quasi-isothermal at the boiling location temperature. When boiling is discrete and convection is negligible, determining the exact temperature profile of the fluid along the leakage path is not very critical to the

analysis. For low leakage seals, the variation in the fluid temperature along the seal faces is often small. The only relevant seal temperature is the temperature at the boiling location, where the boiling interface pressure is equal to the saturation pressure corresponding to this temperature and must be determined by looking up the saturation table. With the exception of saturation pressure, all the relevant physical properties, namely the fluid viscosity and density, are insensitive to small temperature changes. Under the assumption of negligible convection, viscosity is the only fluid property needed to calculate the boiling location temperature. The assumption of an isothermal flow, which in this case means constant viscosity of the fluid, will not introduce any significant error. Since the boiling interface pressure is directly evaluated using the boiling location temperature, the error introduced by the isothermal assumption is also minimal. After the boiling interface pressure is found, the leakage rate and the pressure profile of the seal are evaluated. The isothermal assumption, once again, will not introduce any significant error to the results because the only physical properties needed are viscosity and density.

It should be noted that, the physical meaning of assuming a quasi-isothermal flow is that the temperature variation along the fluid leakage path is assumed not to be large enough to significantly affect the viscosity and density of the fluid. Since it is shown that no unacceptable error will be introduced, this assumption is justified.

6. Boiling is assumed to occur at a discrete location. If the flow is indeed isothermal, then the boiling (change from liquid to vapor) must occur at a discrete interface. This is true because in any two-phase region the temperature and pressure are related by a unique relationship (Clasius-Clapeyron equation). To satisfy momentum balance, the pressure drop must be monotonic through the seal. Hence there can only be one position where the saturation condition is satisfied if the temperature is uniform.

In reality, there must be some heat transfer "to" the fluid to effect boiling. For low leakage seals this amount of heat, and indeed the convection in general, is negligible compared to the total heat generated by viscous dissipation, which is essentially all conducted into the seal plates.

7. The vapor is assumed to behave as an ideal gas. This assumption greatly simplifies the analysis and unless a more precise heat transfer analysis was used it would seem unwarranted to incorporate vapor properties of real fluids. Exact

thermodynamic data were used by Hughes and Chao [88] and quantitatively it was shown to make little difference.

8. Since we assumed quasi-isothermal flow for the low leakage seal with discrete boiling, the model of a two-phase mixture becomes moot. We only consider pure liquid and vapor. However, it is possible that a separated flow may exist with vapor accumulating along the rotating face and liquid along the stationary face because centrifugal inertia would tend to sweep the liquid off the rotor.

3.3 Mathematical Analysis

For the liquid region, using the assumptions of constant density and viscosity, Equation (2.6) can be integrated to obtain a closed form solution of the pressure distribution. The boundary conditions applied are $p = p_o$ at $r = r_o$ and $p = p_b$ at $r = r_b$.

For a parallel faced seal, the expressions for the mass flow rate, m , and the pressure, p , are,

$$m = -\frac{\rho\pi h^3}{6\mu} \frac{(p_o - p_b) - \frac{3\rho\omega^2}{20}(r_o^2 - r_b^2)}{\ln r_o - \ln r_b} \quad (3.1)$$

$$p = \frac{p_o - p_b - \frac{3\rho\omega^2}{20}(r_o^2 - r_b^2)}{\ln \frac{r_o}{r_b}} \ln\left(\frac{r}{r_o}\right) + \frac{3\rho\omega^2}{20}(r^2 - r_o^2) + p_o \quad (3.2)$$

For a seal with constant coning slope, β , the expressions are,

$$m = - \frac{\frac{\rho \pi (h_o - \beta r_o)^3 \left(\frac{3\rho (r_o^2 - r_b^2) \omega^2}{20} - (p_o - p_b) \right)}{6\mu}}{\ln \frac{r_o}{r_b} - \ln \frac{h_o}{h_b} + (h_o - \beta r_o) \left(\frac{1}{h_o} - \frac{1}{h_b} \right) + \frac{(h_o - \beta r_o)^2}{2} \left(\frac{1}{h_o^2} - \frac{1}{h_b^2} \right)} \quad (3.3)$$

$$p = \left[\frac{\left((p_o - p_b) - \frac{3\rho (r_o^2 - r_b^2) \omega^2}{20} \right)}{\ln \frac{r_o}{r_b} - \ln \frac{h_o}{h_b} + (h_o - \beta r_o) \left(\frac{1}{h_o} - \frac{1}{h_b} \right) + \frac{(h_o - \beta r_o)^2}{2} \left(\frac{1}{h_o^2} - \frac{1}{h_b^2} \right)} \right] \times$$

$$\left[\ln \frac{r}{r_o} - \ln \frac{h_o + \beta (r - r_o)}{h_o} + (h_o - \beta r_o) \left(\frac{1}{h_o + \beta (r - r_o)} - \frac{1}{h_o} \right) + \frac{(h_o - \beta r_o)^2}{2} \left(\frac{1}{(h_o + \beta (r - r_o))^2} - \frac{1}{h_o^2} \right) \right]$$

$$+ \frac{3\rho (r^2 - r_o^2) \omega^2}{20} + p_o \quad (3.4)$$

From Equations (3.2) and (3.4), we can see that it is possible for the mass flow rate of an all-liquid seal to go to zero when the centrifugal inertia force balances the pressure force. The speed at which the mass flow rate is zero is called the critical speed and is given by the following expression.

$$\omega_c = \sqrt{\frac{20 (p_o - p_i)}{3\rho (r_o^2 - r_i^2)}} \quad (3.5)$$

When the seal speed is at the critical speed, a liquid front will be formed at the exit. In theory, if the seal is running at above critical speed, the direction of the mass flow will

be reversed (i.e. from the inner radius which has a lower pressure to the outer radius which has a higher pressure). However, it is not possible for most seals to have reversed flows because there is seldom any liquid available at the exit for being "pumped" back into the reservoir. If the seal speed goes higher than the critical speed, the liquid front will move towards the inlet and significantly reduce the seal opening force. For a detail discussion on the effects of centrifugal inertia, the reader is referred to Basu [92].

For the vapor region we assumed ideal gas behavior, negligible inertia effects and vapor viscosity equal to the saturation value at the seal temperature. Integrating Equation (2.6) using the boundary conditions that at $r = r_b, p = p_b$ and at $r = r_i, p = p_i$, we get, for a parallel seal,

$$m = - \frac{\pi h^3 (p_b^2 - p_i^2)}{12\mu RT \ln \frac{r_b}{r_i}} \quad (3.6)$$

$$p^2 = \frac{p_b^2 - p_i^2}{\ln \frac{r_b}{r_i}} \ln \frac{r}{r_i} + p_i^2 \quad (3.7)$$

For a seal with constant coning slope, the expressions are,

$$m = - \frac{\pi(h_o - \beta r_o)^3 (p_b^2 - p_i^2)}{12\mu RT \left(\ln \frac{r_b}{r_i} - \ln \frac{h_b}{h_i} + (h_o - \beta r_o) \left(\frac{1}{h_b} - \frac{1}{h_i} \right) + \frac{(h_o - \beta r_o)^2}{2} \left(\frac{1}{h_b^2} - \frac{1}{h_i^2} \right) \right)} \quad (3.8)$$

$$p^2 = p_i^2 + \left[\frac{(p_b^2 - p_i^2)}{\ln \frac{r_b}{r_i} - \ln \frac{h_b}{h_i} + (h_o - \beta r_o) \left(\frac{1}{h_b} - \frac{1}{h_i} \right) + \frac{(h_o - \beta r_o)^2}{2} \left(\frac{1}{h_b^2} - \frac{1}{h_i^2} \right)} \right] \times$$

$$\left[\ln \frac{r}{r_i} - \ln \frac{h_o + \beta(r - r_o)}{h_i} + (h_o - \beta r_o) \left(\frac{1}{h_o + \beta(r - r_o)} - \frac{1}{h_i} \right) + \left(\frac{(h_o - \beta r_o)^2}{2} \left(\frac{1}{(h_o + \beta(r - r_o))^2} - \frac{1}{h_i^2} \right) \right) \right] \quad (3.9)$$

In addition to the above equations, the thermodynamic data of the sealed fluid must be provided. For the present model, the saturation data, viscosity, density and gas constant of the vapor must be provided. These data may be provided as a function subprogram in the computer code. The present form of the code uses simple fourth-order spline fits of saturation data and incorporates water, nitrogen, oxygen and hydrogen. Additional fluids may be easily added and the routine changed without affecting the main code.

Neglecting convection in the fluid and the inertia terms in the energy equation (2.7), the heat conduction rate into the seal plate is a simple expression,

$$q = \mu \frac{r^2 \omega^2}{h} \quad (3.10)$$

Since most seals operate at temperatures far below the critical temperature of the working fluid, the vapor viscosity is much less than that of the liquid. The heat generation rate in the vapor region is therefore much smaller than in the liquid region and can be neglected. To evaluate the temperature rise at any radial position r_s , we integrate Equation (2.28) only over the area of the liquid region of the seal.

Assuming angular symmetry, the integral can be expanded to,

$$\Delta T_s = \int_{r=r_b, \phi=0}^{r=r_o, \phi=2\pi} \int \frac{\mu \frac{r^2 \omega^2}{4\pi k h} \frac{r d\phi dr}{\sqrt{r_s^2 + r^2 - 2 r_s r \cos \phi}}}{(3.11)}$$

The seal temperature of interest is the temperature evaluated at the boiling location. The pressure at the boiling location must be the same as the saturation pressure of the fluid corresponding to the seal temperature there. Recognizing the angular integral as a complete elliptical integral of the first kind, Equation (3.11) can be simplified to the following, where K represents the complete elliptic integral of the first kind, note that in generally the film thickness h is a function of the radial position r ,

$$\Delta T_s = \begin{cases} \frac{\mu \omega^2}{\pi k} \int_{r_b}^{r_o} \frac{r^2}{h} K\left(\frac{r_s}{r}\right) dr & r_s < r_b \\ \frac{\mu \omega^2}{\pi k} \left(\int_{r_s}^{r_o} \frac{r^2}{h} K\left(\frac{r_s}{r}\right) dr + \int_{r_b}^{r_s} \frac{r^3}{r_s h} K\left(\frac{r}{r_s}\right) dr \right) & r_s > r_b \end{cases} \quad (3.12)$$

The torque, Q , required to overcome the viscous friction is usually very small and can be found using the following expression, where $\tau_{z\theta}$ is the shear stress in the circumferential direction,

$$Q = \int_A r \tau_{z\theta} dA \quad (3.13)$$

Using the same argument as before, we can neglect the frictional torque produced in the vapor region. We can rewrite Equation (3.13) as,

$$Q = \int_{r_b}^{r_o} r \mu \frac{r \omega}{h} 2 \pi r dr \quad (3.14)$$

For a parallel seal, the torque required to overcome viscous friction is,

$$Q = -\frac{\pi \mu \omega}{2h} (r_o^4 - r_b^4) \quad (3.15)$$

For a seal with constant coning slope, the torque required is,

$$Q = -2\pi \mu \omega \left(\frac{r_o^3 - r_b^3}{3\beta} - \frac{(h_o - \beta r_o)(r_o^2 - r_b^2)}{2\beta^2} + \frac{(h_o - \beta r_o)^2 (r_o - r_b)}{\beta^3} - \frac{(h_o - \beta r_o)^3}{\beta^4} \ln \left(\frac{h_o}{h_b} \right) \right) \quad (3.16)$$

3.4 Method of Solution

A computer code suitable for PC operation has been developed which analyzes the low leakage laminar seals which is documented in Appendix D. The boiling location of a low leakage two-phase seal is a operation parameter of significance. When the convection terms are negligible, one may calculate the seal temperature based on the boiling location alone using Equation (3.11). After the seal temperature at the boiling location is found, we can determine the liquid and vapor viscosities and densities and the boiling interface

pressure, which is the saturation pressure corresponding to the seal temperature at the boiling location.

The solution method is as follows,

1. The seal geometry, fluid, inlet and exit conditions, bulk temperature of the sealed liquid, seal thermal conductivity and speed are chosen.
2. A value of the film thickness (inlet value for the case of a coned seal) is chosen.
3. Check whether or not the seal is operating at above critical speed. If the seal is, calculate where the liquid front is located, determine the seal opening force and then go to step 10. If the seal is not, proceed to step 4.
4. Check whether or not the seal is two-phase. If it is all-liquid, determine the pressure profile using Equation (3.1) or (3.3), the seal opening force, and the leakage rate using Equation (3.2) or (3.4), and then go to step 10. If the seal is two-phase, proceed to step 5.
5. A boiling interface location is assumed. The seal temperature at the assumed boiling location is calculated by numerically integrating Equation (3.12). Note that the integrands in Equation (3.12) are singular at the boiling location. An open interval integration scheme such as one of the Gauss quadratures performed over several sub-intervals, with very small ones near the point of singularity, is necessary for an accurate numerical evaluation.
6. The boiling interface pressure and the fluid properties are calculated from the thermodynamic data.
7. Using the liquid equation, (3.1) or (3.3), and the vapor equation, (3.6) or (3.8), the leakage rates are separately determined for both liquid and vapor. These are compared and if the vapor leakage rate is higher then the boiling location must be shifted towards the inlet and vice versa.
8. Steps 5 through 6 are iterated until the proper boiling location is determined.

9. Pressure profiles are found using Equation (3.2) or (3.4) for the liquid region and Equation (3.7) or (3.9) for the vapor region. The opening load is found by numerically integrating the pressure over the seal face.
10. The process is repeated for a different film thickness in order to generate a stiffness curve.

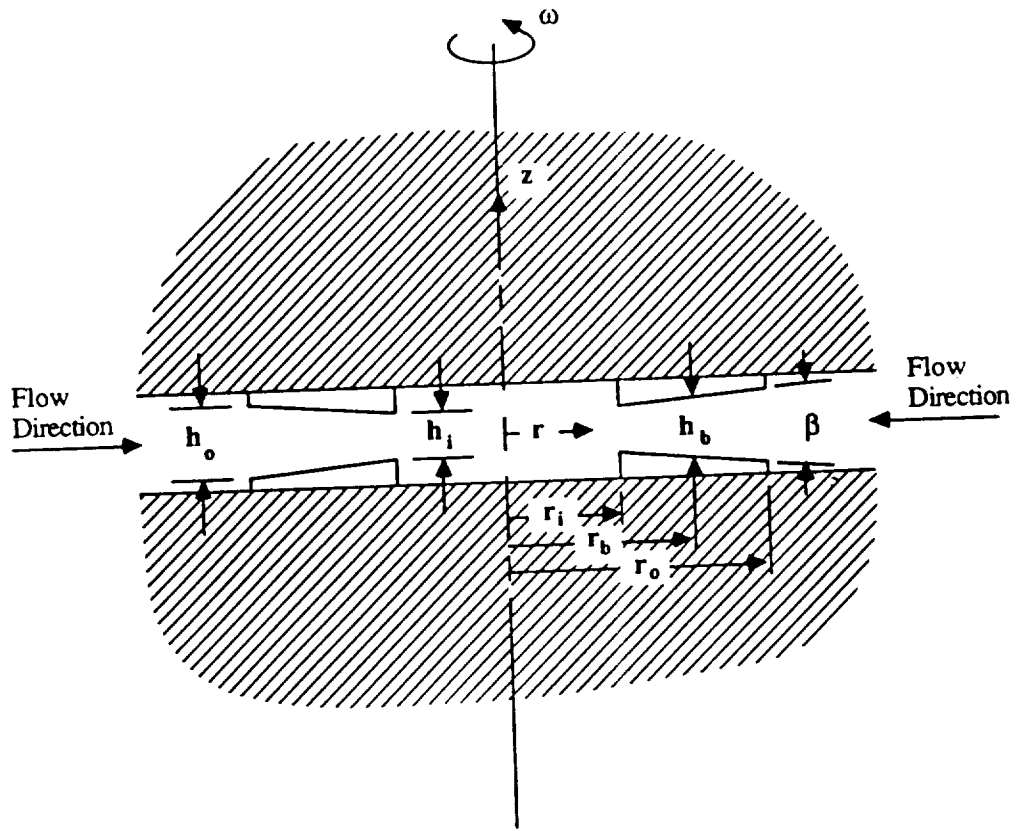


Figure 3.1: The Face Seal Geometry

CHAPTER 4

TURBULENT TWO-PHASE SEALS - THEORY AND EQUATIONS

4.1 Introduction

The full problem of determining the flow through seals in the turbulent regime is a difficult one. It involves the inclusion of the nonlinear fluid inertia terms, the consideration of fluid friction in which the flow has large velocity components in two directions, and in many cases phase change and choking. To make matters worse, the inlet velocities in turbulent seal flows are large enough to cause inlet pressure losses to be significant. Since no simple boundary condition can be specified at the seal inlet *a priori*, the problem domain must be extended beyond the seal proper, upstream to a location where the fluid properties are known. These features of the general turbulent seal problem are in direct contrast to those of classical lubrication theory where nonlinear terms are neglected (making analytical solutions possible in many cases), where frictional effects are easily handled, and where the domain of interest need not extend beyond the flow channel of the device being treated. Solution to the full turbulent seal problem requires sophisticated multi-dimensional numerical techniques which are difficult to produce and verify and are costly to implement on available digital computers.

Fortunately, for any practical seal, the thickness of the flow channel is very small compared to other characteristic dimensions of the device. This fact affords great simplification to the model governing equations for the seal proper. Order of magnitude arguments show that the component of velocity in the direction through the film is essentially zero and that through-the-film variations of temperature and pressure are negligible. One may then write the full basic equations of continuity, momentum, and energy in terms of shear stresses dropping the terms which are small by the above order of

magnitude arguments. It is then possible to integrate through the fluid film to find film-averaged properties in a fashion similar to the Karman-Pohlhausen integral treatment for boundary layer flows. Shear stresses integrated through the film are resolved into wall shear stresses which may be modelled using the film-averaged flow velocities by the semi-empirical law-of-the-wall theory.

By reasonable assumptions yet to be discussed, the problem of determining the flow from the upstream reservoir to the seal inlet may be similarly simplified. Consideration of the extended Bernoulli equation and the First Law of Thermodynamics make it possible to relate the velocity, pressure and specific enthalpy at the seal inlet to the known thermodynamic fluid state in the reservoir. One can then "jump" from the reservoir to the inlet without considering the details of the flow between these stations. This eliminates the necessity of extending the problem domain beyond the seal itself and making multidimensional numerical calculations there.

The advantage of this method is obvious, the number of spatial dimensions of the problem is reduced by one and the computational domain is restricted to the flow passage of the seal. Numerical computation is much simplified and the computer cost to solve an individual problem is reduced to a level where seal designers may realistically do parametric studies.

In the past, some investigators have applied integral methods to problems involving turbulent flow in narrow channels. Constantinescu and Galetuse [115] and Burton and Hsu [116] employed the integral approach in their analyses of turbulent journal bearings. In both cases their analyses were correctly done; however, neither group looked beyond the journal bearing application for this solution method. In both analyses, it was assumed that the gauge pressure on the ends of the bearing were zero. The pressure boundary condition

then was independent of the velocity there so that the problem of the development of flow from the reservoir to the ends of the bearing was not encountered or discussed by these authors. Still others have developed their own methods based on the integral approach and used it to analyze a variety of situations. Ng and Pan [117] proposed what they called "A Linearized Turbulent Lubrication Theory" in which the nonlinear mean fluid inertia terms were dropped from the film-averaged turbulent equations of motion. Linearized turbulence is in this sense logically inconsistent; if the flow is turbulent, the Reynolds number is large enough that the mean fluid inertia terms play a significant role. Hirs [118] developed yet another approach to turbulent lubrication flow. His bulk flow equations are derived from the film-averaged turbulent equations of motion. The turbulent wall shear stresses are related to the mean velocities by a correlation made by considering experiments with turbulent flow in narrow channels. Although the mean fluid inertia terms are present in the equations, Hirs' formulation mixes these terms with those associated with the wall shear stress terms making the role of the inertia terms in any given problem difficult to assess. Extension of Hirs' method to situations which require the inclusion of the energy equation would be extremely awkward.

The underlying philosophy of treating turbulent lubrication in this work is to rely on the fundamental equations. Wall shear stresses are to be calculated by friction factors which have been used extensively and shown to enjoy a wide range of applicability. All the important terms are retained and the inertia terms are isolated from the other terms in the equations. Many problems in turbulent lubrication theory may then be approached in a simple and consistent way by this method.

4.2 Derivation of the Basic Equations for Turbulent Seal Flow

The integral approach will now be applied to the basic governing equations for both the radial face seal and annular seal geometries. In these geometries, a homogeneous fluid is assumed to flow. In the case of two-phase flow, the mixture of liquid and vapor is taken as a pseudo-fluid with properties which are averages of the properties of the component phases. Turbulent flow through these seals is assumed to be adiabatic. This assumption does not mean that no heat transfer takes place between the fluid film and the seal itself, but rather that the amount of heat transferred from the fluid to the seal over some specified time interval is small compared to the amount of heat convected by the flowing fluid or generated in the film during that same time interval. The theoretical adiabatic limit is closely approached in seals over the entire turbulent range where the leakage rates are large. Products of average quantities will be taken as equal to the average of their products in the convective acceleration terms. This assumption is not restrictive in turbulent flows where the velocity profiles for pressure-driven flow are very blunt.

Basic Governing Equations for Radial Face Seals

A schematic representation of a radial face seal is shown in Figure 4. The seal is composed of two rings, one stationary ring mounted to the fluid barrier known as the seal seat, and one ring mounted to the shaft and rotating with it known as the primary ring. Fluid in the clearance space between the rings may velocity components in both the circumferential and radial directions. Radial flow is pressure driven, while circumferential flow is driven by shear from the rotation of the shaft. Depending on the application, one of two different seal configurations may be used. If high pressure is felt on the inside radii of the seal rings, the configuration is referred to as an inside seal and the radial flow is outward; if high pressure is felt on the outside radii of the seal rings, the seal configuration

is referred to as an outside seal and the radial flow is inward. The outside seal configuration is the more commonly used one and that which is depicted in Figure 4.

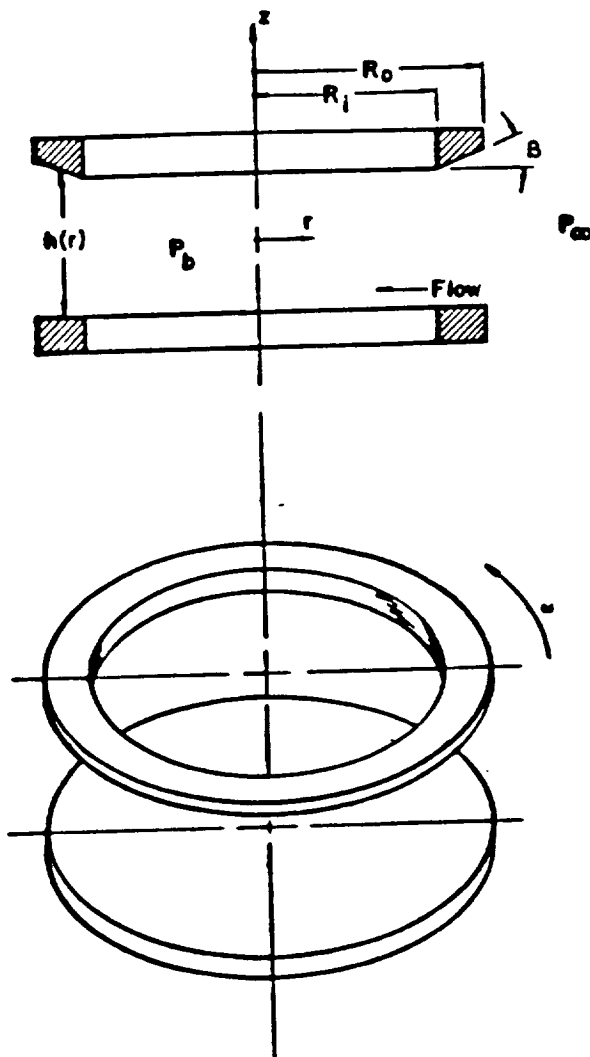


Figure 4-1: Face seal geometry (not to scale).

The opposing surfaces on the face seal rings on either side of the clearance space need not be parallel. It will be shown later that it is advantageous to taper the moving ring seal face as seen in the schematic diagram. This tapering is generally referred to as coning by seal designers.

By restricting the relative motion of the seal rings to be along their common axis only, the problem becomes much simplified; the geometry is axisymmetric and terms for angular

variations in the equations are dropped. Further, time derivatives in the basic equations will be dropped as well. The continuity equation may then be written as:

$$\frac{1}{r} \frac{\partial}{\partial r} (r \rho u) + \frac{\partial}{\partial z} (\rho v_z) = 0$$

where v_z is the axial velocity in the z direction.

Upon integrating from the seal seat to the primary ring, the contribution from the second term is zero since the walls are impermeable, making the axial velocity vanish at both surfaces. Because the film height changes with the radial position, care must be taken to evaluate the remaining integral. Applying Leibnitz's rule, this integral may be expressed as:

$$\int_0^{h(r)} \frac{1}{r} \frac{\partial}{\partial r} (r \rho u) dz = \frac{1}{r} \frac{\partial}{\partial r} \int_0^{h(r)} (r \rho u) dz - r \rho u|_{h(r)} \frac{1}{r} \frac{dh}{dr}$$

where the last term is zero because of the no-slip condition. In the face seal geometry, the radius is never zero so that this equation may be integrated to give:

$$m = 2\pi r h G \tag{4-1}$$

the film thickness, h , being a known function of radial position. In the above equation, the radial velocity, and hence the mass leakage rate and mass velocity, may take either a positive or negative sign. In an inside seal the fluid flows radially outward giving a positive sign, while in an outside seal the fluid flows radially inward giving a negative sign. This convention is used throughout the face seal analysis.

The radial momentum equation can be processed in a similar way. The general form, dropping the angular variations and terms containing the axial velocity, is:

$$\rho u \frac{\partial u}{\partial r} - \rho \frac{w^2}{r} = \frac{1}{r} \frac{\partial}{\partial r} (r\sigma_r) + \frac{\partial}{\partial z} (\sigma_{rz}) - \frac{\sigma_{\theta\theta}}{r} \quad (4-2)$$

The axial velocity is necessarily zero at the walls since they are impermeable. It is presumed that the axial velocity between the walls can not become so large as to be comparable with the velocity components in the other directions. The stress component σ_r is dominated by the pressure. This stress component will be taken to be equal to the negative of the pressure. The stress component $\sigma_{\theta\theta}$ will be small compared to the other components since the mean velocity gradients in the circumferential direction are small compared to those in the other directions.

Special care must be taken to integrate the centrifugal acceleration term through the film. In turbulent Couette flow, the velocity profile for the circumferential velocity is "S" shaped. If the "S" is shallow, the circumferential velocity can be approximated by $w(r,z) = \omega z/h$. This expression is then substituted into the centrifugal acceleration term of equation (4-2) and the integration carried out. Using the stated assumptions and integrating gives:

$$G \frac{du}{dr} - \frac{\omega^2 r}{3\nu} + \frac{dP}{dr} \pm \frac{2}{h} \tau_{rz} = 0 \quad (4-3)$$

where τ_{rz} is the wall shear in the radial direction. The positive sign on the shear term applies to outward radial flow (inside seal), while the negative sign applies to inward radial flow (outside seal).

The energy equation can be written for a ring-shaped control volume of width Δr which occupies the entire space between the seal set and primary ring as:

$$W_s = -m(e_{r+\Delta r} - e_r)$$

where e is the specific energy of the fluid, or:

$$e = i + u^2/2 + w^2/2.$$

The left hand member of the above equation represents work down to the fluid by shear or:

$$W_s = 2 \pi (\Delta r) \omega r \tau_{z\theta}$$

Substituting, and taking the limit as the ring width approaches zero gives the adiabatic energy equation for the face seal:

$$\frac{di}{dr} + \frac{d}{dr} \left(\frac{u^2}{2} \right) + \frac{\omega^2 r}{3} = \frac{\omega r}{Gh} \tau_{z\theta} l_h \quad (4-4)$$

where $\tau_{z\theta} l_h$ is the wall shear stress in the circumferential direction evaluated at the shaft surface. The equations (4-1), (4-3), and (4-4) comprise the set of basic descriptive equations for the axisymmetric radial face seal. The circumferential equation of motion for this situation is trivially satisfied.

Basic Equations for Turbulent Flow in Annular Seals

A schematic representation of an annular seal is shown in Figure 4-4. This seal is made up of the shaft itself and a close fitting opening around it. Fluid in the clearance space is forced through the seal axially by pressure and is dragged along in the circumferential direction by the shearing action of the shaft.

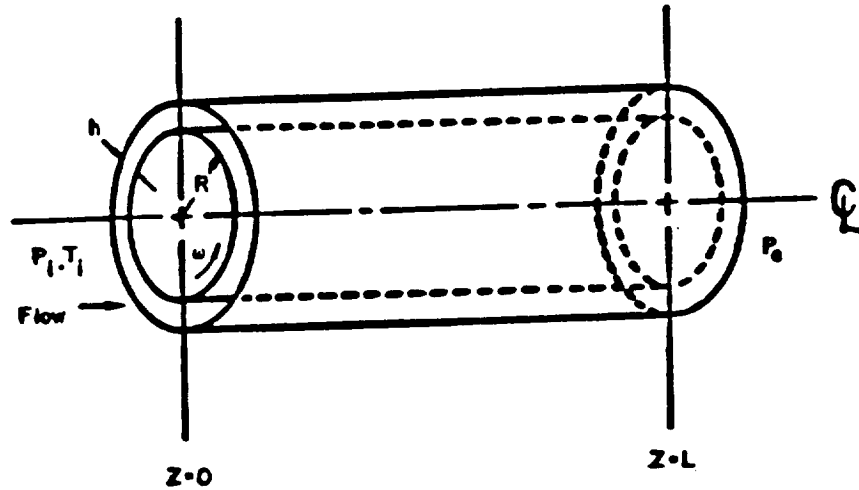


Figure 4-2: Annular seal geometry (not to scale).

The through-the-film integration for the annular seal geometry is proceeded in a similar fashion to that for the radial face seal and all the same assumptions and mathematical techniques applied to the previous case will again be applied. However, the film-averaged annular seal equations given here will be more general and will include circumferential variations. Because the film dimension in the radial direction is very small, the centrifugal acceleration can not build up any appreciable pressure difference. Centrifugal acceleration effects in this case will be neglected.

Since the film thickness is very small compared to the shaft radius, curvature effects can be neglected and the problem domain may be unwrapped; the coordinate system

reduces to a Cartesian system. Integrating through the film of the continuity equation and simplifying gives (Note that here we use u and w for axial and circumferential velocity, respectively):

$$\frac{\partial}{\partial z}(\rho u h) + \frac{1}{R} \frac{\partial}{\partial \theta}(\rho w h) = 0 \quad (4-5)$$

while the equations of motion in the axial and circumferential directions are, respectively:

$$\rho u h \frac{\partial u}{\partial z} + \rho w h \frac{1}{R} \frac{\partial u}{\partial \theta} = - \left(\tau_{rz} |_{R+h} - \tau_{rz} |_R \right) - h \frac{\partial p}{\partial z} \quad (4-6)$$

and

$$\begin{aligned} \rho u h \frac{\partial w}{\partial z} + \rho w h \frac{1}{R} \frac{\partial w}{\partial \theta} \\ = - \left(\tau_{r\theta} |_{R+h} - \tau_{r\theta} |_R \right) - h \frac{1}{R} \frac{\partial p}{\partial \theta} \end{aligned} \quad (4-7)$$

Finally, the adiabatic energy equation becomes:

$$\begin{aligned} \tau_r \theta |_R \omega R \\ = \rho u h \frac{\partial}{\partial z} \left(i + u^2/2 + w^2/2 \right) + \rho w h \frac{1}{R} \frac{\partial}{\partial \theta} \left(i + u^2/2 + w^2/2 \right) \end{aligned} \quad (4-8)$$

The equations (4-5), (4-6), (4-7), and (4-8) make up the set of descriptive equations for the flow within the annular seal. In all the above equations for an annular seal, the variation in radius is neglected. The mean radial position within the film is approximated by the shaft radius.

4.3 Determination of Wall Shear Stresses

Many different approaches to finding wall shear stresses in turbulent flow have been proposed. Burton [119] gives a good catalogue of these approaches, summarizing their origins and salient features. Of all these methods, the semi-empirical law-of-the-wall theory is used here to give wall shear stresses in terms of the components of the mean channel velocity. As stated previously, this choice of turbulent friction theory has advantages over other theories, namely, the theory enjoys wide applicability and the mean inertia terms are separated from other terms in the equations of motion.

From variations in fluid density or channel height, the mean flow velocities and hence the wall shear stresses may change over the area of the seal. These variations may be significant and must be dealt with. In all practical cases, the flow channel height is small compared to other dimensions of the seal and that that channel height varies slowly along the flow path. The flow may then be taken to be quasi-fully developed, and the law-of-the-wall theory, applicable to fully-developed flow, may then be applied locally to give the wall shear stresses in terms of the fluid properties there. The relation:

$$\tau = \frac{f}{8} \rho V^2$$

then holds, where τ is the local wall shear stress, V is the mean velocity in the direction in which the shear acts, and f is a friction factor. Correlations exist which specify the friction factor, depending on the flow situation encountered.

Under typical operating conditions, the flow could have large mean velocity components in two directions simultaneously, giving a complex three-dimensional turbulent structure in which coupling does exist between the velocities in these different

directions. Various treatments for flows of this type have been used. For example, Black and Jenssen [120] apply an elaborate correlation proposed by Yamada [121] to analyze turbulent annular seals. White [122] lists several approaches which account for turbulent flow coupling. However, he also comments that, at present, no good theory exists for treating flows of the type just described. In light of this fact, the use of simple turbulence models which give reasonable results are warranted.

One particularly simple model proposed for coupled turbulent flow treats the flows associated with the different velocity components separately [122]. This approach greatly simplifies the calculations. Trial studies indicate that the fluid property profiles and leakage rates are rather insensitive to variations in the friction factor values in either direction, suggesting that the uncoupled flow model is indeed adequate.

The channel geometry for seals is always such that the aspect ratio, or ratio of channel height to width, is extremely large so that the simple hydraulic radius concept is not applicable. Instead of using a hydraulic radius, it is more accurate to model the channel as one that is infinitely wide. Special friction factor correlations have been made for hydraulically smooth-two-dimensional channels. For pressure-driven or Poiseuille flow, the proper friction factor correlation in turbulent flow is reported by White [122] to be:

$$\frac{1}{\sqrt{f}} = 0.8839 \ln (Re_h \sqrt{f}) + 0.142 \quad (4-9)$$

The Reynolds' number based on film height is defined as: $Re_h = \frac{Gh}{\mu}$. For shear-driven, or Couette, flows the mean velocity profile across the channel assumes an "S" shape. The law-of-the-wall under a zero prevailing pressure gradient may be manipulated to give the following friction factor correlation as derived by that same author [122]:

$$\frac{1}{\sqrt{f}} = 1.768 \ln (\text{Re}_h \sqrt{f}) + 0.831 \quad (4-10)$$

where $\text{Re}_h = \frac{\rho \omega R h}{\mu}$. In addition, it has been shown that this correlation is still valid if the prevailing pressure gradient is negative or moderately positive. Solution of these transcendental equations for the friction factor may be easily accomplished numerically by Newton's root-finding method since the local velocity and fluid properties are known. In the two-phase regime, the mixture density is used and the viscosity is taken to be the volume-weighted average of the viscosities of the component phases.

4.4 Calculation of Inlet Thermodynamic State

It is assumed that the upstream reservoir area is large compared to the flow area at the seal inlet so that the velocity of the reservoir fluid is essentially zero to an observer in the laboratory. Temperature and pressure in this body of fluid far from the seal are measurable and uniform. The possibility does exist that parts of the seal at an elevated temperature can transfer heat to the reservoir fluid, but this effect is assumed to be negligible. The zone of influence of hot seal elements on the temperature of the incoming fluid will not extend far upstream into the reservoir. The fluid entering the zone where heat transfer from the mechanical parts of the seal could be appreciable is travelling at a velocity which is a large fraction of the inlet velocity. It is then reasonable to assume that the flow is nearly adiabatic, as was done for flow in the body of the seal.

With the above assumptions, the first law of thermodynamics may be used to give:

$$i_i = i_\infty - \frac{u_i^2}{2} \quad (4-11)$$

since the difference in potential energy between these two stations is very small. Again neglecting any small potential energy change, the extended Bernoulli equation may be

written for a streamline from a point far upstream in the reservoir to just inside the seal inlet:

$$\int_{\infty}^i v dp = - \frac{k+1}{2} u_i^2 \quad (4-12)$$

where k is an inlet loss coefficient which accounts for the irreversible pressure loss due to sudden contraction of the flow area. The loss coefficient multiplies the mean kinetic energy per unit mass at the inlet. Values for this coefficient may range from 0.01 for a well rounded inlet to 0.5 for a square-edged inlet.

Nowhere in the above equations has the circumferential, or swirl, velocity appeared. It has been assumed that the work done by rotating seal elements on the incoming fluid by shear is approximately equal to the kinetic energy increase of that fluid by increased swirl velocity. These terms then cancel each other and so do not appear in the governing equations. This statement is equivalent to assuming that there is a negligible pressure difference through thin boundary layers surrounding rotating seal parts.

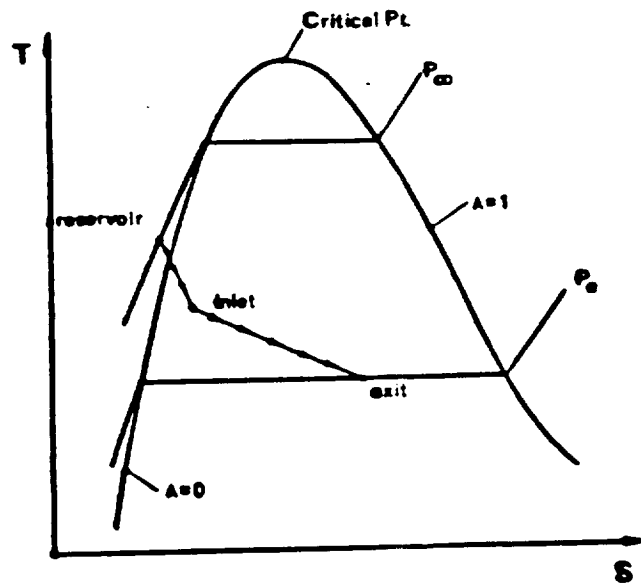


Figure 4-3: Typical trajectory of a fluid element travelling through the seal in the T-s plane.

If the reservoir fluid is very close to its saturation state, it is certainly possible for vaporization to occur as the fluid travels from the reservoir to the inlet as the pressure it experiences decreases. Such a case is shown on the T-s diagram for a typical substance in Figure 4-3 where the first segment of the curve indicates the change of state from the reservoir to the inlet and the second segment shows the change in state through the seal proper. The integral that is the left hand member of the extended Bernoulli equation is then difficult to evaluate because it is path-dependent. Fortunately, for most design situations of interest, the amount of vaporization from inlet pressure drop will be small; most of the boiling of liquid will occur within the body of the seal. Taking the fluid quality just inside the inlet to be small, the integral of Pdv , or the work done on a system of fluid travelling from the reservoir to the seal inlet may be approximated by:

$$\int_{\infty}^i p dv \approx \frac{P_i + P_{\infty}}{2} (v_i - v_{\infty}) \quad (4-13)$$

in other words, the path taken through p-v space is taken as a straight line. Integrating equation (4-12) by parts, and substituting from equation (4-13) gives the following:

$$pv|_{\infty}^i = -\frac{k+1}{2} u_i^2 + \frac{P_i + P_{\infty}}{2} (v_i - v_{\infty}) \quad (4-14)$$

This equation, along with the First Law, from a set of equations which specify the thermodynamic state of the fluid at the inlet.

Simultaneous solution of equations (4-11) and (4-14) is accomplished by iteration. The calculation is begun assuming that the fluid remains a liquid through the inlet process. The specific volume then remains a constant over a streamline and the inlet velocity is found from continuity for a presumed mass flow rate. (To avoid confusion, it should be noted that the mass flow rate is determined independently from this inlet state calculation from pressure boundary conditions imposed upon the entire flow problem. Solution methods to find this mass flow rate will be outlined in subsequent chapters.) Since the specific volume is known for the entire inlet pressure drop, equations (4-11) and (4-14) may be used separately to determine the specific enthalpy and pressure at the inlet. These two fluid properties fully determine its thermodynamic state. If this calculated state indeed corresponds to a subcooled liquid, the initial premise was correct and the inlet state is now known. If the calculated inlet state corresponds to a saturated mixture, however, the iteration must continue. To find the inlet state when that state is under the saturation dome, the estimate for the inlet state is used to find the inlet specific volume. From this estimate and the presumed mass flow rate, an updated inlet velocity is calculated. Substituting the updated inlet velocity and specific volume into equations (4-11) and (4-14) gives updated values of pressure and enthalpy which define a new updated thermodynamic state. This

new estimated state is compared to the previously calculated state. Calculation continues until the relative difference between successive inlet pressure and enthalpy estimates falls below some tolerable error bound. By the nature of the relation between the specific volume and velocity, this procedure will always converge to a solution.

CHAPTER 5

LEAKAGE AND AXIAL STIFFNESS IN TURBULENT RADIAL FACE SEALS

5.1 Introduction

In this chapter, turbulent radial face seals will be analyzed using the basic equations derived in section 4-2 to describe the flow in the seal proper and other equations derived in section 4-5 to relate the inlet conditions to the reservoir conditions. An idealized seal will be considered in which the seal rings: 1) have hydraulically smooth surfaces, 2) are constrained to move only in the axial direction relative to each other rendering the geometry axisymmetric, and 3) move so slowly that squeeze-film damping effects are negligible. In reality, the seal rings in most applications are polished by methods like those used to manufacture telescope mirrors and do approach the hydraulically smooth limit for reasonable clearance gaps. The seal rings are connected to nearby machine elements by elastomeric materials and so actually execute relative motions in directions perpendicular to the axis of the seal; however, these motions are dominated by the axial motion. Finally, it should be noted that damping, though quite important in the dynamics of face seals, does not determine the conditions for seal collapse. One need not be concerned with the degree of damping to investigate the axial stability of the seal. Thus, the highly idealized model presented is not restrictive and gives much useful information about the performance of real face seals.

One may generate a curve of opening force as a function of mean film thickness for any set of operating conditions. Assuming that the seal has sought a film thickness where the forces on the primary ring are in equilibrium, the slope of the opening force curve at that point, multiplied by minus one, gives the restoring force due to a small displacement

from the equilibrium position. The entire response of pressure in the fluid film can then be modelled to the action of an equivalent single axial spring with a variable, but known, spring constant. It is possible for that spring constant to become negative under some operating conditions. If the equivalent spring constant does become negative, the net pressure on the primary ring acts not to restore the seal to equilibrium but instead acts to collapse the seal.

It will be shown that seal leakage and opening force vary with the rotation speed of the spinning face and with the thermodynamic state of the incoming fluid in the two-phase regime. In many situations, the inlet drop is a significant fraction of the total pressure drop through the seal. Further, it will be seen that the inlet drop can give rise to unexpected seal behavior.

Choking may occur in the seal if the back pressure is below a critical value. At choking conditions, the flow velocity is equal to a sonic velocity just at the seal exit and the exit pressure no longer matches the back pressure. Pressure trajectories through the seal are shown in Figure 5-1 for choked and unchoked flow. It is possible for the fluid at the seal exit to be vapor, two-phase mixture, or even pure liquid under choked conditions. The all-liquid choked case may occur when the rate of viscous dissipation is small and the degree of inlet subcooling is large. This mode of choked flow behaves much differently than the two-phase or all vapor choked flow. The previous analysis of Hughes and Beeler [89] allows only for saturated liquid entering the seal and so can not predict this unusual mode of choking. The later paper by Beatty and Hughes connects these deficiencies [90].

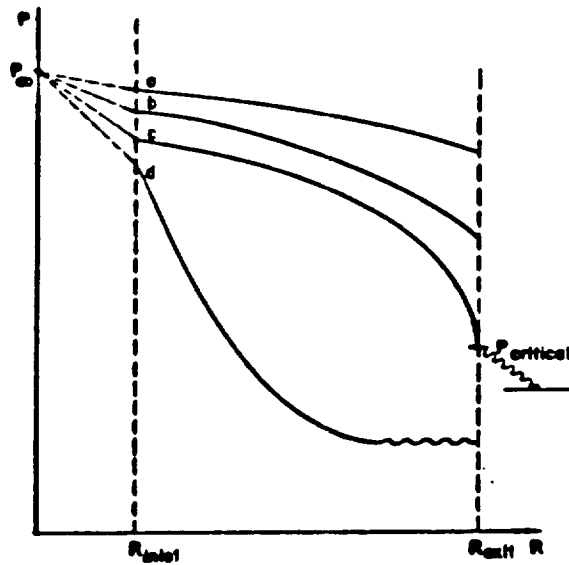


Figure 5-1: Typical pressure profiles through a face seal. Curves "a" and "b" show unchoked flow with exit and back pressures equal. Curve "c" shows the choked flow line and expansion wave with the back pressure lower than the critical pressure. Curve "d" shows the cavitation line for an inside seal.

As discussed by Osterle and Hughes [103], it is possible for cavitation to occur in an inside seal if the quality is low throughout the flow passage and the rotation speed is sufficiently high. In this case the pressure drops to the value of the back pressure within the interior of the seal, rupturing the film without boiling. The net opening force under such circumstances would be extremely low. This possibility is depicted in Figure 5-2.

The criterion for cavitation is that the pressure gradient goes to zero as the pressure approaches the back pressure at some point within the interior of the seal. Although this condition is not complicated, determining whether cavitation occurs is very difficult in that it depends on the specific parameters of the problem. If sufficient boiling occurs within the

seal, the fluid density is low so that the centrifugal inertia term is small and cavitation does not occur. No attempt will be made to do a systematic study of cavitation in turbulent seals in this analysis.

5-2 Specialized Equations for Liquid, Two-Phase, and Vapor Flow

The basic equations are now adapted for liquid, two-phase, or vapor flow. As stated previously, two-phase mixtures are treated as homogeneous fluids. The continuity equation does not change with change of phase and is:

$$m = 2\pi r h G \quad (5-1)$$

Remember that the mass leakage velocity can be positive or negative. It is taken as positive in an inside seal and negative for an outside seal.

Liquid Flow

If the fluid is entirely liquid, it can be assumed with little loss of accuracy that the density is constant with a value corresponding to the density of saturated liquid at the same temperature. This affords some simplification of the radial momentum equation which then can be written:

$$\frac{dp}{dr} = \pm \frac{2}{h} \tau_{rz} + \frac{\omega^2 r}{3v} + \frac{G^2 v}{r} \left(1 + \frac{r}{h} \frac{dh}{dr} \right) \quad (5-2)$$

where the shear stress term takes a negative sign for flow radially outward. Further, the energy equation becomes:

$$\frac{di}{dr} = \frac{\omega r}{Gh} \tau_{z\theta} |_h - \frac{\omega^2 r}{3} + \frac{G^2 v^2}{r} \left(1 + \frac{r}{h} \frac{dh}{dr} \right) \quad (5-3)$$

Note that the derivative of the film thickness with radius in these equations is simply the tangent of the coning angle, β .

Since the liquid compressibility is neglected, the sonic speed for the liquid is infinite and there is no singularity in either the pressure gradient or the enthalpy gradient. Normal choking, where the fluid velocity reaches the acoustic wave speed in the medium, then can not be predicted from the equations above. It should be noted that the acoustic wave speeds for most liquids are so high that choking in a mode as described above is very seldom experienced.

Liquid - Vapor Flow

For a homogeneous saturated two-phase mixture in thermodynamic equilibrium, the specific enthalpy and specific volume may be written in terms of quality:

$$\frac{1}{\rho} = v = v_f + \lambda v_{fg}$$

and,

$$i = i_f + \lambda i_{fg}$$

Further, the radial derivatives of these may be rewritten in terms of other quantities by application of the chain rule, for example:

$$\frac{di}{dr} = \frac{\partial i}{\partial p} \lambda \frac{dp}{dr} + i_{fg} \frac{d\lambda}{dr}$$

where,

$$\frac{\partial i}{\partial p} |_{\lambda} = \frac{di_f}{dp} + \lambda \frac{di_{fg}}{dp}$$

The radial velocity in the radial equation of motion and the energy equation may be expressed in terms of the mass leakage velocity, G . Using this and the relations among the saturation properties above, these equations may be solved for the radial derivative of pressure explicitly, assuming G is known:

$$\begin{aligned} \frac{dp}{dr} = \frac{1}{1-\phi} \left\{ \frac{G^2 v}{r} \left(1 + \frac{r}{h} \frac{dh}{dr} \right) + \frac{\omega r}{3v} \pm \frac{2}{h} \tau_{zr} \right. \\ \left. + G^2 \frac{v_{fg}}{i_{fg}} \left[-\frac{\omega r}{Gh} \tau_{z\theta} + \frac{2\omega r}{3} \pm \frac{2v}{h} \tau_{zr} \right] \right\} \end{aligned} \quad (5-4)$$

where

$$\phi = -G^2 \frac{\partial v}{\partial p} |_{\lambda} - G^2 \frac{v_{fg}}{i_{fg}} \left(v - \frac{\partial i}{\partial p} |_{\lambda} \right)$$

Again, the radial derivative of film thickness is simply the tangent of the coning angle β . In the above expression the negative signs are taken for the radial shear stress terms if the fluid is flowing radially outward. Once the pressure gradient is known, the mixture quality gradient may be expressed as:

$$\begin{aligned} \frac{d\lambda}{dr} = -\frac{1}{i_{fg}} \left[-\frac{\omega r}{Gh} \tau_{z\theta} + \frac{2\omega r}{3} \right. \\ \left. - \left(v - \frac{\partial i}{\partial p} |_{\lambda} \right) \frac{dp}{dr} \pm \frac{2v}{h} \tau_{zr} \right] \end{aligned} \quad (5-5)$$

where, once again, the negative sign applies to the radial shear stress term for radial outward flow. Since temperature is only a function of pressure at saturation, the following is true:

$$\frac{di}{dr} = \left(\frac{di_f}{dp} + \lambda \frac{di_{fg}}{dp} \right) \frac{dp}{dr} + i_{fg} \frac{d\lambda}{dr} \quad (5-6)$$

where the pressure gradient is known from (5-4) and the quality gradient is known from (5-5). Note that equations (5-4) and (5-6) give finite gradients, as in the all-liquid case, unless ϕ becomes greater than or equal to unity. The quantity ϕ corresponds to the square of the Mach number in an ordinary gas dynamics problem; later, it will be related to a characteristic wave speed in a two-phase medium.

All-Vapor Flow

If one assumes an ideal gas with constant specific heats, the continuity, axial momentum, energy, and state equations may be combined in a simple way to give the gradients of the pressure and enthalpy. The pressure gradient may be found explicitly as:

$$\begin{aligned} \frac{dp}{dr} = & \frac{1}{1 - M^2} \left\{ \frac{\gamma p M^2}{r} \left(1 + \frac{r}{h} \frac{dh}{dr} \right) \right. \\ & + \frac{\omega r}{3v} \left(1 + 2(\gamma - 1) M^2 \right) \\ & \left. \pm \frac{2}{h} \left(1 + (\gamma - 1) M^2 \right) \tau_{zr} - \frac{(\gamma - 1) \omega r M^2}{G h v} \tau_{z\theta} \right\} \end{aligned} \quad (5-7)$$

and, the enthalpy gradient, in terms of the pressure gradient expression above, is:

$$\frac{di}{dr} = \frac{\omega r}{Gh} \tau_{z\theta} - \frac{2\omega^2 r}{3} \pm \left(\frac{2v}{h} \tau_{zr} \right) + \left(\frac{\gamma + 1}{\gamma - 1} \right) v \frac{dp}{dr} \quad (5-8)$$

with the radial derivative of film thickness specified as before. Here, M is the Mach number.

5-3 Solution Procedure

Once a mass flow rate is specified, the appropriate set of governing equations may be integrated to give pressure and enthalpy at all points interior to the seal since the upstream reservoir conditions are known and definite relationships exist between the conditions of the reservoir and of the seal inlet. Remember that the mass velocity, G , is related to the flow rate and the local conditions through equation (5-1). These equations are nonlinear and so can not be treated analytically; they are instead integrated in this study numerically by a standard fourth-order Runge-Kutta technique. The choice of the set of governing equations used is made by examining the thermodynamic state of the fluid at the last node where the solution is known. Equations (5-2) and (5-3) apply to the subcooled liquid, equations (5-4) and (5-6) apply to a saturated mixture, and equation (5-7) and (5-8) apply to a superheated vapor.

A solution to the problem as posed is found when a specified mass flow rate either gives an exit pressure equal to the back pressure, or is at its maximum (choked flow). Referring back to Figure 5-1, these possibilities are shown as curves "a", "b", and "c". Since the critical back pressure and mass flow rate are not known *a priori*, a test for choked flow at the outset of the solution procedure is necessary.

When the flow is choked, the radial derivative of pressure is infinite at the seal exit. This condition corresponds to having the denominator of equation (5-4) for two-phase flow

or the denominator of equation (5-7) for vapor flow go to zero just at the exit. The choking condition may be found numerically within preset error limits by a method similar to the bisection method for finding roots to algebraic equations. First, a trial mass flow rate is chosen to insure that the denominator of the appropriate pressure gradient expression does not go to zero or change sign at any node point in the seal. Next, another larger trial mass flow rate is chosen to insure this sign change in the denominator takes place at some interior node. The critical mass flow rate then must occur within the interval defined by the mass flow rates discussed above. The original interval may then be subdivided and the denominator of the pressure gradient expression tested at all nodes down the axis for the intermediate mass velocity. This will further narrow the critical flow rate to one of the subintervals. This process is continued until the possible error in the critical flow rate is within tolerable bounds. The critical back pressure is the exit pressure for the critical mass flow rate.

If the given back pressure is lower than the critical back pressure found by the method described, the problem is solved; the mass flow rate is at its critical value and the procedure is terminated. If not, the problem takes the form of the standard shooting method for a two-point boundary value problem, with mass flow rate as the shooting parameter. Finally, the leakage rate is reported and the opening force is calculated as the area integral of the seal pressure.

5-4 Discussion of All-Liquid Choking

It is possible to have an anomalous situation where the flow is choked but remains liquid up to the seal exit. This is likely to occur if the rate of viscous heat generation is small and the degree of subcooling at the upstream reservoir is large. The liquid pressure will fall, at the exit, to the saturation pressure for the local temperature, but no lower.

Beyond the exit, the liquid flashes immediately into vapor; an outside observer would not see any liquid issuing from the seal.

This peculiar choking mechanism may be understood through the careful study of longitudinal wave propagation in saturated two-phase mixtures as discussed by Pai [126]. In this instance, there are two modes of wave propagation in the medium. One mode is that of ordinary sound waves travelling through the vapor phase, while the other, the so-called vaporization wave mode, is peculiar to the saturated mixture. Unlike the ordinary sound wave, the vaporization wave brings about a change of phase. One then would expect that the propagation speed of the vaporization wave is entirely different than that of an ordinary sound wave. In fact, the speed of the vaporization wave is given by the square root of the expression ϕ in (5-4). Note that this quantity has a finite limit, even as the mixture quality approaches zero. Generally, the vaporization wave speed is much lower than that of the ordinary sound wave under the same background conditions. Thus, the speed at which information can be relayed in a saturated mixture is limited by the vaporization wave speed.

Anomalous all-liquid choking occurs when very slightly subcooled liquid is moving faster than the local vaporization wave speed at the exit. If one imagined that the flow rate could increase, the exit pressure would have to decrease in response and the liquid at the exit would become saturated. But, the saturated mixture exit velocity is limited by the vaporization wave speed. Since the vaporization wave speed is smaller than the presumed exit velocity for the mixture, this situation is physically impossible. Hence the flow in this instance is choked, but is subcooled liquid throughout the seal.

5-5 Numerical Examples and Discussion

Numerical examples are presented based on two applications, namely: a nominal design for the interstage seal of the Space Shuttle Main Engine High Pressure Oxidizer Turbopump, and a high pressure water pump. In both cases, the seal inner radius is taken to be 0.0430 meters, while the outer radius is taken to be 0.0469 meters. The flow inlet is taken to be square-edged with a nominal inlet loss coefficient of 0.5 in all cases.

Figures 5-2 through 5-5 show fluid property profiles for the nominal Space Shuttle interstage seal under various possible conditions. These given conditions do not necessarily correspond to typical operating values, but rather demonstrate some extremes of face seal behavior. In these examples, cryogenic oxygen is taken as the sealed fluid.

Figure 5-2 shows an unchoked flow in an outside seal configuration. The flow enters as a two-phase mixture and remains so throughout. The pressure profile is smooth with a finite gradient everywhere. The predicted leakage in this case is 3.28×10^{-2} kg/s and the predicted opening force is 3670 N.

Figure 5-3 shows profiles for an outside seal with reservoir conditions identical to the previous case, but a back pressure below the critical back pressure. The pressure gradient is extremely steep at the seal exit, demonstrating two-phase choked flow. The flow rate is maximum for the given reservoir conditions with a value of 3.36×10^{-2} kg/s. The opening force is 3600 N, less than the previous case. This is expected since the pressure at any point is less than the corresponding point in the unchoked case.

Figure 5-4 shows nearly straight line profiles for the all-liquid choked flow case for an outside seal configuration. Although the fluid exit velocity is much lower than the sonic

speed of the liquid, the mass flow is at its maximum value and is independent of back pressure, provided it is below a critical value as discussed previously. The leakage rate here is 7.25×10^{-2} kg/s, nearly twice that of the previous cases. The opening force is 3040 N. Large inlet losses partially account for this low opening force value.

Figure 5-5 shows an unchoked flow in an inside seal configuration without cavitation. The operating conditions are identical with those of the case shown in Figure 5-2. One notes that the leakage rate is 3.85×10^{-2} kg/s, significantly higher than in the outside seal configuration, while the opening force is 3620 N, a value less than that of the outside seal case. These differences are a manifestation of the centrifugal inertia. The effect of the centrifugal inertia is to drive, rather than impede, the flow to the exit giving a higher leakage rate. The higher leakage, in turn, gives larger inlet losses so that the pressure throughout the seal is lower than in the outside configuration.

The examples shown in Figures 5-6 through 5-16 are for cryogenic oxygen flow in an outside seal. In each case, the seal leaks fluid to a vacuum for choked flow. The final examples shown in Figures 5-17 and 5-18 are for high pressure water leaking into a space where the ambient pressure is atmospheric.

PROPERTIES OF
OF POOR QUALITY

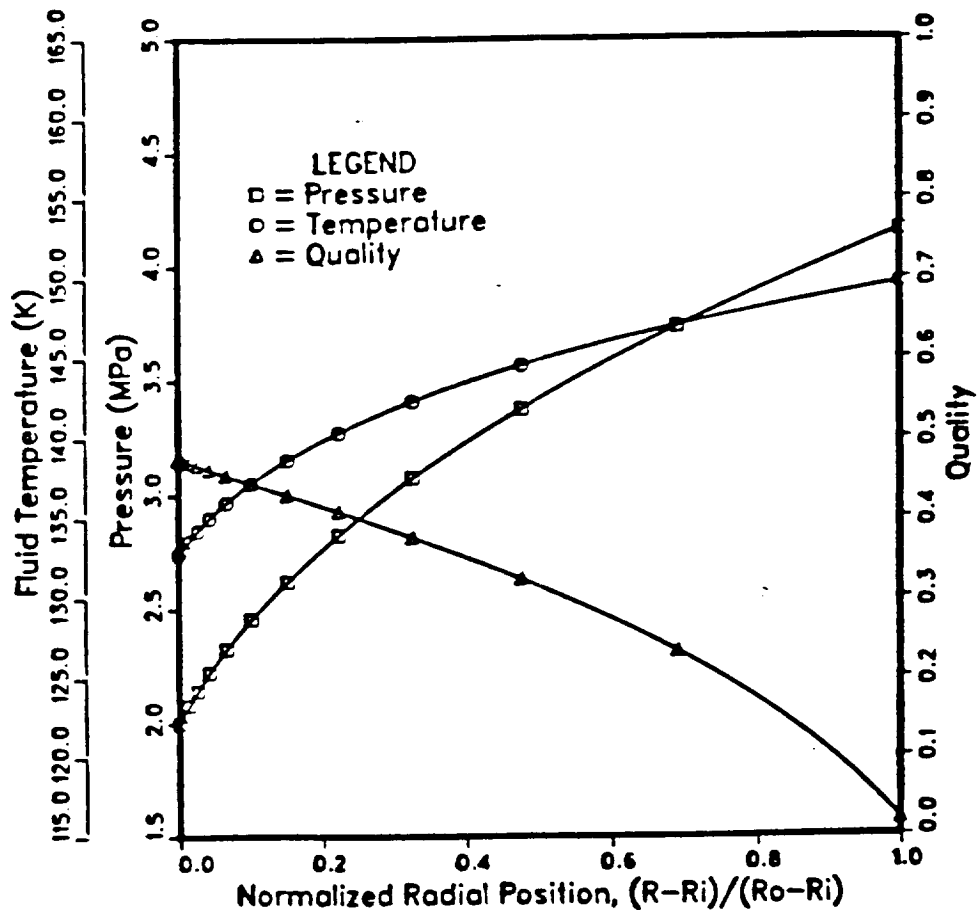


Figure 5-2: Fluid property profiles for an unchoked outside seal.

Sealed fluid is Oxygen

Film Thickness, $h = 1.00 \times 10^{-5}$ m

Shaft Speed, $\omega = 30,000$ RPM

Reservoir Temperature, $T_\infty = 150.0$ K

Reservoir Pressure, $P_\infty = 4.30$ MPa

Back Pressure, $P_b = 2.00$ MPa

Coning Angle, $\beta = 0.0$ radians

ORIGINAL PAGE IS
OF POOR QUALITY

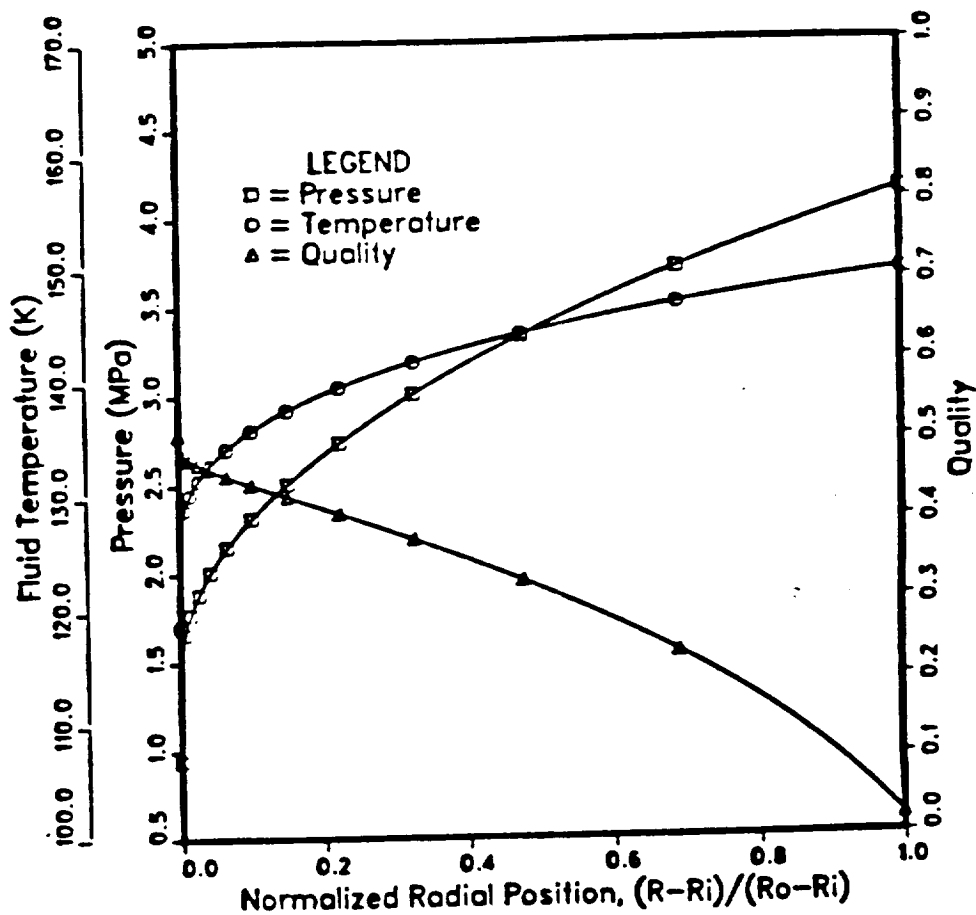


Figure 5-3: Fluid property profiles for a choked outside seal.

Sealed fluid is Oxygen

Film Thickness, $h = 1.00 \times 10^{-5}$ m

Shaft Speed, $\omega = 30,000$ RPM

Reservoir Temperature, $T_\infty = 150.0$ K

Reservoir Pressure, $P_\infty = 4.30$ MPa

Back Pressure, $P_b = 0.0$ MPa

Coning Angle, $\beta = 0.0$ radians

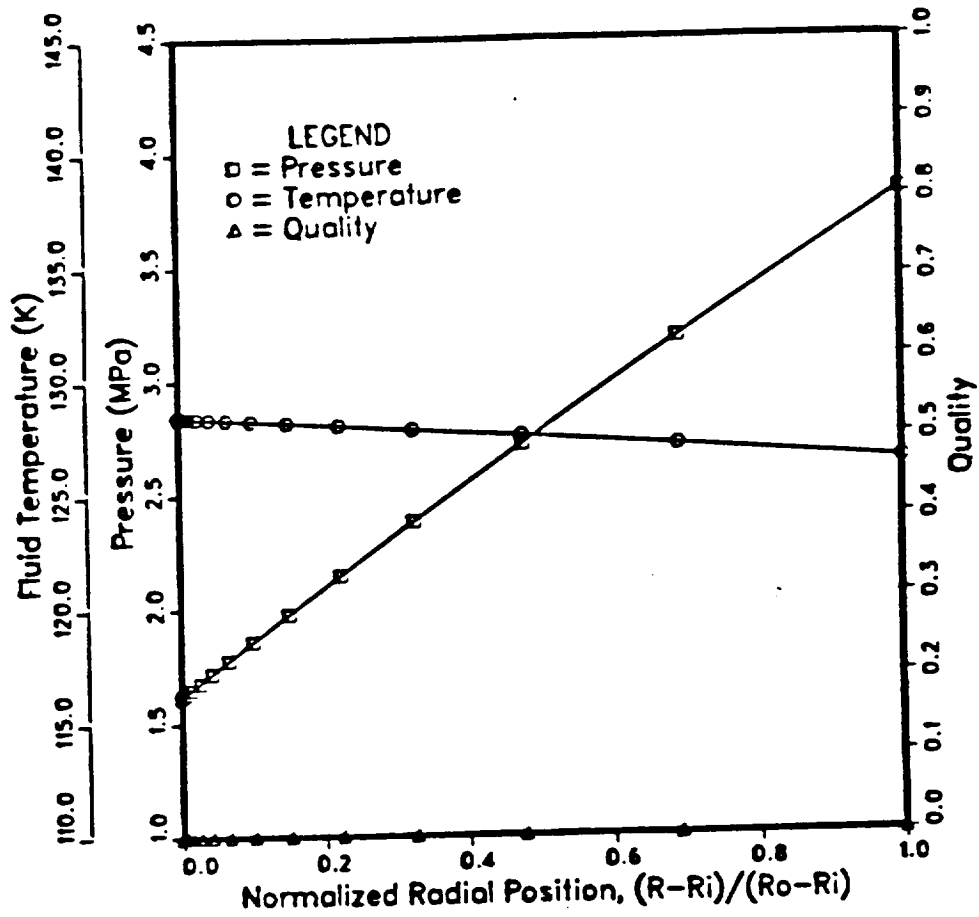


Figure 5-4: Fluid property profiles for an outside seal with all-liquid choked flow.

Sealed fluid is Oxygen

Film Thickness, $h = 1.00 \times 10^{-5}$ m

Shaft Speed, $\omega = 15,000$ RPM

Reservoir Temperature, $T_\infty = 125.0$ K

Reservoir Pressure, $P_\infty = 4.30$ MPa

Back Pressure, $P_b = 0.0$ MPa

Coning Angle, $\beta = 0.0$ radians

ORIGINAL PAGE IS
OF POOR QUALITY

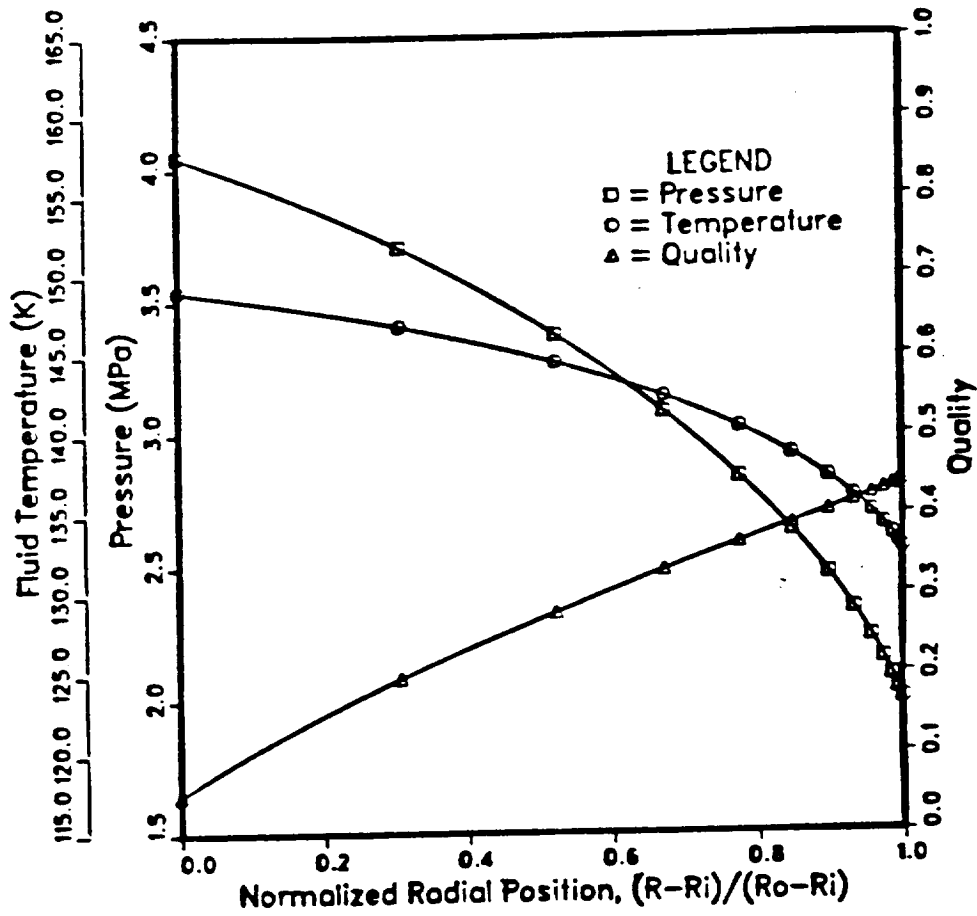


Figure 5-5: Fluid property profiles for an unchoked inside seal without cavitation.

Sealed fluid is Oxygen

Film Thickness, $h = 1.00 \times 10^{-5}$ m

Shaft Speed, $\omega = 30,000$ RPM

Reservoir Temperature, $T_\infty = 150.0$ K

Reservoir Pressure, $P_\infty = 4.30$ MPa

Back Pressure, $P_b = 2.00$ MPa

Coning Angle, $\beta = 0.0$ radians

Figure 5-6 shows the effects of rotation speed and film thickness on the leakage rate. As the speed is increased or the mean film thickness is reduced, more vapor is generated in the seal. Choking is promoted and the leakage is reduced. In addition, for an outside seal configuration, increasing the rotational speed increases the contribution of centrifugal inertia which retards the flow and so further reduces leakage. Similar results are obtained for all cases where the degree of subcooling in the upstream reservoir is moderate.

Figures 5-7 through 5-11 show the effects of film thickness and rotational speed on opening force for various values of initial subcooling. The interesting features of these curves can be largely explained by the competition of two opposing effects, the decrease of opening force by dissipation and the increase of the inlet pressure level through reduced inlet losses. In rough terms, dissipation and pressure loss promote boiling giving increased quality. If the mixture quality is increased, its density decreases. For a nearly constant area channel, the convective acceleration of the fluid is likely to be larger and the wall shear stresses increase. The pressure gradient must then be larger to offset these increases. Larger pressure gradients drive the pressure profile down so that the area under the pressure-radial position curve is reduced. The opening force is directly proportional to the area under that curve. On the other hand, boiling reduces the leakage rate and so decreases the inlet flow velocity. The inlet losses are reduced so that the inlet pressure level increases. This increase raises the pressure profile and so increases the opening force.

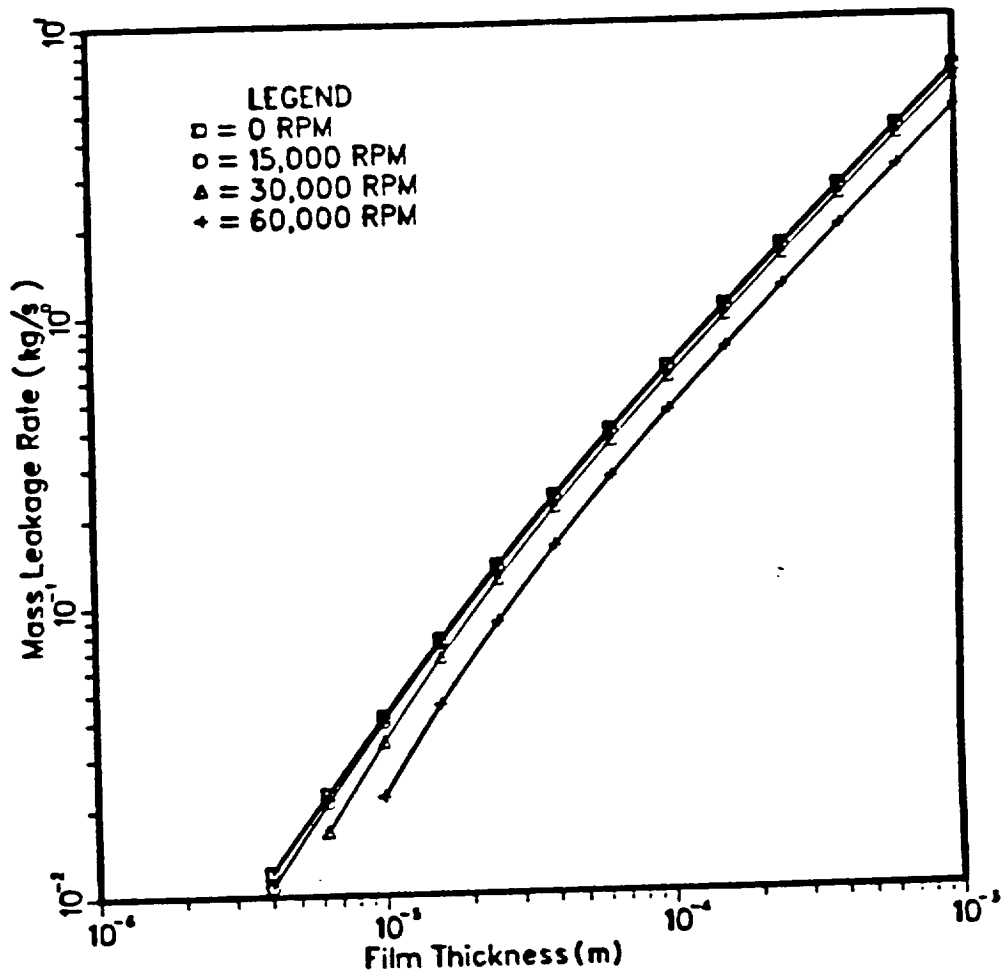


Figure 5-6: Effects of rotation rate and film thickness on leakage with 0.3 K subcooling.
 Sealed fluid is Oxygen
 Reservoir Temperature, $T_{\infty} = 150.0$ K
 Reservoir Pressure, $P_{\infty} = 4.3$ MPa
 Back Pressure, $P_b = 0.0$ MPa
 Coning Angle, $\beta = 0.0$ radians

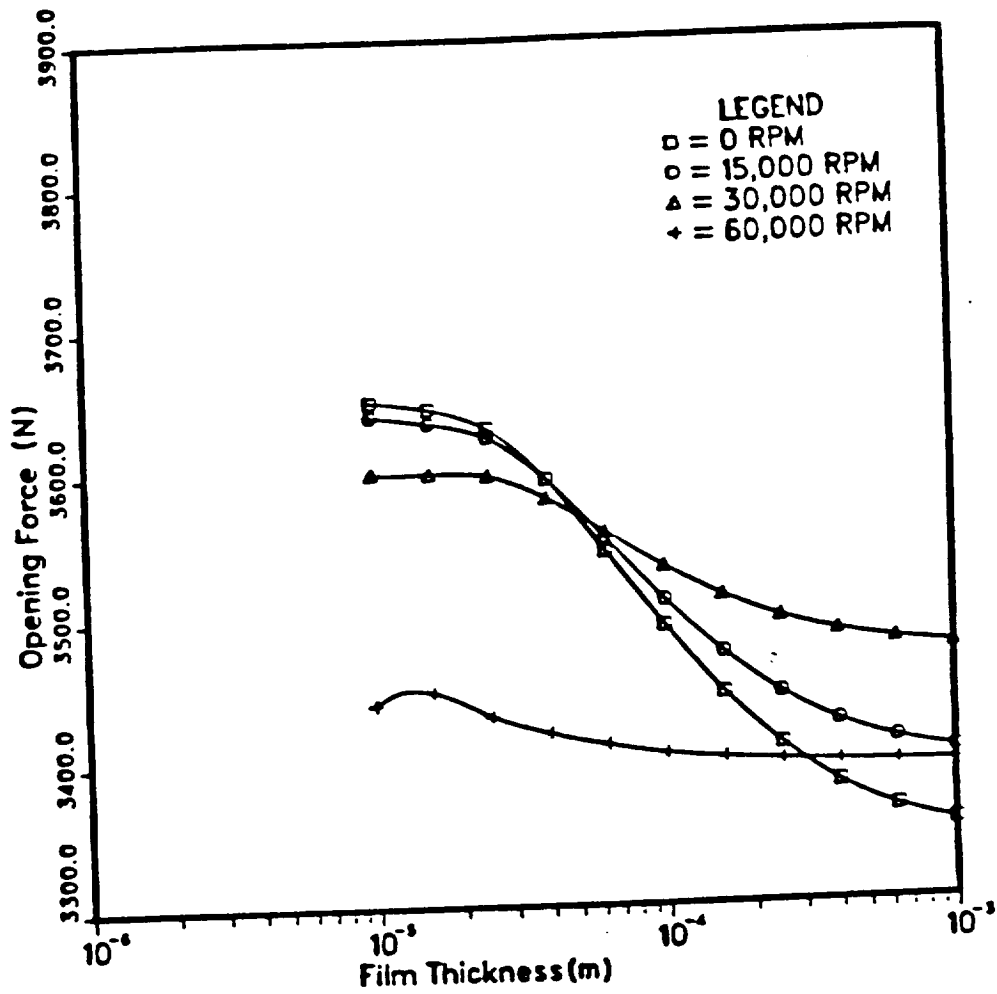


Figure 5-7: Effects of rotation rate and film thickness on leakage with 0.3 K subcooling.
 Sealed fluid is Oxygen
 Reservoir Temperature, $T_{\infty} = 150.0$ K
 Reservoir Pressure, $P_{\infty} = 4.3$ MPa
 Back Pressure, $P_b = 0.0$ MPa
 Coning Angle, $\beta = 0.0$ radians

ORIGINAL COPY
OF POOR QUALITY

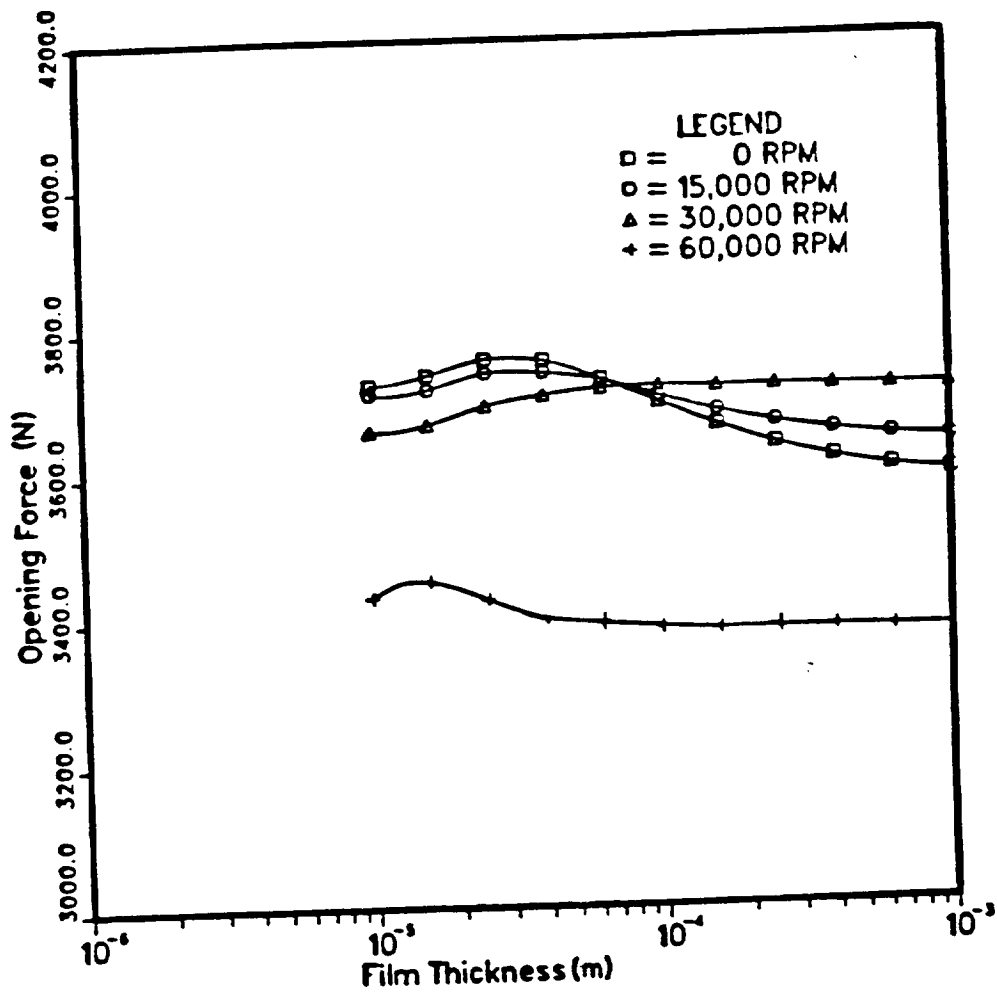


Figure 5-8: Effects of rotation rate and film thickness on opening force with 3.3 K subcooling.
Sealed fluid is Oxygen
Reservoir Temperature, $T_{\infty} = 147.0$ K
Reservoir Pressure, $P_{\infty} = 4.3$ MPa
Back Pressure, $P_b = 0.0$ MPa
Coning Angle, $\beta = 0.0$ radians

Figure 5-7 gives stiffness (i.e., force-displacement) curves for a slight initial subcooling. At large film thicknesses, the three lowest speeds give opening forces that increase with speed. This happens because the inlet loss reduction outweighs the force-reducing effects of dissipation. At small film thicknesses, inlet loss effects are small since the leakage rates are small. Then, the opposing, force-reducing effect dominates and the relative order of the opening forces with speed are reversed. Under the highest speed condition the leakage rates are yet smaller than the cases previous, so the force-reducing effect dominates the inlet loss effect even at large mean film thicknesses. The high speed stiffness curve then lies below the others over most values of film thickness. Note that the curves give positive stiffness (i.e., a negative slope for the force-displacement curve at the point of interest) for large film thicknesses, but give neutral or negative stiffness for small thicknesses.

Figure 5-8 gives stiffness curves for an initial subcooling somewhat greater than the case before it. Results are similar to those of the previous case, but the inlet loss effects are relatively less strong. The curves exhibit stiffnesses that are everywhere less positive than before.

Figure 5-11 gives stiffness curves for a still greater initial subcooling. The inlet loss effect is almost completely dominated. The stiffness curves are flat or slope upward, indicating seal collapse is imminent.

Figure 5-10 gives stiffness curves for yet a greater initial subcooling. The increase in leakage rate due to the suppression of the boiling is large enough to cause the inlet loss effect to again be dominant. This plot is similar to that shown in Figure 5-7.

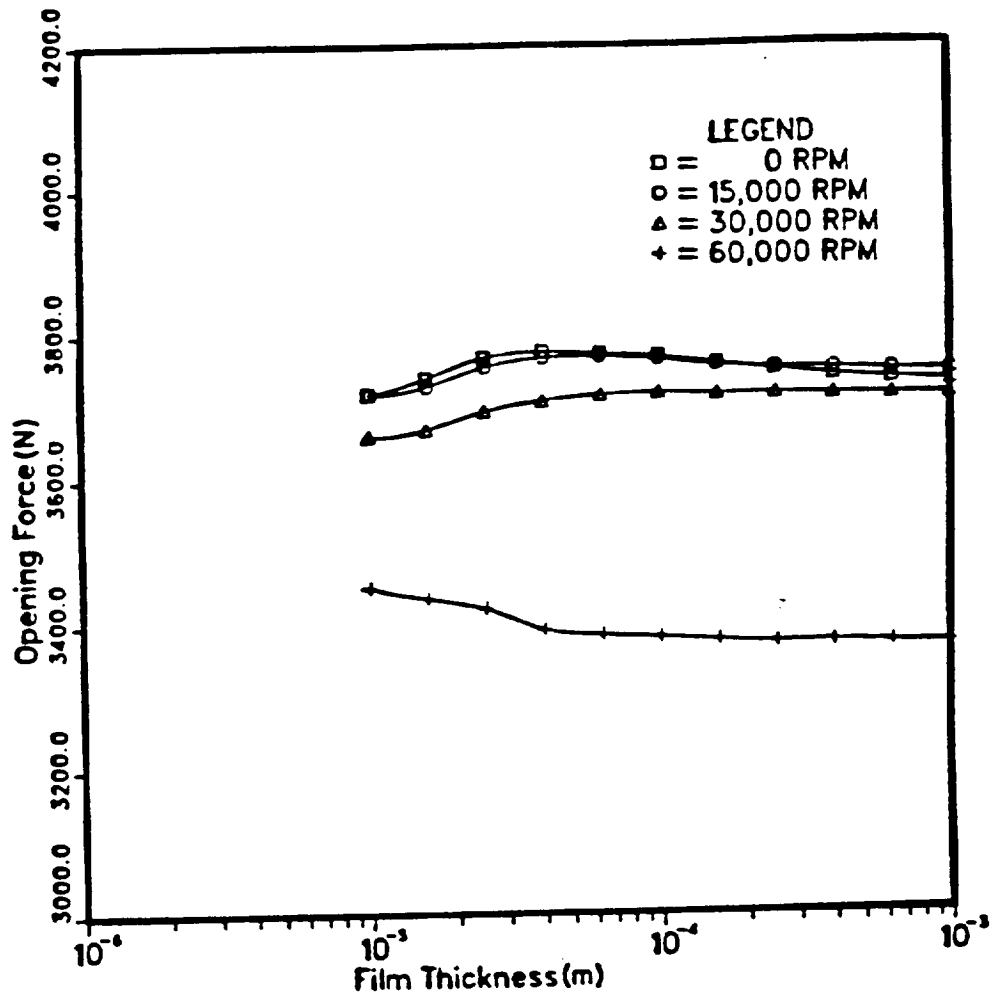


Figure 5-9: Effects of rotation rate and film thickness on opening force with 5.3 K subcooling.
 Sealed fluid is Oxygen.
 Reservoir Temperature, $T_{\infty} = 145.0$ K
 Reservoir Pressure, $P_{\infty} = 4.3$ MPa
 Back Pressure, $P_b = 0.0$ MPa
 Coning Angle, $\beta = 0.0$ radians

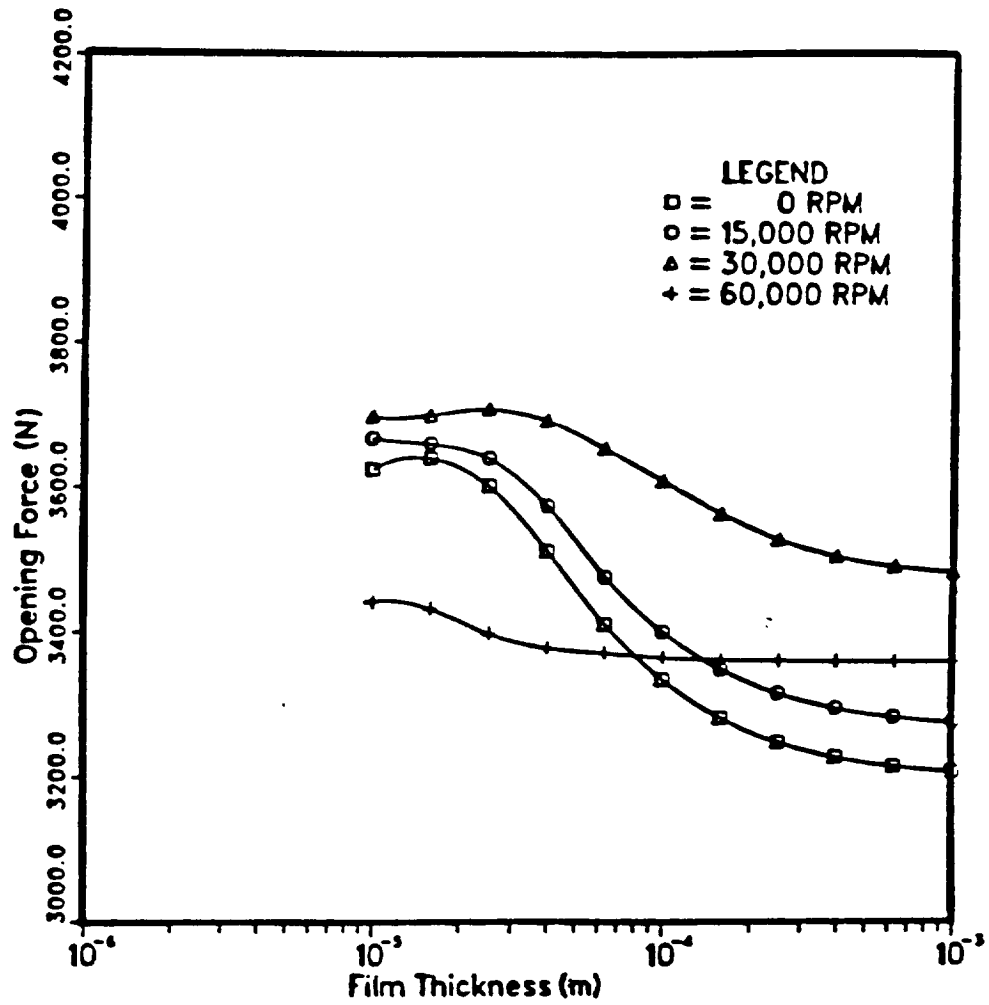


Figure 5-10: Effects of rotation rate and film thickness on opening force with 10.3 K subcooling.
 Sealed fluid is Oxygen.
 Reservoir Temperature, $T_{\infty} = 140.0$ K
 Reservoir Pressure, $P_{\infty} = 4.3$ MPa
 Back Pressure, $P_b = 0.0$ MPa
 Coning Angle, $\beta = 0.0$ radians

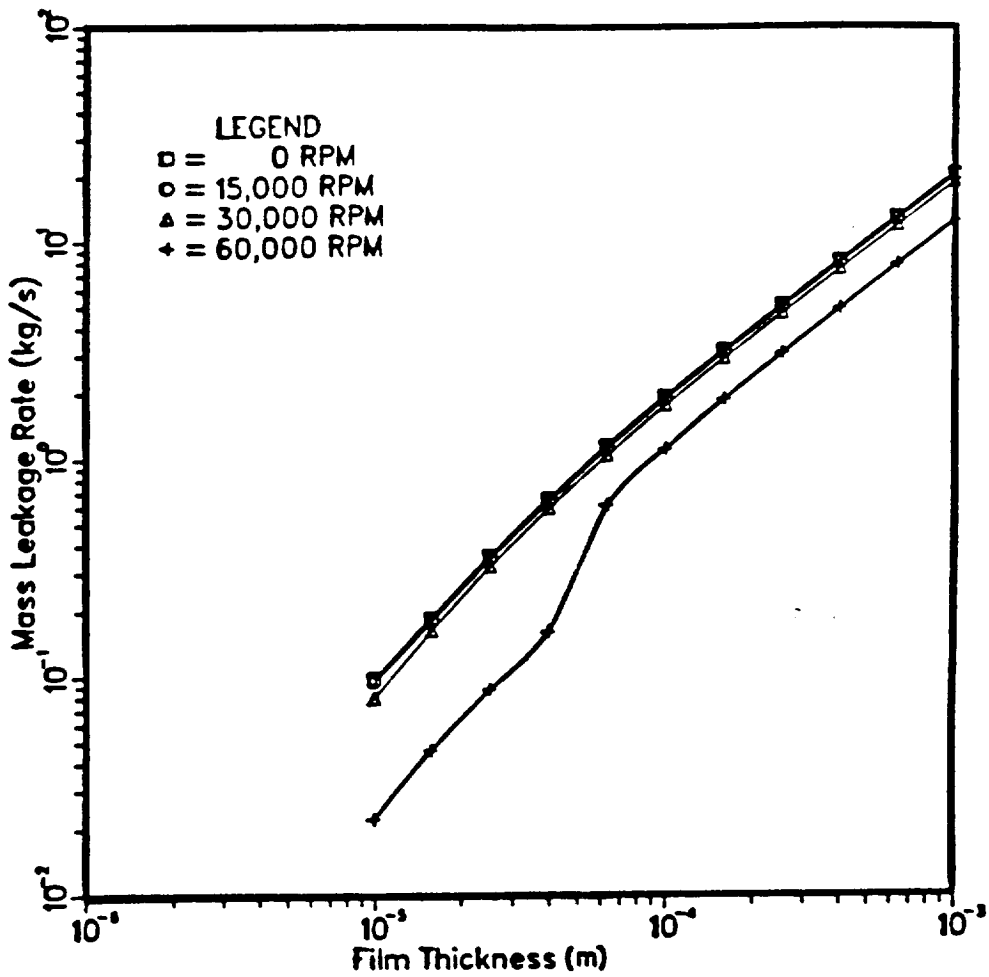


Figure 5-11: Effects of rotation rate and film thickness on leakage rate with 50.3 K subcooling.
 Sealed fluid is Oxygen.
 Reservoir Temperature, $T_{\infty} = 100.0$ K
 Reservoir Pressure, $P_{\infty} = 4.3$ MPa
 Back Pressure, $P_b = 0.0$ MPa
 Coning Angle, $\beta = 0.0$ radians

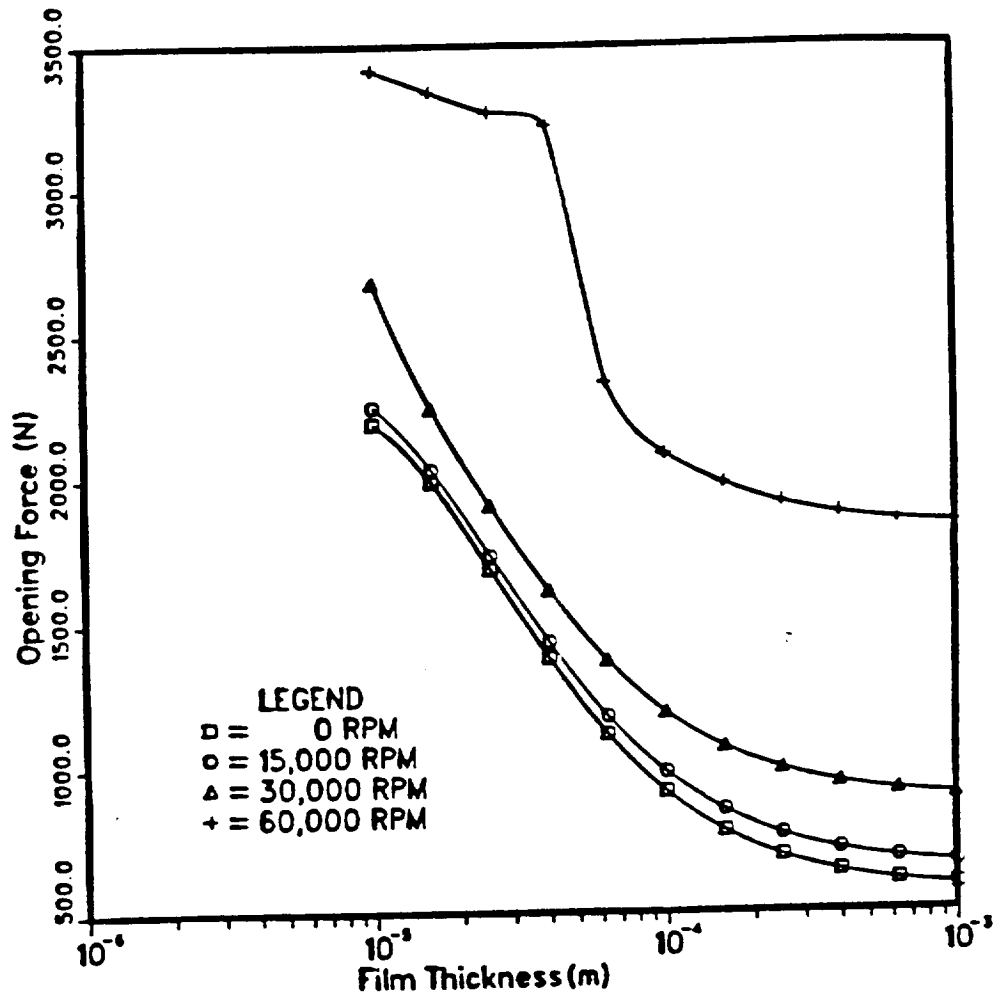


Figure 5-12: Effects of rotation rate and film thickness on opening force with 50.3 K subcooling.
 Sealed fluid is Oxygen.
 Reservoir Temperature, $T_{\infty} = 100.0$ K
 Reservoir Pressure, $P_{\infty} = 4.3$ MPa
 Back Pressure, $P_b = 0.0$ MPa
 Coning Angle, $\beta = 0.0$ radians

Figures 5-11 and 5-12 give leakage rate and stiffness information for a very high degree of initial subcooling. Whereas in the previous cases the flow was in the two-phase regime upon entering the seal or entered as a liquid but became two-phase soon after, in these plots the flow remains liquid throughout much of the flow passage. In fact, the flow is all liquid for all film thicknesses shown for the lowest three speed conditions. An abrupt reduction in leakage under the highest speed condition in Figure 5-12 occurs when the rate of dissipation is just sufficient to boil the fluid within the body of the seal. The stiffness curves for the lowest three speeds in Figure 5-12 exhibit strong positive stiffness due to the dominance of the inlet loss effect. The stiffness curve for the highest speed in that plot undergoes an abrupt change at the outset of boiling and so has a different character than the others.

Figures 5-13 and 5-14 give leakage information for a constant speed of 30,000 RPM for various film thicknesses and degrees of subcooling. Figure 5-13 shows that the leakage rates for a highly subcooled initial state are much higher than those for moderate subcooling. In Figure 5-14, the curve of the highest degree of subcooling shows strong positive stiffness. In that curve, the flow was pure liquid throughout the body of the seal so the effect of the inlet losses were dominant. Note that the opening forces for the large film thicknesses is much lower than their moderately subcooled case counterparts. Among the moderate subcooling cases, the relative order of opening force in terms of degree of subcooling shifts with film thickness for reasons similar to those given for the curve shifts in speed in previous examples. Most importantly, this plot shows that small changes in the degree of subcooling in the upstream reservoir can drastically affect the seal behavior changing the stiffness from positive to neutral or negative at a given mean film thickness.

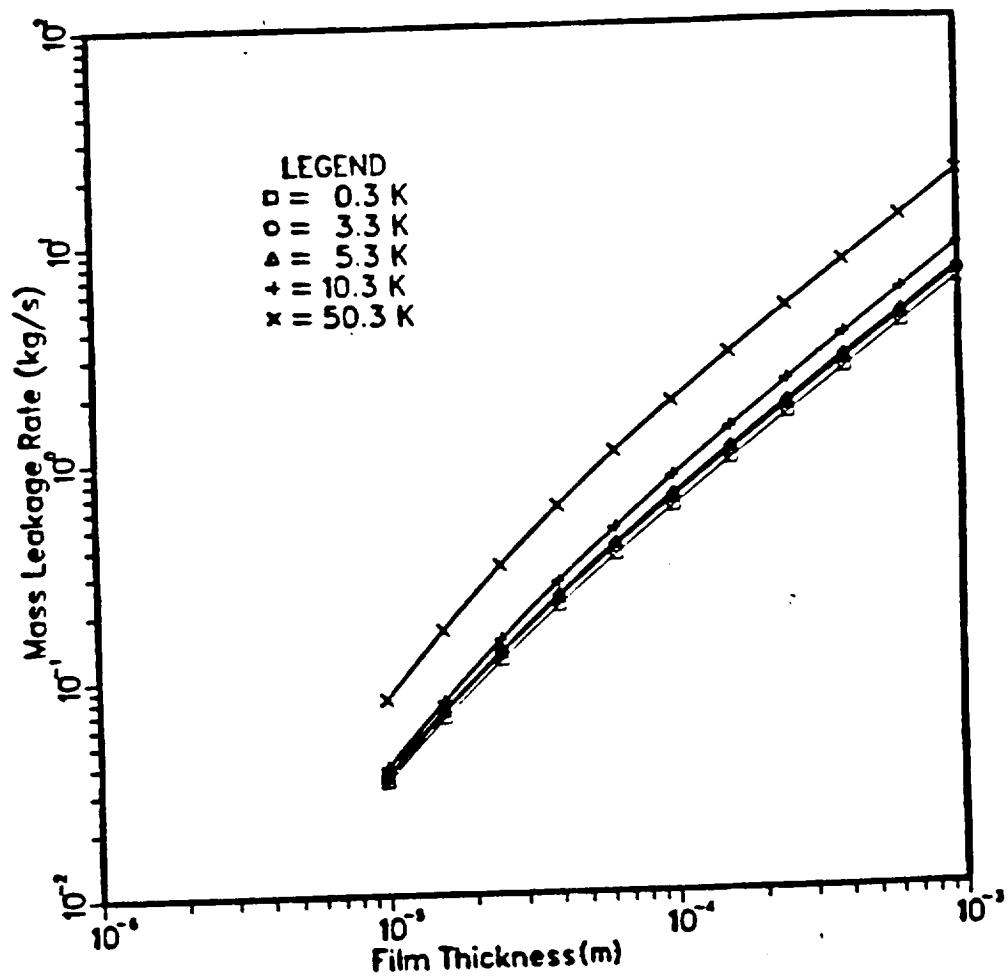


Figure 5-13: Effects of film thickness and subcooling on leakage rate.

Sealed fluid is Oxygen.

Rotation Speed, $\omega = 30,000$ RPM

Reservoir Pressure, $P_{\infty} = 4.3$ MPa

Back Pressure, $P_b = 0.0$ MPa

Coning Angle, $\beta = 0.0$ radians

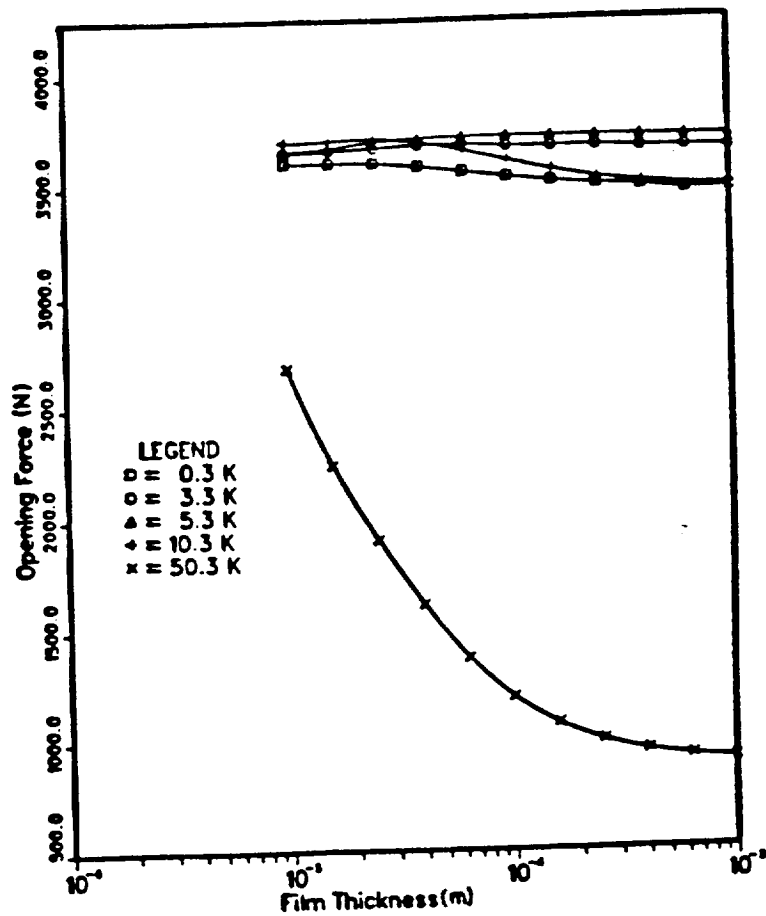


Figure 5-14: Effects of film thickness and subcooling on opening force.

Sealed fluid is Oxygen.

Rotation Speed, $\omega = 30,000$ RPM

Reservoir Pressure, $P_{\infty} = 4.3$ MPa

Back Pressure, $P_b = 0.0$ MPa

Coning Angle, $\beta = 0.0$ radians

Figures 5-15 and 5-16 give leakage rates and opening forces for a seal with various angles of coning. Note that coning not only gives a small decrease in leakage, but also gives the seal a substantial positive stiffness over the entire range of film thicknesses.

Figures 5-17 and 5-18 give leakage and stiffness information with water as the sealed fluid under various degrees of subcooling. The character of the water seal behavior is similar to that of the cryogenic oxygen seal. Note that the force-displacement curves for the two highest degrees of initial subcooling show substantial positive stiffness. For those curves, under the given operating conditions, the flow was all-liquid throughout the seal for every film thickness shown.

Consideration of some trial parametric studies indicate the following salient features of turbulent face seal behavior:

- Vapor production through pressure drop and viscous dissipation within the seal promotes choking and reduces the leakage rate.
- Subcooling the incoming fluid partially negates the effects of dissipation and pressure drop on leakage.
- Centrifugal inertia effects tend to retard flow in outside seals and reduce leakage. In inside seals, the opposite is true.
- All-liquid choked flow may occur at low rotational speeds and high degrees of inlet subcooling. The leakage rates associated with this type of choked flow may be significantly larger than those seen in two-phase flows.
- The interplay of the effects of dissipation, subcooling, and rotational speed is complicated and may give rise to peculiar effects. The character of the seal opening force and stiffness may change radically for small changes in the operating parameters.

- Unexpected positive stiffness (i.e., a force-displacement relation that gives a restoring force) is found in all-liquid flow situations. Decreasing the mean film thickness reduces the inlet losses and so increases the opening force.
- Coning has a beneficial effect on seal leakage and promotes positive seal stiffness.

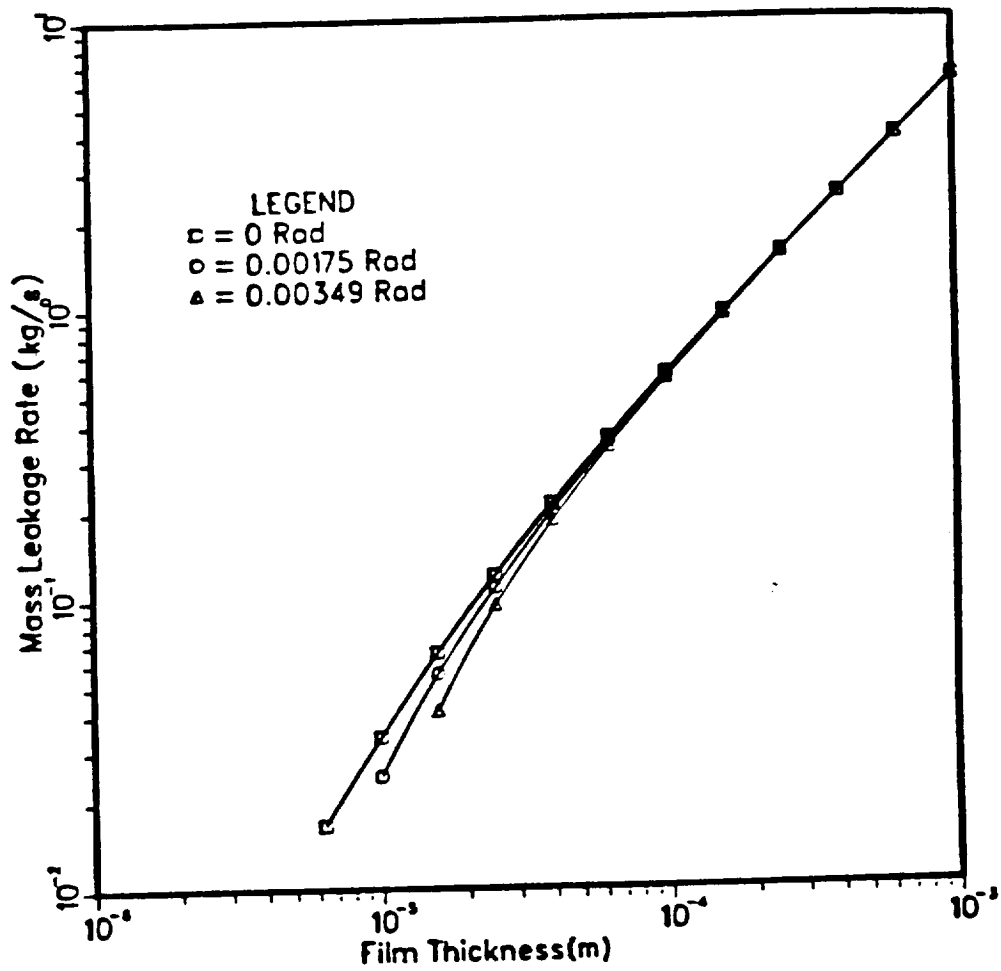


Figure 5-15: Effects of film thickness and coning on leakage.

Sealed fluid is Oxygen.

Rotation Speed, $\omega = 30,000$ RPM
 Reservoir Temperature, $T_{\infty} = 150.0$ K
 Reservoir Pressure, $P_{\infty} = 4.3$ MPa
 Back Pressure, $P_b = 0.0$ MPa

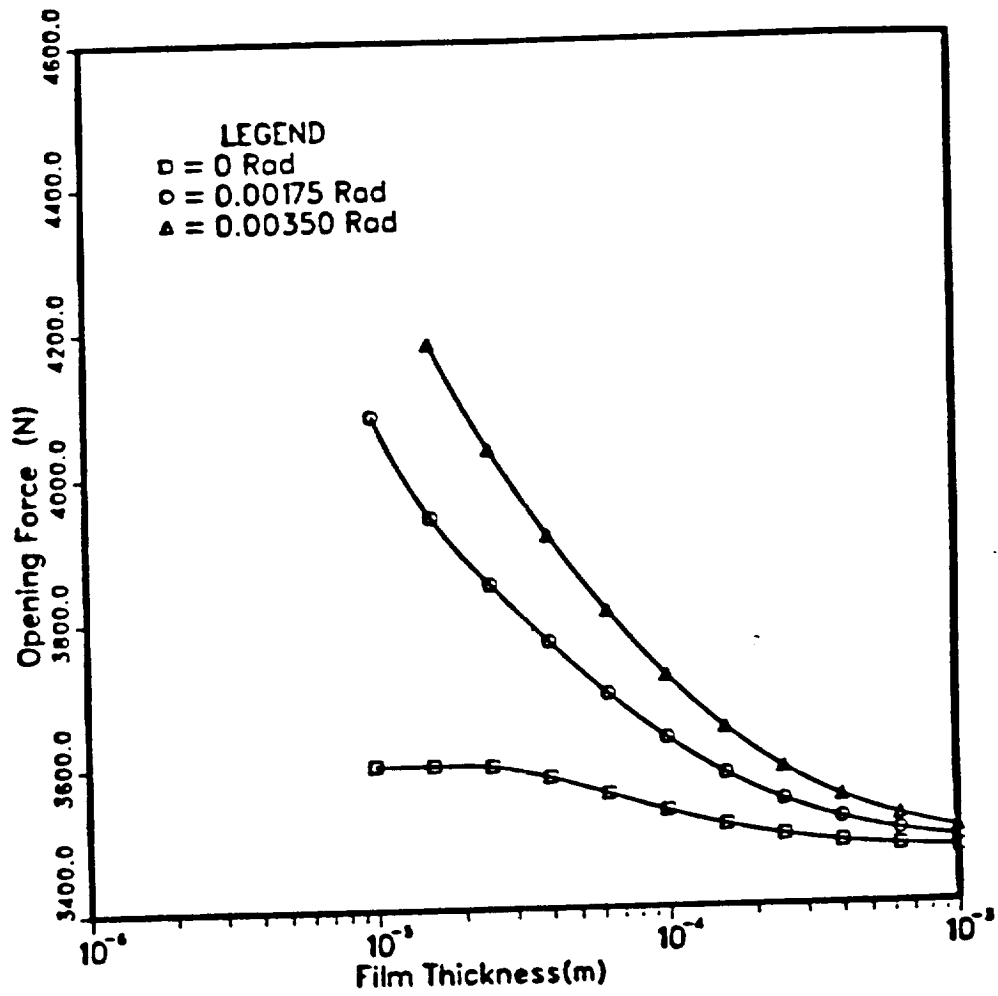


Figure 5-16: Effects of film thickness and coning on opening force.

Rotation Speed, $\omega = 30,000$ RPM
 Reservoir Temperature, $T_{\infty} = 150.0$ K
 Reservoir Pressure, $P_{\infty} = 4.3$ MPa
 Back Pressure, $P_b = 0.0$ MPa
 Coning Angle, $\beta = 0.0$ Radians

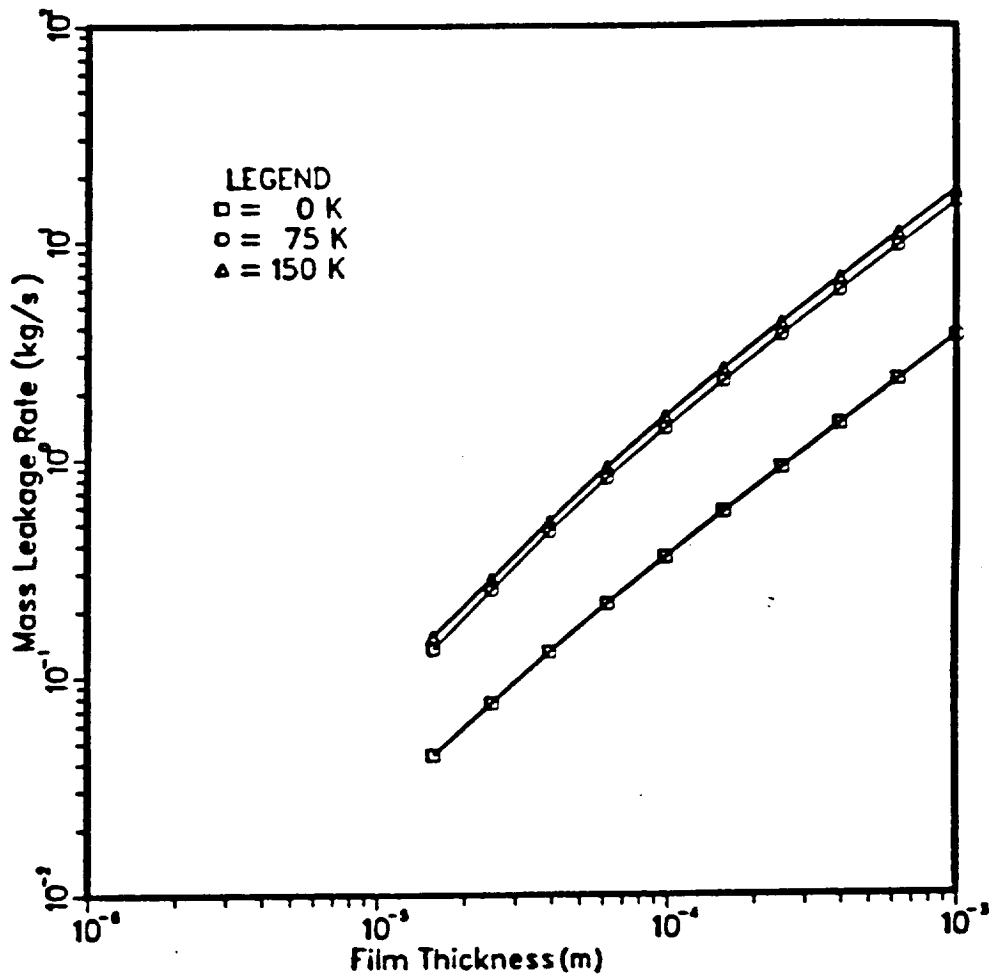


Figure 5-17: Effects of film thickness and subcooling on leakage.

Sealed fluid is Water

Rotation Speed, $\omega = 2,500$ RPM
 Reservoir Pressure, $P_{\infty} = 3.16$ MPa
 Back Pressure, $P_b = 0.100$ MPa
 Coning Angle, $\beta = 0.0$ Radians

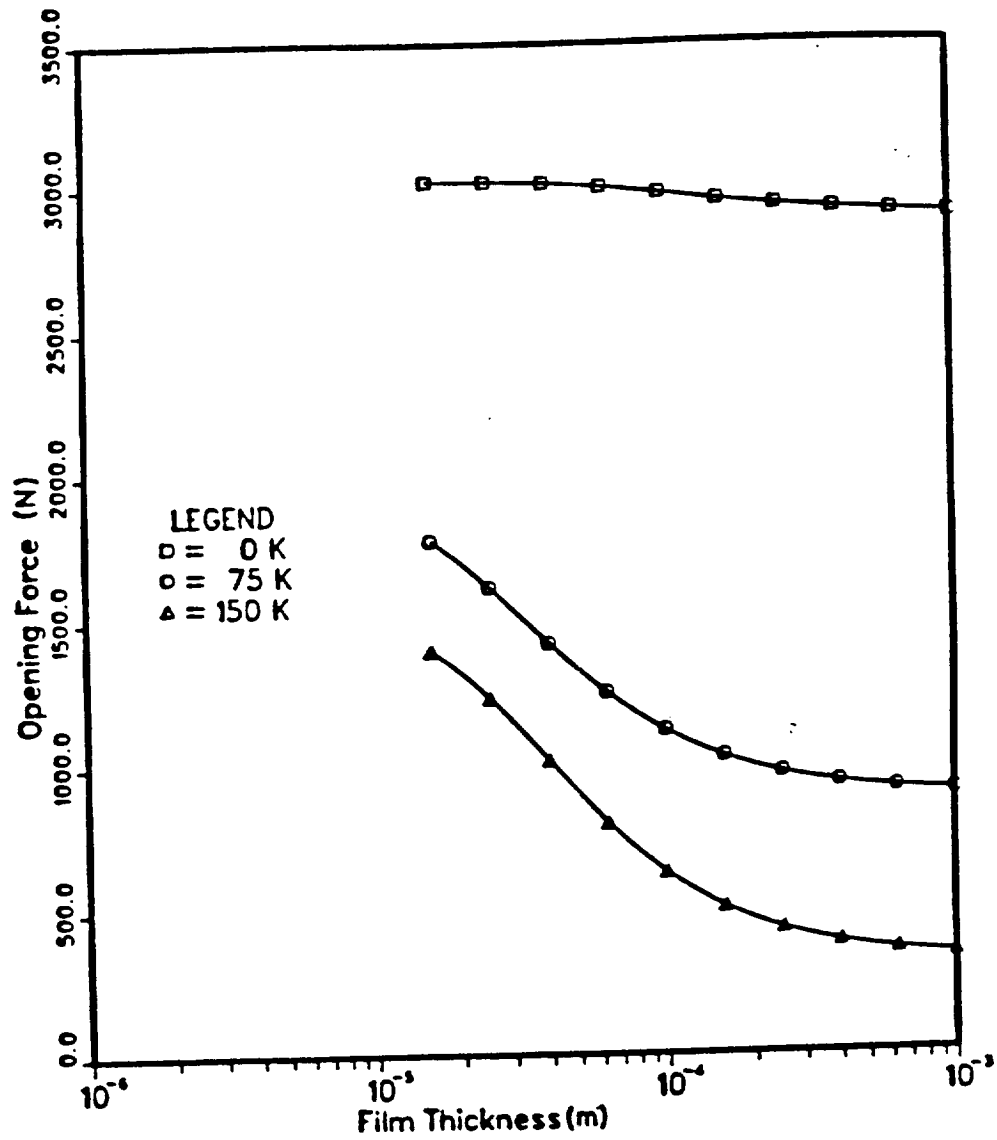


Figure 5-18: Effects of film thickness and subcooling on opening force.

Rotation Speed, $\omega = 2,500$ RPM
 Reservoir Pressure, $P_{\infty} = 3.16$ MPa
 Back Pressure, $P_b = 0.100$ MPa
 Coning Angle, $\beta = 0.0$ Radians

CHAPTER 6

LEAKAGE IN TWO-PHASE ANNULAR SEALS

6.1 Introduction

The quasi-steady analysis of the turbulent annular seal roughly parallels that of the radial face seal. Upon applying the integral approach to the basic equations, equations similar to those governing the face seal flow are obtained. The "jump" conditions relating the reservoir thermodynamic state to the inlet state are identical with those of the previous problem and the general solution method proceeds as before. Moreover, leakage rate solutions to annular seals will be seen to have the same general character as those for radial face seals.

This seal will be idealized as having polished working surfaces which may be considered hydraulically smooth. Further, the seal shaft will be taken to be centered in the bearing surface so that the geometry under study is axisymmetric. For reference, a schematic diagram of a typical annular seal is given in Figure 6-1. Small displacements of the shaft from this centered position are not expected to change the leakage greatly so that the leakage characteristics of annular seals under real operating conditions may be estimated reasonably well by the present model. Of course, no forces lateral to the long axis of the shaft will be developed if the shaft is in its centered position.

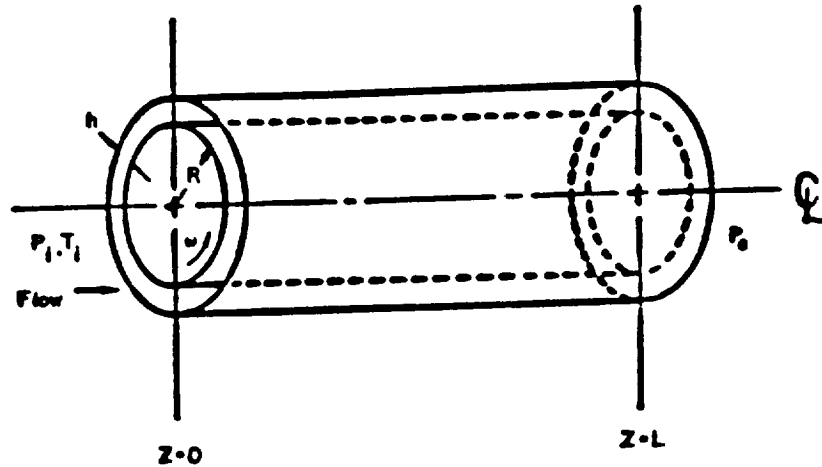


Figure 6-1: Annular seal geometry (not to scale).

It will be seen that the choking, a phenomenon which limits the leakage rate, is sensitive to the rate of internal heat generation through viscous shear and to the inlet thermodynamic state. The previous studies of Childs, et al. [127, 128, 129] do not consider the possibilities of two-phase flow, nor do they account for internal heat generation. This analysis then represents a more complete accounting of the important effects influencing the leakage rate than was previously done.

6-2 Specialized Equations for Liquid, Two-Phase, and Vapor Flow

Dropping the terms dependent on the circumferential location from the basic equations given in section 4-2 gives the following:

Continuity:

$$2\pi R h G = m$$

(6-1)

Axial Momentum:

$$G \frac{du}{dz} + \frac{dp}{dz} + \frac{2\tau_{rz}}{h} = 0 \quad (6-2)$$

Adiabatic Energy Equation:

$$\frac{di}{dz} + \frac{d}{dz} \left(\frac{u^2}{2} \right) = \frac{R\omega}{Gh} \tau_{r\theta} |_R \quad (6-3)$$

It should be noted that the continuity equation requires no specialization; it holds in its present form regardless of the phase of the flowing fluid. Also, the circumferential momentum equation is trivially satisfied as before. The mean circumferential velocity is assumed to be fully developed throughout the interior of the seal with the value of $w = \omega R/2$ since the film thickness, and hence the circumferential flow development region, are very small compared to the other characteristic dimensions of the seal.

Liquid Flow

As before, the liquid density is taken as a constant with a value corresponding to the density of saturated liquid at the same temperature. Equation (6-1) then implies that the axial velocity is constant. This affords further simplification of the axial momentum equation (6-2) which becomes:

$$\frac{dp}{dz} = - \frac{2}{h} \tau_{rz} \quad (6-4)$$

and of the energy equation (4-2-3) which becomes:

$$\frac{di}{dz} = \frac{R\omega}{Gh} \tau_{r\theta} |_R \quad (6-5)$$

These equations are always well behaved, giving a monotonically decreasing pressure and a monotonically increasing enthalpy. Since the liquid compressibility is neglected, the sonic speed for the liquid is infinite. Normal choking, where the fluid velocity reaches the acoustic wave speed in the medium, then can not be predicted from the equations above. It should be noted that the acoustic wave speeds for most liquids are so high that choking in a mode as described above is very seldom experienced.

Liquid - Vapor Flow

The two-phase flow through the seal is assumed to be homogeneous so that the fluid properties are constant through the film. The axial derivatives of quality and enthalpy are expressed in terms of the axial derivative of pressure as was done earlier. The axial velocity in equation (6-2) and (6-3) may be expressed in terms of the mass velocity, G . Using this and the relations among the saturation properties, these equations may be solved for the axial derivative of pressure explicitly, assuming G is known:

$$\frac{dp}{dz} = - \frac{1}{h(1-\phi)} \left[2 \left(1 + \frac{i_{fg}}{G^2 v_{fg}} \right) \tau_{rz} + \left(\frac{R\omega}{Gv} \right) \tau_{r\theta} \right] \quad (6-6)$$

where,

$$\phi = \frac{1}{v} \frac{\partial i}{\partial p} |_{\lambda} - \frac{(1 + G^2 \partial v / \partial p |_{\lambda}) i_{fg}}{G^2 v_{fg}}$$

and, the axial gradient of mixture quality may be simply expressed in terms of the pressure gradient as:

$$\frac{d\lambda}{dz} = - \frac{2\tau_{rz}}{hG^2 v_{fg}} - \frac{(1 + G^2 \partial v / \partial p |_{\lambda})}{G^2 v_{fg}} \frac{dp}{dz} \quad (6-7)$$

Since the temperature is only a function of pressure at saturation, the following is true:

$$\frac{di}{dz} = \left(\frac{di_f}{dP} + \lambda \frac{di_{fg}}{dP} \right) \frac{dp}{dz} + i_{fg} \frac{d\lambda}{dz} \quad (6-8)$$

where the pressure gradient is known from (6-6) and the quality gradient is known from (6-7). Note that equations (6-6) and (6-8) have a singularity at conditions where ϕ equals unity. It is seen that the equations governing two-phase flow in this case are very similar to those of the face seal case and that the nature of their singularities are also similar. Thus, the two-phase, turbulent annular seal can exhibit normal and all-liquid choked behavior much like that of the radial face seal.

All - Vapor Flow

If one assumes an ideal gas with constant specific heats, the continuity, axial momentum, energy, and state equations may be combined in a simple way to give the gradients of the pressure and enthalpy explicitly. The basic equations adapted for vapor flow are then:

$$\frac{dp}{dz} = \frac{1}{1 - M^2} \left(- [2/h] [1 + (\gamma - 1) M^2] \tau_{rz} - (\gamma - 1) \frac{R\omega M^2}{Gh\nu} \tau_{r\theta} \right) \quad (6-9)$$

and,

$$\frac{di}{dz} = \frac{1}{1 + (\gamma - 1) M^2} \left(\frac{R\omega}{Gh\nu} \tau_{r\theta} + \gamma M^2 \nu \frac{dp}{dz} \right) \quad (6-10)$$

This is a well known one-dimensional gas flow problem with heating and friction. Here, M is the Mach number.

6.3 Numerical Examples and Discussion

A nominal design for the interstage seal of the Space Shuttle Main Engine High Pressure Oxidizer Turbopump is taken to be:

Shaft Radius, $R = 0.0325$ m
Seal Length, $L = 0.0260$ m
Radial Clearance, $h = 1.74 \times 10^{-4}$ m

and the range of operating conditions is taken as;

Rotation Speed, $\omega = 20,000$ to $30,000$ RPM

Reservoir Temperature, $T_{\infty} = 116$ to 143 K
Reservoir Pressure, $P_{\infty} = 2.75$ to 4.83 MPa
Back Pressure, $P_b = 0$ to 0.1 MPa

These values will be used unless stated otherwise. The flow inlet is taken to be square-edged with a nominal inlet loss coefficient of 0.5.

Figure 6-2 shows temperature, pressure, and quality profiles for a seal under unchoked conditions in the two-phase regime. Although the back pressure in this instance is out of the design range, it is useful to present this case for comparison with others. Here, the reservoir fluid is sub-cooled by 1 K. Note that boiling had been initiated at the inlet so that the quality there was non-zero. The profiles in this case are smooth with moderate gradients throughout the seal. The leakage rate in this case was 0.575 kg/s.

Figure 6-3 shows the profiles for choked conditions in the two-phase regime. The reservoir fluid is sub-cooled by 5 K and boiling in this case occurs well inside the seal. Discontinuities in the slopes of the pressure and temperature profiles occur at the location where boiling begins. Unlike the case before it, the pressure gradient at the exit has an extremely large negative value. The leakage rate in this case was 0.686 Kg/s.

Figure 6-4 shows the profiles for the anomalous case of all-liquid choked flow. The reservoir fluid is sub-cooled by 24 K. The profiles shown are nearly straight lines and the leakage rate is 1.34 Kg/s, almost twice that of the other cases. Although the fluid exit velocity is much lower than the sonic speed of the liquid, the mass flow is at its maximum value and is independent of back pressure, provided it is below a critical value.

The following three numerical examples are studies of the effects of various parameters on the leakage rate. The geometry and operating conditions will be taken to be the same as in the case presented previously in Figure 6-3 unless stated otherwise.

Figure 6-5 shows the dependence of leakage rate on the length to radius ratio on the shaft rotational speed. As either rotation speed or path length increase, more heat is dumped into an element of fluid as it flows through the seal. This increased heating brings about increased vapor generation. The mixture density is reduced, and the axial velocity is increased. Compressibility effects, however, limit the flow so that the net mass leakage rate decreases.

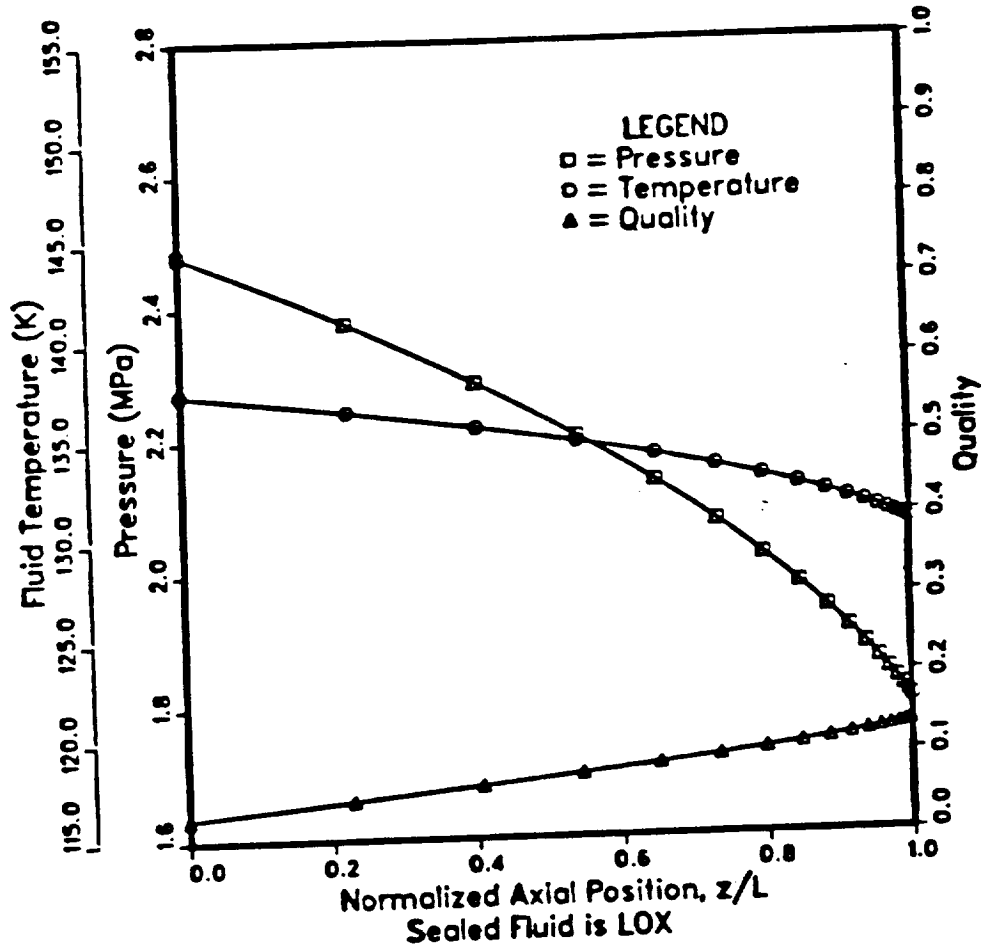


Figure 6-2: Unchoked two-phase flow through the seal.

Shaft Radius, $R = 0.0325$ m

Seal Length, $L = 0.026$ m

Radial Clearance, $h = 1.74 \times 10^{-4}$ m

Shaft Rotation Speed, $\omega = 30,000$ RPM

Reservoir Temperature, $T_{\infty} = 139.0$ K

Reservoir Pressure, $P_{\infty} = 2.79$ MPa

Back Pressure, $P_b = 1.80$ MPa

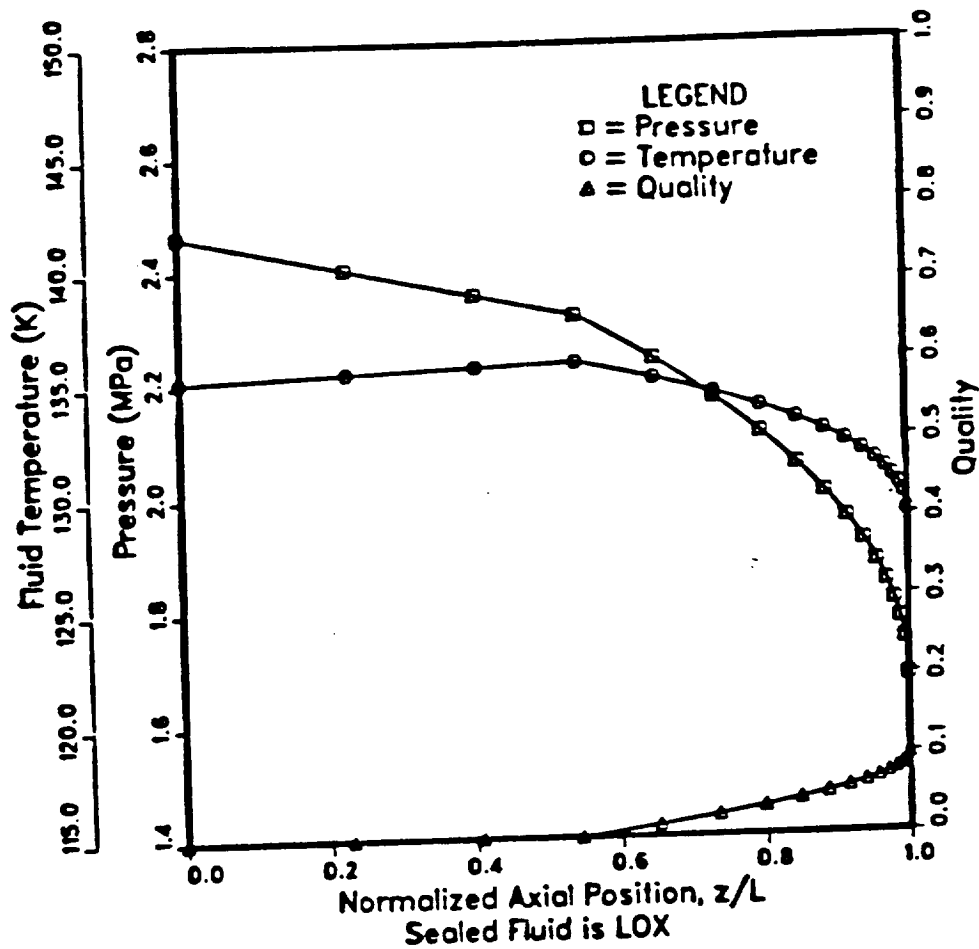


Figure 6-3: Choked two-phase flow through the seal.

Shaft Radius, $R = 0.0325$ m

Seal Length, $L = 0.026$ m

Radial Clearance, $h = 1.74 \times 10^{-4}$ m

Shaft Rotation Speed, $\omega = 30,000$ RPM

Reservoir Temperature, $T_{\infty} = 135.0$ K

Reservoir Pressure, $P_{\infty} = 2.79$ MPa

Back Pressure, $P_b = 0$ MPa

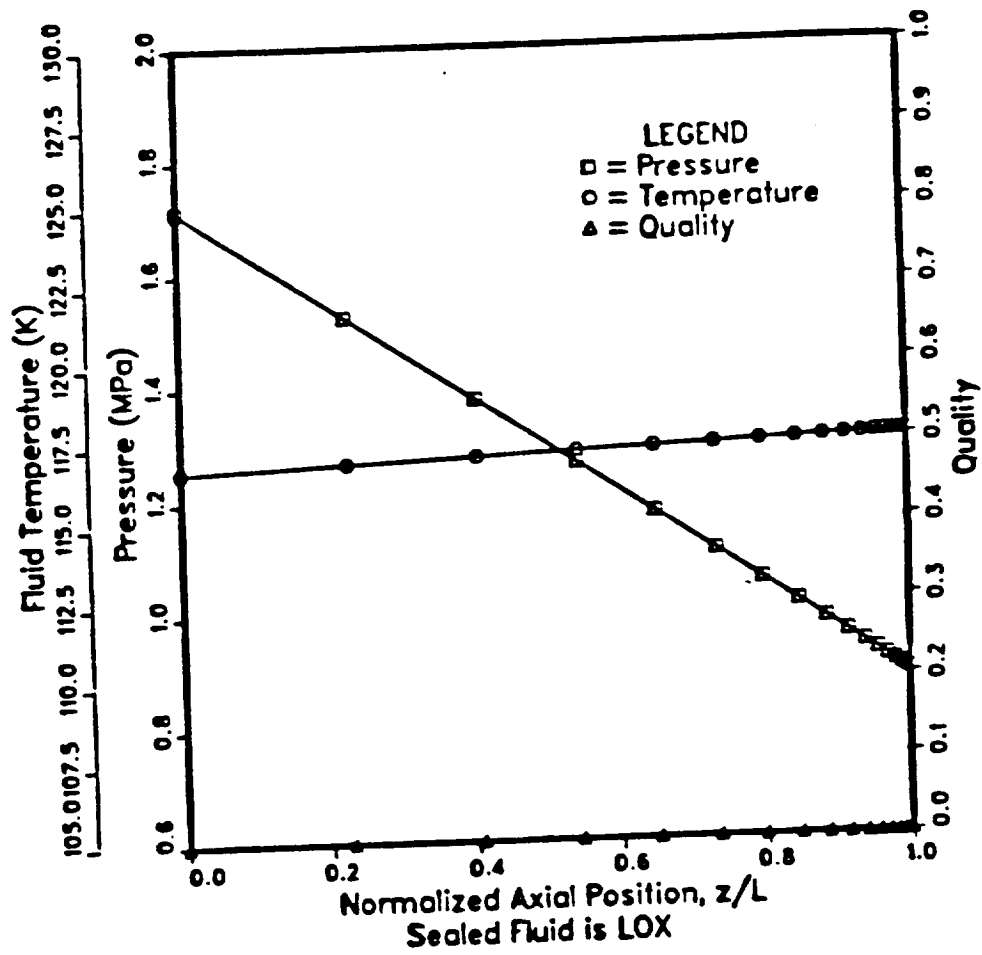


Figure 6-4: Choked all-liquid flow through the seal.
 Shaft Radius, $R = 0.0325$ m
 Seal Length, $L = 0.026$ m
 Radial Clearance, $h = 1.74 \times 10^{-4}$ m
 Shaft Rotation Speed, $\omega = 30,000$ RPM
 Reservoir Temperature, $T_{\infty} = 116.0$ K
 Reservoir Pressure, $P_{\infty} = 2.79$ MPa
 Back Pressure, $P_b = 0$ MPa

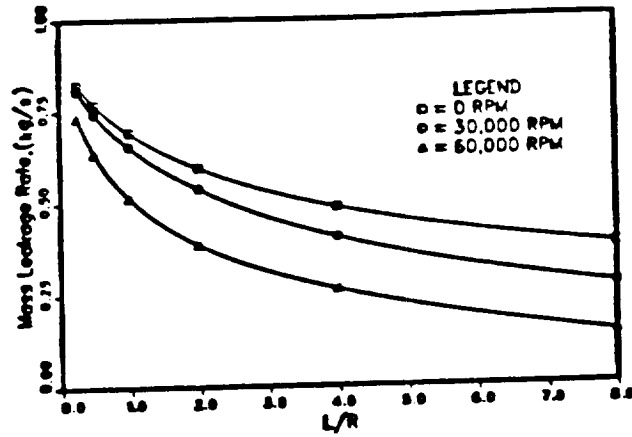


Figure 6-5: Effect of L/R ratio and rotation speed on leakage.

Shaft Radius, $R = 0.0325$ m

Radial Clearance, $h = 1.74 \times 10^{-4}$ m

Shaft Rotation Speed, $\omega = 30,000$ RPM

Reservoir Temperature, $T_{\infty} = 135.0$ K

Reservoir Pressure, $P_{\infty} = 2.79$ MPa

Back Pressure, $P_b = 0$ MPa

Figure 6-6 shows the dependence of leakage rate on the radial clearance and on the shaft rotational speed. Small film thicknesses and high rotational speeds promote high rates of heat generation by viscous dissipation. As in the previous example, the leakage rates associated with high rates of heat generation are small.

Figure 6-7 shows the dependence of leakage rate on the degree of sub-cooling in the upstream reservoir and on the shaft rotational speed. Sub-cooling at the upstream reservoir partially negates the effect of the viscous heat generation in the film and so brings about higher leakage rates.

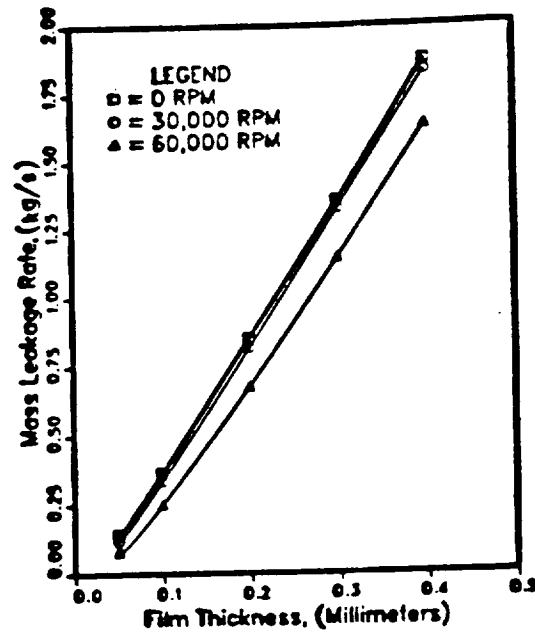


Figure 6-6: Effect of film thickness and rotation speed on leakage.
 Shaft Radius, $R = 0.0325$ m
 Seal Length, $L = 0.026$ m
 Shaft Rotation Speed, $\omega = 30,000$ RPM
 Reservoir Temperature, $T_{\infty} = 135.0$ K
 Reservoir Pressure, $P_{\infty} = 2.79$ MPa
 Back Pressure, $P_b = 0$ MPa

In summary, consideration of some trial parametric studies show that the leakage characteristics of turbulent annular seals are similar to those of radial face seals discussed earlier. Vapor production through pressure drop or viscous heat generation in the seal is an important mechanism for limiting the leakage rate. Small radial clearances, high rotation speeds, and extended seal lengths all aid in reducing leakage. Sub-cooling in the upstream reservoir inhibits vapor production and causes large leakage rates. High degrees of sub-cooling in the upstream reservoir may bring about all-liquid flow, even at very low back pressures. Leakage rates for all-liquid flows can be much higher than two-phase or vapor flows and should be avoided.

ORIGINAL PAGE IS
OF POOR QUALITY

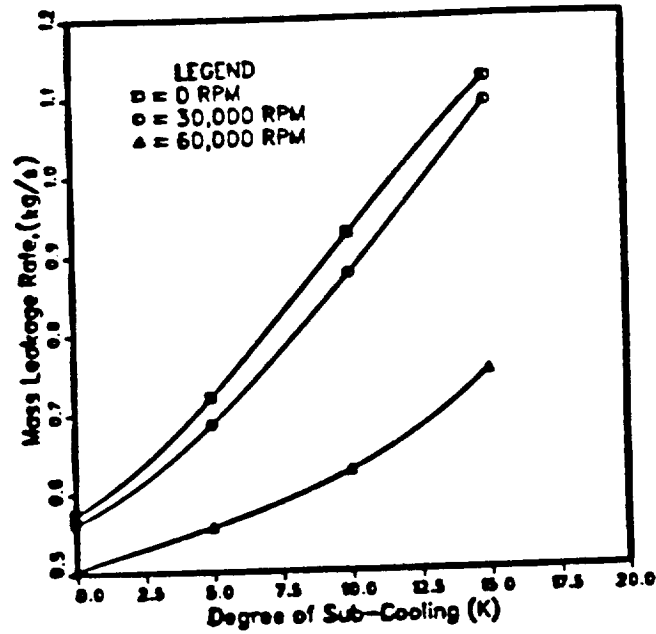


Figure 6-7: Effect of sub-cooling and rotation speed on leakage.

Shaft Radius, $R = 0.0325$ m

Seal Length, $L = 0.026$ m

Radial Clearance, $h = 1.74 \times 10^{-4}$ m

Shaft Rotation Speed, $\omega = 30,000$ RPM

Reservoir Pressure, $P_{\infty} = 2.79$ MPa

Back Pressure, $P_b = 0$ MPa

CHAPTER 7

A COMBINED LAMINAR AND TURBULENT COMPUTER CODE FOR FACE SEAL PERFORMANCE PREDICTION AND DESIGN

7.1 Introduction

A computer code which combines the discrete boiling laminar model developed in Chapter 3 and the adiabatic turbulent model developed in Chapter 5 is presented here. Using this code, we can calculate the performance of a face seal under both low and high leakage conditions. Once we determined how this seal performs under the two limiting conditions, we are able to interpolate the results and predict how the seal will behave in the intermediate region, where both models fail. We performed a parametric study using the computer code to investigate the effects of various operation parameters on face seal performance. The parameters being investigated are the level of subcooling, coning of seal faces, rotational speed, conductivity of the seal materials and the width of seal faces. Because our analysis is based on idealized models, the numerical results may not be exactly the same as those for an actual seal, where a complete analysis must involve consideration of the complex geometry of the seal, its surroundings and other complicated effects such as misalignments of axes and surface roughness. The results presented here are intended to be viewed as a rough guide and are used to indicate the general trends of how seal performance is affected by varying these parameters. The combined laminar and turbulent code is documented in Appendix D.

7.2 Instability of Face Seals

Liquid near saturation condition is notorious in its difficulty to be sealed successfully. Seal instability resulting from phase change has been identified as the cause of numerous failures as for example in the Forties Main Oil Line pump seals [84].

Harrison and Watkins [84] observed that the Forties Main Oil Line pump seal failures usually occurred after the pumps had been operating at above normal temperatures and when the water content in the crude oil was high. Under these operating conditions, fluid vapor was present in a large portion of the seal as vaporization started early on in the leakage path through the seal.

In previous studies using single component fluids as the working fluids [87, 88, 89, 90], the authors show that it is possible for a two phase face seal to have two equilibrium operating points, one stable and the other unstable. The stable operating point is at a higher film thickness and its boiling location is closer to the seal exit than the unstable point. It is shown that if phase change started very close to the inlet, a seal will exhibit negative stiffness and be unstable. This occurs when the sealed liquid is near saturation. Although the fluid in the case of the Forties Main Oil Line [84] was a mixture many components, it is conceivable that the mechanisms that caused the instability of the pump seals were quite similar as the operating temperature was close to the saturation temperature of water.

There are also reports of failures of reactor coolant pump seals during nuclear power station blackouts which were brought about by similar mechanisms [82, 102]. Normally, these seals operate with well-cooled water under high pressure. During a station blackout, external cooling to the coolant system is lost and sometimes there is also a drop in the system pressure. The coolant water can quickly reach near saturation condition and cause the seals to become unstable. The reactor coolant pump seals may "pop open" under these conditions, resulting in uncontrollable and excessive leakage which in severe cases can lead to a loss of coolant accident.

Our results show that, for a parallel seal, there is an absolute minimum amount of subcooling which must be provided to maintain stable operation. A seal will become

unconditionally unstable if the temperature of the sealed liquid rises above this limit. It is shown that stability can be increased by positive seal coning, where the gap between the seal plates converges in the direction of the flow, but at the expense of higher leakage. However, depending on the balance, "popping open" of seals may occur at a temperature lower than the absolute stability limit. It is because at temperatures below the absolute stability limit, any increase in the fluid temperature will lead to an increase in the seal opening force. If the closing force was not high enough to balance the increased opening force, the seal will pop open. The temperature at which this would occur is determined by the balance ratio of the seal.

7.3 Discussion of Sample Calculations and Seal Stability

This study was performed using water as the working fluid. Sample calculations including stiffness curves for parallel and coned face seals are presented to show the effects of the various operation and seal parameters.

7.3.1 Effects of Subcooling

The parameters chosen for the sample calculations are:

$$p_o = 2000 \text{ kPa}$$

$$p_i = 101 \text{ kPa}$$

$$k = 50 \text{ W/(m K)}$$

$$\text{coning slope} = 0.0 \text{ m/m}$$

$$r_o = 0.0428625 \text{ m (1 11/16 in.)}$$

$$r_i = 0.0365125 \text{ m (1 7/16 in.)}$$

$$\text{speed} = 4000 \text{ rpm}$$

To illustrate how subcooling affects the operation of a face seal by changing the boiling location, we look at the pressure profile of the fluid along its leakage path in a typical parallel outside face seal. Figure 7-1 shows plots of pressure profiles along the leakage path for an all liquid, a two-phase and an all vapor seal under low leakage conditions. When subcooling is high, the fluid remains liquid from inlet to exit. In most seals where the widths of the faces are small compared to their radii, the pressure drop is

approximately linear from inlet to exit (see curve A in Figure 7-1). For a parallel face, low leakage seal, where inlet loss and inertial effects are unimportant, the opening force is a function of the pressure differential between the inlet and exit only. Thus, it is quite simple to obtain a good estimate of the opening force of a parallel all liquid face seal. This all liquid opening force is always less than the opening force generated by the same seal under two-phase or all vapor operation. With a sufficient decrease in subcooling (i.e. the sealed liquid approaches saturation), the liquid starts to boil at the exit and the boiling location gradually moves towards the inlet as subcooling is reduced. Pressure drop in the vapor region is much steeper than in the liquid region of the seal, as it is shown in Figure 7-1 (see curve B). As the boiling location move from the exit towards the inlet, the seal opening force initially increases rapidly, reaches a maximum and then decreases eventually to the all vapor seal opening force, which is always higher than the all liquid opening force. Curve C in Figure 7-1 shows the pressure profile of an all vapor seal. If the leakage rate is high and the flow is turbulent, the inlet pressure loss may be significant and if choking occurs, there is a sudden drop in the pressure at the outlet. Hence, depending on the conditions, the opening force of a turbulent seal may be higher or lower that the equivalent low leakage laminar seal.

It should be noted that once the boiling location has moved past the point where the opening force is maximum, the seal is unstable. This instability can be explained by looking at the axial stiffness of the seal. When the boiling location moved past the point at which the opening force is maximum, any decrease in film thickness due to external disturbances will cause the boiling location to move further towards the inlet because of the increased heat generation. This reduces the opening force. The seal plates will move closer together and the seal will eventually collapse. If the seal is perturbed to move apart, the opening force will increase. Depending on the level of subcooling and the balance ratio, the seal will either blow open or reach the stable operating point which is at a higher

film thickness. Therefore, for a parallel face seal, we can see that there is a minimum amount of subcooling we must provide to maintain its stability, regardless of the seal balance.

In actual operations, the closing force of a seal changes very little with the seal film thickness. As subcooling varies, the film thickness adjusts itself such that the opening force is in equilibrium with the closing force. As an example, Figure 7-2 shows a stiffness plot (plot of opening force versus film thickness) of a parallel seal for different degrees of subcooling. In this example, the saturation temperature of the sealed liquid is 485.6K. If we assume a balance such that the seal closing force is constant at 2500N, the seal will operate stably at a very small film when the reservoir liquid is highly subcooled (see Figure 7-2). For example, the operating film thickness for 390K bulk liquid temperature of is less than 10^{-7} m. Surface contacts are likely to occur at such a low film thickness. As subcooling is reduced, the stable operating film thickness increases and as a result, the leakage rate also increases. In Figure 7-2 we show, when the bulk fluid temperature rises above 460K (more than 25K below the saturation temperature of the fluid in the reservoir), there is no stable operating film thickness predicted by the laminar seal model which gives an opening force of 2500N, and the seal pops open. Figure 7-3 shows the plot of leakage rate versus film thickness and Figure 7-4 shows the plot of seal stiffness coefficients versus film thickness. Notice that when the bulk fluid temperature is above 480K, the laminar seal model predicted that the seal would be unconditionally unstable.

Since the quasi-isothermal discrete boiling laminar model is valid only for small leakage rate seals, the sample calculation results given become more and more inaccurate as the film thickness gets higher and higher. Using the computer code developed based on the adiabatic turbulent model, we may determine the seal behavior at large film thicknesses and high leakage rate. The adiabatic model assumes turbulent flow and negligible heat conduction into the seal plates when compared to heat convection within the fluid.

Convection terms in the fluid and inlet pressure loss are considered and boiling is allowed to be continuous in this model. Full account is taken for all liquid, two-phase and vapor choking. Figure 7-2 shows the sample results of the parallel seal using both the quasi-isothermal laminar model and the adiabatic turbulent model. When subcooling is high, the seal opening force given by the adiabatic turbulent model decreases with increasing film thickness. This is due to the increased inlet pressure loss as the radial fluid velocity increases with film thickness. As subcooling reduces, the opening force increases dramatically as the flow starts choking at the exit. The trends of how opening force varies with film thickness predicted by both models are very similar. When the laminar model predicts that the opening force drops as film thickness increases, the turbulent model predicts a similar behavior. When the laminar model predicts that the seal opening force increases as film thickness increases, the turbulent model predicts that as film thickness increases even further, the seal opening force will increase even more. The intermediate region, where both heat conduction into the seal plates and heat convection within the fluid are important, is bounded quite well by the two limiting models. This close agreement of the predicted behavior of seals using both models gives us confidence in applying the laminar model to predict seal failures.

Figure 7-5 shows the absolute minimum reservoir temperature for stable operation of a parallel face seal as determined using the laminar model. When rotational speed is zero, a low leakage seal with negligible inlet loss is always neutrally stable because the opening force is constant with film thickness. The opening force of a two phase stationary parallel face seal is determined by the boiling location and is a function of the reservoir fluid temperature alone. The reservoir temperature at which the opening force of this seal is maximum is the highest temperature the seal can maintain stable operation. We can reason this by looking at a seal running at an infinitesimally slow speed. If the seal temperature is at the stability limit, any decrease in the film thickness will generate more heat, thereby

moving the boiling location closer to the inlet and lowering the seal opening force. Since the seal closing force remains constant, the seal plates are pushed together until the seal collapses. This temperature limit calculated from an infinitesimally slowly rotating seal can be considered as the absolute stability limit. It represents the best case and is by no means a conservative estimate. Any seal running at an appreciable speed will have a different temperature limit which will always be at a lower temperature than the one derived using the stationary seal. Also, in order to maintain successful seal operation, the seal temperature often can not exceed a temperature limit which is much lower than the stability limit. This operating temperature limit is dependent on the seal balance ratio. If the seal balance ratio chosen is low, the increase in seal opening force due to the reduction of subcooling can pop open a seal and result in a seal failure. Using the models and computer code presented here, one can calculate this limit for a seal given the balance ratio. A line representing such a limit is shown in Figure 7-5 for an arbitrary seal balance ratio.

7.3.2 Effect of Coning

Figures 7-6 through 7-11 show results of sample calculations for seals with coning (converging in the direction of flow) using the same operation parameters and seal dimensions as in the last section. Two cases of seal coning are presented. Figures 7-6 through 7-8 show the results of a seal with a minute coning slope (10^{-5}m/m) and Figure 7-9 through 11 a larger coning slope ($1.5 \times 10^{-3}\text{m/m}$). For the seal with the smaller coning slope, the effects of coning are not very noticeable at the larger film thicknesses (see Figure 7-6) and the opening force and leakage rate characteristics are quite similar to that of the parallel seal (see Figures 7-6 and 7-7). When the film thickness is small, coning effectively restricts the flow and thereby increases the seal opening force and stability (see Figures 7-6 and 7-8). As the film thickness gets very small, there is little pressure drop in the liquid region of the seal. When the film thickness decreases further, unlike a parallel face seal, the boiling location moves back closer to the seal exit and the opening force asymptotically

approaches the maximum opening force the seal can produce due to hydrostatic pressure. This maximum opening force can be calculated by taking the fluid pressure inside the seal to be uniformly at the reservoir fluid pressure. The asymptotic limit can be explained by looking at the limiting case that, when the plates of a coned seal just touch each other at the exit, there is no leakage and if the centrifugal effects are not important, the fluid inside the seal gap will be uniformly at the reservoir pressure. For high speed seals, the maximum opening force will be lower.

For the seal with the smaller coning slope, the film thickness at the seal exit is only a minuscule $6 \times 10^{-8} \text{m}$ smaller than at the inlet but the effects of coning are already significant. Any wear of the seal plates at the outer radius resulted from surface contacts will produce a much higher coning slope. Figures 7-9 through 7-11 show the results of a seal with a more realistic coning slope. The difference between the inlet and exit film thicknesses is about 10^{-5}m . If we assume the same seal balance as in the previous example, the stable operating film thickness is much higher for the coned face seal than for the parallel face seal. At 450K bulk fluid temperature, the equilibrium film thicknesses are about $4 \times 10^{-7} \text{m}$ for the parallel seal (see Figure 7-2) and $3 \times 10^{-5} \text{m}$ at the inlet for the coned seal (see Figure 7-9) and the predicted leakage rates are $1 \times 10^{-6} \text{kg/s}$ and $3 \times 10^{-1} \text{kg/s}$ respectively. The high leakage rate of the coned seal, however, invalidated the assumptions made in the laminar seal model. Using the results from the adiabatic turbulent seal model, the equilibrium film thickness predicted is a lower $1.7 \times 10^{-5} \text{m}$ and the leakage rate is about $6 \times 10^{-2} \text{kg/s}$ (the results of the leakage rate calculations using the adiabatic turbulent model are not shown). Since the leakage rate is very high in this case, the predictions using the turbulent model should be more accurate. A leakage rate this high is unacceptable for most sealing requirements and therefore, in order to maintain an acceptable leakage rate, we should choose a higher balance ratio for a coned seal than we would for a

parallel seal. At higher temperatures, the stable operating film thicknesses are so high that the seal can be considered popped open.

It is interesting to note that, unlike the parallel face seal, the unstable operating region of a coned seal is either very small or non-existing. Since the seal opening force drops when the temperature exceeds the value at which the opening force is maximum, the seal stiffness characteristics at a temperature very close to saturation can be quite similar to that of a much lower temperature (see Figure 7-9). It is possible that a seal with a certain balance ratio can operate satisfactorily when subcooling is high or very low but not in between. However, once a seal is popped open at a lower temperature, it is not very likely that the seal will regain stable operation by itself. Figures 7-10 and 7-11 show the leakage rate and stiffness coefficients as predicted using the laminar seal model; because of the higher operating film thicknesses, the stiffness coefficients of the coned seal are much lower than those of the parallel seal (note the change of scale of the vertical axis).

7.3.3 Effect of Speed

Figures 7-12 through 7-17 show the stiffness curves for seals running at speeds from 0 rpm to 10000 rpm and at constant bulk fluid temperatures. The basic operation parameters and seal dimensions used in the calculation were the same as in the previous two sections. Figures 7-12 through 7-14 show the results of a parallel seal operating at bulk liquid temperatures of 400K, 450K and 470K respectively. Figure 7-15 through 7-17 show, under the same operating conditions, the results of a coned seal with a converging coning slope of $1.5 \times 10^{-3} \text{m/m}$. From Figures 7-12 through 7-14 we can see, for the parallel seal with a given seal balance, as the speed increases, the stable operating point shifts towards higher film thicknesses and as a result, the leakage rate also increases. This is because when the seal speed increases, the rate of heat generation, and therefore the seal temperature, increases. This moves the boiling location closer towards the inlet and

increases the seal opening force when the seal is operating in the stable region. Thus for a given balance, the stable equilibrium operating point must move to a higher film thickness when the seal speed is increased so that it can maintain the same opening force (and also a similar boiling interface location). For the turbulent region, the heat generation rate is relatively small and the effect of speed is not very significant.

It can be seen from the figures that, even at 10000 rpm, the centrifugal inertia effects are not very significant. However, if either the seal speed gets much higher or the pressure differential between the inlet and exit becomes much lower, the centrifugal effects can become important.

For the coned seal, where heat generation cannot be very high because of the seal geometry, the effects of speed is not significant in both the laminar and the turbulent regions (see Figures 7-15 through 7-17).

7.3.4 Effects of the Thermal Conductivity of Seal Materials

Figures 7-18 through 7-25 show the stiffness curves of seals made with materials of different thermal conductivities. In our studies presented in previous sections, the average conductivity of the seal materials used is 50W/m-K. To illustrate the effects of varying thermal conductivity, analyses are performed using the same operating parameters and dimensions for seals made with lower and higher thermal conductivity materials. Figures 7-18 and 7-19 show the stiffness plots of two parallel seals for different seal speeds with average seal material conductivities of 15W/m-K and 100W/m-K respectively. Figures 7-20 and 7-21 show the stiffness plots of the same seals for different bulk temperatures. It can be seen from these curves (and from Figures 7-13 and 7-2), for seals made of lower conductivity materials, the stable equilibrium operating film thicknesses are higher. This is because for the seals with lower thermal conductivities, under the same

operation conditions for the same film thicknesses, the seal temperatures is higher than the ones with higher conductivities and thus they have higher opening forces.

Figures 7-22 through 7-25 show stiffness curves for different temperatures and seal speeds for coned seals (coning slope $1.5 \times 10^{-3} \text{m/m}$) with average thermal conductivities of 15W/m-K and 100W/m-K . Since the heat generation rates are relatively small, the effects of seal material conductivity is not very significant.

For the high leakage turbulent region, since our model is adiabatic, the values of seal material thermal conductivity have no effect on the results.

7.3.5 Effects of the Width of Seal Faces

Figures 7-26 through 7-29 illustrate the effects of varying the widths of the seal faces. Figure 7-26 shows the stiffness curve for a parallel seal with a face width half of that of the seal used for the studies in the previous sections and Figure 7-27 shows the curve for a seal with a face width twice as wide. From these curves we can see that the opening forces is almost direct proportional to the seal face areas. When compared to the results of the original seal shown in Figure 7-2, the stability characteristic for all three seals are very similar to each other (i.e. the shape of the stiffness curves are very similar) and the temperatures at which the seal become unstable are almost identical.

Figure 7-28 and 7-29 show the stiffness plots for coned seals with face widths half and double the width of the seal used in the studies in the previous sections. Again, when compared to the results of the original coned seal (see Figure 7-9), the effects of the width of seal faces on the stability characteristics are shown not to be significant.

7.4 A Summary of Our Results and a Discussion of the Implications to Face Seal Designs

Using the computer code base on the quasi-isothermal low leakage model and the adiabatic high leakage model, we can determine the stability criteria and stiffness coefficients of face seals. Our results show that these important seal operation characteristics predicted by the two extreme models tend to overlap each other in a reasonable manner. This gives us confidence that the simplified quasi-isothermal model is capable of being a useful tool for face seal design and can be used to form the basis of a face seal design methodology.

Subcooling is a critical factor in determining seal stability. The simplified model allows us to predict very quickly how the seal opening force and stiffness characteristics vary with subcooling. As subcooling of the sealed fluid is reduced, the seal opening force increases rapidly. It is shown in our results that, even when the seal stiffness coefficient is positive (i.e. the seal is operating stably), given a sufficient reduction in the subcooling of the sealed fluid, the seal may still pop open if the balance force is exceeded. Using the model and the computer code presented here, one can establish the temperature limit for successful seal operation for different inlet pressures given a seal balance ratio, such as the example shown in Figure 7-5.

The effects of seal coning has also been discussed. In actual seal operations, any surface contact caused by wobbling of the seal plates tends to wear the plates at the outer radius. A parallel face seal can become coned very quickly once it enters into service. It is shown in our sample calculation results that a small amount of seal coning can dramatically alter the operation characteristics of a face seal, in particular its stiffness characteristics. A coned seal is in general more stable than a parallel face seal (compare Figure 7-2, 7-6 and 7-9). Although coning tends to stabilize a seal, given the same balance ratio, a coned seal

operates at a higher film thickness and thus has a much higher leakage rate than a parallel seal. It should be realized that when determining the seal balance ratio, a higher value is needed for a coned seal than for an otherwise equivalent parallel seal. Besides the wear of seal plates, during actual operations, effective coning can also be caused by temperature and pressure distortion. An equivalent amount of coning can be added to account for these effects.

The effects of speed, thermal conductivity of seal materials and the width of the seal faces are also discussed. It is found that, under normal operating conditions (i.e. high pressure differential between the inlet and exit and seal speed much lower than the critical speed), the centrifugal inertia effects are not very significant. As seal speed increases, given the seal balance, the stable equilibrium operating point moves towards higher film thicknesses and the leakage increases. It is also shown that, for the same balance, the equilibrium operating film thickness of a seal made with lower thermal conductivity materials is higher than that of a seal made with higher conductivity materials. Both these effects can be explained by looking at the seal temperature. When the seal is operating in the stable region, an increase in seal temperature due to any reason, such as an increase in the bulk fluid temperature, an increase in seal speed or because the seal is made from lower thermal conductivity materials, will increase the seal opening force. It is found that, the width of seal faces has relatively little effects on the temperature limit for successful and stable seal operations and the seal opening force is almost directly proportional to the area of the seal faces.

To ensure a long and reliable face seal operation, a seal designer must know the level of subcooling of the sealed fluid, anticipate how much it will vary and take into account the effects of coning resulting from wear and pressure and thermal distortions, and then the balance ratio can be chosen accordingly.

The computer code presented here currently incorporates the physical and thermodynamic properties of water, nitrogen, oxygen and hydrogen. Other fluids can be easily added into the code with only minor modifications. Also, the solution to the heat transfer problem is based on an idealized model in which the seal area is surrounded by two semi-infinite solids. If higher accuracy of the seal temperature profile is needed, a geometry specific heat transfer calculation, such as a finite element analysis, can be incorporate into the present code.

Although no experimental results are presented here, published field observations and some unpublished experimental data tend to corroborate our results.

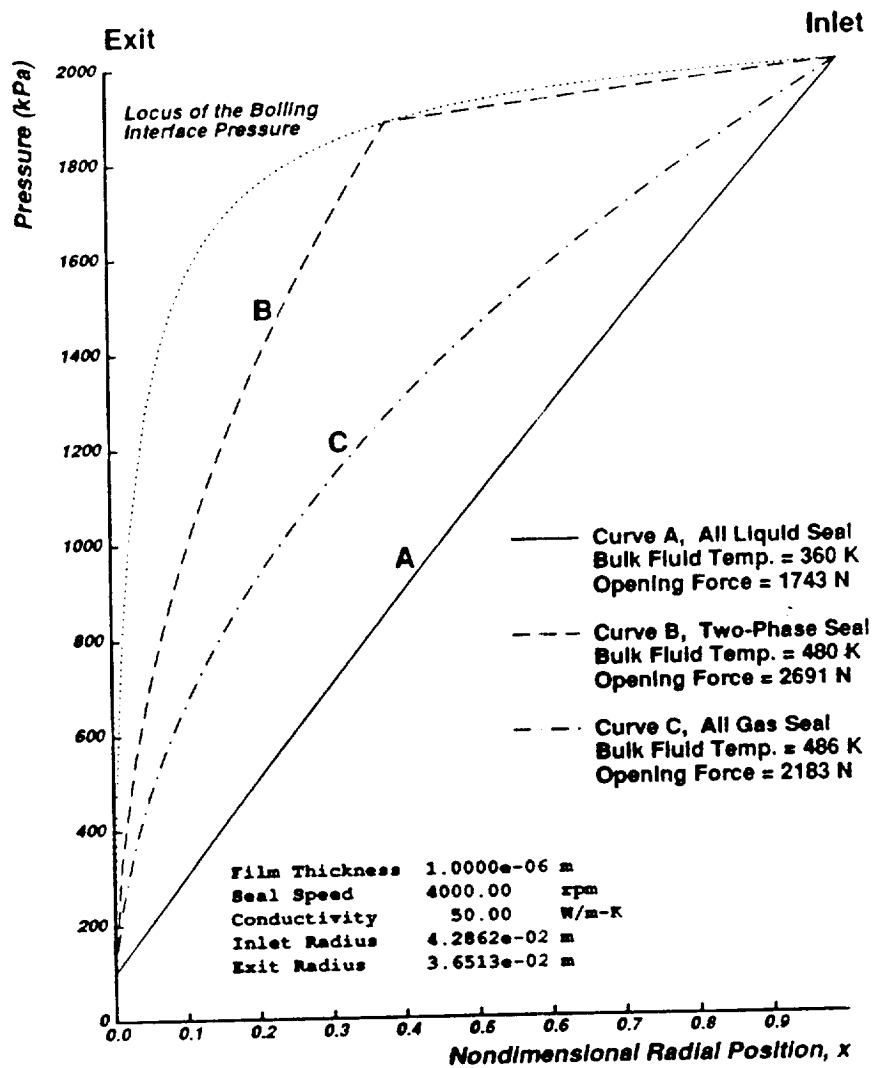


Figure 7-1: Plot of Pressure Profiles of a Typical Face Seal Under All Liquid, Two-Phase and All Vapour Operations

ORIGINAL SOURCE OF INFORMATION

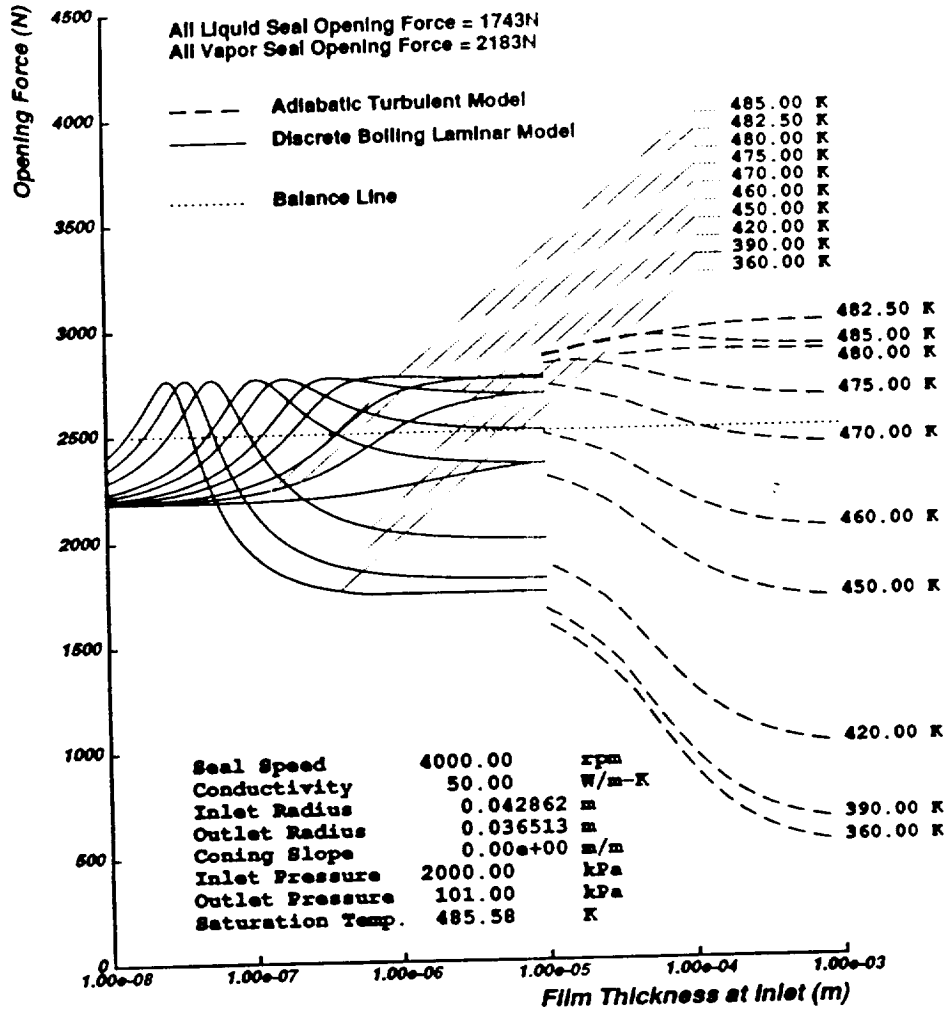


Figure 7-2: Stiffness Curves of a Parallel Face Seal For Different Bulk Fluid Temperatures

ORIGINAL PAGE IS
OF POOR QUALITY

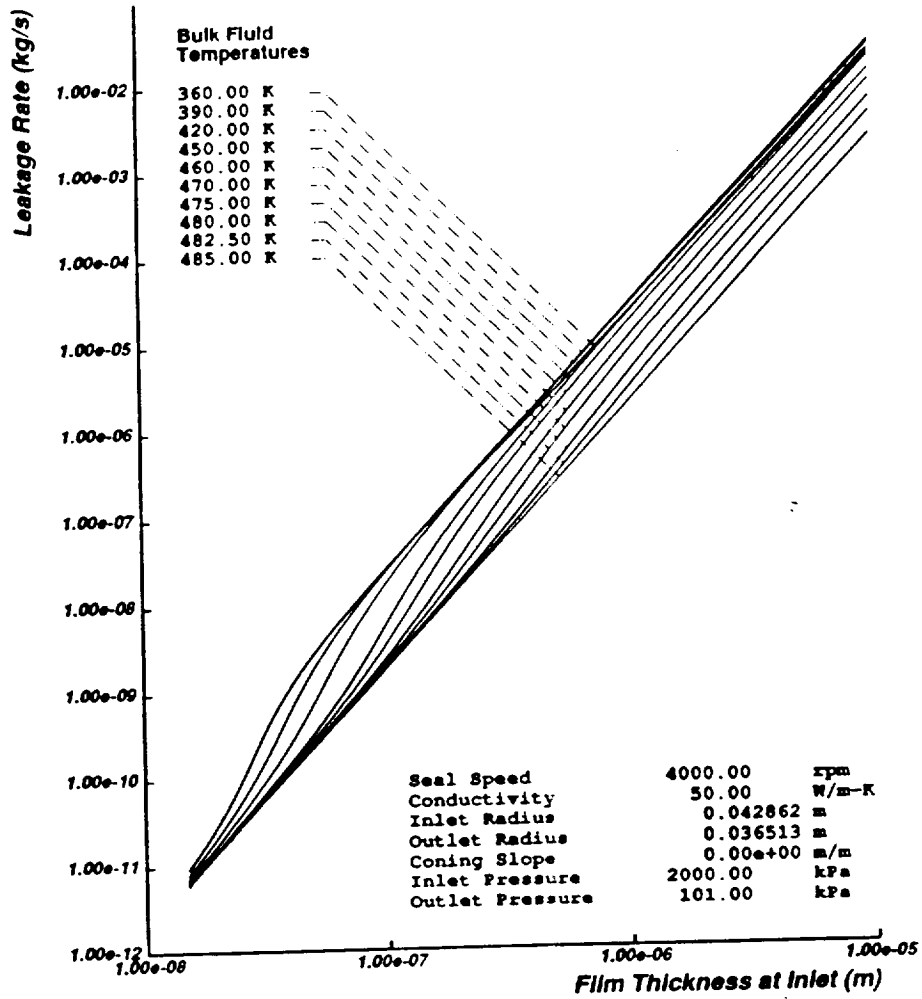


Figure 7-3: Leakage Curves of a Parallel Face Seal For Different Bulk Fluid Temperatures

ORIGINAL PAGE IS
OF POOR QUALITY

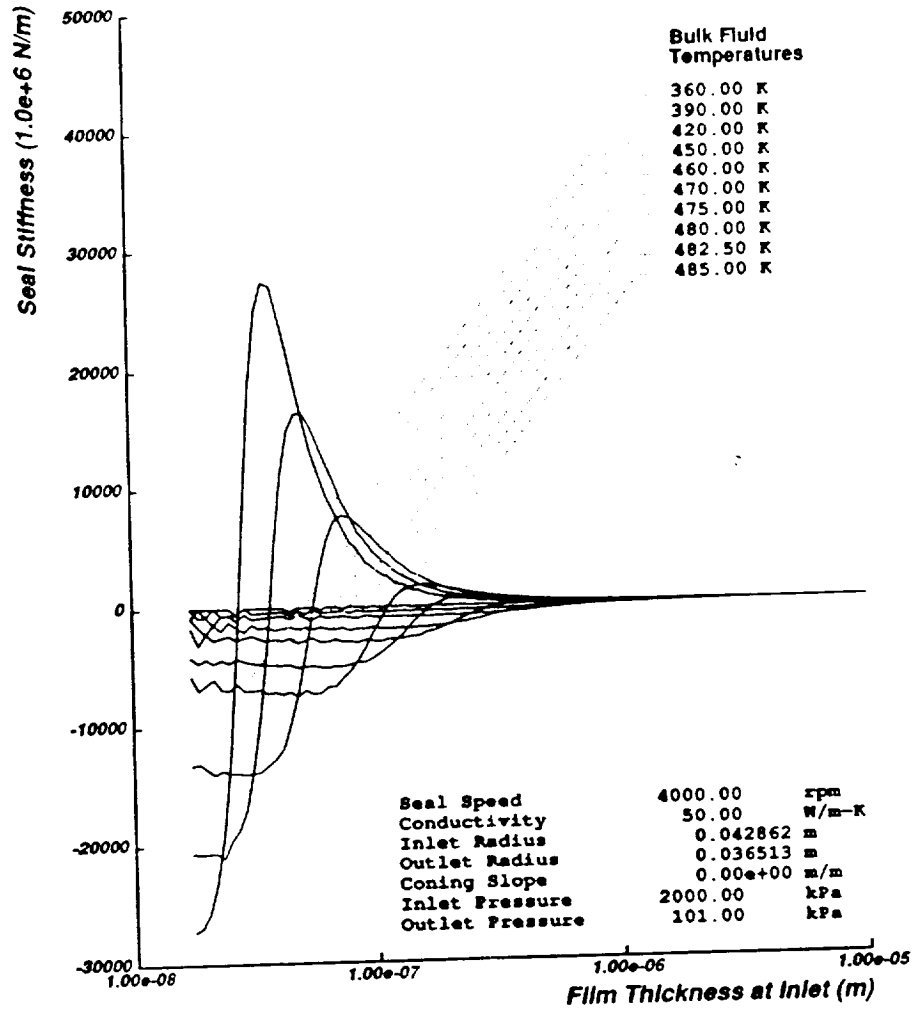


Figure 7-4: Plot of Stiffness Coefficient versus Film Thickness for a Parallel Face Seal for Different Bulk Fluid Temperatures

ORIGINAL PAGE IS
OF POOR QUALITY

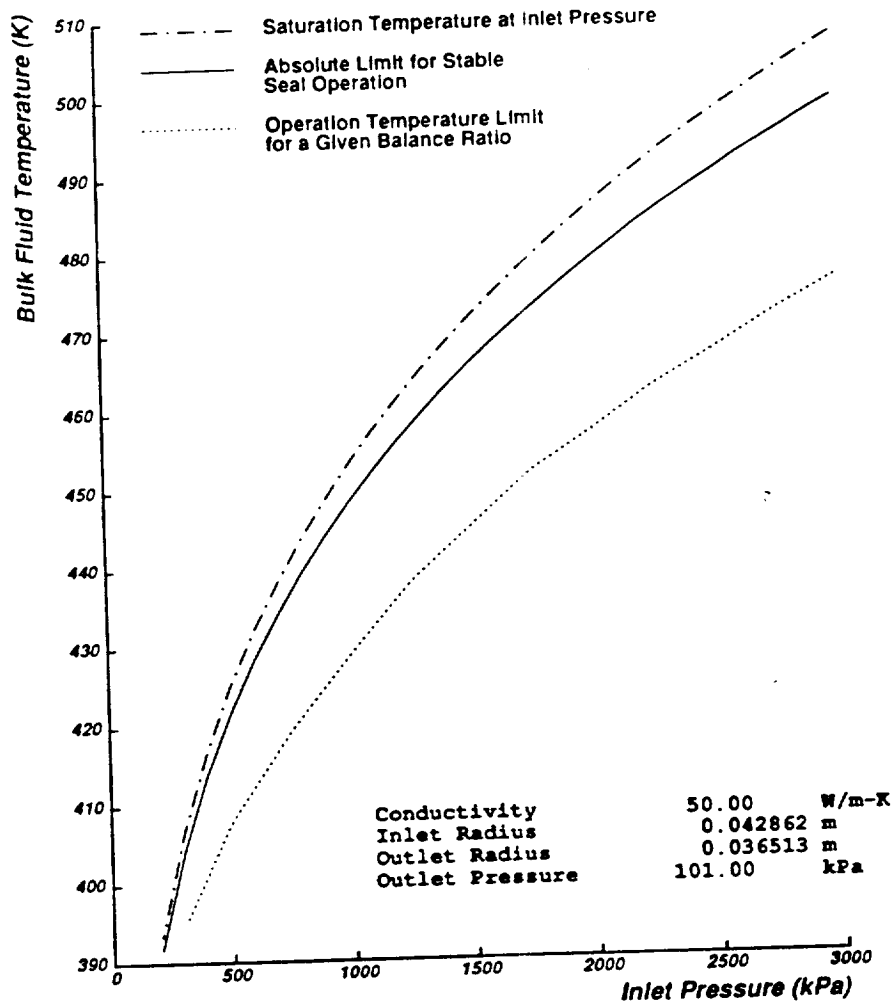


Figure 7-5: Plot of the Absolute Stability Limit for a Parallel Face Seal

ORIGINAL PAGE IS
OF POOR QUALITY

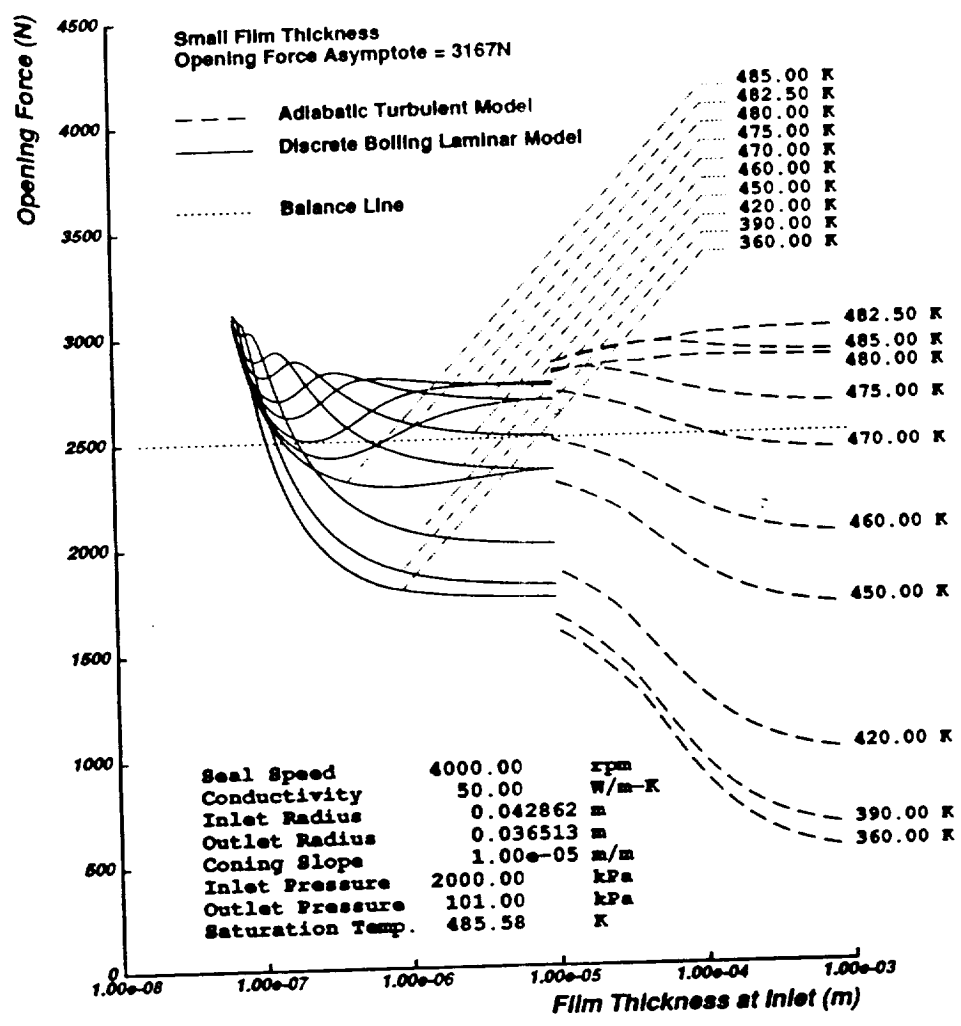


Figure 7-6: Stiffness Curves of a Coned Face Seal with a Small Coning Slope for Different Bulk Fluid Temperatures

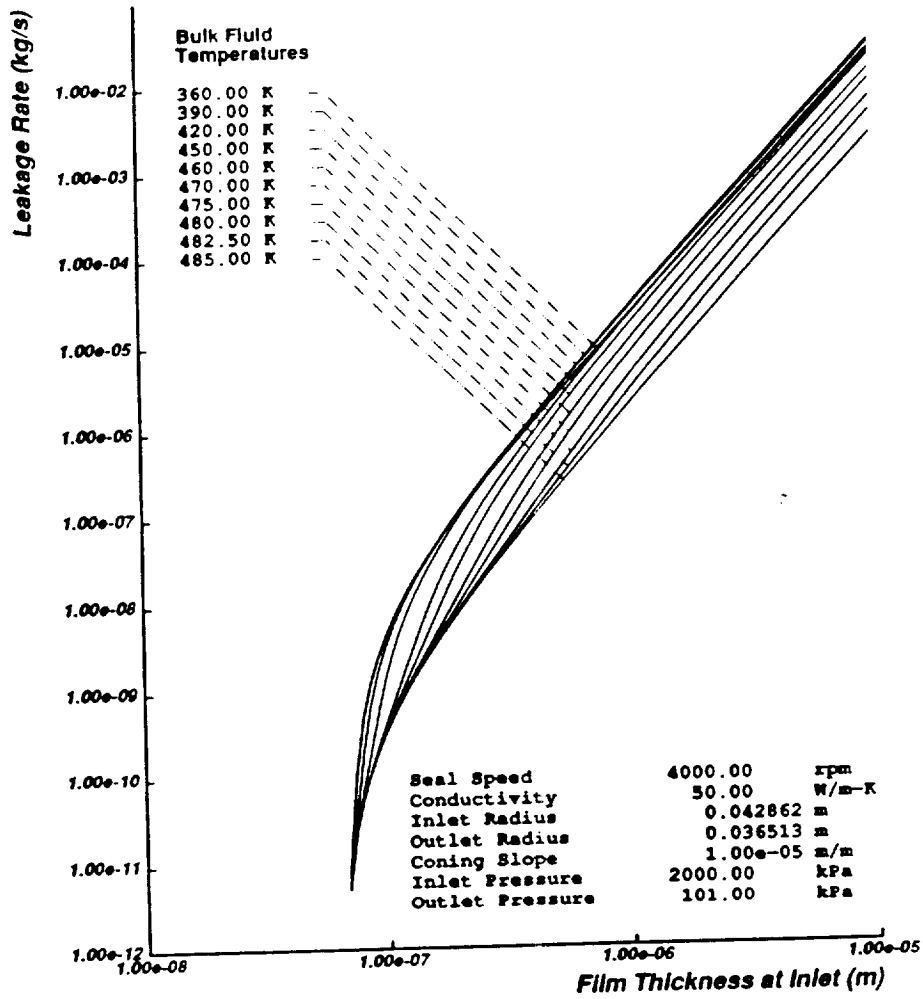


Figure 7-7: Leakage Curves of a Coned Face Seal with a Small Coning Slope for Different Bulk Fluid Temperatures

ORIGINAL PAGE IS
OF POOR QUALITY

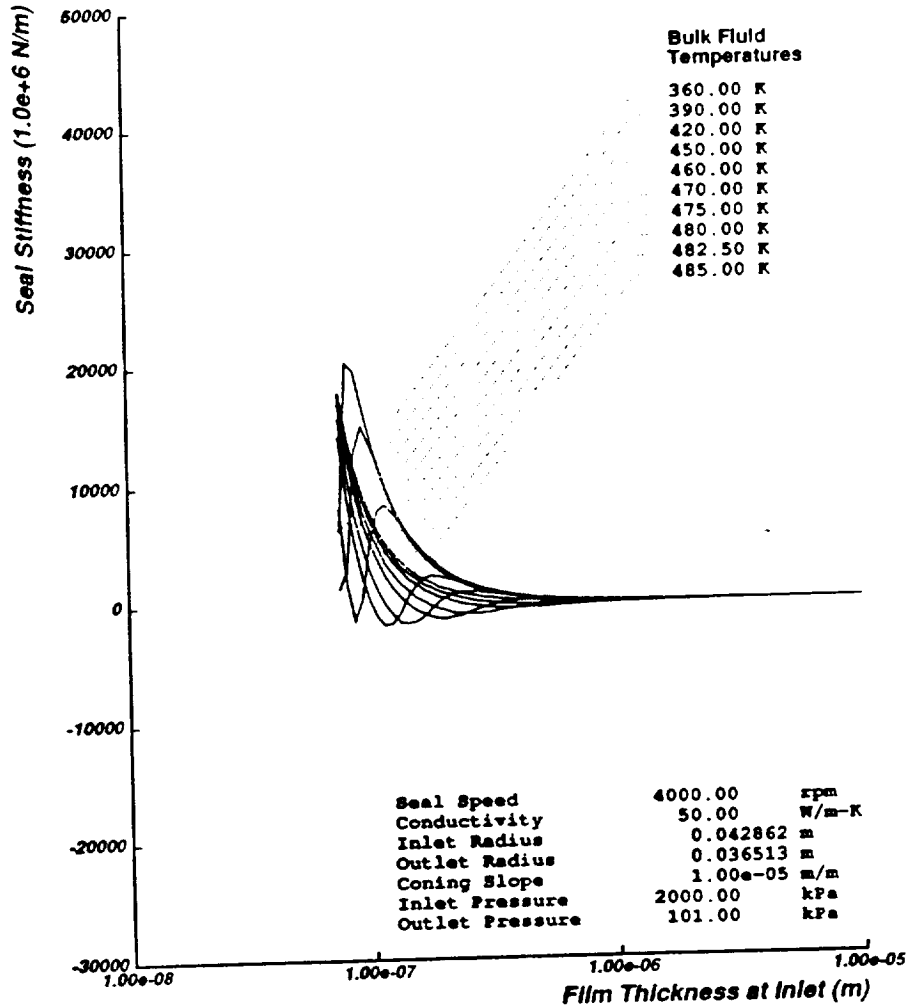


Figure 7-8: Plots of Stiffness Coefficients versus Film Thickness of a Face Seal with a Small Coning Slope for Different Bulk Fluid Temperatures

ORIGINAL DESIGN
OF POOR QUALITY

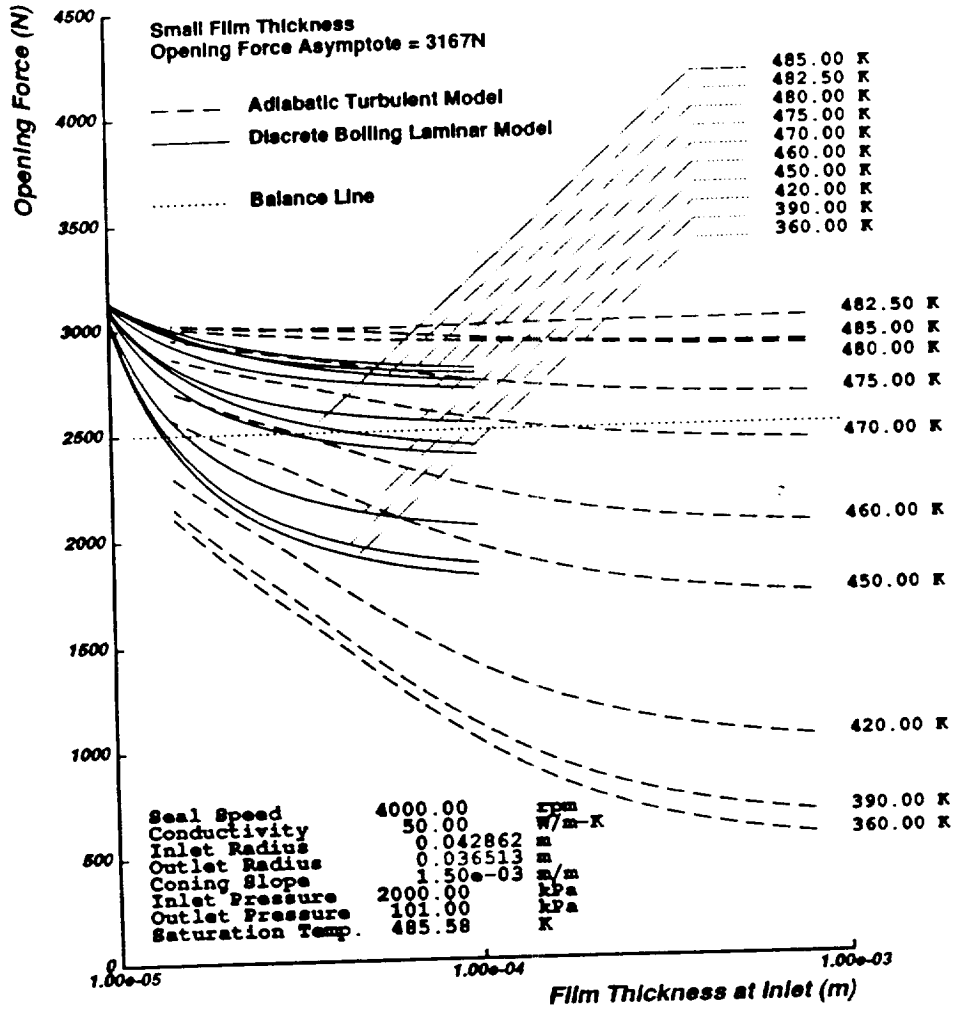


Figure 7-9: Plot of Stiffness Curves of a Coned Face Seal with a Typical Coning Slope for Different Bulk Fluid Temperatures

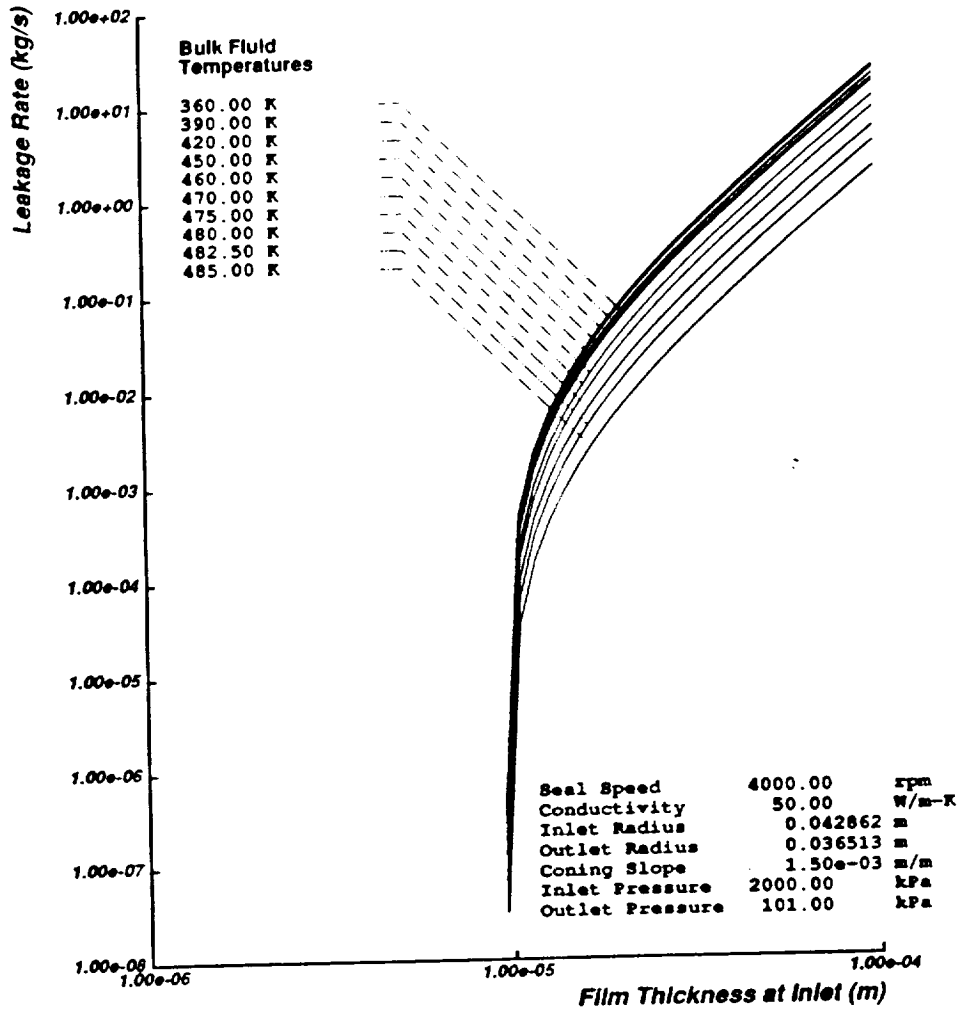


Figure 7-10: Plot of Leakage Curves of a Coned Face Seal with a Typical Coning Slope for Different Bulk Fluid Temperatures

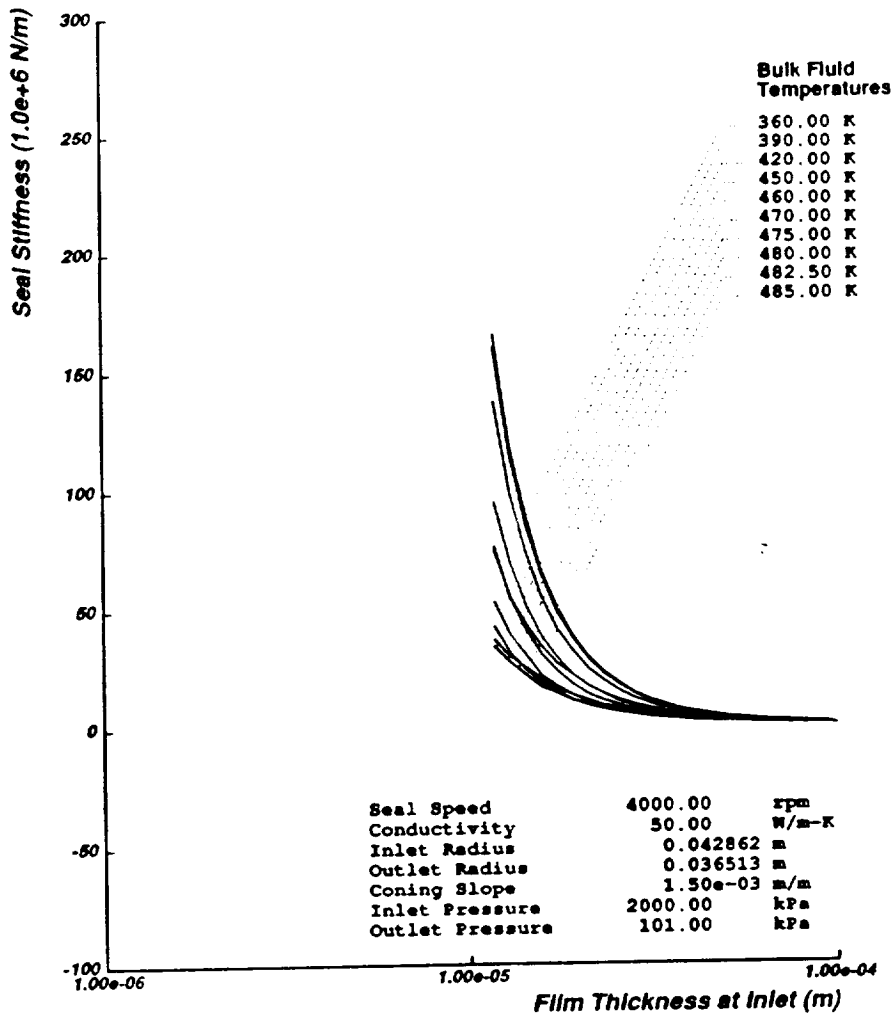


Figure 7-11: Plot of Stiffness Coefficients versus Film Thickness of a Coned Face Seal with a Typical Coning Slope for Different Bulk Fluid Temperatures

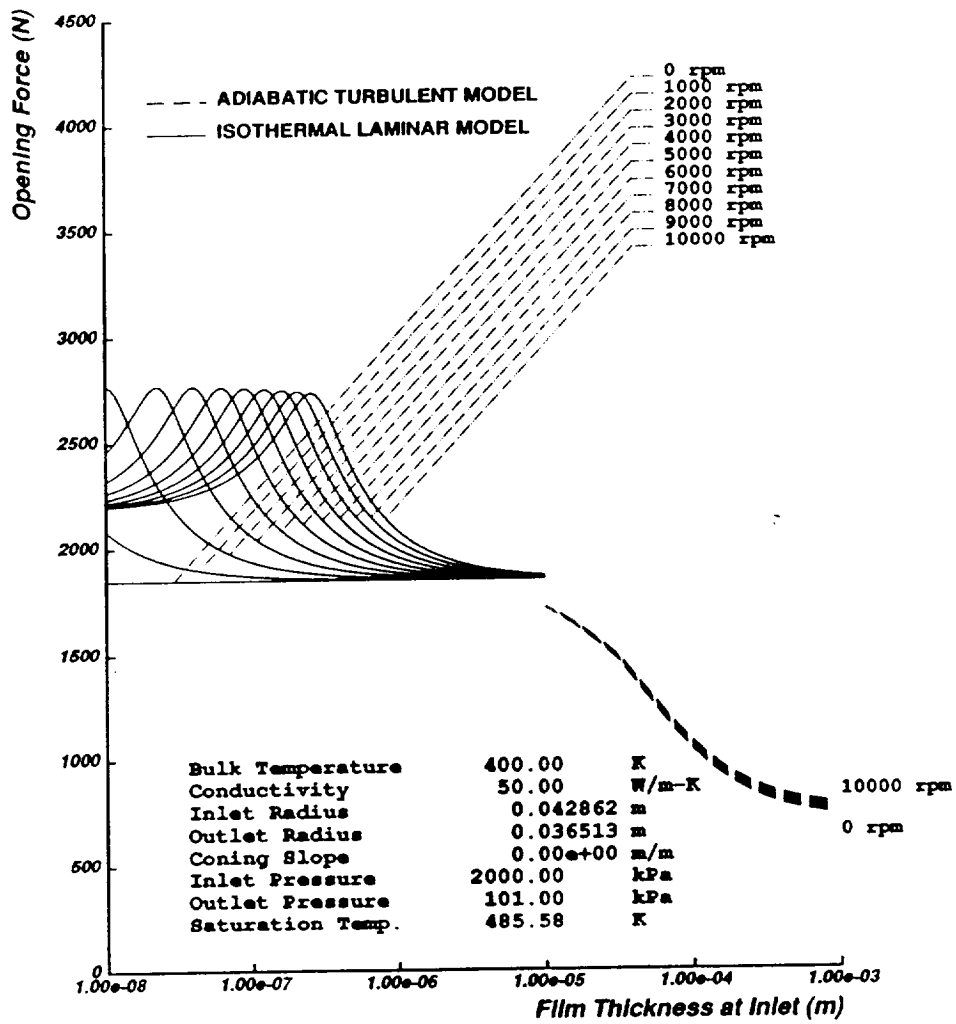


Figure 7-12: Stiffness Curves of a Parallel Face Seal for Different Seal Speeds at 400K Bulk Fluid Temperature

ORIGINAL PAGE IS
OF POOR QUALITY

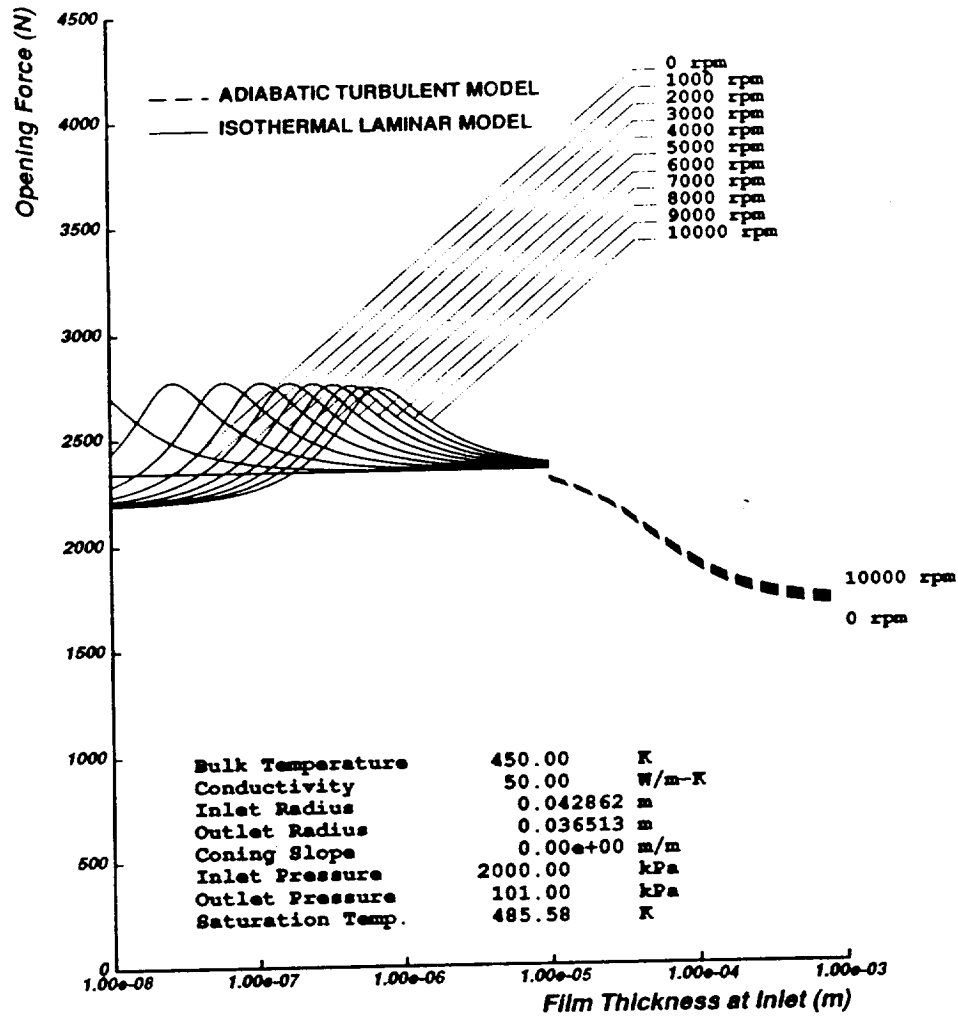


Figure 7-13: Stiffness Curves of a Parallel Face Seal for Different Seal Speeds at 450K Bulk Fluid Temperatures

ORIGINAL PAGE IS
OF POOR QUALITY.

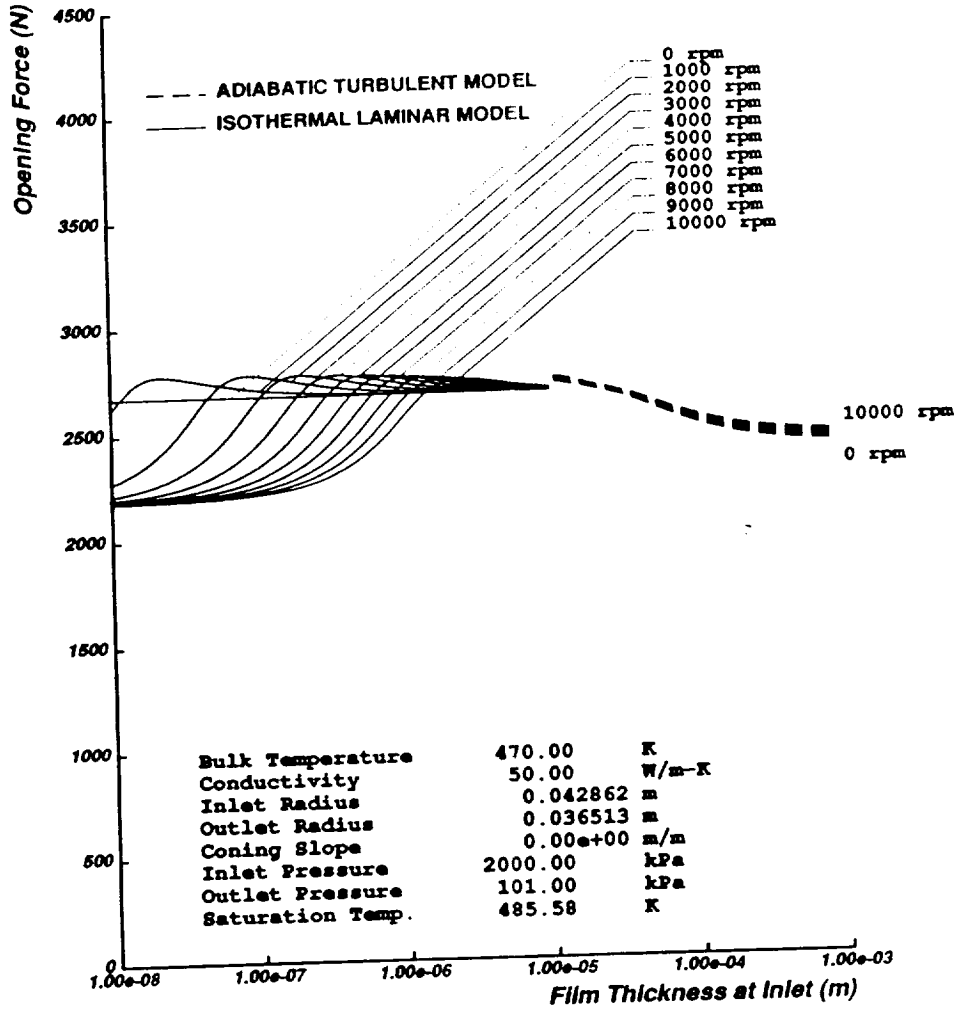


Figure 7-14: Stiffness Curves of a Parallel Face Seal for Different Seal Speeds at 470K Bulk Fluid Temperature

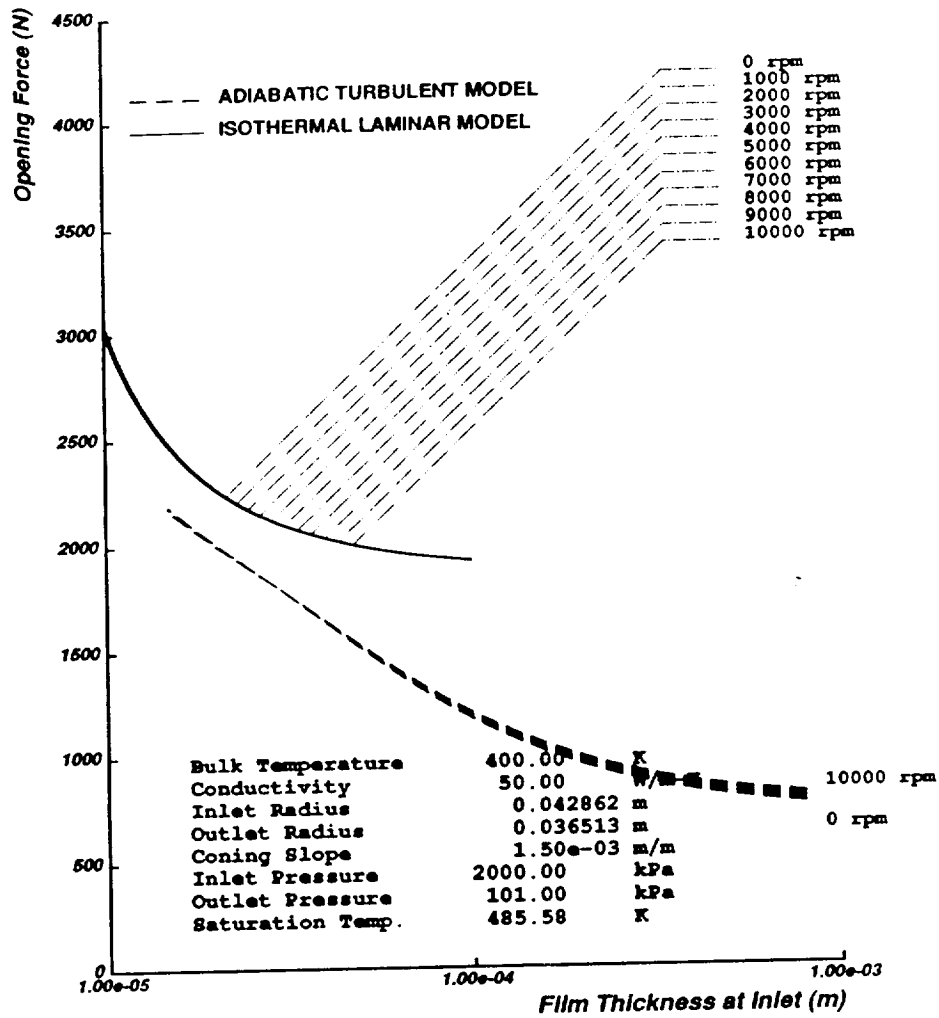


Figure 7-15: Stiffness Curves of a Coned Face Seal for Different Seal Speeds at 400K Bulk Fluid Temperature

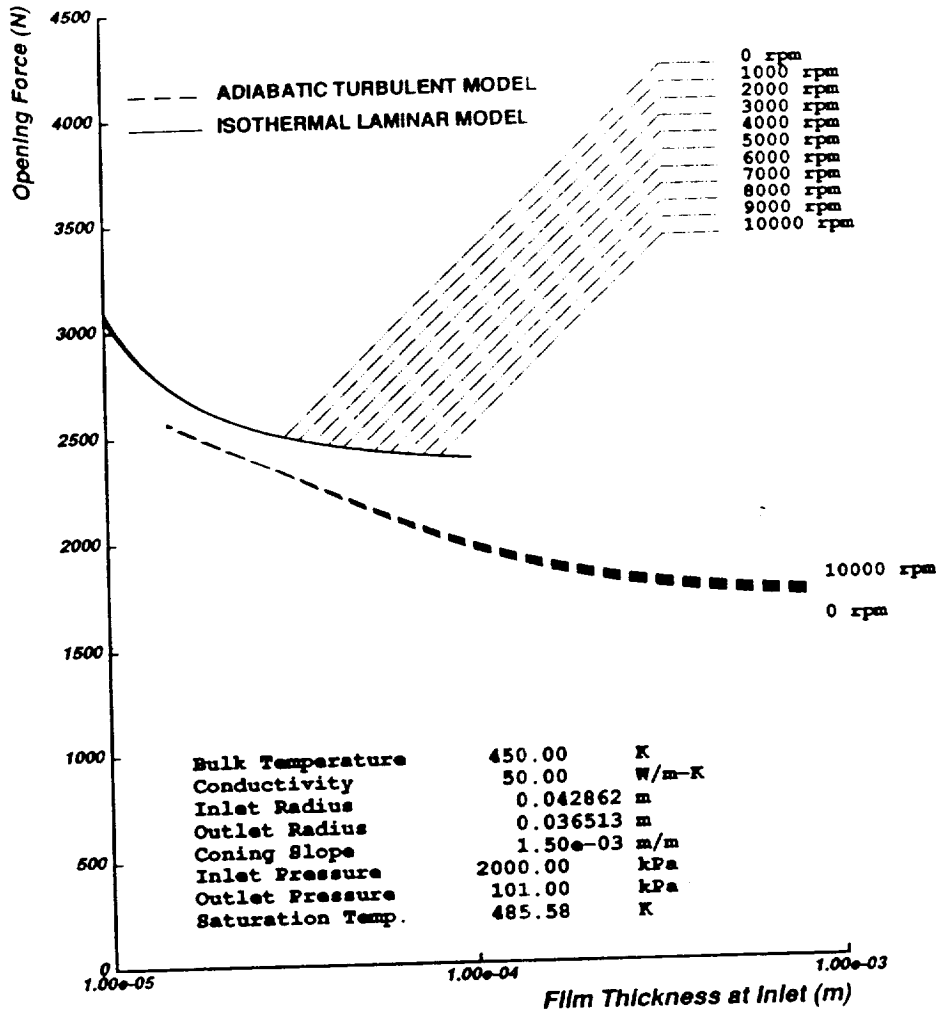


Figure 7-16: Stiffness Curves of a Coned Face Seal for Different Seal Speeds at 450K Bulk Fluid Temperatures

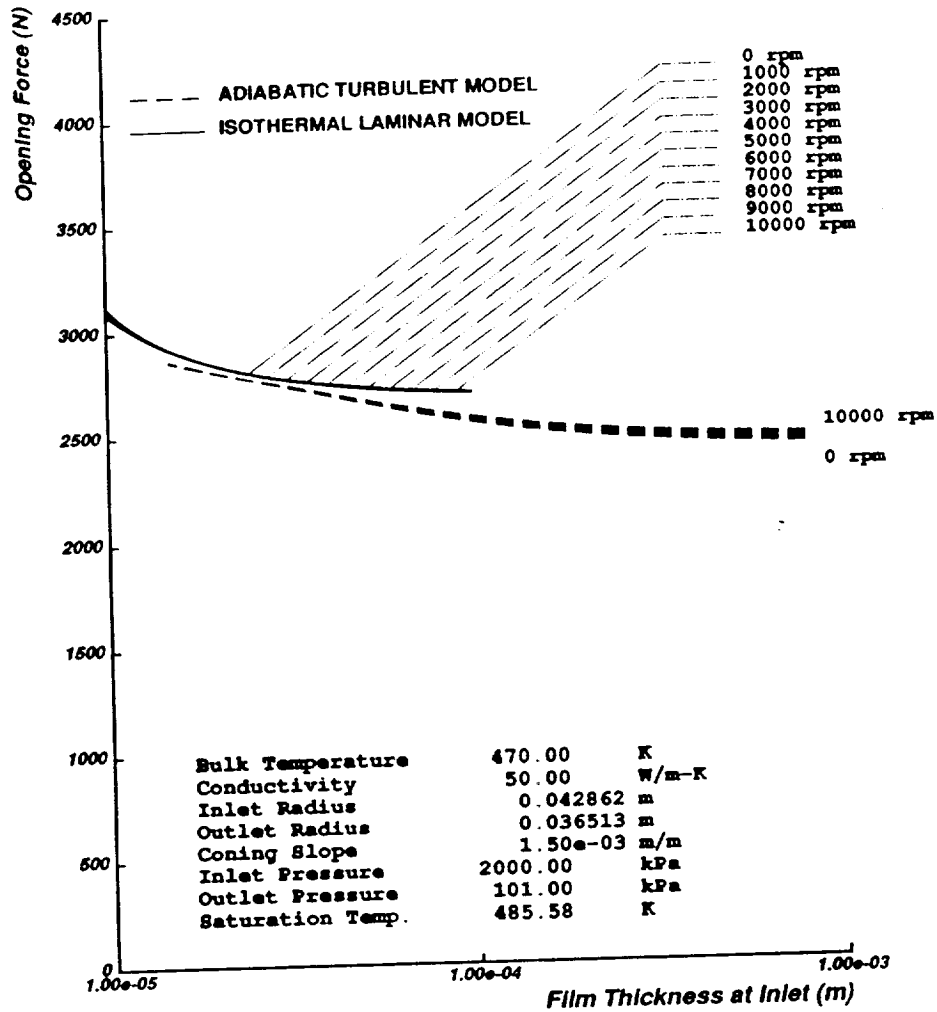


Figure 7-17: Stiffness Curves of a Coned Face Seal for Different Seal Speeds at 470K Bulk Temperature

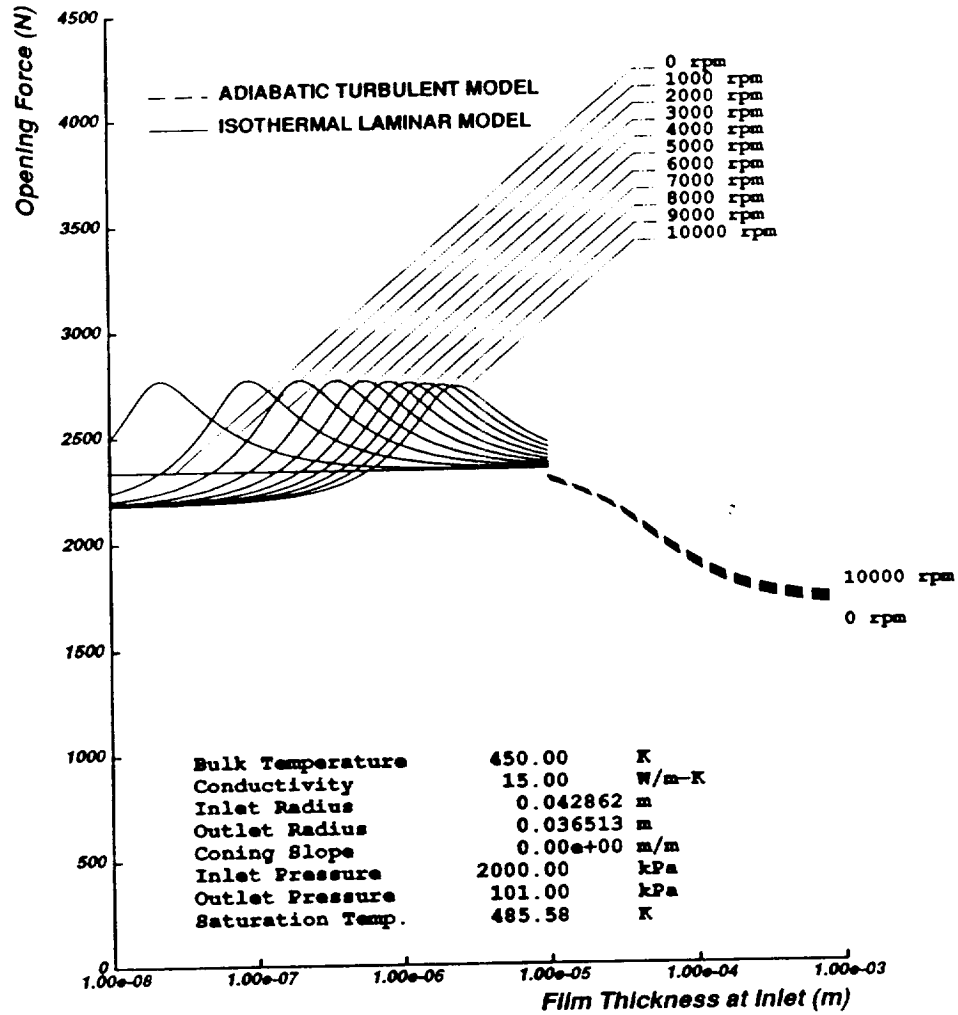


Figure 7-18: Stiffness Curves of a Parallel Face Seal with a Low Thermal Conductivity for Different Seal Speeds at 450K Bulk Fluid Temperature

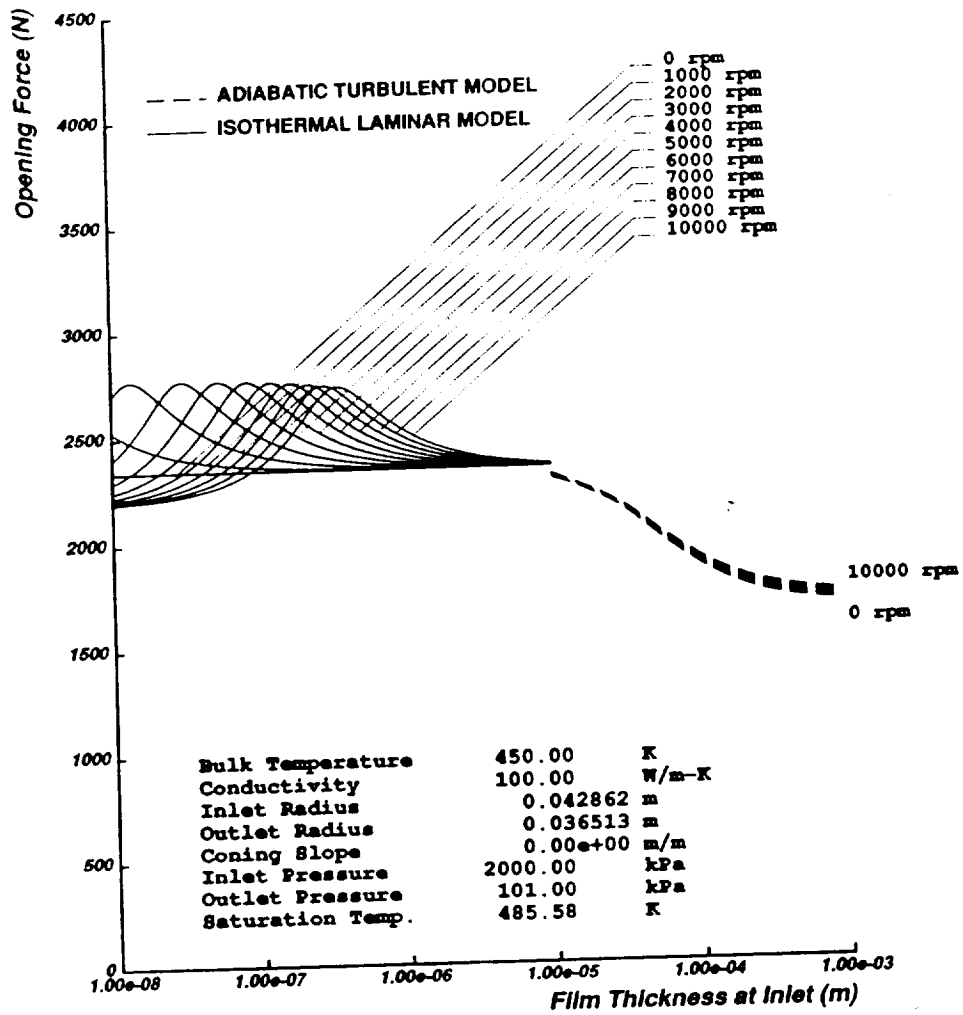


Figure 7-19: Stiffness Curves of a Parallel Face Seal with a High Thermal Conductivity for Different Seal Speeds at 450K Bulk Fluid Temperature

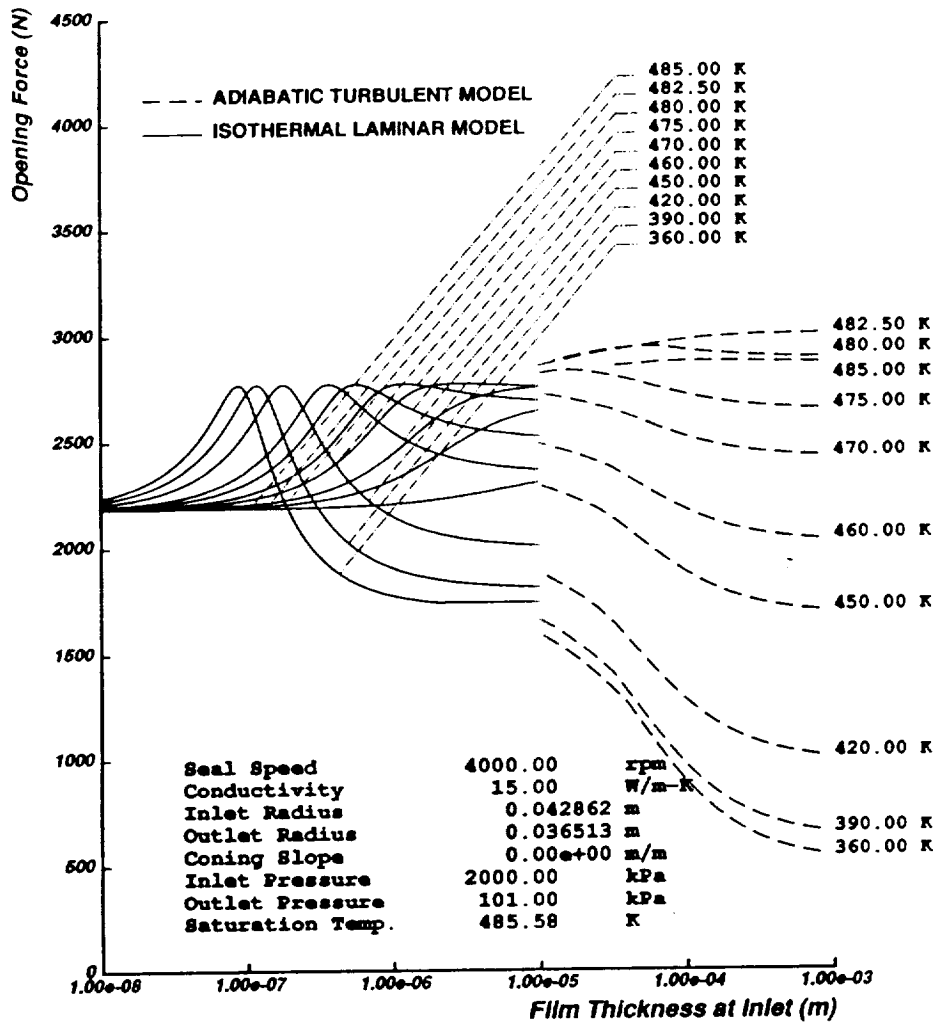


Figure 7-20: Stiffness Curves of a Parallel Face Seal with a Low Thermal Conductivity for Different Bulk Fluid Temperatures

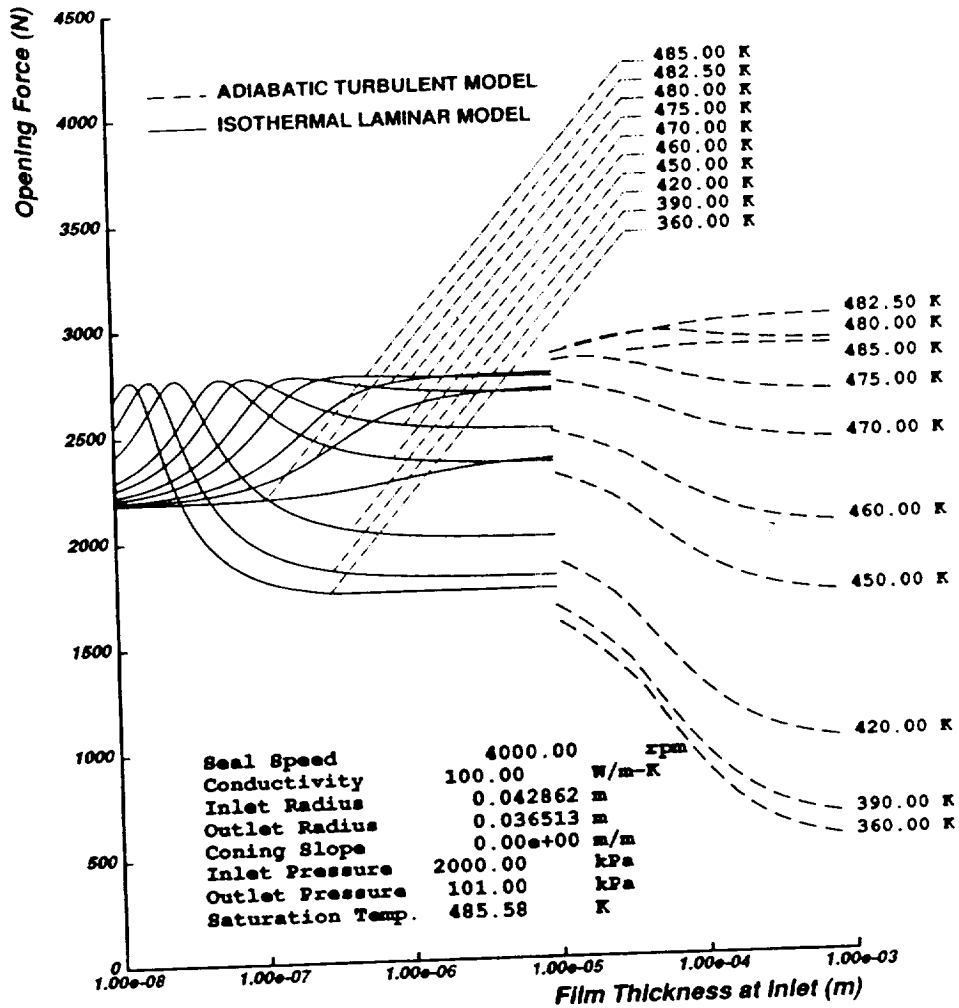


Figure 7-21: Stiffness Curves of a Parallel Face Seal with a High Thermal Conductivity for Different Bulk Fluid Temperatures

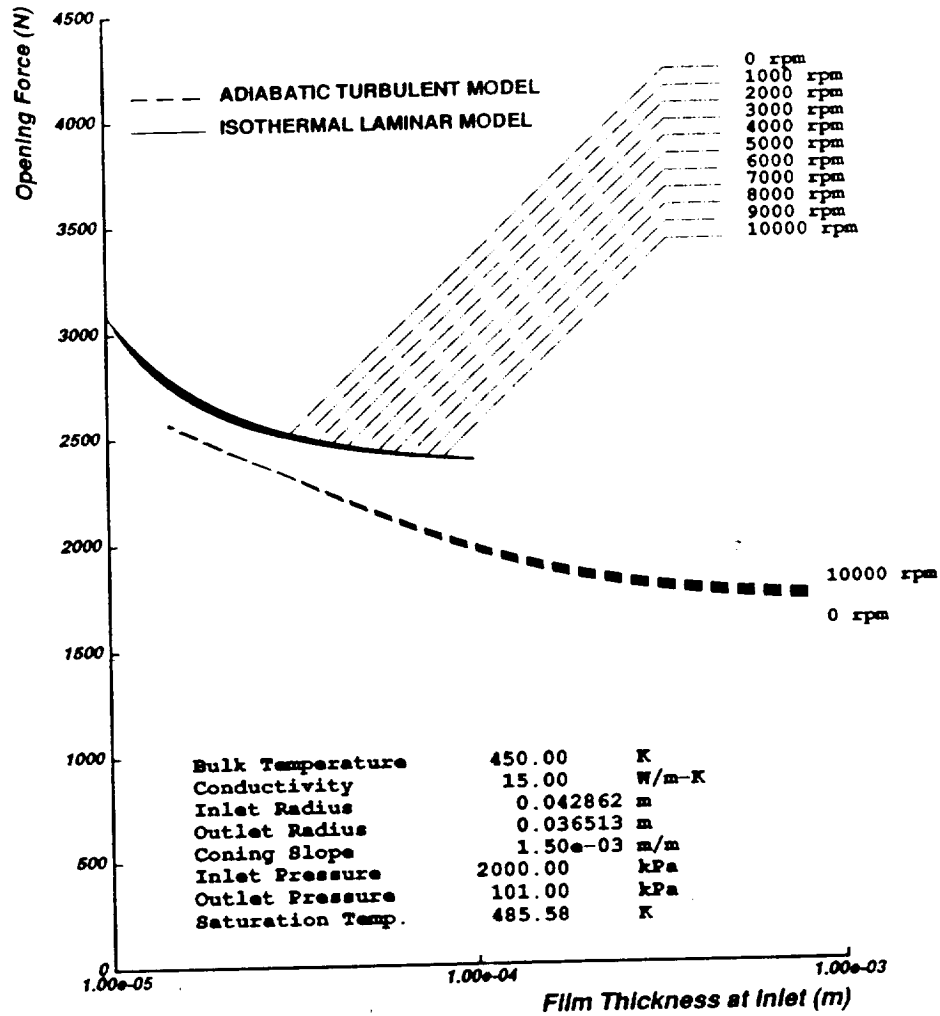


Figure 7-22: Stiffness Curves of a Coned Face Seal with a Low Thermal Conductivity for Different Seal Speeds at 450K Bulk Fluid Temperature

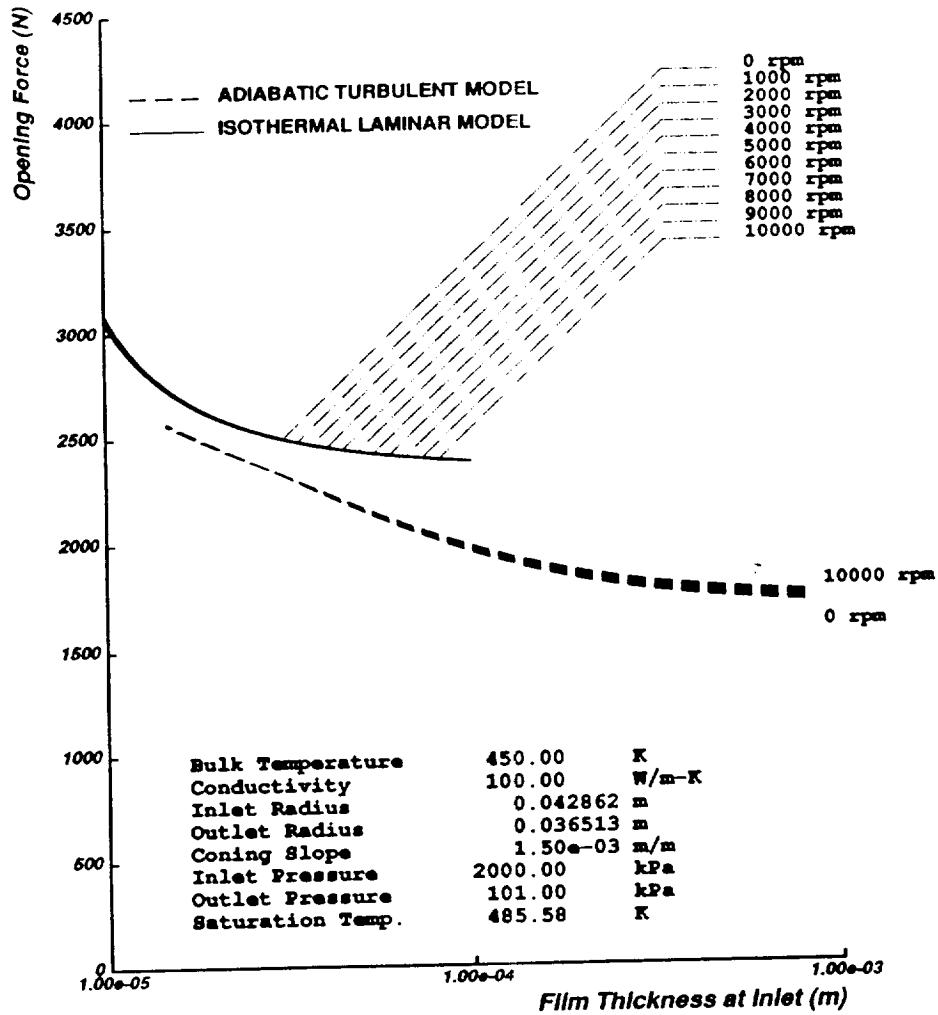


Figure 7-23: Stiffness Curves of a Coned Face Seal with a High Thermal Conductivity for Different Seal Speeds at 450K Bulk Fluid Temperature

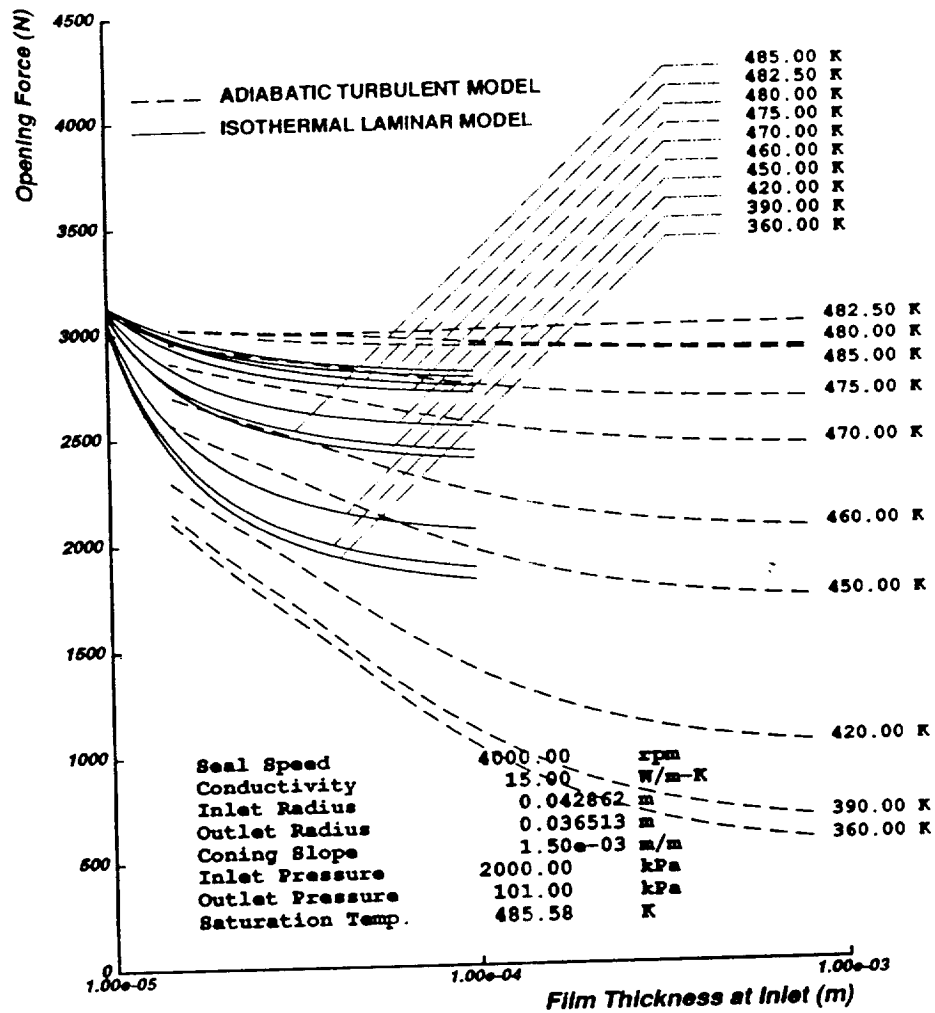


Figure 7-24: Stiffness Curves of a Coned Face Seal with a Low Thermal Conductivity for Different Bulk Fluid Temperatures

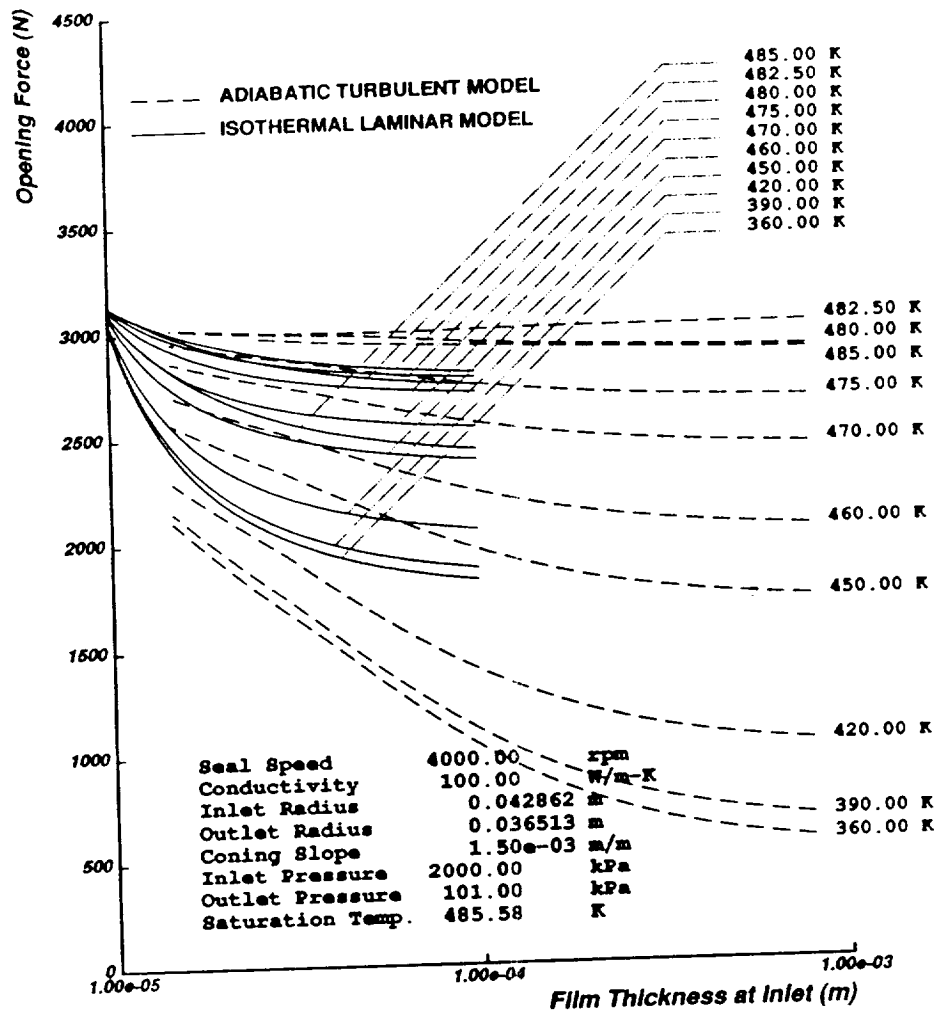


Figure 7-25: Stiffness Curves of a Coned Face Seal with a High Thermal Conductivity for Different Bulk Fluid Temperatures

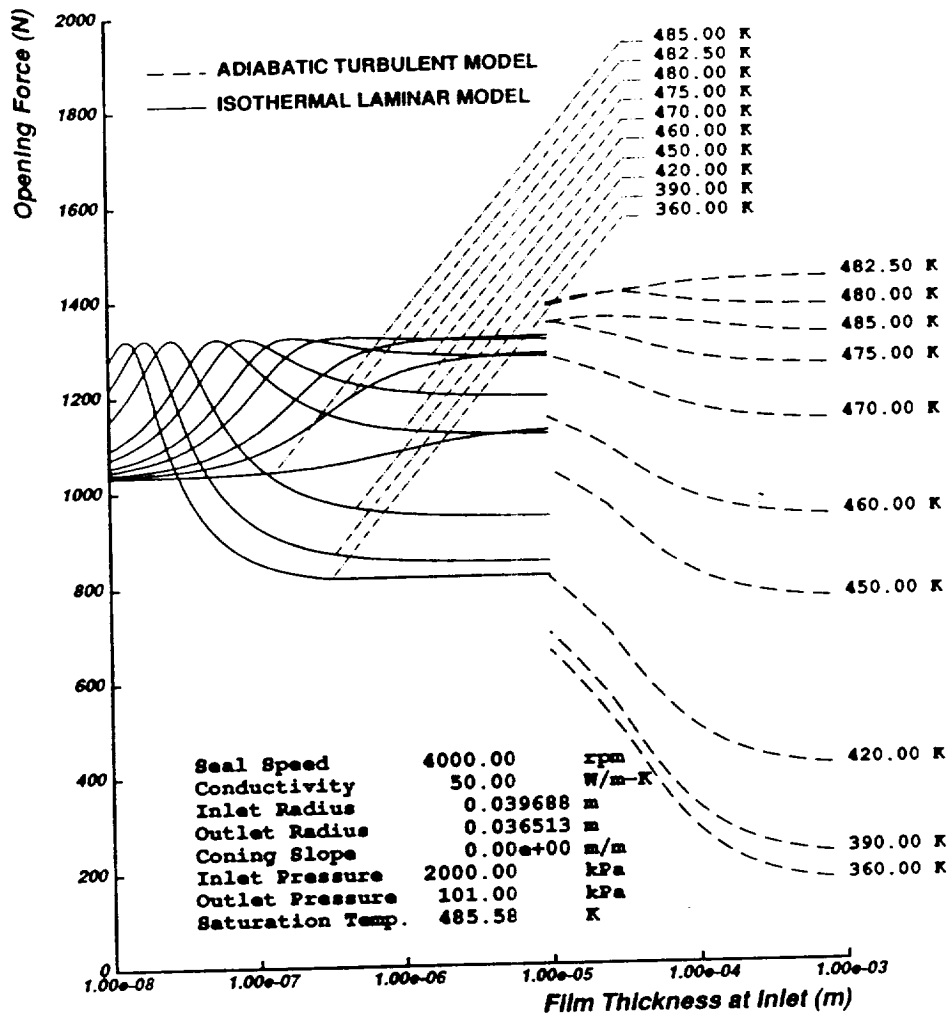


Figure 7-26: Stiffness Curves of a Parallel Face Seal with a Narrow Face Width for Different Bulk Fluid Temperatures

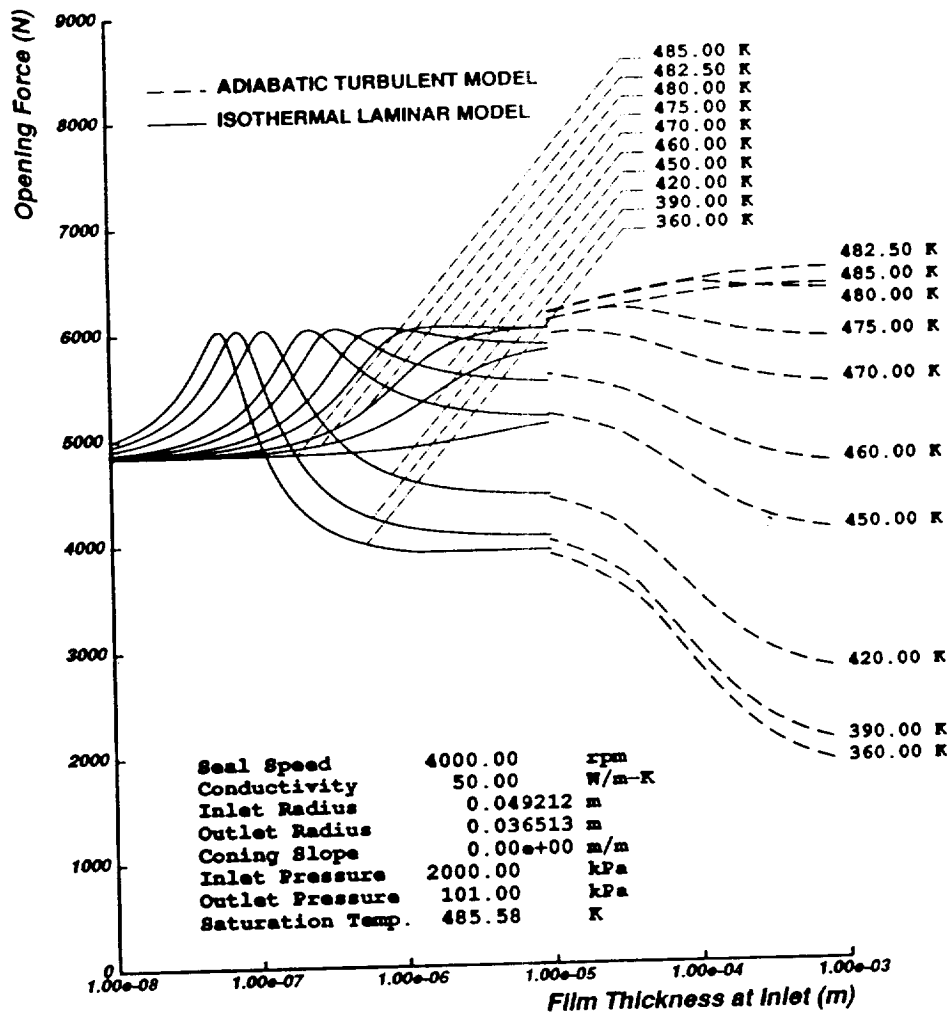


Figure 7-27: Stiffness Curves of a Parallel Face Seal with a Wide Face Width for Different Bulk Fluid Temperatures

ORIGINAL FILE IS
OF POOR QUALITY

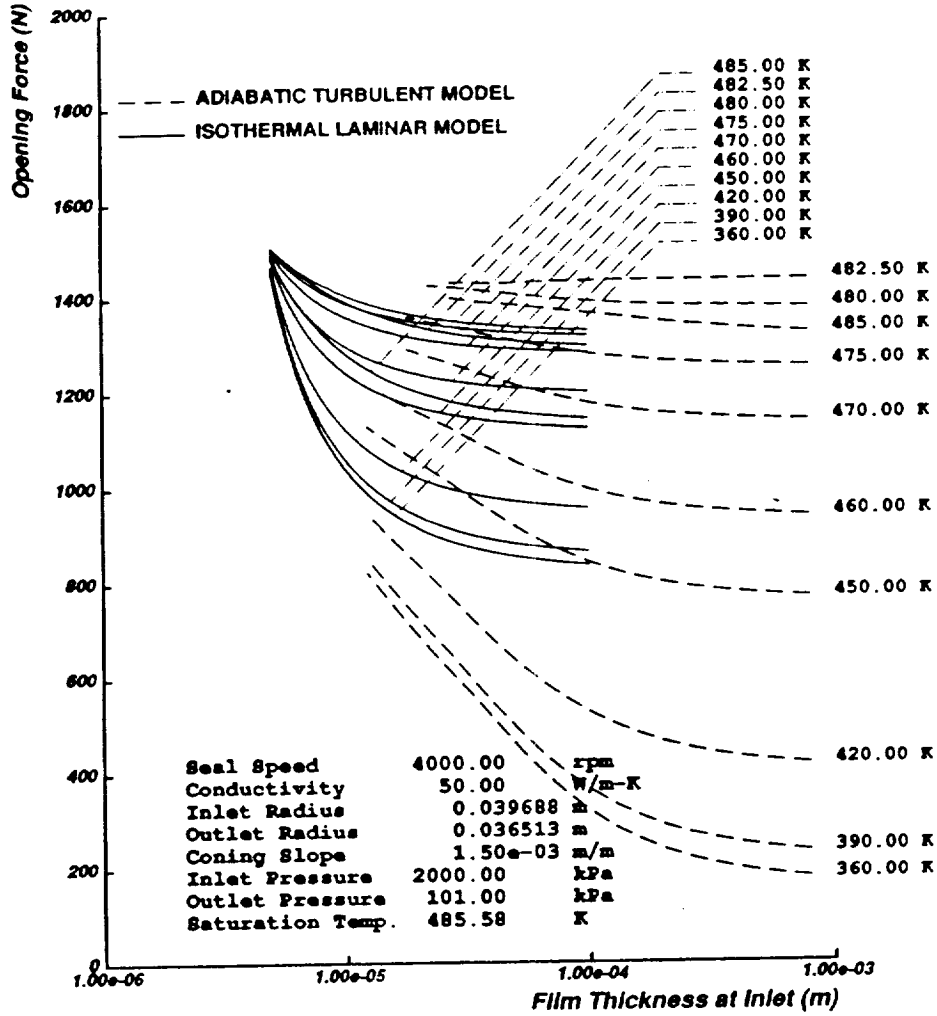


Figure 7-28: Stiffness Curves of a Coned Face Seal with a Narrow Face Width for Different Bulk Fluid Temperatures

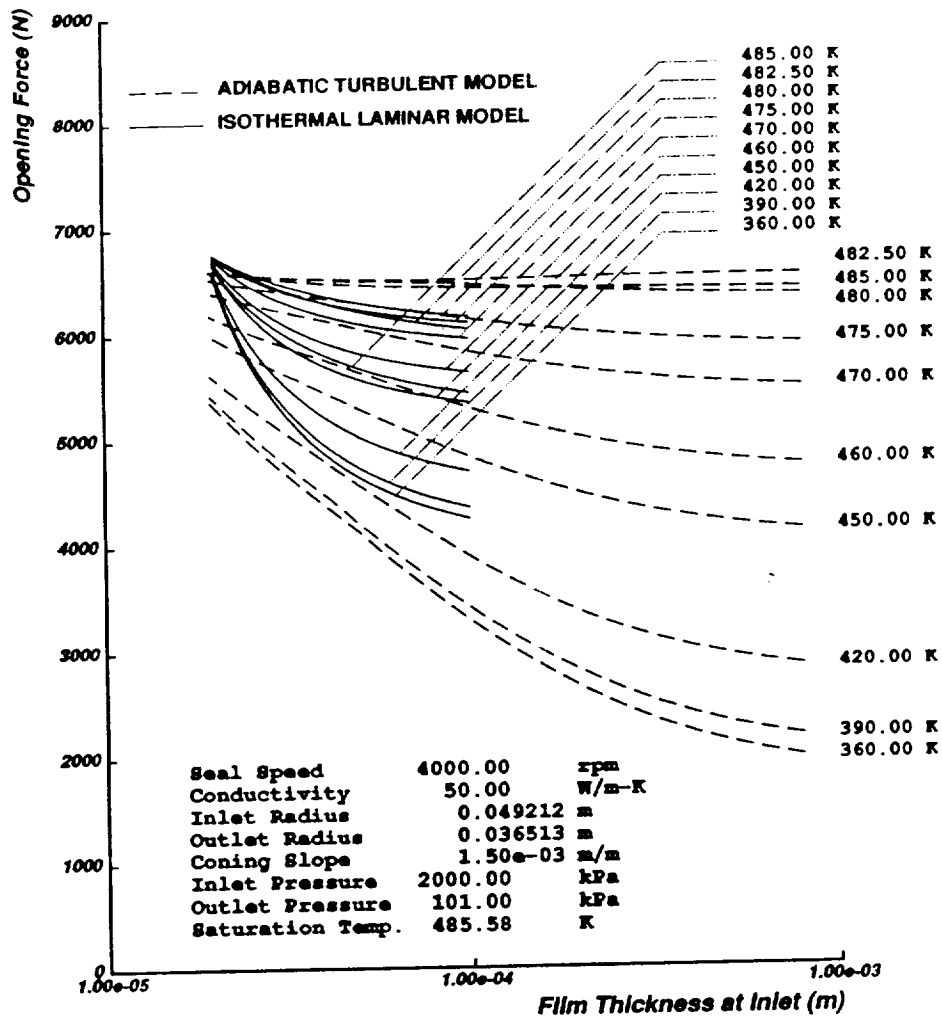


Figure 7-29: Stiffness Curves of a Coned Face Seal with a Wide Face Width at Different Bulk Fluid Temperatures

Chapter 8

A Summary of Detailed Work and Key to Publications

We have discussed some of the distinctive behavior characteristics of two-phase seals, particularly their axial stability. While two-phase seals probably exhibit instability to disturbances of other degrees of freedom such as wobble, etc., under certain conditions, such analyses are too complex to be treated at present. Since an all liquid seal (with parallel faces) has a neutral axial stiffness curve, and is stabilized axially by convergent coning, other degrees of freedom stability analyses are necessary. However, the axial stability behavior of the two-phase seal is always a consideration no matter how well the seal is aligned and regardless of the speed. Hence, we might think of the axial stability as the primary design consideration for two-phase seals and indeed the stability behavior under sub-cooling variations probably overshadows other concerns. The main thrust of this work has been the dynamic analysis of axial motion of two-phase face seals, principally the determination of axial stiffness, and the steady behavior of two-phase annular seals.

A chart is shown below which identifies the problems and we have considered and indicates location of the detailed analyses and computer codes in the listed publications.

Type of Seal	Program Description	Application	Reference for details and computer codes
Face Seal High Leakage Laminar	Adiabatic Laminar: Steady, Stability, Dynamic Response, Limit Cycles	High leakage laminar seal, not encountered under normal operating conditions.	Papers: 2, 4 Thesis 1
Face Seal Low Leakage	Quasi-Isothermal Laminar: Steady, Stability, Elevated temperature calculated with heat transfer model	Good for most face seals under normal conditions with low leakage	Papers: 2, 6 Thesis 1 Chapter 7, this report
Face Seal Low and Moderate Leakage	Continuous boiling with variable temperature. Laminar film coefficients considered in boiling region. homogeneous T-P model. Convection included in energy equation: Steady, Stability, Transient	Refinement of above model. Good for virtually all low and moderate leakage face seals.	Paper: 8 Thesis 3
Face Seals Turbulent High Leakage	Adiabatic turbulent face seals including inertia, heat generation and entrance losses Steady, Stability	High leakage seals, special applications such as cryogenic pumps: LOX-GOX	Papers: 3, 5 Thesis 2 Chapter 7, this report
Annular Seals Turbulent High Leakage	Adiabatic turbulent annular seals including inertia, heat generation and entrance losses Steady, Stability	Cryogenic LOX-GOX Turbo Pumps for Rocket Engines	Papers: 3, 7 Thesis 2 Chapter 7, this report
General Design Codes	A simplified combined computer program for laminar and turbulent face seals including effects listed in items 2 and 4 above		Chapter 7, this report (disk inside back cover)

List of published references cited in above Table:

1. N.S. Winowich, M.J. Birchak, W.C. Kennedy, and W.F. Hughes, "Phase Change in Liquid Face Seals," ASME Paper No. 77-LUB-12, *Trans. ASME, Journal of Lubrication Technology*, Vol. 100, No. 1, January 1978, p. 74.
2. N.H. Chao and W.F. Hughes, "Phase Change in Liquid Face Seals II--Isothermal and Adiabatic Bounds with Real Fluids," *Transactions of the ASME, Journal of Lubrication Technology*, Vol. 102, No. 3, July 1980, p. 350.
3. R.M. Beeler and W.F. Hughes, "Turbulent Two-Phase Flow in Ring and Face Seals," Proceedings of *Ninth International Conference on Fluid Sealing, BHRA Fluid Engineering*, April 1-3, 1981, pp. 185-202.
4. R.M. Beeler and W.F. Hughes, "Dynamics of Two-Phase Face Seals," *Trans. A.S.L.E.*, Vol. 27, No. 2, April 1984, p. 146.
5. P.A. Beatty and W.F. Hughes, "Turbulent Two-Phase Flow in Face Shaft Seals," , *Journal of Tribology*, Trans. of the A.S.M.E., Vol. 109, No. 1, January 1987, pp. 91-99.
6. P. Basu, R.M. Beeler, and W.F. Hughes, "Centrifugal Inertia Effects in Two-Phase Face Seal Films" *Trans. A.S.L.E.*, Vol. 30, No. 2, April 1987, pp. 177-186.
7. P.A. Beatty and W.F. Hughes, "Turbulent Two-Phase Flow in Annular Seals" . *Trans. A.S.L.E.*, Vol. 30, No. 1, January 1987, p. 11.
8. P. Basu and W.F. Hughes, "Thermal Instability in Two-Phase Face Seals" , Proceedings of 11th International Conference on Fluid Sealing, BHRA, Cannes, France, 1987, pp. 423-441.

Ph.D. Theses:

1. Beeler, R.M., 'Effects of Two-Phase Flow in Shaft Seals,' Ph.D. Thesis, Carnegie Mellon University, May 1985, Pittsburgh, Pennsylvania.
2. Beatty, P.A., 'Inertial Effects in Turbulent Fluid Seals,' Ph.D. Thesis, Carnegie Mellon University, May 1986, Pittsburgh, Pennsylvania.
3. Basu, P., 'Thermal Effects in Two-Phase Flow Through Face Seals,' Ph.D. Thesis, Carnegie Mellon University, May 1988, Pittsburgh, Pennsylvania.

9. REFERENCES

- [1] Buchter, H.H., 'Industrial Sealing Technology,' John Wiley & Sons, 1979.
- [2] Ludwig, L.P. & Griener, H.F., 'Designing Mechanical Face Seals for Improved Performance. Part 1 - Basic Configurations,' Mechanical Engineering, November 1978, pp. 38-46.
- [3] Ludwig, L.P. & Griener, H.F., 'Designing Mechanical Face Seals for Improved Performance. Part 2 - Lubrication,' Mechanical Engineering, December 1978, pp. 18-23.
- [4] Salant, R.F., 'Seminar on Seal Design & Analysis,' EG&G Sealol, Rhode Island, 1987.
- [5] Etsion, I., 'Radial Forces in a Misaligned Radial Face Seal,' Trans., ASME, Journal of Lubrication Technology, Vol. 101, January 1979, pp. 81-85.
- [6] Etsion, I. & Sharoni, A., 'The Effect of Coning on Radial Forces in Misaligned Radial Face Seals,' Trans., ASME, Journal of Lubrication Technology Preprint, 1979, Paper No. 79-Lub-17.
- [7] Findlay, J.A., 'Inward Pumping in Mechanical Face Seals,' Trans. ASME, Journal of Lubrication Technology, July 1969, pp. 417-426.
- [8] Findlay, J.A., 'Measurement of Leakage in Mechanical Face Seals,' Trans. ASME, Journal of Lubrication Technology, October 1969, pp. 687-694.
- [9] Etsion, I., 'Nonaxisymmetric Incompressible Hydrostatic Pressure Effects in Radial Face Seals,' Trans., ASME, Journal of Lubrication Technology, Vol. 100, July 1978, pp. 379-385.
- [10] Etsion, I., 'Hydrodynamic Effects in a Misaligned Radial Face Seal,' Trans., ASME, Journal of Lubrication Technology, Vol. 101, July 1979, pp. 283-292.
- [11] Etsion, I. & Sharoni, A., 'Performance of End-Face Seals with Diametral Tilt and Coning - Hydrostatic Effects,' ASLE Transactions, Vol. 23, 1980, 3, pp. 279-288.
- [12] Sharoni, A. & Etsion, I., 'Performance of End-Face Seals with Diametral Tilt and Coning - Hydrodynamic Effects,' ASLE Transactions, Vol. 24, 1981, 1, pp. 61-70.
- [13] Etsion, I., 'The Accuracy of the Narrow Seal Approximation in Analyzing Radial Face Seals,' ASLE Transactions, Vol. 22, 2, pp. 208-216.
- [14] Findlay, J., 'Cavitation in Mechanical Face Seals,' Trans., ASME, Journal of Lubrication Technology, April 1968, pp. 356-364.
- [15] Sneek, H.J., 'The Effects of Geometry and Inertia on Face Seal Performance - Laminar Flow,' Trans., ASME, Journal of Lubrication Technology, April 1968, pp. 333-341.

- [16] Sneck, H.J., 'Reversed Flow in Face Seals,' Trans., ASME, Journal of Lubrication Technology, July 1969, pp. 427-433.
- [17] Sneck, H.J., 'The Effects of Geometry and Inertia on Face Seal Performance - Turbulent Flow,' Trans., ASME, Journal of Lubrication Technology, April 1968, pp. 342-350.
- [18] Sneck, H.J., 'The Eccentric Face Seal with Tangentially Varying Film Thickness,' Trans., ASME, Journal of Lubrication Technology, October 1969, pp. 748-755.
- [19] Sneck, H.J., 'Misaligned, Eccentric Face Seal,' Trans., ASME, Journal of Lubrication Technology, October 1969, pp. 695-703.
- [20] Sneck, H.J., 'Thermal Effects in Face Seals,' Trans., ASME, Journal of Lubrication Technology, July 1969, pp. 434-437.
- [21] Khonsari, M.M., 'A Review of Thermal Effects in Hydrodynamic Bearings Part 1: Slider and Thrust Bearings,' ASLE Transactions, Vol. 30, 1987, 1, pp. 19-25.
- [22] King, V.W. & Lauer, J.L., 'Temperature Gradients Through EHD Films and Molecular Alignment Evidenced by Infrared Spectroscopy,' Trans., ASME, Journal of Lubrication Technology, Vol. 103, January 1981, pp. 65-73.
- [23] Pinkus, O. & Lund, J.W., 'Centrifugal Effects in Thrust Bearings and Seals under Laminar Conditions,' Trans., ASME, Journal of Lubrication Technology, Vol. 103, January 1981, pp. 126-136.
- [24] Koga, T. & Fujita, T., 'The Hydrostatic Noncontact Seal Including Fluid Inertia Effect,' ASLE Transactions, Vol. 29, 1986, 1, pp. 35-42.
- [25] Nau, B.S., 'Observations and Analysis of Mechanical Seal Film Characteristics,' Trans. ASME, Journal of Lubrication Technology, Vol. 102.
- [26] Allaire, P.E., 'Noncontacting Face Seals for Nuclear Applications - a Literature Review,' Lubrication Engineering, June 1984, pp. 344-351.
- [27] Metcalfe, R., 'Predicted Effects of Sealing Gap Convergence on Performance of Plain End Face Seals,' ASLE Transactions, Vol. 21, 1978, 2, pp. 134-142.
- [28] Metcalfe, R., 'End-Face Seal Deflection Effects - The Problems of Two-Component Stationary or Rotating Assemblies,' ASLE Transactions, Vol. 23, 1980, 4, pp. 393-400.
- [29] Metcalfe, R., et al., 'Effects of Pressure and Temperature Changes on End-Face Seal Performance,' ASLE Transactions, Vol. 25, 1982, 3, pp. 361-371.
- [30] Salant, R.F. & Key, W.E., 'Development of an Analytical Model for Use in Mechanical Seal Design,' Proceedings of the Tenth International Conference on Fluid Sealing, BHRA, 1984, Paper No. G3.
- [31] Salant, R.F., et al., 'Development of an Electronically Controlled Mechanical Seal,' Proceedings of the Eleventh International Conference on Fluid Sealing, BHRA, 1987, Paper No. H3.

- [32] Li, C.H., 'Thermal Deformation in a Mechanical Face Seal,' ASLE Transactions, Vol. 19, 2, pp. 146-152.
- [33] Doust, T.G. & Parmer, A., 'An Experimental and Theoretical Study of Pressure and Thermal Distortions in a Mechanical Seal,' ASLE Transactions, Vol. 29, 1986, 2, pp. 151-159.
- [34] Doust, T.G. & Parmer, A., 'Hydrostatic Effects in a Mechanical Face Seal,' ASLE Transactions, Vol. 29, 1986, 4, pp. 467-472.
- [35] Doust, T.G. & Parmer, A., 'Transient Thermoelastic Effect in a Mechanical Face Seal,' Proceedings of the Eleventh International Conference on Fluid Sealing, BHRA, 1987, Paper No. F3.
- [36] Lebeck, A.O., 'A Mixed Friction Hydrostatic Mechanical Face Seal Model with Thermal Rotation and Wear,' ASLE Transactions, Vol. 23, 1980, 4, pp. 375-387.
- [37] Young, L.A. & Lebeck, A.O., 'Experimental Evaluation of a Mixed Friction Hydrostatic Mechanical Face Seal Model Considering Radial Taper, Thermal Taper and Wear,' Trans., ASME, Journal of Lubrication Technology, Vol. 104, October 1982, pp. 439-448.
- [38] Lebeck, A.O., 'Contacting Mechanical Seal Design Using a Simplified Hydrostatic Model,' Proceedings of the Eleventh International Conference on Fluid Sealing,' BHRA, 1987, Paper No. F1, July 1980, pp. 341-349.
- [39] Kennedy, F.E. & Grim, J.N., 'Observation of Contact Conditions in Mechanical Face Seals,' ASLE Transactions, Volume 27, 2, pp. 122-128.
- [40] Kiryu, K., et al., 'An Analysis of Ringing Phenomena on a Water Pump Mechanical Seal,' ASLE Transactions, Vol. 28, 1985, 2, pp. 261-267.
- [41] Kiryu, K., et al., 'An Analysis of Ringing Phenomena in a Water Pump Mechanical Seal (Part II),' ASLE Transactions, Vol. 29, 1986, 1, pp. 25-34.
- [42] Haardt, R. & Godet, M., 'Axial Vibration of a Misaligned Radial Face Seal, Under a Constant Closure Force,' ASLE Transactions, Vol. 18, 1975, 1, pp. 55-61.
- [43] Etsion, I. & Burton, R.A., 'Observation of Self-Excited Wobble in Face Seals,' Trans. ASME, Journal of Lubrication Technology, Vol. 101, October 1979, pp. 526-528.
- [44] Etsion, I., 'Squeeze Effects in Radial Face Seals,' Trans., ASME, Journal of Lubrication Technology, Vol. 102, April 1980, pp. 145-152.
- [45] Etsion, I. & Dan, Y., 'An Analysis of Mechanical Face Seal Vibrations,' Trans., ASME, Journal of Lubrication Technology, Vol. 103, July 1981, pp. 428-435.
- [46] Etsion, I., 'Dynamic Response to Rotating Seat Runout in Noncontacting Face Seals,' Trans., ASME, Journal of Lubrication Technology, Vol. 103, October 1981, pp. 587-592.
- [47] Metcalfe, R., et al., 'Dynamic Tracking of Angular Misalignment in Liquid-Lubricated End-Face Seals,' ASLE Transactions, Vol. 24, 1981, 4, pp. 509-516.

- [48] Etsion, I. & Auer, B.M., 'Simulation and Visualization of Face Seal Motion Stability by Means of Computer Generated Movies,' NASA Technical Memorandum 81581, 1981.
- [49] Metcalfe, R., 'Dynamic Whirl in Well-Aligned, Liquid-Lubricated End-Face Seals with Hydrostatic Tilt Instability,' ASLE Transactions, Vol. 25, 1982, 1, pp. 1-6.
- [50] Etsion, I., 'A Review of Mechanical Face Seal Dynamics,' Shock & Vibration Digest, March 1982, pp. 9-14.
- [51] Green, I. & Etsion, I., 'Fluid Film Dynamic Coefficients in Mechanical Face Seals,' Trans. ASME, Journal of Lubrication Technology, Vol. 105, April 1983, pp. 297-302.
- [52] Green, I. & Etsion, I., 'Stability Threshold and Steady State Response of Noncontacting Coned Face Seals,' ASLE Transactions, Vol. 28, 4, pp. 449-460.
- [53] Etsion, I. & Constantinescu, I., 'Experimental Observation of the Dynamic Behavior of Noncontacting Coned-Face Mechanical Seals,' ASLE Transactions, Vol. 27, 1984, 3, pp. 263-270.
- [54] Green, I. & Etsion, I., 'Pressure and Squeeze Effects on the Dynamic Characteristics of Elastomeric O-Rings under Small Reciprocating Motion,' Trans., ASME, Journal of Tribology, Vol. 108, July 1986, pp. 439-445.
- [55] Green, I. & Etsion, I., 'Nonlinear Dynamic Analysis of Noncontacting Coned-Face Mechanical Seals,' ASLE Transactions, Vol. 29, 1986, 3, pp. 383-393.
- [56] Green, I. & Etsion, I., 'Stiffness and Damping Characteristics of Elastomer O-Rings Secondary Seals Subjected to Reciprocating Twist,' Proceedings of the Tenth International Conference on Fluid Sealing, BHRA, 1984, Paper No. E3.
- [57] Smally, A.J., et al., 'The Dynamic Characteristics of O-Rings,' ASME Journal of Mechanical Design, Vol. 100, No. 1, January 1978, pp. 132-138.
- [58] Sedy, J., 'Improved Performance of Film-Riding Gas Seals through Enhancements of Hydrodynamic Effects,' ASLE Transactions, Vol. 23, 1, pp. 35-44.
- [59] Shapiro, W. & Colsher, R., 'Steady-State and Dynamic Analysis of a Jet Engine, Gas Lubricated Shaft Seal,' ASLE Transactions, Vol. 17, 1974, 3, 190-200.
- [60] Ludwig, L.P. & Lynwander, P., 'Mainshaft Seals for Small Gas Turbine Engines,' ASLE Transactions, Vol. 19, 1, pp. 33-47.
- [61] Cheng, H.S., et al., 'Behavior of Hydrostatic and Hydrodynamic Noncontacting Face Seals,' Trans., ASME, Journal of Lubrication Technology, April 1968, pp. 510-519.
- [62] Gardner, J.F., 'Combined Hydrostatic and Hydrodynamic Principles Applied to Non-Contacting Face Seals,' presented at the Fourth International Conference on Fluid Sealing at Philadelphia, 1969.

- [63] Gardner, J.F., 'Recent Developments on Non-Contacting Face Seals,' *Lubrication Engineering*, Vol. 29, September 1973, pp. 406-412.
- [64] Zuk, J., 'Analysis of Face Deformation Effects on Gas Film Seal Performance,' *ASLE Transactions*, Vol. 16, 1973, 4, 267-275.
- [65] Hsing, F.C. & Carraro, M.J., 'Analysis of Compressible Fluid Flow in Gas Turbine Mainshaft Seals,' *ASLE Transactions*, Vol. 23, 3, pp. 237-243.
- [66] Sneek, H.J. & McGovern, J.F., 'Analytical Investigation of the Spiral Groove Face Seal,' *Journal of Lubrication Technology*, October 1973, pp. 499-510.
- [67] Boyce, M.P. & Desai, A.R., 'A Theoretical Analysis of Non-Isentropic Flow of a Compressible, Viscous Gas in Narrow Passages,' *ASLE Transactions*, Vol. 16, 2, pp. 132-140.
- [68] Zuk, J., 'Analytical Study of Pressure Balancing in Gas Film Seals,' *ASLE Transactions*, Vol. 17, 2, pp. 97-104.
- [69] Kupperman, D.S., 'Dynamic Tracking of Non-Contacting Face Seals,' *ASLE Transactions*, Vol. 18, 4, pp. 306-311.
- [70] Zuk, J., 'Compressible Seal Flow Analysis Using the Finite Element Method with Galerkin Solution Technique,' *ASLE Transactions*, Vol. 19, 1, pp. 61-71.
- [71] DiRusso, E., 'Design Analysis of a Self-Acting Spiral-Groove Ring Seal for Counter-Rotating Shafts,' *NASA Technical Paper 2143*, 1983.
- [72] Koga, T. & Fujita, T., 'The Hydrostatic Gas Noncontact Seal,' *ASLE Transactions*, Vol. 29, 4, pp. 505-514.
- [73] Milligan, M.W., 'Rarefied Gas Flow Through Passages with Static Boundaries,' *ASLE Transactions*, Vol. 11, pp. 228-234.
- [74] Hsing, F.C. & Malanoski, S.B., 'Mean Free Path Effect in Spiral-Grooved Thrust Bearings,' *Trans., ASME, Journal of Lubrication Technology*, January 1969, pp. 69-78.
- [75] Gans, R.F., 'Lubrication Theory at Arbitrary Knudsen Number,' *Journal of Tribology*, Vol. 107, July 1985, pp. 431-433.
- [76] Fukui, S. & Kaneko, R., 'Analysis of Ultra-Thin Gas Film Lubrication Based on Linearized Boltzmann Equation: First Report - Derivation of a Generalized Lubrication Equation Thermal Creep Flow,' presented at STLE/ASME Tribology Conference, San Antonio, Texas, October, 1987, Paper No. 87-Trib-14.
- [77] Fukui, S. & Kaneko, R., 'Experimental Investigation of Externally Pressurized Bearings Under High Knudsen Number Conditions,' presented at STLE/ASME Tribology Conference, San Antonio, Texas, October 1987, Paper No. 87-Trib-15.
- [78] Kubo, M., et al., 'Finite Element Solution for the Rarefied Gas Lubrication Problems,' presented at STLE/ASME Tribology Conference, San Antonio, Texas, October 1987, Paper No. 87-Trib-24.

- [79] Wallace, W.W., 'The Design & Application of Seals for Light Hydrocarbon Service,' Ninth Technical Conference of the British Pump Manufacturers' Association, 1985, Paper 21.
- [80] Suzuki, M., et al., 'Research and Development of a Rotating-Shaft Seal for a Liquid Hydrogen Turbopump,' *Lubrication Engineering*, March 1986, pp. 162-169.
- [81] Adams, W.V. & Lytwyn, P., 'Retrofit of an Unspared Main Boiler Feed Pump to End Face Mechanical Seals,' presented at the Joint ASME/IEEE Power Generation Conference, 1986.
- [82] Hill, R.C. & Rhodes, D.B., 'Behavior of Primary Coolant Pump Shaft Seals,' presented at International ANS/ENS Topical Meeting on Operability of Nuclear Power Systems in Normal and Adverse Environments, 1986.
- [83] Orcutt, F.K., 'An Investigation of the Operation and Failure of Mechanical Seals,' *Trans., ASME, Journal of Lubrication Technology*, October 1969.
- [84] Harrison, D. & Watkins, R., 'Evaluation of Forties Main Oil Line Pump Seals,' *Proceedings of the Tenth International Conference on Fluid Sealing, BHRA, 1984, Paper No. A1, p. 713-725.*
- [85] Barnard, P.C. & Weir, R.S.L., 'A Theory for Mechanical Seal Face Thermodynamics,' *Proceedings of the Eighth International Conference on Fluid Sealing, BHRA, 1978, Paper No. H1.*
- [86] Will, T.P., 'Experimental Observations of a Face-Contact Mechanical Shaft Seal Operating on Water,' *Lubrication Engineering*, December, 1982, pp. 767-772.
- [87] Hughes, W.F., Winowich, N.S., Birchak, M.J., and Kennedy, W.C., 'Phase Change in Liquid Face Seals,' *Trans., ASME, Journal of Lubrication Technology, Vol. 100, No. 1, January 1978, pp. 74-80.*
- [88] Hughes, W.F. & Chao, N.H., 'Phase Change in Liquid Face Seals II - Isothermal and Adiabatic Bounds with Real Fluids,' *Trans., ASME, Journal of Lubrication Technology, Vol. 102, No. 3, July 1980, pp. 350-359.*
- [89] Hughes, W.F. & Beeler, R.M., 'Turbulent Two-Phase Flow in Ring and Face Seals,' *Proceedings of the Ninth International Conference on Fluid Sealing, BHRA, 1981, Paper No. E3.*
- [90] Beatty, P. & Hughes, W.F., 'Turbulent Two Phase Flow in Face Shaft Seals,' *Journal of Tribology, Trans. of the A.S.M.E., Vol. 109, No. 1, January 1987, pp. 91-99..*
- [91] Lebeck, A.O., 'A Mixed Friction Hydrostatic Face Seal Model with Phase Change,' *Trans., ASME, Journal of Lubrication Technology, Vol. 102, April 1980, pp. 133-138.*
- [92] Basu, P., Hughes, W.F. & Beeler, R.M., 'Centrifugal Inertia Effects in Two-Phase Face Seal Films,' *ASLE Transactions, Vol. 30, 1987, 2, pp. 177-186.*

- [93] Basu, P. & Hughes, W.F., 'Thermal Instability in Two Phase Face Seals,' Proceedings of the Eleventh International Conference on Fluid Sealing, BHRA, 1987, Paper No. F5.
- [94] Zuber, N. & Dougherty, D.E., 'The Field Equations for Two-Phase Reynolds Film Flow with a Change of Phase,' ASLE Transactions, Vol. 25, 1982, 1, pp. 108-116.
- [95] Hudelson, J.C., 'Dynamic Instability of Undamped Bellows Face Seal in Cryogenic Liquid,' ASLE Transactions, 9, pp. 381-390.
- [96] Cieslik, W.J., 'A Helium Face Seal Application in a Liquid Oxygen Pump,' Trans., ASME, Journal of Lubrication Technology, October 1969, pp. 668-674.
- [97] Adams, W.V., 'Advancements in Sealing Ethylene and Other L.P.G. Pumps,' Hydrocarbon Processing, January 1982, 126-130.
- [98] Beeler, R.M. & Hughes, W.F., 'Dynamics of Two-Phase Face Seals,' ASLE Transactions, Vol. 27, 1984, 2, pp. 146-153.
- [99] Shapiro, W., et al., 'Analysis of Spiral-Groove Face Seals for Liquid Oxygen,' ASLE Transactions, Vol. 27, 1984, 3, 177-188.
- [100] Will, T.P., 'Effects of Seal Face Width on Mechanical Seal Performance - Hydrocarbon Tests,' Lubrication Engineering, September, 1984, pp. 522-527.
- [101] Feng, N.S. & Hahn, E.J. 'Density and Viscosity Models for Two-Phase Homogeneous Hydrodynamic Damper Fluids,' ASLE Transactions, Vol. 29, 1986, 3, pp. 361-369.
- [102] Rhodes, D.B. & Metcalfe, R., 'Preventing Dryout and Popping-Open Failures in End Face Seals,' presented at Fourth ACOT Research Seminar, 1987.
- [103] Osterle, J.F. & Hughes, W.F., 'The Effect of Lubricant Inertia in Hydrostatic Thrust-Bearing Lubrication,' Wear, 1, p. 465, 1957/58.
- [104] Beeler, R.M., 'Effects of Two-Phase Flow in Shaft Seals,' Ph.D. Thesis, Carnegie Mellon University, May 1985, Pittsburgh, Pennsylvania.
- [105] Wallis, G.B., 'One-Dimensional Two-Phase Flow,' McGraw-Hill Book Company.
- [106] Abramowitz, M. & Stegun, I.A., Editors, 'Handbook of Mathematical Functions,' Dover Publications, Inc., New York, 1965.
- [107] Byrd, P.F. & Friedman, M.D., 'Handbook of Elliptical Integrals for Engineers and Scientists,' Lange, Maxwell, and Springer Ltd., New York, 1954.
- [108] Carslaw, H.S. & Jaeger, J.C., 'Conduction of Heat in Solids,' Oxford University Press, 1950.
- [109] Gear, W.C., 'Numerical Initial Value Problems in Ordinary Differential Equations,' Prentice-Hall, Inc.

- [110] Press, W.H., et al., 'Numerical Recipes - The Art of Scientific Computing,' Cambridge University Press, 1987.
- [111] Kays, W.M. & Crawford, M.E., 'Convective Heat and Mass Transfer,' McGraw-Hill Book Company, 1980.
- [112] Beatty, P.A., 'Inertial Effects in Turbulent Fluid Seals,' Ph.D. Thesis, Carnegie Mellon University, May 1986, Pittsburgh, Pennsylvania.
- [113] Reynolds, W.C., 'Thermodynamic Properties in SI,' Department of Mechanical Engineering, Stanford University.
- [114] Irvine, T.F. & Liley, P.E., 'Steam and Gas Tables with Computer Equations,' Academic Press, Inc., 1984.
- [115] Constantinescu, V.N. and Galetuse, S., 'Operating Characteristics of Journal Bearings in Turbulent Inertial Flow,' J. Lubr. Technol., Trans. ASME 104(2):173-179, 1982.
- [116] Burton, R.A. and Hsu, Y.C., 'The Incompressible-Turbulent-Thin-Film Short Bearing With Inertial Effects,' J. Lubr. Technol., Trans. ASME 96(1):158-163, 1974.
- [117] Ng, C.W. and Pan, C.H.T., 'A Linearized Turbulent Lubrication Theory,' J. Basic Eng., Trans. ASME 87(4):675-688, 1965.
- [118] Hirs, G.G., 'A Bulk-Flow Theory for Turbulence in Lubricant Films,' J. Lubr. Technol., Trans. ASME 95(2):137-146, 1973.
- [119] Burton, R.A., 'Approximations in Turbulent Film Analysis,' J. Lubr. Technol., Trans. ASME 96(1):103-109, 1974.
- [120] Black, H.F. and Jenssen, D.W., 'Dynamic Hubrid Bearing Characteristics of Annular Controlled Leakage Seals,' Proc. Inst. Mech. Engrs. 184(Part 3N):92-100, 1970.
- [121] Yamade, Y., 'Resistance of Flow Through a Rotating Annulus with an Inner Cylinder Rotating,' Bull, JSME 5(18):302-310, 1962.
- [122] White, F.M., "Viscous Fluid Flow,' McGraw-Hill, New York, 1974, p. 543, p. 486, p. 575.
- [123] Roder, H.M. and Weber, L.A. (editors), ASRDI Oxygen Technology Survey, National Aeronautics and Space Administration, Washington, D.C., 1972.
- [124] McCarty, R.D. (editor), 'Hydrogen Technical Survey - Thermophysical Properties,' National Aeronautics and Space Administration, Washington, D.C., 1975.
- [125] Electrical Research Association (editor), 1967 Steam Tables, St. Martin's Press, New York, 1967.
- [126] Pai, S.I., 'Two-Phase Flows,' Brunschweig, Vieweg, 1977, pp. 64-67.

- [127] Childs, D.W., Dressman, J.B., and Childs, S.B., 'Testing of Turbulent Seals for Rotordynamic Coefficients,' in NASA Conference Publication 2133, pages 121-138, National Aeronautic and Space Administration, 1980.
- [128] Childs, D.W., 'Finite-Length Solutions for Rotordynamic Coefficients of Turbulent Seals,' J. Lubr. Technol., Trans. ASME 105(3):437-445, 1983.
- [129] Childs, D.W. and Dressman, J.B., 'Convergent-Tapered Annular Seals: Analysis and Testing for Rotordynamic Coefficients,' J. Tribology, Trans. ASME 107(3):307-317, 1985.

10. APPENDICES

Appendix A

Derivation of the Energy Equation

Consider radial viscous flow with properties uniform across the film. The temperature is assumed to vary only with r (but small variations across the film account for gradients in that direction and consequent conduction into the seal rings). The energy equation is written below,

$$\rho \frac{Di}{Dt} = \frac{Dp}{Dt} + \Phi + k\nabla^2 T$$

where k is the thermal conductivity of the fluid and Φ is the dissipation function given to a high degree of accuracy by

$$\Phi = \mu \left[\left(\frac{\partial w}{\partial z} \right)^2 + \left(\frac{\partial u}{\partial z} \right)^2 \right]$$

Integrating the energy equation across the film

$$\begin{aligned} \int_0^h \rho u \frac{di}{dr} dz &= \int_0^h u \frac{dp}{dr} dz + \mu \int_0^h \left[\left(\frac{\partial w}{\partial z} \right)^2 + \left(\frac{\partial u}{\partial z} \right)^2 \right] dz \\ &\quad \int_0^h k \left(\frac{\partial^2 T}{\partial r^2} + \frac{1}{r} \frac{\partial T}{\partial r} + \frac{\partial^2 r}{\partial z^2} \right) dz \end{aligned}$$

Multiplying the r -momentum equation (2.1) by u and integrating across the film,

$$\begin{aligned} \int_0^h u \frac{dp}{dr} &= \mu \int_0^h u \frac{\partial^2 r}{\partial z^2} dz + \rho \int_0^h \frac{uu^2}{r} dz \\ &= \mu \left[u \frac{\partial u}{\partial z} \Big|_0^h - \int_0^h \left(\frac{\partial u}{\partial z} \right)^2 dz \right] + \rho \int_0^h \frac{uu^2}{r} dz \end{aligned}$$

Combining with the energy equation and neglecting conduction along the film

$$\frac{m}{2\pi r} \frac{di}{dr} = \mu u \left. \frac{\partial u}{\partial z} \right|_0^h + \rho \int_0^h \frac{u w^2}{r} dz + \int_0^h \mu \left(\frac{\partial w}{\partial z} \right)^2 dz + \int_0^h k \frac{\partial^2 T}{\partial z^2} dz$$

Since $u = 0$ at $z = 0, h$, the first term of the right-hand side goes to zero. The term

$$\int_0^h k \frac{\partial^2 T}{\partial z^2} dz$$

integrates to

$$k \left. \frac{\partial T}{\partial z} \right|_{z=h} - k \left. \frac{\partial T}{\partial z} \right|_{z=0} = -q$$

where q is the conduction heat flux into the seal rings from the fluid.

Using the expression for u and w from equations [2.4] and [2.3], the following form of the integrated energy equation is obtained,

$$\frac{m}{2\pi r} \frac{di}{dr} = \mu \frac{r^2 \omega^2}{h} + \frac{3\omega^2 m}{20\pi} + \frac{\rho^2 r^2 h^3 \omega^4}{700\mu} - q$$

Appendix B

The Steady State Influence Coefficient Matrix

In this appendix, the relationship between the heat-conduction profile and the temperature profile is derived. The result is a coefficient matrix, $[C]$, which relates the temperature and heat conduction vectors, $\{T\}$ and $\{q\}$, whose n elements correspond to finite difference points that have been placed along the fluid film. The elements of this matrix involve the complete elliptic integrals of the first and second kind, K and E , respectively. These are defined as follows :

$$K(x) = \int_0^{\pi/2} (1 - x^2 \sin^2 \theta)^{-1/2} d\theta$$
$$E(x) = \int_0^{\pi/2} (1 - x^2 \sin^2 \theta)^{1/2} d\theta$$

where x is referred to as the modulus.

It is required to find the temperature T_s at a point on the surface of the seal ring faces due to a heat source at another position. The background temperature is T_∞ . The radial position r_s at which temperature is to be determined, corresponds to the mid-width of the s^{th} element of the fluid film. The heat source q_t is due to uniform heat generation over the t^{th} element. The heat flux leaves the fluid film and enters the rings normal to the faces. The heat flux is assumed constant across each element and is thus discontinuous at the edge between two adjacent elements. The inner and outer radii of the t^{th} element are designated as r_{t-} and r_{t+} respectively.

The temperature T at \vec{r}_s due to a point heat source q_t at \vec{r}_t in the solid is

$$T(\vec{r}_s, \vec{r}_t) = \frac{q_t}{4\pi k |\vec{r}_s - \vec{r}_t|} + T_\infty$$

which is easily derived by considering the heat flux across a sphere of radius $|\bar{r}_s - \bar{r}_t|$ centered around a point heat source of intensity q_t at \bar{r}_t . The temperature T_{st} is now given by integrating the above Green's function over the entire t^{th} element as follows:

$$T_{st} = \int_{r_{t-}}^{r_{t+}} \int_0^{2\pi} \frac{r q_t d\phi d\tau}{4\pi k |r_s - r_t|} + T_\infty$$

Carrying out this integration, according to the formulas provided by Abramowitz and Stegun [106], and Byrd and Friedman [107], the following expressions are obtained,

$$T_{st} - T_\infty = \frac{q_t r_s}{\pi k} \left[E \left[\frac{r_{t+}}{r_s} \right] - E \left[\frac{r_{t-}}{r_s} \right] + \left[\frac{r_{t+}^2 - r_s^2}{r_s^2} \right] K \left[\frac{r_{t+}}{r_s} \right] - \left[\frac{r_{t-}^2 - r_s^2}{r_s^2} \right] K \left[\frac{r_{t-}}{r_s} \right] \right]; r_{t+} < r_s \quad (\text{B.1})$$

$$T_{st} - T_\infty = \frac{q_t r_s}{\pi k} \left[\left[\frac{r_{t+}}{r_s} \right] E \left[\frac{r_s}{r_{t+}} \right] - \left[\frac{r_{t-}}{r_s} \right] E \left[\frac{r_s}{r_{t-}} \right] \right]; r_{t-} > r_s \quad (\text{B.2})$$

and

$$T_{st} - T_\infty = \frac{q_t r_s}{\pi k} \left[\left[\frac{r_{s+}}{r_s} \right] E \left[\frac{r_s}{r_{s+}} \right] + \left[\frac{r_s^2 - r_{s-}^2}{r_s^2} \right] K \left[\frac{r_{s-}}{r_s} \right] - E \left[\frac{r_{s-}}{r_s} \right] \right]; r_s = r_t \quad (\text{B.3})$$

Equation (B.1), (B.2), or (B.3) is used depending on whether the temperature in question is at a radial position outside, inside or equal to the corresponding position of the heat source, respectively. Since, in general, all of the elements making up the fluid film will be releasing or absorbing heat, it is summed over all the heat sources to get the total temperature elevation at a point.

$$T_s = \sum_{t=1}^n T_{st} + T_\infty$$

The temperature T_s and the heat fluxes q_t are grouped into column vectors $\{T\}$ and $\{q\}$, respectively, which are then related by the square coefficient matrix $[C]$,

$$\{T\} = [C]\{q\} + \{T_\infty\}$$

where $\{T_\infty\}$ is the column vector, each element of which is equal to the background temperature T_∞ .

Appendix C

Derivation of the Time-Dependent Influence Coefficient Matrix

Referring to the Figure (C.1), the temperature at the mid-point of the element 'k' due to heat generation over the element 'l' over the time interval (0, t) is given by the following Equation [108],

$$T_{kl}(t) = \frac{2\pi q_l r_l \Delta r_l \alpha}{k} \underbrace{\int_0^t \frac{1}{8[\pi\alpha(t-\tau)]^{3/2}} \exp\left[-\frac{r_k^2 + r_l^2}{4\alpha(t-\tau)}\right] I_0\left[\frac{r_k r_l}{2\alpha(t-\tau)}\right] d\tau}_{J_1} \quad (C.1)$$

where, Δr_l is the width of the 'lth' element and I_0 is the modified Bessel function. Here a time invariant concentrated line ring source is assumed to exist at the radius ' r_l '.

C.1 Off-Diagonal Terms ($k \neq l$)

Evaluate the integral J_1 .

Assume $t_d = t - \tau$. Hence $dt_d = -d\tau$. For different ranges of t_d , different approximations are to be used.

C.1.1 Case 1

For $\frac{r_k r_l}{2\alpha t_d} > 3.75$ or $t_d < \frac{r_k r_l}{7.5\alpha} = (t_c)_{kl}$ (say), the following series representation of Bessel function I_0 can be made according to the Equation (9.8.2) in [106],

$$I_0(x)x^{1/2}e^{-x} = b_1 + h.o.t \quad (C.2)$$

where $b_1 = 0.39894228$ and higher order terms (*h.o.t*) can be neglected.

Using the Equation (C.2), the integral J_1 can be written as

$$\begin{aligned} J_1 &= \frac{b_1}{31.499 \alpha \sqrt{r_k r_l}} \int_0^{t_1} \frac{1}{t_d} \exp\left[-\frac{(r_k - r_l)^2}{4\alpha t_d}\right] dt_d \\ &= \frac{b_1}{31.499 \alpha \sqrt{r_k r_l}} E_1\left[\frac{(r_k - r_l)^2}{4\alpha t_1}\right] \end{aligned} \quad (C.3)$$

where E_1 is the 'Exponential Integral Function' the series representation of which is given by the Equation (5.1.53) in [106].

Substituting Equation (C.3) in (C.1),

$$\begin{aligned} T_{kl}(0, t_1) &= 0.199471 b_1 \frac{1}{k} \sqrt{r_l/r_k} \Delta r_l E_1\left[\frac{(r_k - r_l)^2}{4\alpha t_1}\right] q_l \\ &= C_{kl}(0, t_1) q_l; \quad 0 \leq t_d \leq (t_c)_{kl} \end{aligned} \quad (C.4)$$

where C_{kl} is the (k, l)th element of the time-dependent influence coefficient matrix.

C.1.2 Case 2

For $(t_c)_{kl} < t_d < \infty$, the modified Bessel function I_0 can be expressed by the following series expression according to the Equation (9.8.1) in [106] with the values of the coefficients a_0 through a_4 given,

$$\begin{aligned} I_0\left[\frac{r_k r_l}{2\alpha t_d}\right] &= a_0 + a_1 \left[\frac{(t_c)_{kl}}{t_d}\right]^2 + a_2 \left[\frac{(t_c)_{kl}}{t_d}\right]^4 + a_3 \left[\frac{(t_c)_{kl}}{t_d}\right]^6 + \\ &\quad a_4 \left[\frac{(t_c)_{kl}}{t_d}\right]^8 + h.o.t \end{aligned} \quad (C.5)$$

Using the Equation (C.5) in evaluating the integral J_1 , one obtains

$$\begin{aligned}
 J_1 &= \frac{1}{8\pi^{3/2}\alpha} \frac{1}{\sqrt{r_k^2 + r_l^2}} \left[3.5449 f_{10}(y) + 0.56889 a_1 R_{kl}^2 f_{11}(y) + \right. \\
 &\quad \left. 0.16182 a_2 R_{kl}^4 f_{12}(y) + 0.04603 a_3 R_{kl}^6 f_{13}(y) + 0.0131 a_4 R_{kl}^8 f_{14}(y) \right]_{y_2}^{y_1} \\
 &= \frac{1}{8\pi^{3/2}\alpha} \frac{1}{\sqrt{r_k^2 + r_l^2}} [g(y)]_{y_2}^{y_1} \quad (C.6)
 \end{aligned}$$

where $g(y)$ is the function inside the parentheses and the limits of integration are given by

$$\begin{aligned}
 y_1 &= \frac{r_k^2 + r_l^2}{4\alpha t_1} \\
 y_2 &= \frac{r_k^2 + r_l^2}{4\alpha t_2}
 \end{aligned}$$

The other functional definitions, used in the Equation (C.6) are

$$\begin{aligned}
 R_{kl} &= \frac{1}{\left(\frac{r_k}{r_l} + \frac{r_l}{r_k}\right)} \\
 f_{10}(y) &= \operatorname{erf}(\sqrt{y}) \\
 f_{11}(y) &= 1.32934 \operatorname{erf}(\sqrt{y}) - (y + 1.5)\sqrt{y}e^{-y} \\
 f_{12}(y) &= 11.63173 \operatorname{erf}(\sqrt{y}) - (y^3 + 3.5y^2 + 8.75y + 13.125)\sqrt{y}e^{-y} \\
 f_{13}(y) &= 287.8853 \operatorname{erf}(\sqrt{y}) - (y^5 + 5.5y^4 + 24.75y^3 + 86.625y^2 + 216.5625y + \\
 &\quad 324.8438)\sqrt{y}e^{-y} \\
 f_{14}(y) &= 14034.407 \operatorname{erf}(\sqrt{y}) - (y^7 + 7.5y^6 + 48.75y^5 + 268.125y^4 + 1206.563y^3 + \\
 &\quad 4222.969y^2 + 10557.422y + 15836.13)\sqrt{y}e^{-y}
 \end{aligned}$$

Substituting Equation (C.6) in (C.1) with the limits of integration,

$$\begin{aligned}
 T_{kl}(t_1, t_2) &= \frac{1}{4\pi^{1/2}k} \frac{r_l}{\sqrt{r_k^2 + r_l^2}} \Delta r_l \left[g\left(\frac{r_k^2 + r_l^2}{4\alpha t_1}\right) - g\left(\frac{r_k^2 + r_l^2}{4\alpha t_2}\right) \right] q_l \\
 &= C_{kl}(t_1, t_2) q_l ; (t_c)_{kl} \leq t_d \leq \infty \quad (C.7)
 \end{aligned}$$

Again q_l is assumed to be constant over the time interval t_1 and t_2 .

C.2 Diagonal Terms ($k = l$)

Considering an heat source extended over the 'kth' ring, the temperature at the mid-point of the ring 'k' due to self heat generation over the period $(0, t)$ is given by

$$T_{kk}(0, t) = \int_0^t \int_{r_{k-}}^{r_{k+}} \frac{2\pi q_k}{\rho C} \frac{1}{8[\pi\alpha(t-\tau)]^{3/2}} \exp\left[-\frac{r_k^2 + r^2}{4\alpha(t-\tau)}\right] I_0\left[\frac{r_k r}{2\alpha(t-\tau)}\right] r dr d\tau \quad (C.8)$$

Again let $t_d = t - \tau$. Using this substitution in Equation (C.8), there obtains,

$$T_{kk}(0, t) = \frac{2\pi q_k \alpha}{k} \int_0^t \frac{1}{8[\pi\alpha(t_d)]^{3/2}} \int_{r_{k-}}^{r_{k+}} \exp\left[-\frac{r_k^2 + r^2}{4\alpha t_d}\right] I_0\left[\frac{r_k r}{2\alpha t_d}\right] r dr dt_d \quad (C.9)$$

C.2.1 Case 1

For $0 < t_d < (t_c)_{kk}$, using the series representation (C.2) of the modified Bessel function, the Equation (C.9) can be written as

$$T_{kk}(0, t) = \frac{q_k b_1}{\sqrt{8\pi r_k k}} \int_0^t \frac{1}{t_d} \int_{r_{k-}}^{r_{k+}} \exp\left[-\frac{(r_k - r)^2}{4\alpha t_d}\right] \sqrt{r} dr dt_d \quad (C.10)$$

The function \sqrt{r} inside the spatial integral does not vary that much over the interval (r_{k+}, r_{k-}) and it can be assumed as $\sqrt{r_k}$ over the same interval. However, the first function $\exp\left[-\frac{(r_k - r)^2}{4\alpha t_d}\right]$ varies dramatically over the region specially when $t_d \rightarrow 0$.

Hence the Equation (C.10) becomes,

$$\begin{aligned} T_{kk}(0, t) &= \frac{q_k b_1}{\sqrt{8\pi k}} \int_0^t \frac{1}{t_d} \int_{r_{k-}}^{r_{k+}} \exp\left[-\frac{(r_k - r)^2}{4\alpha t_d}\right] dr dt_d \\ &= \frac{b_1}{k} \left[\frac{\Delta r_k}{\sqrt{8\pi}} E_1\left(\frac{\Delta r_k^2}{16\alpha t}\right) + \sqrt{2\alpha t} \operatorname{erf}\left(\frac{\Delta r_k}{4\sqrt{\alpha t}}\right) \right] q_k \\ &= C_{kk} q_k ; 0 < t_d < (t_c)_{kk} \end{aligned} \quad (C.11)$$

C.2.2 Case 2

For $(t_c)_{kk} < t_d < \infty$, the same Equation (C.7) as in $k \neq l$ can be used.

ORIGINAL DESIGN
OF POOR QUALITY

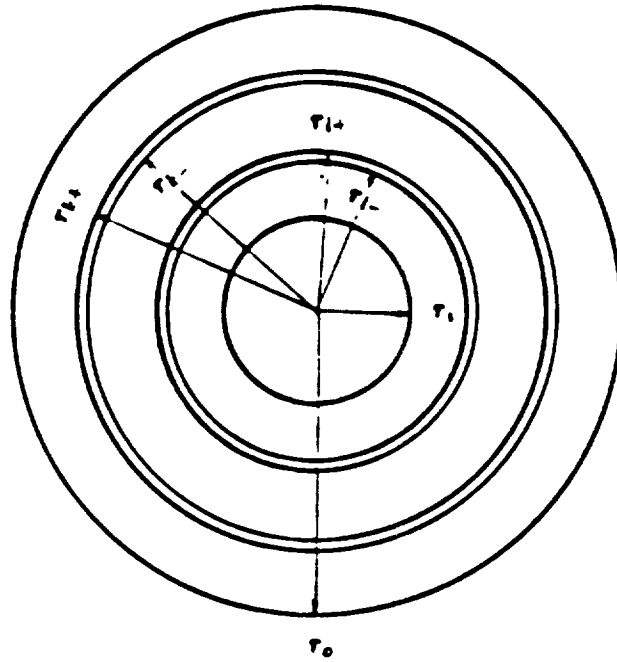


Figure C.1: Discretization of Annular Seal Interface

Appendix D

The Combined Laminar and Turbulent Computer Code for Low and High Leakage Operations

D.1 Input File Description

The default name of the input file is 'seal.in'. If a file named 'seal.in' is found in the current working directory, the program will assume this file to be the intended input file and will try reading input data from it without asking the user any question. If such a file does not exist in the working directory, the user is prompted for the name of the input data file.

The format of an input file is tabulated below:

Line	Variable	Format	Description
1	outfnm	a15	Name of the output data file, maximum 15 characters. However, for machines running MS-DOS, this is limited by the MS-DOS file naming convention (8 character file name + 3 character extension).
2	fluid	a8	Name of the working fluid. The current fluids incorporated in this program are 'water', 'nitrogen', 'hydrogen' and 'oxygen'.
3	pinlet	f20.0	Pressure at the seal inlet (i.e. reservoir pressure). [kPa]
4	pback	f20.0	Pressure at the seal exit (i.e. back pressure). [kPa]
5	rinlet	f20.0	Radius of the seal inlet. For an outside seal, this is the outer radius; for an inside seal, this is the inner radius. [m]
6	routlt	f20.0	Radius of the seal outlet. For an outside seal, this is the inner radius; for an inside seal, this is the outer radius. [m]
7	cone	f20.0	Seal coning slope. A positive value means that the seal gap diverges with increasing radial distance from the seal axis. [m/m]
8	conduc	f20.0	Average conductivity of the seal face materials. [W/m-K]

Line	Variable	Format	Description
9	both	a1	To decide whether the analysis will be performed for both low leakage and high leakage operations or only for the low leakage operation. If a 'Y' or 'y' is entered, the analysis will be performed for both flow regimes. If any other character is entered (an 'N' or 'n' is recommended) the analysis will only be performed for the low leakage laminar operation. Note that a combined analysis for both flow regimes typically takes 40 times (depending on the number of different film thicknesses calculated in the high leakage analysis ¹) longer to run than an analysis for low leakage operation only.
10	choose	a1	To choose whether the analysis will be repeated for different seal speeds or for different bulk (reservoir) fluid temperatures. If an 'S' or 's' is entered, the analysis will be repeated for different seal speeds. If a 'T' or 't' is entered, the analysis will be repeated for different bulk temperatures.
11	tinf or rpm	f20.0	If the analysis is going to be repeated for different seal speeds (choose = 'S'), the bulk temperature tinf is entered here. If the analysis is going to be repeated for different bulk temperatures (choose = 'T'), the seal speed rpm is entered here. [K] if choose = 'S' ; [rpm] if choose = 'T'
12	ncurve	i10	Number of times the analysis will be performed for different seal speeds or bulk temperatures. This is the same as the number of stiffness and leakage curves to be calculated. The limit on the number of curves is 50.
next ncurve lines	tinf or rpms	f20.0	The ncurve different seal speeds (if choose = 'S') or bulk fluid temperatures (if choose = 'T') for which analyses are performed are entered here. Each seal speed or bulk fluid temperature is entered on a separated line. [rpm] if choose = 'S' ; [K] if choose = 'T'

¹Section D.3 describes how to vary the range and the number of film thicknesses.

A sample input file is given below. Columns 21 to 80 of each input line are reserved for comments.

```

seal.out          ; output file name (max 15 characters, less for DOS)
water             ; fluid (either: water, nitrogen, oxygen or hydrogen)
2000.             ; pinlet (kPa)
101.              ; pback (kPa)
0.0428625        ; rinlet (m)
0.0365125        ; routlt (m)
1.5e-03          ; cone (m/m)
50.0             ; conduc (W/m-K)
y                ; both, 'n' if laminar analysis only; 'y' for both
t                ; choose, 's' for speeds, 't' for bulk temperatures
4000.0           ; if 's', bulk temp. (degrees K); seal RPM if 't'
10               ; number of curves (max 50)
360.0            ; tinf(1)
390.0            ; tinf(2)
420.0            ; tinf(3)
450.0            ; tinf(4)
460.0            ; tinf(5)
470.0            ; tinf(6)
475.0            ; tinf(7)
480.0            ; tinf(8)
482.5            ; tinf(9)
485.0            ; tinf(10)

```

The ranges of allowable temperatures and pressures for the various fluids currently incorporated in this program are listed below:

Water	-	305.00 K <	tinf	<	647.29 K
		4.718 kPa <	pinlet, pback	<	22.089 MPa
Nitrogen	-	63.15 K <	tinf	<	126.20 K
		12.54 kPa <	pinlet, pback	<	3.400 MPa
Oxygen	-	80.00 K <	tinf	<	154.58 K
		30.09 kPa <	pinlet, pback	<	5.043 MPa
Hydrogen	-	13.80 K <	tinf	<	32.94 K
		7.042 kPa <	pinlet, pback	<	1.284 MPa

D.2 Output File Description

The contents of output file is self descriptive. An output file begins with a heading showing the input seal operating parameters. It is followed by tabulated results of the seal analyses for each seal speed or bulk fluid temperature. The tabulated results are all given in S.I. units. If an analysis is performed for both low and high leakage operations, the results for each seal speed or bulk temperature will be tabulated in two tables, the first table contains the results from the quasi-isothermal laminar model and the second table contains the results from the adiabatic turbulent model. If the analysis is performed only for low leakage operations, the results will be tabulated in only one table.

The output data contains :

For each seal speed or bulk fluid temperature, a sub-heading is printed to identify either the speed or the bulk temperature:

rpm: Seal speed, [rpm]; or
tin: bulk fluid temperature of the reservoir, [K].

For the laminar low leakage model, the tabulated results are:

hrin: The inlet film thickness, [m].
xboil: The non-dimensional boiling location. The non-dimension radial position, x , is defined as fraction of the seal width from the seal exit:

$$x = \frac{r - r_{\text{exit}}}{r_{\text{inlet}} - r_{\text{exit}}}$$

pboil: The fluid pressure at the boiling locations, [Pa].
tseal: The temperature of the seal at the boiling location, [K].
leakage: The leakage rate [in kg/s], where positive values indicate that the leakage path is radially outwards and negative values indicate that the leakage path is radially inwards.
load: The seal opening force, [N].

- Note that if the **xboil** and **pboil** columns are blank, the seal is either all-liquid or all-vapor. For an all-liquid seal, the temperature **tseal** is the temperature evaluated at the seal exit. For an all-vapor seal, since we assumed that the viscous dissipation is negligible, **tseal** will be the same as the bulk fluid temperature.

- If the **pboil** and **leakage** columns are blank, the seal is non-boiling and is operating at above critical speed. In this case, the non-dimensional radial location of the stationary liquid front is given as **xboil** and the leakage rate is zero.

For the turbulent high leakage model, the tabulated results are:

- hrin:** The inlet film thickness, [m].
- Reyc:** The maximum Reynold's number in the circumferential direction.
- Reyr:** The maximum Reynold's number in the radial direction.
- qexit:** The quality of the fluid exiting the seal.
- leakage:** The leakage rate [in kg/s], where positive values indicate that the leakage path is radially outwards and negative values indicate that the leakage path is radially inwards.
- load:** The seal opening force, [N].

D.3 Preset Program Parameters

There are several parameters preset (hard coded) in the computer code. Some of these parameters are problem specific and may be adjusted to suit the specific needs of individual problems. They are initialized immediately upon program execution. The location of the code which initializes these parameters is in the main program following the variable declarations. A brief description of each of these parameters are tabulated below:

Preset parameters for the turbulent analysis:

Variable	Type	Preset Value	Description
nspac	integer*4	50	Size of the finite difference grid.
closs	real*8	0.5	Inlet pressure loss coefficient. The inlet pressure loss is given by the product of the inlet loss coefficient and the dynamic pressure. The preset value is for inlets with square edges.
epsi	real*8	0.95	Grid contraction factor. The factor by which the finite difference grid contracts along the leakage path. Since pressure drop is usually much steeper near the exit, we can obtain better resolution using a variable sized grid with grid points closer to each other near the exit.
error	real*8	0.001	The iteration error bound for the exit pressure.

Preset parameters for the number and range of film thicknesses to be calculated:

Variable	Type	Preset Value	Description
npntst	integer*4	21	Number of points (different film thicknesses) on the turbulent curves. The points are chosen in such a way that they are equally spaced between hinupt and hinlot in log scale.
hinupt	real*8	10^{-3}	The upper limit of the inlet film thickness of the turbulent curves. [m]
hinlot	real*8	10^{-5}	The lower limit of the inlet film thickness of the turbulent curves. [m]
npntsl	integer*4	31	Number of points (different film thicknesses) on the laminar curves. The points are chosen in such a way that they are equally spaced between hinupl and hinlol in log scale.
hinupl	real*8	10^{-5}	The upper limit of the inlet film thickness of the laminar curves. [m]
hinlol	real*8	10^{-8}	The lower limit of the inlet film thickness of the laminar curves. [m]

In the original turbulent code, the user is required to input **floor**, an estimate of the minimum allowable mass flow rate. This value is used as the first mass flow rate estimate when solving the boundary value problem using the shooting method. If this estimate is too large and gives a choked flow in the first iteration of the shooting method, the program will abort (return without a solution) with an error message. If the estimate is too low, the program may not converge.

Fortunately, the range of values of **floor** for which the program will converge is quite large. Since the mass leakage rate is directly proportional to the film thickness, in the combined program, the value of **floor** is initialized in the turbulent analysis code subroutine **face**. The current preset values are, where h_{mean} is the mean film thickness:

$$\text{floor} = \begin{cases} 10^{-2} \text{ kg/s,} & \text{if } h_{\text{mean}} > 10^{-4} \text{ m} \\ 10^{-4} \text{ kg/s,} & \text{if } h_{\text{mean}} \leq 10^{-4} \text{ m} \end{cases}$$

Note that the optimal choices for the values of **floor** are problem specific and the preset values may not be suitable for all cases. If the turbulent code does not run properly, the user should try adjusting the preset values of **floor**.

D.4 Source Code of the Combined Laminar and Turbulent Program

```
c-----c
c
c      Steady State Analysis for a Two-Phase Face Seal Operating in
c      Low Leakage Laminar and the High Leakage Turbulent Regimes
c
c      This program analyzes the steady state performance of a
c      two-phase face seal operating under both low leakage
c      conditions using the quasi-isothermal laminar model and
c      under high leakage operations using the adiabatic turbulent
c      model.
c
c      Units:
c      S.I. units are used in all calculations. With the exception
c      of input pressures being in kPa, all input values are in
c      S.I. units. All output values are in S.I. units unless
c      they are stated otherwise.
c
c      Acceptable Ranges of Temperature and Pressure Input Data:
c
c      Water      - 305.00 K < tinf          < 647.29 K
c                  4.718 kPa < pinlet, pback < 22.089 MPa
c
c      Nitrogen   - 63.15 K < tinf          < 126.20 K
c                  12.54 kPa < pinlet, pback < 3.400 MPa
c
c      Oxygen     - 80.00 K < tinf          < 154.58 K
c                  30.09 kPa < pinlet, pback < 5.043 MPa
c
c      Hydrogen   - 13.80 K < tinf          < 32.94 K
c                  7.042 kPa < pinlet, pback < 1.284 MPa
c
c      Please direct any questions or comments to:
c
c      Professor William F. Hughes or Stephen Lau
c      Department of Mechanical Engineering
c      Carnegie Mellon University
c      Pittsburgh, Pennsylvania 15213
c-----c
c-----c
c      Main program.
c
c      program seal
c-----c
```

```

-----+c
cc      implicit logical ( a - z )
cc      implicit undefined ( a - z )

real*8  rinlet, routlt, cone, conduc
real*8  pinlet, pback, rpm, omega, rolinf, tinf
real*8  closs, epsi, error
real*8  hinupt, hinlot, hinupl, hinlol
cc      real*8  hinlet, pboil, rboil
cc      real*8  tseal, visgas, visliq, rolliq, rgas

integer nspace
integer npntst, npntsl

common /geomty/ rinlet, routlt, cone, conduc
common /operat/ pinlet, pback, rpm, omega, rolinf, tinf
common /turbin/ nspace, closs, epsi, error
common /curves/ npntst, hinupt, hinlot, npntsl, hinupl, hinlol
cc      common /iterat/ hinlet, pboil, rboil
cc      common /fluid / tseal, visgas, visliq, rolliq, rgas

real*8  rpms(50), tinf(50)
cc      real*4  tarray(2), dtime
integer i, ncurve
logical exstf
character fluid*8, respon*1, inpfm*15, outfm*15, choose*1,
2       both*1, dummy*60

```

```

-----c
c The built-in turbulent program parameters are initialized below. c
c Some of these parameters are problem specific and may be adjusted c
c according to individual problems. c
c c
c      NSPACE - Size of the finite difference grid. c
c      CLOSS - Inlet loss coefficient. The inlet pressure loss c
c              is given by the product of the inlet loss c
c              coefficient and the dynamic pressure. c
c      EPSI - Grid contraction factor. The factor of which the c
c              grid size contracts along the leakage path. c
c              Since pressure drop is usually much steeper near c
c              the exit, we can obtain better resolution using c
c              a variable sized grid with grid points closer to c
c              each other near the exit. c
c      ERROR - The iteration error bound for the exit pressure. c
c
c There is one other preset parameter FLOOR - an estimate of the c
c minimum allowable leakage rate. In the original turbulent c
c program written by Paul Beatty, the user is required to input c
c FLOOR. This value is used as the starting estimate in solving c
c the boundary value problem using the shooting method. If the c
c value of FLOOR is too high and gives a choked flow in the first c
c iteration of the shooting method, the turbulent routine will c
c abort (return without a solution) with an error message. If c

```

```

c FLOOR is too low, the program may not converge.
c Fortunately, the range of values of FLOOR for which the program
c will converge is quite wide. Since the leakage rate is directly
c related to the film thickness, the value of FLOOR is initial-
c ized in the turbulent analysis SUBROUTINE FACE. The current
c preset values are, where HMEAN is the mean film thickness:
c
c      FLOOR = 1.0d-02 [kg/s] ; if HMEAN > 1.0d-04 [m]
c          = 1.0d-04 [kg/s] ; if HMEAN <= 1.0d-04 [m]
c
c Note that the optimal choices for the values of FLOOR are
c problem specific and these preset values may not be suitable for
c all cases. If the turbulent part of the code does not run
c properly, the user should try adjusting the preset values of
c FLOOR.
c-----c

```

```

      nspace = 50
      closs = 0.5d0
      epsi = 0.95d0
      error = 1.0d-3

```

```

c-----c
c FLOOR is initialized in the turbulent analysis code SUBROUTINE
c FACE.
c-----c

```

```

c-----c
c The upper and lower limits of film thicknesses in the study and
c the number of points are decided below. They may be changed to
c suit specific needs.
c
c      NPNTST - Number of points (different film thicknesses) on
c              the turbulent curves. The points are chosen in
c              such a way that they are equally spaced between
c              HINUPT and HINLOT in log scale.
c      HINUPT - The upper limit of the inlet film thickness of
c              the turbulent curves (in meters).
c      HINLOT - The lower limit of the inlet film thickness of
c              the turbulent curves (in meters).
c      NPNTSL - Number of points (different film thicknesses) on
c              the laminar curves. The points are chosen in
c              such a way that they are equally spaced between
c              HINUPL and HINLOL in log scale.
c      HINUPL - The upper limit of the inlet film thickness of
c              the laminar curves (in meters).
c      HINLOL - The upper limit of the inlet film thickness of
c              the laminar curves (in meters).
c-----c

```

```

      npntst = 21
      hinupt = 1.0d-03
      hinlot = 1.0d-05
      npntsl = 31

```

```
hinupl = 1.0d-05
hinlol = 1.0d-08
```

```
-----C
c Open the input data file. Default name of the input file is      c
c 'seal.in'.                                                       c
-----C
```

```
inquire(file='seal.in',exist=existf)
if (existf) then
  open(11,file='seal.in',status='old')
else
  write(*,(' File "seal.in" does not exist ...'))
  write(*,(' Please enter the input file name',
2      ' (max. 15 characters): '))
  read(*,'(a15)') inpfrm
  open(11,file=inpfrm,status='old')
end if
```

```
-----C
c Read the inputs ...                                             c
-----C
```

```
-----C
c For some reason, Microsoft FORTRAN compiler (at least V3.31)  c
c requires the read statement to read in the comment field along  c
c with the relevent input data on each input line or the program  c
c bombs out with an I/O error. To get round this, the comment    c
c field of each line is read in as a character string DUMMY.     c
-----C
```

```
read(11,'(a15,5x,a60)') outfrm, dummy
read(11,'(a8,12x,a60)') fluid, dummy
read(11,'(bn,f20.0,a60)') pinlet, dummy
read(11,'(bn,f20.0,a60)') pback, dummy
read(11,'(bn,f20.0,a60)') rinlet, dummy
read(11,'(bn,f20.0,a60)') routlt, dummy
read(11,'(bn,f20.0,a60)') cone, dummy
read(11,'(bn,f20.0,a60)') conduc, dummy
read(11,'(bn,a1,19x,a60)') both, dummy
read(11,'(bn,a1,19x,a60)') choose, dummy
```

```
cc read(11,'(a15)') outfrm
cc read(11,'(a8)') fluid
cc read(11,'(f20.0)') pinlet
cc read(11,'(f20.0)') pback
cc read(11,'(f20.0)') rinlet
cc read(11,'(f20.0)') routlt
cc read(11,'(f20.0)') cone
cc read(11,'(f20.0)') conduc
cc read(11,'(a1)') both
cc read(11,'(a1)') choose
```

```
if ((choose.eq.'S') .or. (choose.eq.'s')) then
```

```

      read(11, '(bn, f20.0, a60)') tinf, dummy
cc      read(11, '(f20.0)') tinf
      read(11, '(bn, i10, 10x, a60)') ncurve, dummy
cc      read(11, '(i10)') ncurve
      do 10, i = 1, ncurve
cc          read(11, '(bn, f20.0, a60)') rpms(i), dummy
10          read(11, '(f20.0)') rpms(i)
          continue
      else if ((choose.eq.'T') .or. (choose.eq.'t')) then
cc          read(11, '(bn, f20.0, a60)') rpm, dummy
          read(11, '(f20.0)') rpm
cc          read(11, '(bn, i10, 10x, a60)') ncurve, dummy
          read(11, '(i10)') ncurve
cc          do 20, i = 1, ncurve
          read(11, '(bn, f20.0, a60)') tinfs(i), dummy
cc          read(11, '(f20.0)') tinfs(i)
20          continue
      else
2          write(*, '(' Invalid input for CHOOSE, '
          ' program terminates ... ')')
          stop
      end if

      close(11)

```

```

-----c
c Read the spline curve fitting coefficients of the fluid properties c
c at saturation, the ideal gas constant and a few other necessary c
c information from the fluid properties data file. c
-----c

```

```

      call rsatdt(fluid)

```

```

-----c
c Open the output file ... c
-----c

```

```

-----c
c Microsoft FORTRAN doesn't know about the file status 'unknown!' c
-----c

```

```

      inquire(file=outfnm, exist=exstf)
      if (exstf) then
2          write(*, '(' File "", a15, "" already exists, type',
          ' "" ""y"" to overwrite it, ')') outfnm
          write(*, '(48x, ' else to exit : '))'
          read(*, '(a1)') respon
          if ((respon.eq.'Y') .or. (respon.eq.'y')) then
cc              open(12, file=outfnm)
                  open(12, file=outfnm, status='unknown')
          else
          stop
          end if
      else

```

```

        open(12,file=outfrm,status='new')
    end if

-----c
c Write the input seal parameters as the heading of the output file c
c so as to identify the output file. c
-----c

    if ((choose.eq.'S') .or. (choose.eq.'s')) then
        write(12,501) pinlet, pback, rinlet, routlt, cone, conduc,
2          tinf, fluid
501      format(1x,'Inlet Pressure = ',0pf10.4,4x,' kPa' /
2          1x,'Exit Pressure = ',0pf10.4,4x,' kPa' /
3          1x,'Inlet Radius = ',1pel4.4,' m' /
4          1x,'Exit Radius = ',1pel4.4,' m' /
5          1x,'Coning Slope = ',1pel4.2,' m/m' /
6          1x,'Conductivity = ',0pf10.4,4x,' W/m-K' /
7          1x,'Bulk Temperature = ',0pf8.2, 6x,' K' /
8          1x,'Fluid = ',3x,a8 /)
    else
        write(12,502) pinlet, pback, rinlet, routlt, cone, conduc,
2          rpm, fluid
502      format(1x,'Inlet Pressure = ',0pf10.4,4x,' kPa' /
2          1x,'Exit Pressure = ',0pf10.4,4x,' kPa' /
3          1x,'Inlet Radius = ',1pel4.4,' m' /
4          1x,'Exit Radius = ',1pel4.4,' m' /
5          1x,'Coning Slope = ',1pel4.2,' m/m' /
6          1x,'Conductivity = ',0pf10.4,4x,' W/m-K' /
7          1x,'Seal Speed = ',0pf8.2, 6x,' rpm' /
8          1x,'Fluid = ',3x,a8 /)
    end if

    pinlet = 1.0d3*pinlet
    pback = 1.0d3*pback

-----c
c Crunch the curves out ... c
-----c

    do 30, i = 1, ncurve
        if ((choose.eq.'S') .or. (choose.eq.'s')) then
            omega = 3.141592653589793d0*rpms(i)/30.0d0
            write(12,'(//' RPM = ',f11.4)') rpms(i)
            write(12,'( ' Omega = ',f11.4)') omega
            write(*,'(' RPM('',i2,'') = ',f12.4)') i, rpms(i)
            call match(tinf, rpms(i))
            if ((both.eq.'y') .or. (both.eq.'Y')) then
                call face(tinf, rpms(i))
            end if
        else
            omega = 3.141592653589793d0*rpm/30.0d0
            write(12,'(//' Tinf = ',f11.4,' K'//)') tinf(i)
            write(*,'(' Tinf('',i2,'') = ',f12.4)') i, tinf(i)
            call match(tinf(i), rpm)
        end if
    end do

```

```

        if ((both .eq. 'y') .or. (both .eq. 'Y')) then
            call face(tinfs(i), rpm)
        end if
    end if
30    continue

    close(12)

    stop
    end

```

```

-----+c
c+-----+c
c
c    subroutine match ( tresvr, rpmsl )
c
c    The routine which calculates the seal temperaturea, leakage rates
c    and opening forces for various film thickness given a set of
c    operating conditions using the subroutines ALLLIQ and PHAS2L.
c
c-----+c

```

```

cc    implicit logical ( a - z )
cc    implicit undefined ( a - z )

    real*8 rinlet, routlt, cone, conduc
    real*8 pinlet, pback, rpm, omega, rolinf, tinf
    real*8 hinlet, pboil, rboil
    real*8 hinupt, hinlot, hinupl, hinlol
cc    real*8 tseal, visgas, visliq, rolliq, rgas

    integer npntst, npntsl

    common /geomty/ rinlet, routlt, cone, conduc
    common /operat/ pinlet, pback, rpm, omega, rolinf, tinf
    common /iterat/ hinlet, pboil, rboil
    common /curves/ npntst, hinupt, hinlot, npntsl, hinupl, hinlol
cc    common /fluid / tseal, visgas, visliq, rolliq, rgas

    real*8 tresvr, rpmsl, pi, houtlt, rbmax, delh, sat
    integer i
    logical boil, boiled
    external sat

    parameter (pi = 3.141592653589793d0)

    rpm = rpmsl
    tinf = tresvr
    omega = pi*rpm/30.0d0
    boiled = .false.
    rbmax = routlt

    if (tinf .ge. sat(1, pinlet)) then

```

```

        write(*,'(/ '' Seal is all-vapor ...'' /)')
    end if

    delh = (hinlol/hinupl)**(1.0d0/dble(npntsl - 1))
    hinlet = hinupl

501  write(12,501)
2    format(/,'          hrin          xboil          pboil          tseal ',
           '          leakage          load'//)

    do 10, i = 1, npntsl

        rboil = routlt

        if (cone .ne. 0.0d0) then
            houtlt = hinlet + (routlt - rinlet)*cone
            if (houtlt .le. 0.0d0) then
                write(*,'(/ '' WARNING: Coning angle specified is'',
                    '' too large.'')')
2                write(*,'(''          Calculations for film '',
2                    ''thicknesses less than or equal to'')')
2                write(*,'(10x,1pe10.3,'' m are skipped ...'' /)')
                hinlet
                return
            end if
        end if

        if (tinf .ge. sat(1, pinlet)) then
ccc         write(*,'('' All vapor seal ... ''')')
ccc         call allvap
ccc

        else

            call heat(boil)

            if (boil .or. boiled) then
ccc         write(*,'('' Two-phase seal ... ''')')
ccc
ccc         call phas2l(rbmax, boiled)

            else
ccc         write(*,'('' All liquid seal ... ''')')
ccc
ccc         call allliq

            end if

        end if

    end if

```

```

        hinlet = hinlet * delh
10      continue

        return
        end

c+-----+c
c
c      subroutine allliq
c
c      This is an all liquid seal.  But we need to check if the critical
c      seal speed is exceeded.
c
c+-----+c

cc      implicit logical ( a - z )
        implicit undefined ( a - z )

        real*8  rinlet, routlt, cone, conduc
        real*8  pinlet, pback, rpm, omega, rolinf, tinf
        real*8  hinlet, pboil, rboil
        real*8  tseal, visgas, visliq, rolliq, rgas

        common /geomty/ rinlet, routlt, cone, conduc
        common /operat/ pinlet, pback, rpm, omega, rolinf, tinf
        common /iterat/ hinlet, pboil, rboil
        common /fluid / tseal, visgas, visliq, rolliq, rgas

        real*8  crt, rbold, pi, rerr, load, leak, xboil, wliq, lkliq
        logical  boil
        external wliq, lkliq

        parameter (pi = 3.141592653589793d0, rerr = 1.0d-8)

        crt = pinlet - pback - 0.15d0*rolliq*omega*omega
2          *(rinlet*rinlet - routlt*routlt)

c-----c
c  If CRT is negative, the seal is operating at super-critical
c  speed.
c-----c

        if (crt .lt. 0.0d0) then
ccc
ccc      write(*,(' Crit''''ed, Hinlet = ',1pe12.3,
ccc 2      ', RPM = ',0pf10.2)') hinlet, rpm
ccc
10      rbold = rboil
2      rboil = dsqrt(rinlet*rinlet - 20.0d0*(pinlet - pback)
          / (3.0d0*rolliq*omega*omega))

```

```

        call heat(boil)
        if (dabs(1.0d0 - rbold/rboil) .gt. rerr) go to 10

        pboil = pback
        load = dabs(wliq(rboil)
2          + pback*pi*dabs(rboil*rboil - routlt*routlt)
        xboil = (routlt - rboil)/(routlt - rinlet)
        write(12,501) hinlet, xboil, tseal, load
501      format(2(1x,1pe12.3),14x,0pf10.3,14x,1pe12.3)

        else

ccc      write(*,'(' AOKay, Hinlet = ',1pe12.3,
ccc      ', RPM = ',0pf10.2)') hinlet, rpm
ccc
        pboil = pback
        load = dabs(wliq(routlt))
        leak = lkliq(routlt)
        write(12,502) hinlet, tseal, leak, load
502      format(1x,1pe12.3,27x,0pf10.3,2(1x,1pe12.3))

        end if

        rboil = routlt

        return
        end

-----+c
c
c      subroutine phas21 ( rbmax, boiled )
c
c      This seal is likely to be a two-phase seal. But we need to check
c      if the critical speed is exceeded.
c
c-----+c

cc      implicit logical ( a - z )
cc      implicit undefined ( a - z )

        real*8 rinlet, routlt, cone, conduc
        real*8 pinlet, pback, rpm, omega, rolinf, tinf
        real*8 hinlet, pboil, rboil
        real*8 tseal, visgas, visliq, rollic, rgas

        common /geomty/ rinlet, routlt, cone, conduc
        common /operat/ pinlet, pback, rpm, omega, rolinf, tinf
        common /iterat/ hinlet, pboil, rboil
        common /fluid / tseal, visgas, visliq, rollic, rgas

        real*8 rbmax, rerr, lkerr, crt, rbold, load, leak, xboil,

```

```

2      dir, talgas, rleft, rright, glkage, check, llkage, sat,
3      lkgas, lkliq, wgas, wliq
logical boiled, boil
external lkgas, lkliq, wgas, wliq

parameter (rerr = 1.0d-8, lkerr = 1.0d-4)

crt = pinlet - pback
2      - 0.15d0*rolliq*omega*omega
3      *(rinlet*rinlet - rboil*rboil)

ccc
ccc  write(*, '(' CRT = ',1pe12.3)') crt
ccc

      if (crt .lt. 0.0d0) then

10         rbold = rboil
           rboil = dsqrt(rinlet*rinlet - 20.0d0*(pinlet - pback)
2           / (3.0d0*rolliq*omega*omega))

           call heat(boil)
           if (dabs(1.0d0 - rbold/rboil) .gt. rerr) go to 10

           if (.not.boil) then
               boiled = .false.
               pboil = pback
               load = dabs(wliq(rboil))
               xboil = (routlt - rboil)/(routlt - rinlet)
               write(12,501) hinlet, xboil, tseal, load
501          format(2(1x,1pe12.3),14x,0pf10.3,14x,1pe12.3)
               rboil = routlt
               return
           end if

           end if

      if (rinlet .lt. routlt) then
          dir = 1.0d0
      else
          dir = -1.0d0
      end if

      boiled = .true.
      rleft = rboil
      rright = rinlet

20         rboil = 0.5d0*(rleft + rright)
           call heat(boil)
           talgas = sat(1, pinlet)
           if (tseal .ge. talgas) then
               rleft = rboil
               go to 20
           end if
           glkage = lkgas()

```

```

llkage = lkliq()
check = dir*(glkage - llkage)
if (((dabs(check/glkage) .gt. lkerr) .or.
2   (dabs(check/llkage) .gt. lkerr)) .and.
3   (dabs(1.0d0 - rright/rleft) .gt. rerr)) then
    if (check .gt. 0.0d0) then
        rleft = rboil
    else
        rright = rboil
    end if
    go to 20
end if

ccc
ccc write(*,'(' XBoil = ',1pe12.3)')
ccc 2   (roult - rboil)/(roult - rinlet)
ccc write(*,'(' PBoil = ',1pe12.3)') pboil
ccc
ccc if ((dabs(check/glkage) .gt. lkerr) .or.
ccc 2   (dabs(check/llkage) .gt. lkerr)) then
ccc   if (dabs(check/glkage) .gt. dabs(check/llkage)) then
ccc     check = dabs(check/glkage)
ccc   else
ccc     check = dabs(check/llkage)
ccc   end if
ccc   write(*,'(/ ' WARNING: Leakage rates did not converge',
ccc 2   ' to within the specified limit'))
ccc   write(*,'(11x,'at HRIN = ',1pe10.3,' m,')') hinlet
ccc   write(*,'(11x,' ERR = ',f10.7,'.' /)') check
ccc   end if
ccc
load = dabs(wliq(rboil) + wgas(rboil))
leak = 0.5d0*(llkage + glkage)
xboil = (roult - rboil)/(roult - rinlet)
write(12,502) hinlet, xboil, pboil, tseal, leak, load
502   format(3(1x,1pe12.3),1x,0pf10.3,2(1x,1pe12.3))

return
end

```

```

c+-----+c
c
c   subroutine allvap
c
c   This is an all vapor seal. Heat generation by viscous dissipation
c   is assumed negligible.
c
c+-----+c

```

```

cc   implicit logical ( a - z )
cc   implicit undefined ( a - z )

real*8 rinlet, roult, cone, conduc

```

```

real*8 pinlet, pback, rpm, omega, rolinf, tinf
real*8 hinlet, pboil, rboil
real*8 tseal, visgas, visliq, rollic, rgas

common /geomty/ rinlet, routlt, cone, conduc
common /operat/ pinlet, pback, rpm, omega, rolinf, tinf
common /iterat/ hinlet, pboil, rboil
common /fluid / tseal, visgas, visliq, rollic, rgas

real*8 load, leak, sat, wgas, lkgas
external sat, wgas, lkgas

tseal = tinf
visgas = sat(8, tseal)
rboil = rinlet
pboil = pinlet
load = wgas(rinlet)
leak = lkgas(rinlet)
write(12,501) hinlet, tseal, leak, load
501  format (1x,1pe12.3,27x,0pf10.3,2(1x,1pe12.3))

return
end

```

```

c+-----+c
c
c      subroutine heat ( boil )
c
c      Subroutine that calculates, for a given boiling interface location,
c      the temperature at the boiling interface using the semi-infinite
c      solid heat transfer model. The leakage flow is assumed to be
c      quasi-isothermal at this temperature. The pressure at the boiling
c      interface and the saturation fluid properties are then obtained
c      from the steam table ( real*8 function SAT ).
c
c+-----+c

```

```

cc      implicit logical ( a - z )
      implicit undefined ( a - z )

real*8 rinlet, routlt, cone, conduc
real*8 pinlet, pback, rpm, omega, rolinf, tinf
real*8 hinlet, pboil, rboil
real*8 tseal, visgas, visliq, rollic, rgas
real*8 gamma, cpgas, tcrit, vcrit, pcrit, psmall

common /geomty/ rinlet, routlt, cone, conduc
common /operat/ pinlet, pback, rpm, omega, rolinf, tinf
common /iterat/ hinlet, pboil, rboil
common /fluid / tseal, visgas, visliq, rollic, rgas
common /gas / gamma, cpgas, tcrit, vcrit, pcrit, psmall

```

```

real*8 ttemp, intgr1, deltt, terr, tsmall, pi, blkpt1, blkpt2,
2     blkpt3, talgas, ttrial, termht, sat, gss4, hcondc
cc   real*8 intgl1, intgl2, intgl3, intgl4
     logical boil
     external sat, gss4, hcondc

```

```

parameter (pi=3.141592653589793d0, terr=1.0d-2, tsmall=10.0d0)

```

```

-----c
c Since the integrand function has a singularity at R = RBOIL, an c
c open interval integration scheme (4 points Gauss-Legendre c
c integration over 4 sub-intervals) is chosen. c
-----c

```

```

     blkpt1 = rboil + 0.1d0*(rinlet - rboil)
     blkpt2 = rboil + 0.01d0*(rinlet - rboil)
     blkpt3 = rboil + 0.001d0*(rinlet - rboil)
     intgr1 = gss4(rinlet, blkpt1, hcondc)
2         + gss4(blkpt1, blkpt2, hcondc)
3         + gss4(blkpt2, blkpt3, hcondc)
4         + gss4(blkpt3, rboil, hcondc)

cc   intgl1 = gss4(rinlet, blkpt1, hcondc)
cc   write(*,(''INT(LOW =',1pe10.3,'' UP =',1pe10.3,') =',
cc   2     1pe10.3)') rinlet, blkpt1, intgl1
cc   intgl2 = gss4(blkpt1, blkpt2, hcondc)
cc   write(*,(''INT(LOW =',1pe10.3,'' UP =',1pe10.3,') =',
cc   2     1pe10.3)') blkpt1, blkpt2, intgl2
cc   intgl3 = gss4(blkpt2, blkpt3, hcondc)
cc   write(*,(''INT(LOW =',1pe10.3,'' UP =',1pe10.3,') =',
cc   2     1pe10.3)') blkpt2, blkpt3, intgl3
cc   intgl4 = gss4(blkpt3, rboil, hcondc)
cc   write(*,(''INT(LOW =',1pe10.3,'' UP =',1pe10.3,') =',
cc   2     1pe10.3)') blkpt3, rboil, intgl4
cc   write(*,('1x)')

cc   intgr1 = intgl1 + intgl2 + intgl3 + intgl4

     if (rboil .gt. rinlet) then
         intgr1 = -1.0d0*intgr1
     end if
cc   write(*,('/' INTGRL = ',f20.8)') intgr1

     talgas = sat(1, pinlet)
     visliq = sat(7, talgas)
cc   write(*,('' VisLiq(TALGas =',f9.3,') =',f20.8)')
cc   2     talgas, visliq
     termht = omega*omega*intgr1/(pi*conduc)
     deltt = visliq*termht
     ttemp = tinf + deltt

cc   if (ttemp .gt. talgas) then
     write(*,('' Seal will be all gas ...''))
     tseal = talgas

```

```

        boil = .true.
        return
    end if

20    visliq = sat(7, ttemp)
    deltt = visliq*termht
    ttrial = tinf + deltt
    if (dabs(ttemp - ttrial) .gt. terr) then
        if (ttrial .gt. talgas) then
            ttemp = 0.5d0*(talgas + ttemp)
        else
            ttemp = ttrial
        end if
    go to 20
    end if

    tseal = ttrial
    pboil = sat(6, tseal)
    visgas = sat(8, tseal)
    rolliq = 1.0d0/sat(10, tseal)
    if (pboil .gt. pback) then
        boil = .true.
    else
        boil = .false.
    end if
cc    write(*, '(' Tseal = ',f20.8)') tseal
cc    write(*, '(' Pboil = ',f20.8)') pboil/1000.0d0
cc    write(*, '(' VisGas = ',f20.8)') visgas
cc    write(*, '(' Rolliq = ',f20.8)') rolliq

    return
    end

```

```

-----+c
c+-----+c
c
c      real*8 function hcondc ( radius )
c
c      The integrand function of the heat transfer model.
c
c-----+c

```

```

cc      implicit logical ( a - z )
cc      implicit undefined ( a - z )

cc      real*8 rinlet, routlt, cone, conduc
cc      real*8 pinlet, pback, rpm, omega, rolinf, tinf
cc      real*8 hinlet, pboil, rboil
cc      real*8 tseal, visgas, visliq, rolliq, rgas

cc      common /geonty/ rinlet, routlt, cone, conduc
cc      common /operat/ pinlet, pback, rpm, omega, rolinf, tinf
cc      common /iterat/ hinlet, pboil, rboil

```

```

cc      common /fluid / tseal, visgas, visliq, rollic, rgas
      real*8 radius, ellipl
      external ellipl
      if (radius .lt. rboil) then
        hcondc = radius*radius*radius*ellipl(radius/rboil)
2         / (rboil*(hinlet + (radius - rinlet)*cone))
      else
        hcondc = radius*radius*ellipl(rboil/radius)
2         / (hinlet + (radius - rinlet)*cone)
      end if
cc      write(*, '( " HCOND(C(r = ', f10.8, ') = ', f20.8) ') radius,
cc      2      hcondc
      return
      end

```

```

c+-----+c
c
c      real*8 function ellipl ( x )
c
c      A double precision function that evaluates the complete elliptical
c      integral of the 1st kind using the series approximation given in
c      the "Handbook of Mathematical Functions."
c      The absolute error of this approximation is less than 3.0e-5.
c
c      Reference : Abramowitz, M., and Stegun, I. A.,
c                  "Handbook of Mathematical Functions", pp 591,
c                  Equation 17.3.34, Ninth Printing, Dover Publications
c
c      Note that the relationship between the parameter M1 as defined
c      in equation 17.3.34 and the input parameter of this function, X,
c      is :
c
c          M1 = 1.0 - X**2
c
c+-----+c

```

```

cc      implicit logical ( a - z )
cc      implicit undefined ( a - z )
      real*8 x, m1, m2, a0, a1, a2, b0, b1, b2
      parameter ( a0 = 1.38629 44 d0, b0 = 0.50000 00 d0,
2         a1 = 0.11197 23 d0, b1 = 0.12134 78 d0,
3         a2 = 0.07252 96 d0, b2 = 0.02887 29 d0)
      m1 = 1.0d0 - x * x
      m2 = m1 * m1
      ellipl = (a0 + a1 * m1 + a2 * m2)
2         - (b0 + b1 * m1 + b2 * m2)*dlog(m1)

```

```

return
end

```

```

-----+c
c+-----+c
c
c      subroutine rsatdt ( fluid )
c
c      Subroutine that reads in the spline coefficients for the steam
c      tables from the saturation fluid properties data files.
c
c-----+c

```

```

cc      implicit logical ( a - z )
      implicit undefined ( a - z )

      real*8 gamma, cpgas, tcrit, vcrit, pcrit, psmall
      real*8 satdat, ddatdp, visdat, pvisc, tvisc, tmin, tmax,
2      pmin, pmax
      real*8 tseal, visgas, visliq, rollic, rgas
      integer ndata, jprops, irows, jcols, i, j, k
      character*8 fluid

      common /gas / gamma, cpgas, tcrit, vcrit, pcrit, psmall
      common /thermo/ satdat(11,50,4), ndata, jprops, ddatdp(5,60,3),
2      visdat(65,15), pvisc(15), tvisc(65), irows,
3      jcols, tmin, tmax, pmin, pmax
      common /fluid / tseal, visgas, visliq, rollic, rgas

      jprops = 1
      if (fluid .eq. 'water ') then
          open(10, file='water.dat', status='old')
          rgas = 461.51d0
      else if (fluid .eq. 'hydrogen') then
          open(10, file='hydrogen.dat', status='old')
          rgas = 4124.289d0
      else if (fluid .eq. 'oxygen ') then
          open(10, file='oxygen.dat', status='old')
          rgas = 259.832d0
      else if (fluid .eq. 'nitrogen') then
          open(10, file='nitrogen.dat', status='old')
          rgas = 296.798d0
      else
          write(*, '(' Program cannot handle this fluid ... ')')
          stop
      end if

      read(10,701) gamma, cpgas, tcrit, vcrit, pcrit, psmall
      read(10,702) ndata
      read(10,703) (((satdat(i,j,k),i=1,11),j=1,ndata),k=1,4)
      read(10,703) (((ddatdp(i,j,k),i=1,5),j=1,ndata),k=1,3)
      read(10,702) irows, jcols

```

```

        read(10,701) tmin, tmax, pmin, pmax
        do 10, j = 1, jcols
10         read(10,701) pvisc(j)
        do 20, i = 1, irows
20         read(10,701) tvisc(i)
        do 30, j = 1, jcols
        do 30, i = 1, irows
30         read(10,*) visdat(i,j)
        close(10)

        return

701     format (bn,e13.6)
702     format (bn,i13)
703     format (bn,6(1pe13.6))

end

```

```

c+-----+c
c
c      real*8 function sat(i, x)
c
c      This function calculates saturation properties as functions of
c      either pressure, temperature, or saturated liquid enthalpy. The
c      data is stored in the array SATDAT(I,J,K) where I denotes the
c      the fluid property as follows:
c
c      1 : Tsat (Psat)      5 : Ifg (Psat)      9 : If (Tsat)
c      2 : Vf (Psat)       6 : Psat (Tsat)     10 : Vf (Tsat)
c      3 : Vfg (Psat)      7 : VISCf (Tsat)    11 : Tsat (If)
c      4 : If (Psat)       8 : VISCg (Tsat)
c
c      The index K takes on values 1 through 4 where K = 1 denotes the
c      property for the particular J. K = 2,3,4 contains the cubic
c      spline coefficient for the curve of property type I (e.g. If)
c      between point J and J + 1.
c
c+-----+c

        implicit real*8 (a-h,o-z)
        common /gas / gamma, cpgas, tcrit, vcrit, pcrit, psmall
        common /thermo/ satdat(11,50,4), ndata, jprops, ddatdp(5,60,3),
2         visdat(65,15), pvisc(15), tvisc(65), irows, jcols,
3         tmin, tmax, pmin, pmax

        dimension ipropx(11)
        data ipropx /6,6,6,6,6,1,1,1,1,1,4/

c-----c
c      Remember what property is used as the independent variable for this
c      I.
c-----c

```

```

ix = ipropx(i)
-----c
c Go straight to the calculations if we're still between J and      c
c J + 1.                                                            c
c-----c

      if ((x .ge. satdat(ix,jprops ,1)) .and.
2      (x .le. satdat(ix,jprops+1,1))) go to 200

-----c
c Find the correct J for this property.                             c
c-----c

      jmove = int(dsign(1.0d0, x - satdat(ix,jprops,1)))

100      jprops = jprops + jmove
      if ((x .lt. satdat(ix,jprops ,1)) .or.
2      (x .gt. satdat(ix,jprops+1,1))) go to 100

-----c
c Calculate the property from the cubic spline.                    c
c-----c

200      z = x - satdat(ix,jprops,1)
      sat = satdat(i,jprops,1) + z * (satdat(i,jprops,2) +
2      z * (satdat(i,jprops,3) + z * satdat(i,jprops,4)))

      return
      end

-----+c
c+-----c
c      real*8 function wliq ( rboil )                                c
c      Function that calculates the opening force from the all-liquid c
c      portion of the seal given the boiling interface location.    c
c-----+c

cc      implicit logical ( a - z )
      implicit undefined ( a - z )

      real*8 rboil, rombrg, tprliq
      real*8 rinlet, routlt, cone, conduc
      external rombrg, tprliq

      common /geomty/ rinlet, routlt, cone, conduc

      wliq = rombrg(rinlet, rboil, tprliq)

```

```

return
end

```

```

-----+c
c
c      real*8 function tprliq ( radius )
c
c      Function that calculates the value of : 2.0 * pi * r * P(r)
c      for the all-liquid portion of the seal.
c      To find the seal opening force from the all-liquid portion of the
c      seal, this function is integrated with respect to RADIUS from
c      the inlet to the boiling interface location.
c
c-----+c

```

```

cc      implicit logical ( a - z )
cc      implicit undefined ( a - z )

      real*8 radius, press, twopi, pliq
      integer ncalls
      external pliq
      parameter (twopi = 6.283185307179586d0)
      data ncalls /0/

      ncalls = ncalls + 1
      press = pliq(radius)
      tprliq = twopi * radius * press
cc      write(*,501) ncalls, radius, press, tprliq
cc501    format(' Call #',i3,', P(r = ',f10.8,') =',f20.6 /
cc      2      23x,'2*pi*P =',f20.6)

      return
      end

```

```

-----+c
c
c      real*8 function pliq ( radius )
c
c      Function that calculates the pressure at RADIUS for the all-
c      liquid portion of the seal.
c
c-----+c

```

```

cc      implicit logical ( a - z )
cc      implicit undefined ( a - z )

      real*8 rinlet, routlt, cone, conduc
      real*8 pinlet, pback, rpm, omega, rolinf, tinf
      real*8 hinlet, pboil, rboil
      real*8 tseal, visgas, visliq, rollic, rgas

```

```

common /geomty/ rinlet, routlt, cone, conduc
common /operat/ pinlet, pback, rpm, omega, rolinf, tinf
common /iterat/ hinlet, pboil, rboil
common /fluid / tseal, visgas, visliq, rollicq, rgas

```

```

2 real*8 radius, term1, centrf, h, ho, hboil, numer1, numer2,
denom

```

```

if (cone .eq. 0.0d0) then
2 term1 = (pinlet - pboil
3 - 0.15d0*rollicq*omega*omega
4 *(rinlet*rinlet - rboil*rboil))
centrf = 0.15d0*rollicq*omega*omega
2 *(radius*radius - rinlet*rinlet)
pliq = pinlet + term1 + centrf

```

```

else
h = hinlet + (radius - rinlet)*cone
hboil = hinlet + (rboil - rinlet)*cone
ho = hinlet - rinlet*cone
numer1 = pinlet - pboil
2 - 0.15d0*rollicq*omega*omega
3 *(rinlet*rinlet - rboil*rboil)
numer2 = dlog((radius*hinlet)/(rinlet*h))
2 + ho*(1.0d0/h - 1.0d0/hinlet)
3 + 0.5d0*ho*ho*(1.0d0/(h*h)
4 - 1.0d0/(hinlet*hinlet))
denom = dlog((rinlet*hboil)/(rboil*hinlet))
2 + ho*(1.0d0/hinlet - 1.0d0/hboil)
3 + 0.5d0*ho*ho*(1.0d0/(hinlet*hinlet)
4 - 1.0d0/(hboil*hboil))
centrf = 0.15d0*rollicq*omega*omega
2 *(radius*radius - rinlet*rinlet)
pliq = pinlet + numer1*numer2/denom + centrf
end if

```

```

return
end

```

```

-----+c
c
c      real*8 function lkliq ( )
c
c      Function that calculates the mass leakage rate from the liquid seal
c      equations.
c
c-----c
cc      implicit logical ( a - z )
      implicit undefined ( a - z )

```

```

real*8 rinlet, routlt, cone, conduc
real*8 pinlet, pback, rpm, omega, rolinf, tinf
real*8 hinlet, pboil, rboil
real*8 tseal, visgas, visliq, rollic, rgas

common /geomty/ rinlet, routlt, cone, conduc
common /operat/ pinlet, pback, rpm, omega, rolinf, tinf
common /iterat/ hinlet, pboil, rboil
common /fluid / tseal, visgas, visliq, rollic, rgas

real*8 pi, ho, hboil, numer, denom

parameter (pi = 3.141592653589793d0)

cc write(*,501) pi, rollic, hinlet, omega, rinlet, rboil, pinlet,
cc 2 pboil
cc501 format(' Pi = ',f20.8 / ' RolLiq = ',f20.8 /
cc 2 ' Hinlet = ',f20.8 / ' Omega = ',f20.8 /
cc 3 ' Rinlet = ',f20.8 / ' Rboil = ',f20.8 /
cc 4 ' Pinlet = ',f20.8 / ' Pboil = ',f20.8 )

if (cone .eq. 0.0d0) then
  numer = rollic*pi*hinlet*
  2 * (0.15d0*rollic*omega*omega
  3 *(rinlet*rinlet - rboil*rboil)
  4 - (pinlet - pboil))

  denom = 6.0d0*visliq*dlog(rinlet/rboil)
cc write(*,'(' Numer = ',f20.8)') numer
cc write(*,'(' Denom = ',f20.8)') denom
  lkliq = numer/denom
cc write(*,'(' LkLiq = ',f20.8)') lkliq
else
  ho = hinlet - rinlet*cone
  hboil = ho + rboil*cone
cc write(*,'(' Hinlet = ',f20.8)') hinlet
cc write(*,'(' Ho = ',f20.8)') ho
cc write(*,'(' Hboil = ',f20.8)') hboil
  numer = rollic*pi*ho*ho*ho
  2 * (0.15d0*rollic*omega*omega
  3 *(rinlet*rinlet - rboil*rboil)
  4 - (pinlet - pboil))

  denom = 6.0d0*visliq
  2 *(dlog(rinlet/rboil) - dlog(hinlet/hboil)
  3 + ho*(1.0d0/hinlet - 1.0d0/hboil)
  4 + 0.5d0*ho*ho*(1.0d0/(hinlet*hinlet)
  5 - 1.0d0/(hboil*hboil)))
cc write(*,'(' Numer = ',f20.8)') numer
cc write(*,'(' Denom = ',f20.8)') denom
  lkliq = numer/denom
cc write(*,'(' LkLiq = ',f20.8)') lkliq
end if

return
end

```

```

c+-----+c
c
c      real*8 function wgas ( rboil )
c
c      Function that calculates the opening force from the all-vapor
c      portion of the seal given the boiling interface location.
c
c-----c

```

```

cc      implicit logical ( a - z )
cc      implicit undefined ( a - z )

      real*8 rboil, rombrg, tprgas
      real*8 rinlet, routlt, cone, conduc
      external rombrg, tprgas

      common /geomty/ rinlet, routlt, cone, conduc

      wgas = rombrg(rboil, routlt, tprgas)

      return
      end

```

```

c+-----+c
c
c      real*8 function tprgas ( radius )
c
c      Function that calculates the value of :  $2.0 * \pi * r * P(r)$ 
c      for the all-vapor portion.
c      To find the seal opening force from the all-vapor portion of the
c      seal, this function is integrated with respect to RADIUS from
c      the inlet to the boiling interface location.
c
c-----c

```

```

cc      implicit logical ( a - z )
cc      implicit undefined ( a - z )

      real*8 radius, twopi, press, pgas
      integer ncalls
      external pgas
      parameter (twopi = 6.283185307179586d0)
      data ncalls /0/

      ncalls = ncalls + 1
      press = pgas(radius)
      tprgas = twopi * radius * press

cc      write(*,501) ncalls, radius, press, tprgas

```



```

return
end

```

```

-----+C
C                                             C
C      real*8 function lkgas ( )                                             C
C                                             C
C Function that calculates the mass leakage rate from the vapor seal C
C equations.                                                                 C
C                                             C
C-----+C

cc      implicit logical ( a - z )
cc      implicit undefined ( a - z )

      real*8 rinlet, routlt, cone, conduc
      real*8 pinlet, pback, rpm, omega, rolinf, tinf
      real*8 hinlet, pboil, rboil
      real*8 tseal, visgas, visliq, rollic, rgas

      common /geomty/ rinlet, routlt, cone, conduc
      common /operat/ pinlet, pback, rpm, omega, rolinf, tinf
      common /iterat/ hinlet, pboil, rboil
      common /fluid / tseal, visgas, visliq, rollic, rgas

      real*8 pi, ho, hboil, houtlt, numer, denom

      parameter (pi=3.141592653589793d0)

cc      write(*,501) pi, pback, pboil, hinlet, cone, visgas, rgas,
cc 2      tseal, rboil, routlt
cc501    format(' Pi      = ',f20.8 / ' Pback = ',f20.8 /
cc 2      ' Pboil = ',f20.8 / ' Hinlet = ',f20.8 /
cc 3      ' Cone   = ',f20.8 / ' VisGas = ',f20.8 /
cc 4      ' Rgas   = ',f20.8 / ' Tseal = ',f20.8 /
cc 5      ' Rboil = ',f20.8 / ' Routlt = ',f20.8 )

      if (.false.) then
2        numer = pi*(pback*pback - pboil*pboil)*hinlet*hinlet
          *hinlet
          denom = 12.0d0*visgas*rgas*tseal*dlog(rboil/routlt)
cc        write(*,(' Numer = ',f20.8)) numer
cc        write(*,(' Denom = ',f20.8)) denom
          lkgas = numer/denom
cc        write(*,(' LkGas = ',f20.8)) lkgas
      else
          ho = hinlet - rinlet*ccone
          hboil = ho + rboil*ccone
          houtlt = ho + routlt*ccone
cc        write(*,(' Ho      = ',f20.8)) ho
cc        write(*,(' Hboil  = ',f20.8)) hboil
cc        write(*,(' Houtlt = ',f20.8)) houtlt

```

```

numer = pi*(pback*pback - pboil*pboil)*ho*ho*ho
denom = 12.0d0*visgas*rgas*tseal
2          *(dlog(rboil/routlt) - dlog(hboil/houtlt)
3          + ho*(1.0d0/hboil - 1.0d0/houtlt)
4          + 0.5d0*ho*ho*(1.0d0/(hboil*hboil)
5          - 1.0d0/(houtlt*houtlt)))
cc        write(*,'('' Numer = ',f20.8)') numer
cc        write(*,'('' Denom = ',f20.8)') denom
          lkgas = numer/denom
cc        write(*,'('' LkGas = ',f20.8)') lkgas
          end if

          return
          end

```

```

-----+c
c                                             c
c          real*8 function gss4 ( up, low, func )                               c
c                                                                                   c
c          This routine calculates the integral of FUNC from LOW to UP             c
c          using 4 points Gauss-Legendre Quadratures.                             c
c                                                                                   c
c-----+c

```

```

cc        implicit logical ( a - z )
cc        implicit undefined ( a - z )

          real*8 up, low, xmid, hdelx, xpt, g1, g2, g3, g4, sum, func
          real*8 xi, wt
          dimension xi(2), wt(2)
          external func

          data xi /0.33998 10435 84856 d0, 0.86113 63115 94053 d0/
          data wt /0.65214 51548 62546 d0, 0.34785 48451 37454 d0/

          xmid = 0.5d0*(up + low)
          hdelx = 0.5d0*(up - low)

          xpt = xmid + hdelx * xi(1)
          g1 = func(xpt)
          xpt = xmid - hdelx * xi(1)
          g2 = func(xpt)
          xpt = xmid + hdelx * xi(2)
          g3 = func(xpt)
          xpt = xmid - hdelx * xi(2)
          g4 = func(xpt)
          sum = wt(1) * (g1 + g2) + wt(2) * (g3 + g4)

          gss4 = hdelx * sum

          return

```

end

```
+-----+c
c
c      real*8 function rombrg ( up, low, func )
c
c      Romberg integration routine.  Modified from "Numerical Recipes."
c
c      Reference :  Press, W. H., Flannery, B. P., Teukolsky, S. A., and
c                   Vetterling, W. T.,
c                   Numerical Recipes, The Art of Scientific Computing
c                   ( 1st ed., Cambridge University Press, 1986 )
c                   pp 114-115.
c
c+-----+c
```

```
cc      implicit logical ( a - z )
cc      implicit undefined ( a - z )

      real*8 up, low, errmax, s, h, ss, dss, func
      integer nmax, nmaxpl, k, kml, j
      external func

      parameter (errmax=1.0d-8, nmax=20, nmaxpl=21, k=5, kml=4)

      dimension s(nmaxpl), h(nmaxpl)

      h(1) = 1.0d0
      do 10, j = 1, nmax
         call trapzd(func, low, up, s(j), j)
         if (j .ge. k) then
            call polint(h(j-kml), s(j-kml), k, 0.0d0, ss, dss)
            if (dabs(dss) .lt. errmax*dabs(ss)) then
               rombrg = ss
               return
            end if
         end if
         s(j+1) = s(j)
         h(j+1) = 0.25d0*h(j)
10      continue

      write(*, '(' Too many steps ... ')')

      stop
      end
```

```
+-----+c
c
c      subroutine trapzd (func, low, up, s, n)
c
c
```

```

c This routine computes the N'th stage of refinement of an extended
c trapezoidal rule. Modified from "Numerical Recipes."
c
c Reference : Press, W. H., Flannery, B. P., Teukolsky, S. A., and
c Vetterling, W. T.,
c Numerical Recipes, The Art of Scientific Computing
c ( 1st ed., Cambridge University Press, 1986 )
c pp 111.
c
c-----+c

```

```

cc      implicit logical ( a - z )
      implicit undefined ( a - z )

      real*8 func, low, up, s, trm, del, x, sum
      integer n, it, j
      external func

      if (n.eq.1) then
        s = 0.5d0*(up - low)*(func(low) + func(up))
        it = 1
      else
        trm = dble(it)
        del = (up - low)/trm
        x = low + 0.5d0*del
        sum = 0.0d0
        do 10, j = 1, it
          sum = sum + func(x)
          x = x + del
10      continue
        s = 0.5d0*(s + (up - low)*sum/trm)
        it = 2*it
      end if

      return
      end

```

```

c-----+c
c
c      subroutine polint ( xa, ya, n, x, y, dy )
c
c This routine does polynomial interpolation or extrapolations.
c Modified from "Numerical Recipes."
c
c Reference : Press, W. H., Flannery, B. P., Teukolsky, S. A., and
c Vetterling, W. T.,
c Numerical Recipes, The Art of Scientific Computing
c ( 1st ed., Cambridge University Press, 1986 )
c pp 82.
c
c-----+c

```

```

cc      implicit logical ( a - z )
      implicit undefined ( a - z )

      real*8 xa, ya, x, y, dy, dif, dift, c, d, den ,ho, hp, w
      integer nmax, n, ns, i, m

      parameter (nmax=10)

      dimension xa(n), ya(n), c(nmax), d(nmax)

      ns = 1
      dif = dabs(x - xa(1))
      do 10, i = 1, n
         dift = dabs(x - xa(i))
         if (dift.lt.dif) then
            ns = i
            dif = dift
         end if
         c(i) = ya(i)
         d(i) = ya(i)
10      continue
      y = ya(ns)
      ns = ns - 1
      do 30, m = 1, n-1
         do 20, i = 1, n-m
            ho = xa(i) - x
            hp = xa(i+m) - x
            w = c(i+1) - d(i)
            den = ho - hp
            if (den .eq. (0.0d0)) then
               write(*, '( " XA" 's are identical ....' )')
               stop
            end if
            den = w/den
            d(i) = hp * den
            c(i) = ho * den
20      continue
         if ((2*ns).lt.(n-m)) then
            dy = c(ns + 1)
         else
            dy = d(ns)
            ns = ns - 1
         end if
         y = y + dy
30      continue

      return
      end

      subroutine face (tinf, rpm)

      implicit real*8 (a-h,o-z)

```

```

common /gas / gamma, cpgas, tcrit, vcrit, pcrit
common /geomry/ hmean, radius, rin, rout, rinlet, dhdr, nspace,
$ delta, epsi, pi, rmean
common /flow / flux, omega, pinfty, pback, iinfty, tinfty, choke,
$ cflux, pchoke, closs, signum, ifluid, psmall
common /thermo/ satdat(11,50,4), ndata, jprops, ddatdp(5,60,3),
$ visdat(65,15), pvisc(15), tvisc(65), irows, jcols,
$ tmin, tmax, pmin, pmax
common /var / p(120), h(120)
common /stress/ tauzr, tauzth, v, mu

```

```

-----+c
c
c Common blocks to connect the variables from Lau's laminar program c
c to Beatty's turbulent program. c
c c

```

```

common /geomty/ srin, sroul, scone, scondc
common /operat/ spinlt, spback, srpm, somega, srol, stinf
common /fluid/ stseal, svisg, svisl, sroll, srgas
common /turbin/ nsspac, scloss, sepsi, serror
common /curves/ npntst, hinupt, hinlot, npntsl, hinupl, hinlol

```

```

c
c-----+c

```

```

real*8 mu, iinfty, isat

```

```

-----+c
c
c Put the values of each variable in Lau's program into the corres- c
c ponding ones in beatty's program. c
c c

```

```

icase = 1
if (srin.lt.sroul) then
  rin = srin
  rout = sroul
  pin = spinlt
  pout = spback
else
  rin = sroul
  rout = srin
  pin = spback
  pout = spinlt
end if
dhdr = scone
nspace = nsspac
closs = scloss
epsi = sepsi
error = serror
tinfty = tinf
iplot = 0

```

```

c
c+-----+c
      pi = 4.0d0*datan(1.0d0)
      omega = pi*rpm/30.0d0

c      Specify finite difference grid. By making each successive step
c      smaller than the last by a set factor, high gradients near the
c      exit may be better resolved.

      sum = (1.0d0 - epsi**nspace)/(1.0d0 - epsi)
      delta = (rout - rin)/sum
      rmean = (rout + rin)/2.0d0

c      The error bound for the iteration to match the pressure boundary
c      condition (error) has already been set in the input file. Set the
c      error bound for the critical mass velocity and exit pressure,
bound.

      bound = 1.0d-04

c+-----+c
c
c      Modifications made to this subroutine (which was originally a
c      separate program) so that it calculates the seal performance for
c      a range of film thicknesses instead of at only one thickness as
c      in the original program. This is done to make the task of
c      plotting stiffness curves a little easier.
c

      hstep = (hinupt/hinlot)**(1.0d0/dble(npntst - 1))
      hrin = hinupt

c
c+-----+c

c      Determine the direction of flow through the seal.

      if(pin.eq.pout) check = 0.0d0
      if(pin.ne.pout) check = (pin - pout)/dabs(pin - pout)

      if (check) 12,13,13

12  pinfty = pout
    pback = pin
    rinlet = rout
    signum = -1.0d0
    go to 14

13  pinfty = pin
    pback = pout
    rinlet = rin
    signum = 1.0d0

```

```

        go to 14

14 delta = signum*delta

c+-----+c
c
c   The big do loop ...
c
c
c
c
c   write(12,510)
510 format(/,'          hrin          Reyc          Reyr          qexit ',
2          '          leakage          load'/)

c   do 100 iloops = 1, nptst

c   hmean = hrin + 0.5d0*dhdr*(rout - rin)
c   iterat = 1

c+-----+c
c
c   FLOOR is hard coded in this subroutine.  It MAY NOT be appropriate
c   for all conditions.  If you found that the turbulent part of this
c   program doesn't run properly, you may have to adjust the
c   values in the following statements.
c
c
c   if (hmean .le. (1.0d-4)) then
c     floor = 1.0d-4
c   else
c     floor = 1.0d-2
c   end if

c
c+-----+c
c
c   write(*,'(' Hmean = ',1pe12.3,',      Iloops = ',i4)')
2          hmean, iloops

c+-----+c
c
c   Flush all buffered output to save the already computed stuff
c   into the output file in case this routine enters an infinite loop
c   and needs to be killed.
c   Does not work when running under DOS, of course.
c
c   call flush(12)

c+-----+c

c   Initialize the check for choking.

c   choke = -1.0d0

c   Calculate the specific enthalpy of the fluid in the reservoir.
c   The sub-cooled liquid there is assumed to be incompressible.

```

```

volume = sat(10,tinfy)
deltap = pinfty - sat(6,tinfy)
isat = sat(9,tinfy)
iinfty = isat + volume*deltap

```

c Find the lowest back pressure for which a physically realize-
c able matching exit pressure may be found.

```

fluxl = floor
flux = fluxl
call shoot(pexit)

if (choke.ne.(1.d0)) go to 21
write(*,9)
return

```

```

21 fluxr = fluxl
22 flux = fluxr
   call shoot(pexit)
   fluxr = 3.162d0*fluxr
   if (choke.ne.(1.d0)) go to 22
   choke = -1.0d0

```

c Find the mass flux for incipient choking by the bisection
c method.

```

fluxr = fluxr/3.162d0
23 flux = fluxl
cc  iterat = iterat + 1
cc
   call shoot(pexit)
   a = choke
   choke = -1.0d0
   flux = fluxr
   call shoot(pexit)
   b = choke
   choke = -1.0d0
   test = a*b
   if(test.lt.(0.d0)) go to 24

   fluxr = fluxl
   fluxl = temp
   fluxl = (fluxl + fluxr)/2.0d0
   go to 23

24 check = dabs(fluxl - fluxr)/fluxl
   cflux = fluxl
   pchoke = pexit
   if(check.lt.bound) go to 25
   temp = fluxl
   fluxl = (fluxl + fluxr)/2.0d0
   go to 23

```

```

25 continue

c   Test now whether the back pressure desired can be matched.  If
c   it can not be matched store the profiles for the choked flow, If
c   it can be matched proceed to find the proper mass flux and
c   exit pressure.

    if(pback.ge.pchoke) go to 26

    call output (iplot,icase)
    go to 100

26 continue

c   Input the first two guesses for the mass flux.

    flux00 = floor
    flux0 = cflux

c   Calculate the exit pressures for the guessed mass flux.  Abort
c   the procedure if the initial guess for flux gives choked flow.

    flux = flux00
    call shoot(pend00)
    if(choke.ne.(1.d0)) go to 30
    write(*,9)
    return

30 flux = flux0
cc
    iterat = iterat + 1
cc
    call shoot(pend0)

c   Correct the guess for flux.  If it was found that the last guess
c   for flux gave an infinite or negative pressure gradient in the
c   computational domain, average that guess with the previous one,
c   reset the choked flow flag and shoot again.

    if(choke.eq.(-1.d0)) go to 40
    flux0 = 0.5d0*(flux0+flux00)
    choke = -1.0d0
    go to 30

40 deltaf = (pback - pend0)*(flux0 - flux00)/(pend0 - pend00)
    flux1 = flux0 + deltaf
    flux00 = flux0
    flux0 = flux1
    pend00 = pend0

c   test for convergence.

    check = dabs(pend0-pback)/pback

```

```

        if (iterat.ge.100) then
            write(*, '(' program did not converge, returned to caller. ')')
            return
        end if
        if(check.ge.error) go to 30

c    call output routine to store information for printing and
plotting.

cc    write(*, '(' iterations = ',i5)') iterat
        call output (iplot, icase)

        100 hrin = hrin/hstep
            continue

c
c    end of the big do loop.
c
c+-----+c

c    Format statements.

        9 format (11x, 'Note: Initial guess for flux gives choked flow')

        60 return
            end

c-----c

        subroutine dsatdp (dvfdp, dvfgdp, difdp, difgdp, press)

c-----c
c    This subroutine calculates derivatives of certain saturation
c    properties as functions of pressure. The data is stored in the
c    array ddatdp(i,j,k) where i denotes the fluid property as follows:
c
c        1:d(vf)/dp        2:d(vfg)/dp        3:d(if)/dp        4:d(ifg)/dp
c
c    For a particular j, k=2,3,4 contains the coefficients of a
c    quadratic which is the derivative of the cubic spline for the
c    curve of property type i (e.g. if) between point j and j+1.
c
c-----c

        implicit real*8 (a-h,o-z)

        common /gas / gamma, cpgas, tcrit, vcrit, pcrit
        common /geomry/ hmean, radius, rin, rout, rinlet, dhdr, nspace,
$         delta, epsi, pi, rmean
        common /flow / flux, omega, pinfty, pback, iinfty, tinfty, choke,
$         cflux, pchoke, closs, signum, ifluid, psmall
        common /thermo/ satdat(11,50,4), ndata, jprops, ddatdp(5,60,3),
$         visdat(65,15), pvisc(15), tvisc(65), irows, jcols,
$         tmin, tmax, pmin, pmax

```

```

common /var / p(120), h(120)
common /stress/ tauzr, tauzth, v, mu

real*8 mu, iinfy

c --- Jump to the calculations if pressure is still between p(j) and
c p(j+1).

      if ((press .ge. satdat(6, jprops, 1)) .and.
$         (press .le. satdat(6, jprops+1, 1)))          go to 200

c --- Find the correct j for this property.

      jmove = int(dsign(1.0d0, press - satdat(6, jprops, 1)))
100 jprops = jprops + jmove
      if ((press .lt. satdat(6, jprops, 1)) .or.
$         (press .gt. satdat(6, jprops+1, 1)))          go to 100

c --- Calculate the property from the cubic spline derivative.

200 z = (press - satdat(6, jprops, 1))
      dvfdp = ddatdp(1, jprops, 1) + z * (ddatdp(1, jprops, 2)
$         + z * (ddatdp(1, jprops, 3)))
      dvfgdp = ddatdp(2, jprops, 1) + z * (ddatdp(2, jprops, 2)
$         + z * (ddatdp(2, jprops, 3)))
      difdp = ddatdp(3, jprops, 1) + z * (ddatdp(3, jprops, 2)
$         + z * (ddatdp(3, jprops, 3)))
      difgdp = ddatdp(4, jprops, 1) + z * (ddatdp(4, jprops, 2)
$         + z * (ddatdp(4, jprops, 3)))

      return
      end

```

```

c      subroutine grad

c-----
c
c      This subroutine finds fluid properties and their derivatives
c      with pressure and calculates the axial gradients of pressure and
c      enthalpy derived from the equations of motion and energy.
c      Multiple entry points are used here to calculate the appropriate
c      properties for three separate flow regimes: sub-cooled liquid,
c      saturated liquid - vapor mixture, and superheated vapor.
cc
cc      Multiple entry points are, unfortunately, not supported by
cc      Microsoft FORTRAN compiler version 3.31. The three entry points
cc      in the original subroutine are broken up into three separate
cc      subroutines.
cc      - Stephen Lau
c
c-----

```

```

cc  implicit real*8 (a-h,o-z)

cc  common /gas    / gamma, cpgas, tcrit, vcrit, pcrit
cc  common /geomry/ hmean, radius, rin, rout, rinlet, dhdr, nspace,
cc  $              delta, epsi, pi, rmean
cc  common /flow  / flux, omega, pinfty, pback, iinfty, tinfy, choke,
cc  $              cflux, pchoke, closs, signum, ifluid, psmall
cc  common /thermo/ satdat(11,50,4), ndata, jprops, ddatdp(5,60,3),
cc  $              visdat(65,15), pvisc(15), tvisc(65), irows, jcols,
cc  $              tmin, tmax, pmin, pmax
cc  common /var   / p(120), h(120)
cc  common /stress/ tauzr, tauzth, v, mu

cc  real*8 mu, iinfty

```

c-----

```

subroutine liquid (press,enthpy,dhdr, didr)

```

c-----

```

implicit real*8 (a-h,o-z)

common /gas    / gamma, cpgas, tcrit, vcrit, pcrit
common /geomry/ hmean, radius, rin, rout, rinlet, dhdr, nspace,
$              delta, epsi, pi, rmean
common /flow  / flux, omega, pinfty, pback, iinfty, tinfy, choke,
$              cflux, pchoke, closs, signum, ifluid, psmall
common /thermo/ satdat(11,50,4), ndata, jprops, ddatdp(5,60,3),
$              visdat(65,15), pvisc(15), tvisc(65), irows, jcols,
$              tmin, tmax, pmin, pmax
common /var   / p(120), h(120)
common /stress/ tauzr, tauzth, v, mu

real*8 mu, iinfty

```

c Find the local film thickness.

```

hfilm = hmean + (radius - rmean)*dhdr

```

c Find the mass velocity, g.

```

g = signum*flux/(2.0d0*pi*radius*hfilm)

```

c Take the viscosity and specific volume of the sub-cooled liquid
c to be that of the saturated liquid at the same temperature.

```

temp = sat(11,enthpy)
v = sat(10,temp)
mu = sat(7,temp)
call shear

```

```

thing = g*g*v/radius*(1.0d0 + radius/hfilm*dhdr)
term1 = -2.0d0*signum/hfilm*tauzr

```

```
term2 = omega*omega*radius/(3.0d0*v)
term3 = thing
```

```
dpdr = term1 + term2 + term3
```

```
term1 = radius*omega/(g*hfilm)*tauzth
term2 = -omega*omega*radius/3.0d0
term3 = v*thing
```

```
didr = term1 + term2 + term3
```

```
return
end
```

```
c-----
```

```
subroutine phas2t (press,enthpy,dpdr, didr)
```

```
c-----
```

```
implicit real*8 (a-h,o-z)
```

```
common /gas / gamma, cpgas, tcrit, vcrit, pcrit
common /geomry/ hmean, radius, rin, rout, rinlet, dhdr, nspace,
$ delta, epsi, pi, rmean
common /flow / flux, omega, pinfty, pback, iinfty, tinfty, choke,
$ cflux, pchoke, closs, signum, ifluid, psmall
common /thermo/ satdat(11,50,4), ndata, jprops, ddatdp(5,60,3),
$ visdat(65,15), pvisc(15), tvisc(65), irows, jcols,
$ tmin, tmax, pmin, pmax
common /var / p(120), h(120)
common /stress/ tauzr, tauzth, v, mu
```

```
real*8 mu, iinfty
```

```
c Find the local film thickness.
```

```
hfilm = hmean + (radius - rmean)*dhdr
```

```
c Find the mass velocity, g.
```

```
g = signum*flux/(2.0d0*pi*radius*hfilm)
```

```
c Find the saturation temperature.
```

```
temp = sat(1,press)
```

```
c Find vfg, if, and ifg for the given pressure.
```

```
vfg = sat(3,press)
if = sat(4,press)
ifg = sat(5,press)
```

```
c Calculate the quality.
```

```

quality = (enthpy - if)/ifg
c   Find the specific volume of the saturated mixture at a given
c   pressure.

vf = sat(2,press)
v = vf + quality*vfg

c   Find the derivatives of vf, vfg, if, and ifg with pressure.

call dsatdp( dvfdp, dvfgdp, difdp, difgdp, press)

c   Find the derivatives of volume and enthalpy with respect to
c   pressure at constant quality.

dvdp = dvfdp + quality*dvfgdp
didp = difdp + quality*difgdp

c   Find the mixture viscosity by weighting the liquid and vapor
c   viscosities with the volume fraction.

vg = vfg + vf
mu = (quality*vg*sat(8,temp) + (1.d0 - quality)*vf*sat(7,temp))/v

c   Calculate the denominator of the gradient expressions and
c   check for a singularity.

phi = -g*g*(dvdp + vfg/ifg*(v - didp))

if(phi.lt.(1.d0)) go to 100
choke = 1.0d0
return

100 continue

c   Find the shear stresses.

call shear

c   Calculate the pressure and enthalpy gradients.

quant = 1.0d0 + radius/hfilm*dhdr
factor = g*g*v/radius
quod1 = g*g*vfg/ifg
quod2 = -omega*radius*tauzth/(g*hfilm)
quod3 = omega*omega*radius/1.5d0
quod4 = -2.0d0*signum*v*tauzr/hfilm

term1 = factor*quant
term2 = omega*omega*radius/(3.0d0*v)
term3 = -2.0d0*signum*tauzr/hfilm
term4 = quod1*(quod2+quod3+quod4)

```

```
dpdr = (term1+term2+term3+term4)/(1.0d0 - phi)
```

```
factor = -1.0d0/ifg
```

```
term1 = -omega*radius*tauzth/(g*hfilm)
```

```
term2 = omega*omega*radius/1.5d0
```

```
term3 = -(v - didp)*dpdr
```

```
term4 = -2.0d0*signum*v*tauzr/hfilm
```

```
dqdr = factor*(term1+term2+term3+term4)
```

```
didr = (difdp + quality*difgdp)*dpdr + ifg*dqdr
```

```
return
```

```
end
```

```
c-----
```

```
subroutine vapor (press,enthpy,dpdr, didr)
```

```
c-----
```

```
implicit real*8 (a-h,o-z)
```

```
common /gas / gamma, cpgas, tcrit, vcrit, pcrit
```

```
common /geomry/ hmean, radius, rin, rout, rinlet, dhdr, nspace,  
$ delta, epsi, pi, rmean
```

```
common /flow / flux, omega, pinfty, pback, iinfty, tinfty, choke,  
$ cflux, pchoke, closs, signum, ifluid, psmall
```

```
common /thermo/ satdat(11,50,4), ndata, jprops, ddatdp(5,60,3),  
$ visdat(65,15), pvisc(15), tvisc(65), irows, jcols,  
$ tmin, tmax, pmin, pmax
```

```
common /var / p(120), h(120)
```

```
common /stress/ tauzr, tauzth, v, mu
```

```
real*8 mu, iinfty
```

```
c Find the local film thickness.
```

```
hfilm = hmean + (radius - rmean)*dhdr
```

```
c Find the mass velocity, g.
```

```
g = signum*flux/(2.0d0*pi*radius*hfilm)
```

```
c Find the temperature and determine the viscosity.
```

```
temp = sat(1,press)
```

```
$ + (enthpy - sat(4,press) - sat(5,press))/cpgas
```

```
mu = superv(press,temp)
```

```
c Find the specific volume (through ideal gas law).
```

```
r = cpgas*(gamma - 1.0d0)/gamma
```

```
v = r*temp/press
```

```
c Determine the mach number and check for a singularity.
```

```

machsq = g*g*v/(gamma*press)
if(machsq.lt.(1.d0)) go to 200
choke = 1.0d0
return

200 continue

c Find the shear stresses.

call shear

c Calculate the pressure and enthalpy gradients.

term1 = -2.0d0*signum*tauzr/hfilm*(1.0d0 +
$ (gamma - 1.0d0)*machsq)
term2 = -(gamma - 1.0d0)*radius*omega*machsq*tauzth/(g*hfilm*v)
term3 = omega*omega*radius/(3.0d0*v)
$ *(1.0d0 + 2.0d0*(gamma - 1.0d0)*machsq)
term4 = gamma*press*machsq/radius*(1.0d0 + radius/hfilm*dhdr)
dpdr = (term1 + term2 + term3 + term4)/(1.0d0 - machsq)

term1 = radius*omega/(g*hfilm)*tauzth
term2 = omega*omega*radius/1.5d0
term3 = -2.0d0*signum*v*tauzr/hfilm
term4 = (gamma + 1.0d0)/(gamma - 1.0d0)*v*dpdr
dhdr = term1 + term2 + term3 + term4

return
end

-----
c
subroutine output (iplot, icense)
-----
c
c This subroutine prints out point by point information about
c temperature, pressure, and quality in the file "face.dat".
c if the variable iplot = 1 , this routine also generates
c a file "fprof.dat" which may be further processed by the program
c fprof.for. This post-processor prepares a plot of pressure,
c temperature, and quality profiles on a single graph.
c
c Most of the output statements in the routine are commented out.
cc This subroutine is modified so that it outputs only the inlet film
cc thickness, the maximum Reynold's numbers, the fluid quality at the
cc seal exit, the mass leakage rate and the seal opening force.
cc Since a different post-processor program is used, the statements
cc for generating the plot file are also commented out.
cc - Stephen Lau
c
-----
c

```

```
implicit real*8 (a-h,o-z)
```

```
common /gas / gamma, cpgas, tcrit, vcrit, pcrit  
common /geomry/ hmean, radius, rin, rout, rinlet, dhdr, nspace,  
$ delta, epsi, pi, rmean  
common /flow / flux, omega, pinfty, pback, iinfty, tinfty, choke,  
$ cflux, pchoke, closs, signum, ifluid, psmall  
common /thermo/ satdat(11,50,4), ndata, jprops, ddatdp(5,60,3),  
$ visdat(65,15), pvisc(15), tvisc(65), irows, jcols,  
$ tmin, tmax, pmin, pmax  
common /var / p(120), h(120)  
common /stress/ tauzr, tauzth, v, mu
```

```
real*8 mu, iinfty, leak
```

```
dimension r(120), t(120), quality(120)
```

```
c Back out properties of interest from the enthalpy array.
```

```
do 10 i=1,nspace+1  
check = (h(i) - sat(4,p(i)))/sat(5,p(i))  
if (check.lt.(0.d0)) check = -1  
check = dint(check)  
if (check) 11, 12, 13  
11 quality(i) = 0.0d0  
t(i) = sat(11,h(i))  
go to 10  
12 quality(i) = (h(i) - sat(4,p(i)))/sat(5,p(i))  
t(i) = sat(1,p(i))  
go to 10  
13 quality(i) = 1.0d0  
t(i) = sat(1,p(i)) + (h(i)-sat(5,p(i))-sat(4,p(i)))/cpgas  
10 continue
```

```
c Calculate the leakage rate and maximum leakage rate.
```

```
leak = flux  
cleak = cflux
```

```
c calculate shaft rpm.
```

```
rpm = omega*30.0d0/pi
```

```
c Report if the flow was choked.
```

```
iflow = 0  
if(pback.le.pchoke) iflow = 1
```

```
c Integrate the pressure over the seal area by the trapezoidal  
c rule to find the opening force
```

```
delr = delta  
r(1) = rinlet  
sum = 0.0d0
```

```

do 31 i=2,nspace+1
  r(i) = r(i-1) + delr
  tleft = p(i-1)*r(i-1)
  tright = p(i)*r(i)
  sum = sum + signum*delr*pi*(tleft + tright)
31 delr = delr*epsi

  force = sum

c      Check circumferential and radial flow reynold's numbers.
c      Print out the minimum values of each for reference.

  reyc = 1.0d+20
  reyr = 1.0d+20

  delr = delta

do 1000 i = 1,nspace+1
  radius = rinlet + delr*float(i-1)
  hfilm = hmean + (radius - rmean)*dhdr
  g = flux/(2.0d0*pi*radius*hfilm)
  vf = sat(2,p(i))
  vfg = sat(3,p(i))
  v = vf + quality(i)*vfg
  den = 1.0d0/v
  vg = vfg + vf
  visc = (quality(i)*vg*sat(8,t(i))
$      + (1.0d0 - quality(i))*vf*sat(7,t(i)))/v
  rr = 2.0d0*g*hfilm/visc
  rc = den*omega*radius*hfilm/(2.0d0*visc)
  if(rr.lt.reyr) reyr = rr
  if(rc.lt.reyc) reyc = rc
  delr = delr*epsi
1000 continue

c      Store output information in files for printing and plotting.
cc     open(unit=15,file='test.dat',access='sequential',status='new')

cc     write(15,20)
cc     write(15,21)
cc     if(ifluid.eq.1) write(15,36)
cc     if(ifluid.eq.2) write(15,46)
cc     if(ifluid.eq.3) write(15,47)
cc     if(ifluid.eq.4) write(15,48)
cc     write(15,37) icase
cc     write(15,22) rin
cc     write(15,23) rout
cc     write(15,24) hmean
cc     write(15,42) dhdr
cc     write(15,25) rpm
cc     write(15,26) pinfty
cc     write(15,27) pback

```

```

cc  write(15,28) tinfy
cc  write(15,38) closs
cc  write(15,29) leak
cc  write(15,33) cleak
cc  write(15,34) pchoke
cc  write(15,45) reyr
cc  write(15,44) reyc
cc  write(15,43) force
cc  if(iflow.eq.(1.d0)) write(15,39)

cc  write(15,30)
cc  do 35 i=1,nspace+1
cc 35 write(15,32) i, r(i), t(i), p(i), quality(i)

cc  write(15,'(///)')
cc  close (unit=15)

cc  if(iplot.eq.0) go to 40

cc  open(unit=14,file='fprof.dat',access='sequential',status='old')

cc  write(14,*)  icase
cc  write(14,*)  ifluid
cc  write(14,*)  rin
cc  write(14,*)  rout
cc  write(14,*)  hmean
cc  write(14,*)  dhdr
cc  write(14,*)  rpm
cc  write(14,*)  pinfty
cc  write(14,*)  pback
cc  write(14,*)  tinfy
cc  write(14,*)  leak
cc  write(14,*)  nspace
cc  write(14,*)  closs
cc  write(14,*)  force
cc  write(14,*)  iflow

cc  do 41 i = 1,nspace+1
cc  write(14,*) r(i)
cc  write(14,*) t(i)
cc  write(14,*) p(i)
cc 41 write(14,*) quality(i)

cc  close (unit=14)

c+-----+c
c
c  Tabulate results in format similar to Lau's laminar program.  c
c
c  rmean = 0.5d0*(rin + rout)
c  hrin = hmean - 0.5d0*dhdr*(rout - rin)
c  write(12,501) hrin,reyc,reyr,quality(nspace+1),leak*signum,force
501  format(3(1x,1pe12.3),1x,0pf10.3,2(1x,1pe12.3))

```

c
c+-----+c

40 return

c Format statements.

```
cc 20 format (10x,1h 'Steady State Analysis for a Face Shaft
cc $ seal operating',//,22x,1h 'in the Two-phase Regime'//)
cc 21 format (5x, ' Operating Conditions: '/')
cc 22 format (5x, ' Inner Seal Radius = ',1pe10.3, ' meters')
cc 23 format (5x, ' Outer Seal Radius = ',1pe10.3, ' meters')
cc 24 format (5x, ' Mean Film Thickness = ',1pe10.3, ' meters')
cc 25 format (5x, ' Shaft Rotation Speed = ',1pe10.3, ' rpm')
cc 26 format (5x, ' Reservoir Pressure = ',1pe10.3, ' Pascals')
cc 27 format (5x, ' Back Pressure = ',1pe10.3, ' Pascals')
cc 28 format (5x, ' Reservoir Temperature = ',1pe10.3,
cc $ ' degrees Kelvin')
cc 29 format (5x, ' Leakage Rate = ',1pe12.5,
cc $ ' kg/second')
cc 30 format (1x, ' Point R Temperature
cc $ Pressure Quality'//)
cc 32 format (2x,i3,7x,1pe10.4,7x,1pe10.4,10x,1pe10.3,10x,f5.3)
cc 33 format (5x, ' Maximum Leakage Rate = ',1pe12.5,
cc $ ' kg/second')
cc 34 format (1x, ' Exit Pressure for Choked Flow = ',1pe10.3,
cc $ ' Pascals')
cc 36 format (1x, ' Sealed Fluid is WATER'//)
cc 37 format (1x, ' case # ',i3/)
cc 38 format (5x, ' Inlet Loss Coefficient = ',e10.3)
cc 39 format (5x, ' Flow is Choked'//)
cc 42 format (5x, ' Coning Angle = ',1pe10.3, ' radians')
cc 43 format (5x, ' Opening Force = ',1pe12.5, ' Newtons'//)
cc 44 format (5x, ' Minimum Circumferential Re = ',1pe10.3)
cc 45 format (5x, ' Minimum Radial Re = ',1pe10.3)
cc 46 format (1x, ' Sealed Fluid is PARA - H2'//)
cc 47 format (1x, ' Sealed Fluid is LOX - GOX'//)
cc 48 format (1x, ' Sealed Fluid is NITROGEN'//)
end
```

c-----

subroutine runge (n,y,f,r,h,m,k)

c
c
c this subroutine performs numerical quadrature of coupled dif-
c ferential equations by gill's method, a variant of the Runge-Kutta
c technique. This routine was drawn from appendix c of "Viscous
c Fluid Flow" by Frank M. White.
c
c-----

implicit real*8 (a-h,o-z)

```

dimension y(10), f(10), q(10)

m = m + 1
go to (1,4,5,3,7), m
1 do 2 i = 1,n
2 q(i) = 0.0d0
  a = 0.5d0
  go to 9
3 a = 1.0d0 + dsqrt(0.5d0)
4 r = r + 0.5d0*h
5 do 6 i = 1,n
  y(i) = y(i) + a*(f(i)*h - q(i))
6 q(i) = 2.0d0*a*h*f(i) + (1.0d0 - 3.0d0*a)*q(i)
  a = 1.0d0 - dsqrt(0.5d0)
  go to 9
7 do 8 i = 1,n
8 y(i) = y(i) + h*f(i)/6.0d0 - q(i)/3.0d0
  m = 0
  k = 2
  go to 10
9 k = 1
10 return
end

```

subroutine shear

C
C
C This subroutine computes the radial (TAUZR) and circumferential
C (TAUZH) shear stresses at the seal faces. Expressions for
C both shear stresses are in a form:

$$\frac{1}{P} - C1 \ln(P) - C2 = 0$$

C
C where p is the square root of the friction factor. The
C stresses may be recovered from the formula:

$$T_{wall} = \frac{2}{(8v)} (PU)^2$$

C
C where U is the mean velocity and v is the specific volume.
C The constants c1 and c2 are determined by the fluid properties,
C the operating conditions of the seal, and the stress component
C under consideration. Solution of this transcendental
C equation is accomplished by Newton's method.
C

implicit real*8 (a-h,o-z)

```

common /gas / gamma, cpgas, tcrit, vcrit, pcrit
common /geomry/ hmean, radius, rin, rout, rinlet, dhdr, nspace,
$ delta, epsi, pi, rmean
common /flow / flux, omega, pinfty, pback, iinfty, tinfty, choke,
$ cflux, pchoke, closs, signum, ifluid, psmall
common /thermo/ satdat(11,50,4), ndata, jprops, ddatop(5,60,3),
$ visdat(65,15), pvisc(15), tvisc(65), irows, jcols,
$ tmin, tmax, pmin, pmax
common /var / p(120), h(120)
common /stress/ tauzr, tauzth, v, mu

```

```

real*8 mu, iinfty

```

```

c --- Find the local film thickness.

```

```

hfilm = hmean + (radius - rmean)*dhdr

```

```

c --- Find the mass velocity, g.

```

```

g = flux/(2.0d0*pi*radius*hfilm)

```

```

c --- Set error bound for iteration.

```

```

error = 1.0d-06

```

```

c --- Solve for axial shear stress.

```

```

tauzr = dabs(tauzr)
arg = 8.0d0*tauzr/(g*g*v)
prs = dsqrt(arg)
c1 = 0.8838d0
c2 = 0.142d0 + c1*dlog(g*hfilm/mu)
pcrit = dexp(-c2/c1)
if (prs .lt. pcrit) prs = pcrit * 10.0d0

```

```

100 pold = prs
top = 2.0d0 + c1*pold*(1.0d0 - dlog(pold)) - c2*pold
bot = 1.0d0/pold + c1
prs = top/bot
if (prs .lt. pcrit) prs = dsqrt(pold*pcrit)
if (dabs(pold - prs) / prs .gt. error) go to 100

```

```

c Limit the friction factor for transition flows.

```

```

reyn = g*hfilm/mu
if(reyn.lt.(4.0d3)) prs = 0.1694d0

```

```

temp = prs*g
tauzr = temp*temp*v/8.0d0

```

```

c --- Solve for circumferential shear stress.

```

```

if (omega .eq. (0.d0)) return

```

```

tauzth = dabs(tauzth)
u = radius*omega
arg = 8.0d0*v*tauzth/(u*u)
prs = dsqrt(arg)
c1 = 1.763d0
arg = u*hfilm/(mu*v)
c2 = 0.83d0 + c1*dlog(arg)
pcrit = dexp(-c2/c1)
if (prs .lt. pcrit) prs = pcrit * 10.0d0

200 pold = prs
top = 2.0d0 + c1*pold*(1.0d0 - dlog(pold)) - c2*pold
bot = 1.0d0/pold + c1
prs = top/bot
if (prs .lt. pcrit) prs = dsqrt(pold*pcrit)
if (dabs(pold - prs) / prs .gt. error) go to 200
temp = prs*u
tauzth = temp*temp/(8.0d0*v)

return
end

```

```

subroutine shoot (pexit)

```

```

c
c
c   This function returns the value of the pressure at the exit
c   boundary of the computational domain and records the pressure
c   and enthalpy at each finite difference point in that domain.
c
c

```

```

implicit real*8 (a-h,o-z)

```

```

common /gas / gamma, cpgas, tcrit, vcrit, pcrit
common /geomry/ hmean, radius, rin, rout, rinlet, dhdr, nspace,
$           delta, epsi, pi, rmean
common /flow / flux, omega, pinfty, pback, iinfty, tinfy, choke,
$           cflux, pchoke, closs, signum, ifluid, psmall
common /thermo/ satdat(11,50,4), ndata, jprops, ddatdp(5,60,3),
$           visdat(65,15), pvisc(15), tvisc(65), irows, jcols,
$           tmin, tmax, pmin, pmax
common /var / p(120), h(120)
common /stress/ tauzr, tauzth, v, mu

```

```

real*8 mu, iinfty, iinlet

```

```

dimension y(10), f(10)

```

```

c   Define number of equations to be solved and initialize para-
c   meters for integration scheme.

```

```

m = 0
n = 2
radius = rinlet

c   Find the local film thickness.

hfilm = hmean + (radius - rmean)*dhdr

c   Find the mass velocity, g.

g = signum*flux/(2.0d0*pi*radius*hfilm)

c   Calculate the entrance losses and modify inlet pressure and
c   enthalpy.

c --- Define error bound for iteration.

error = 1.0d-04

c --- Make initial guess that the end state corresponds to pure liquid.

volume = sat(10,tinfty)
thing = g*volume
iinlet = iinfty - thing*thing/2.0d0
pinlet = pinfty - (closs + 1.0d0)/volume*thing*thing/2.0d0

c --- Check for unrealistic pressure loss at the inlet.

if(pinlet.ge.psmall) go to 3
choke = 1.0d0
return
3 continue

c --- Check if end state is indeed pure liquid.

test = sat(4,pinlet)
if(iinlet.le.test) go to 5

c --- Iterate for saturated mixture end state.

voll = volume

1 ptemp = pinlet
volf = sat(2,pinlet)
volfg = sat(3,pinlet)
hf = sat(4,pinlet)
hfg = sat(5,pinlet)
qualty = (iinlet - hf)/hfg
vol2 = volf + qualty*volfg

thing = g*vol2
iinlet = iinfty - thing*thing/2.0d0
vol = (voll + vol2)/2.0d0

```

```

pinlet = pinfty - (closs + 1.0d0)*thing*thing/(2.0d0*vol)
c   Test for unrealistic pressure loss at inlet.

   if(pinlet.ge.psmall) go to 2
   choke = 1.0d0
   return

c   Check for convergence.

2 test = dabs(pinlet-ptemp)/pinlet
   if(test.ge.error) go to 1

5 continue

c   Initialize index to mark variable arrays and apply the initial
c   conditions in the shooting algorithm.

   jpoint = 1
   delr = delta
   y(1) = pinlet
   y(2) = inlet

c   Store the current values of pressure and enthalpy and integrate
c   both the axial momentum and energy equations.

8 p(jpoint) = y(1)
   h(jpoint) = y(2)
   if(jpoint.eq.(nspace+1)) go to 7
6 call runge (n,y,f,radius,delr,m,k)
   press = y(1)

c   Abort procedure if pressure goes below known saturation data.

   if(press.ge.psmall) go to 4
   choke = 1.0d0
   go to 18

4 enthpy = y(2)
   go to (10,20), k
10 check = (y(2) - sat(4,y(1)))/sat(5,y(1))
   if(check.lt.(0.d0)) check = -1.0d0
   check = dint(check)
   if (check) 12, 14, 16
12 call liquid (press,enthpy,dpdr, didr)
   f(1) = dpdr
   f(2) = didr
   go to 6
14 call phas2t (press,enthpy,dpdr, didr)
   if(choke.eq.(1.d0)) go to 18
   f(1) = dpdr
   f(2) = didr
   go to 6
16 call vapor (press,enthpy,dpdr, didr)

```

```

        if(choke.eq.(1.d0)) go to 18
        f(1) = dhdr
        f(2) = didr
        go to 6
20    jpoint = jpoint + 1
        delr = epsi*delr
        go to 8

c      Give pexit the pressure calculated at the end of the compu-
c      tational domain.

        7 pexit = y(1)

18    return
        end

-----
real*8 function superv (press, temp)

-----
c
c      this function computes superheated vapor viscosity by interpol-
c      ating from from a table.
c
c
c
-----

implicit real*8 (a-h,o-z)

common /gas      / gamma, cpgas, tcrit, vcrit, pcrit
common /geomry/  / hmean, radius, rin, rout, rinlet, dhdr, nspace,
$               / delta, epsi, pi, rmean
common /flow     / flux, omega, pinfty, pback, iinfty, tinfy, choke,
$               / cflux, pchoke, closs, signum, ifluid, psmall
common /thermo/  / satdat(11,50,4), ndata, jprops, ddatdp(5,60,3),
$               / visdat(65,15), pvisc(15), tvisc(65), irows, jcols,
$               / tmin, tmax, pmin, pmax
common /var      / p(120), h(120)
common /stress/  / tauzr, tauzth, v, mu

real*8 mu, iinfty

c --- Test to determine whether thermodynamic state is within the
c      bounds of the table.

        serror = 0.0d0
        if((press.lt.pmin).or.(press.ge.pmax)) serror = 1.0d0
        if((temp.lt.tmin).or.(temp.ge.tmax)) serror = 1.0d0
        if(serror.eq.(1.d0)) go to 100

c --- Find the appropriate pressure range.

        k = 0
10    k = k + 1

```

```

    if (press.ge.pvisc(k)) go to 10
    j = k - 1
c --- Find the appropriate temperature range.

    k = 0
20 k = k + 1
    if (temp.ge.tvisc(k)) go to 20
    i = k - 1

c --- Test for proximity to the saturation dome.

    if (temp.ge.tcrit) go to 40
    psat = sat(6,temp)
    if (pvisc(j+1).gt.psat) go to 30

c --- Bilinear interpolation by inverse-area rule.

40 a1 = temp - tvisc(i)
    a2 = tvisc(i+1) - temp
    b1 = press - pvisc(j)
    b2 = pvisc(j+1) - press

    fact1 = a1*b1
    fact2 = a2*b1
    fact3 = a2*b2
    fact4 = a1*b2
    factor = 1.0d0/(fact1 + fact2 + fact3 + fact4)

    superv = factor*(fact3*visdat(i,j) + fact4*visdat(i+1,j)
$          + fact1*visdat(i+1,j+1) + fact2*visdat(i,j+1))

    go to 200

c --- Special interpolation routine near the saturation dome.

30 vhigh = sat(8,temp)
    temp1 = sat(1,pvisc(j))
    vlow1 = sat(8,temp1)
    vlow2 = visdat(i+1,j)
    fact1 = temp - temp1
    fact2 = tvisc(i+1) - temp
    factor = 1.0d0/(fact1 + fact2)
    vlow = factor*(fact2*vlow1 + fact1*vlow2)

    fact1 = press - pvisc(j)
    fact2 = psat - press
    factor = 1.0d0/(fact1 + fact2)

1000 continue

    superv = factor*(fact2*vlow + fact1*vhigh)

    go to 200

```

```
100 write(5,101)
```

```
200 return
```

```
c --- Format statement.
```

```
101 format(1h 'Pt. of interest is out of bounds')
```

```
end
```